Insulin Secretory Granule Biogenesis and VPS41

Yousun An

In fulfilment of the requirements of the degree

Doctor of Philosophy

Faculty of Medicine and Health

The University of Sydney

2023

Insulin Secretory Granule Biogenesis and VPS41

Table of Contents

Declaration

I declare that this thesis represents my own writing which has been done after registering for the degree of PhD at the University of Sydney. This project was a collaborative study, and the following details were described the individuals who contributed to the results.

Dr. Ben Crossett performed label-free quantification proteomics on WT, VSP41 KO INS1 cells, control & VPS41 KD INS1 cells and then, I conducted analysis on the MaxQuant (version 2.0.2.0) data in section 2.5 using Perseus software (version 1.6.15.0), R package (version 4.1.1) and R studio.

Most of the experiments on VPS41 KO and VPS41 KD INS1 cells in chapter II and III, respectively was performed by me. The immunofluorescence images in sections 2.3.1, 3.3.1, 3.3.3 and 3.3.4 on INS1 cells were obtained by Dr. Belinda Yau and Dr. Mark Germanos.

Characterization of βVPS41 mice was performed by myself together with Dr. Belinda Yau. Especially, data in sections 4.3.4 were collected by Belinda and they were visualized by myself after my own analysis using Prism (version 9).

My supervisor, Associate Professor Melkam Kebede contributed to supervising this study, designs of experiments, interpretation of new findings and editing of this thesis.

Signed, Yousun An

June 2023

Acknowledgement

I would like to acknowledge my PhD supervisor, Associate Professor Melkam Kebede. Thanks to her great support and guidance for 4 years, I finally made the final fruit. She also taught me to be patient along with the strong confidence to become a researcher. Many thank you, Melkam, it was a great honour to be your student and hope to see your little angel with Melikt. I also thank Dr. Belinda for her great help and guidance throughout my PhD project, it was an honour to work with you and I enjoyed it a lot more than any experience. Thank you of course to my lab members, Mark, and Nick, it's been great fun working with you guys! I also thank a new member of my lab, Gabrielle. Thanks to her huge support for my thesis, I could finalise that.

My friend, Sheyda, I really thank for her encouragement, friendship as well as sincere advice to get through the darkness. I've been so pleased to know Sheyda here and become her friend.

I am also grateful to Dr. Yi. my previous supervisor in Korea. Even after I left Korea, she's been still supporting me along with sincere advice to find my way.

Thanks of course to my family, especially the two Kangs for supporting and endless love! Please always remember, we are one team and I love you with all my heart.

Finally, I thank everyone I've met through my PhD at Sydney University. It was a wonderful opportunity to make a new path in my life. I am truly sure that I can become a better person for my career in a new place thanks to the valuable experiences I had here.

Publication

Chapter 4.3.1, 4.3.2 and 4.3.3 of this thesis was published in Diabetes 2021; 70:436-448. I conducted in vivo experiments and acquired and analyzed data as a co-author.

List of Abbreviations

ALPS	Amphipathic lipid-packing sensor
AP-3	Adaptor protein-3
ARF6	ADP-ribosylation factor 6
ATP	Adenosine triphosphate
AUC	Area under the curve
BAR	Bin/anphiphysin/Rvs
BCA	Bicinchoninic acid
BSA	Bovine serum albumin
CgA	Chromogranin A
CgB	Chromogranin B
CHCR	Clathrin heavy-chain repeat domain
Co-IP	Co-immunoprecipitation
CORVET	Class c core vacuole/endosome tethering
CPE	Carboxypeptidase
CRISPR	Clustered regularly interspaced short palindromic repeats
Ctrl si	non-targeting siRNA control
DAPI	4,6'-diamidino-2-phenylindole, dihydrochloride
DMSO	Dimethyl sulfoxide
EGF	Epidermal growth factor
EGFR	Epidermal growth factor receptor
ELISA	Enzymes-linked immunosorbent assay
EM	Electron microscopy
ER	Endoplasmic reticulum
FBS	Foetal bovine serum
FFA	Free fatty acid
GFP	Green fluorescent protein
GLP-1	Glucagon-like peptide-1
GLUT-2	Glucose transporter type-2
GLUT-4	Glucose transporter type-4
GSIS	Glucose-stimulated insulin secretion
GSV	GLUT4 storage vesicle
GWAS	Genome-wide association studies

HA	Hemagglutinin
HA-VPS41	HA-tagged VPS41 rescue
HET	Heterozygous knockout
HID-1	High-temperature-induced dauer formation domain-containing protein-1
HOPS	Homotypic fusion and protein sorting
HTRF	Homogeneous time resolved fluorescence
ICA69	Islet cell autoantigen of 69kDa
ICC	Immunocytochemistry
IF	Immunofluorescence
IP	Immunoprecipitation
IP-GTT	Intraperitoneal glucose tolerance test
IP-ITT	Intraperitoneal insulin tolerance test
KD	Knockdown
KO	Homozygous knockout
KRBH	Krebs Ringer buffer
LAMP	Lysosome-associated membrane protein
LFQ	Label free quantification
MVB	Multivesicular bodies
OGTT	Oral glucose tolerance test
PBS	Phosphate buffered saline
PBS-T	PBS containing 0.1% Tween 20
PC1/3	Proprotein convertase 1
PC2	Proprotein convertase 2
PFA	Paraformaldehyde
PICK1	Protein interacting with C-kinase 1
PKD1	Protein kinase D1
RER	Rough endoplasmic reticulum
RES	VPS41 rescue INS1 cells
RILP	Rab-interacting lysosomal protein
ROS	Reactive oxygen species
SDS	Sodium dodecyl sulfate
SDS-PAGE	Sodium dodecyl sulphate-polyacrylamide gel electrophoresis
SEM	Standard error of mean
SG	Secretory granule

SgII	Secretogranin II
SINGD	Stress-induced nascent insulin granules degradation
SNAP23	Synaptosome-associated protein 23kDa
SNAP25	Synaptosome-associated protein 25kDa
SNARE	Soluble N-ethylmaleimide-sensitive factor attachment protein receptor
SNPs	Single nucleotide polymorphisms
T2D	Type 2 diabetes
TBS	Tris buffered saline
TBS-T	TBS containing 0.1% Tween 20
TCA	Tricarboxylic acid cycle
TE	Tris-EDTA buffer
TGN	Trans-Golgi network
UCP	Uncoupling protein
UniPort	Universal protein resource
VAMP2	Vesicle-associated membrane protein-2
VPS41	Vacuolar protein sorting-associated protein 41
VPS41si	siRNA to VPS41
WT	Wild-type

List of antibodies used in this thesis.

Antibody	*Supplier (source, cat.no.)*	*Application*
VPS41(D-12)	SC (Mouse, sc-377118)	1:500 (WB)
Insulin	SC (Mouse, sc-8033)	1:200 (WB)
Insulin	Dako	1:1 (IF, ICC)
proinsulin	DSHB (Mouse, GS-9A8)	2.5ug/ml (WB), 35ug/ml (IF)
β-actin	Sigma-Al. (Mouse, A5441)	1:1000 (WB)
GAPDH	SC (Rabbit, sc-25778)	1:1000 (WB)
HA	Abcam. (Mouse, ab18181)	1:1000 (WB)
Flag	Sigma-Al. (Mouse, F3165)	1:1000 (WB)
Poly_Ubi.	Invitrogen (Mouse, LF-MA0118)	0.5ug/ml (WB)
AP-3	DSHB (Mouse, anti-delta SA4)	0.5ug/ml (WB & IF)
TGN38	Sigma-Al. (Rabbit, T9826)	1:1000 (WB)1:100 (IF)
IgGK-BP HRP	SC (Mouse, sc-516102)	1:1000 (WB)
LAMP1	Abcam. (Rabbit, ab24170)	1:1000 (WB), 1:100 (IF)
LC3A/B	CST (Rabbit, #12741)	1:1000 (WB), 1:100 (IF)
Rab5A	CST (Rabbit, #2143)	1:1000 (WB), 1:100 (IF)
Chromogranin A	NOUVS (Rabbit,NB120-15160SS)	1:1000 (WB), 1:100 (IF)
Glucagon	Sigma-Al. (Mouse, G2654)	1:100 (ICC)
Goat @GP488 (Alexa Fluor) IgG	Invitrogen A11073	1:500 (IF, ICC)
Goat @mouse 488 (Alexa Fluor) IgG	Invitrogen A11001	1:500 (IF, ICC)
Goat @rabbit 594 (Alexa Fluor) IgG	Invitrogen A11032	1:500 (IF, ICC)
Goat @mouse 594 (Alexa Fluor) IgG	Invitrogen A11012	1:500 (IF, ICC)

WB = western blot, IF = immunofluorescence, ICC = immunocytochemistry

Abstract

The pancreatic β cells are not only the fundamental source of insulin production but also the predominant regulator of its storage and release upon appropriate stimuli to maintain glucose homeostasis. Insulin is stored in membrane-bounded structures called secretory granules (SGs), which are specialized secretory units of the regulated secretory pathway. Synthesized proinsulin as an inactive precursor form transports into the Golgi apparatus, where proinsulin is sorted and packaged into immature SGs. Soluble cargo proteins, membrane proteins, as well as ions are critical components for insulin production as well as insulin storage in pancreatic β cells. Type 2 diabetes (T2D) is a prevalent and complex disease that is defined by chronic hyperglycemia and insulin resistance, which are strongly correlated with dysregulated insulin production machinery in β cells. Recently, vacuolar protein sorting-associated protein 41 (VPS41) was identified as a regulator in the trafficking pathways of synthesized secretory proteins. In this thesis, I show that VPS41 plays a critical role in insulin storage capacity and insulin granule biogenesis in β cells using both an *in vitro* rat insulinoma β cell VPS41 knockout line and an *in vivo* mouse model with a conditional deletion of VPS41 in β cells. I show for the first time that deletion of VPS41 in a mouse model leads to severe diabetes associated with extensive depletion of insulin in pancreatic β cells. Together, my *in vivo* and *in vitro* data illustrate that VPS41 is a potent regulator of insulin secretory biology and is required for the maintenance of normal glucose homeostasis.

1 Chapter I: Literature Review

1.1 β cells and Insulin

1.1.1 Properties of islet cells

The *islets of Langerhans* are regions of the pancreas containing well-organized clusters of multiple endocrine cell types that produce and secrete peptide hormones to control glucose homeostasis in response to nutrient stimuli [25]. In a human islet, insulin-producing β cells and glucagon-producing α cells are the majority of the cells, accounting for 70 % and 20 % of total islet mass respectively, whereas somatostatin-producing δ cells, ghrelin-producing ε cells and pancreatic polypeptide-producing PP cells altogether make up about 10 % of total islet mass [25–27]. These hormonal endocrine cells are surrounded by well-developed fine capillary structures, suggesting that there are cellular communications between multiple hormone-producing endocrine cells ultimately to maintain blood glucose homeostasis in the body (**Figure 1-1**) [27,28]. The fine capillary network surrounding the endocrine cells has functional features to allow rapid access of insulin into the blood circulation in the body by releasing peptide hormones or growth factors [29].

Under the fasting state with plasma glucose levels around 5 mmol/L, α cell produces and releases glucagon resulting in its concentrations below 20 pmol/L, while the circulating glucagon concentration is within picomolar ranges in normal physiological conditions [1,20]. The released glucagon increases blood glucose levels *via* activation of glycogenolysis and gluconeogenesis in muscles and the liver (**Figure 1-1A**)[18,30]. Human δ cells comprise less than 10 % of the total islet cells and are distributed across the islet, secreting somatostatin in response to glucose stimulation [31]. Somatostatin inhibits the secretion of both insulin and glucagon from β cells and α cells respectively. Somatostatin also acts as a negative regulator of cell growth through inhibition of β cell proliferation [26,32].

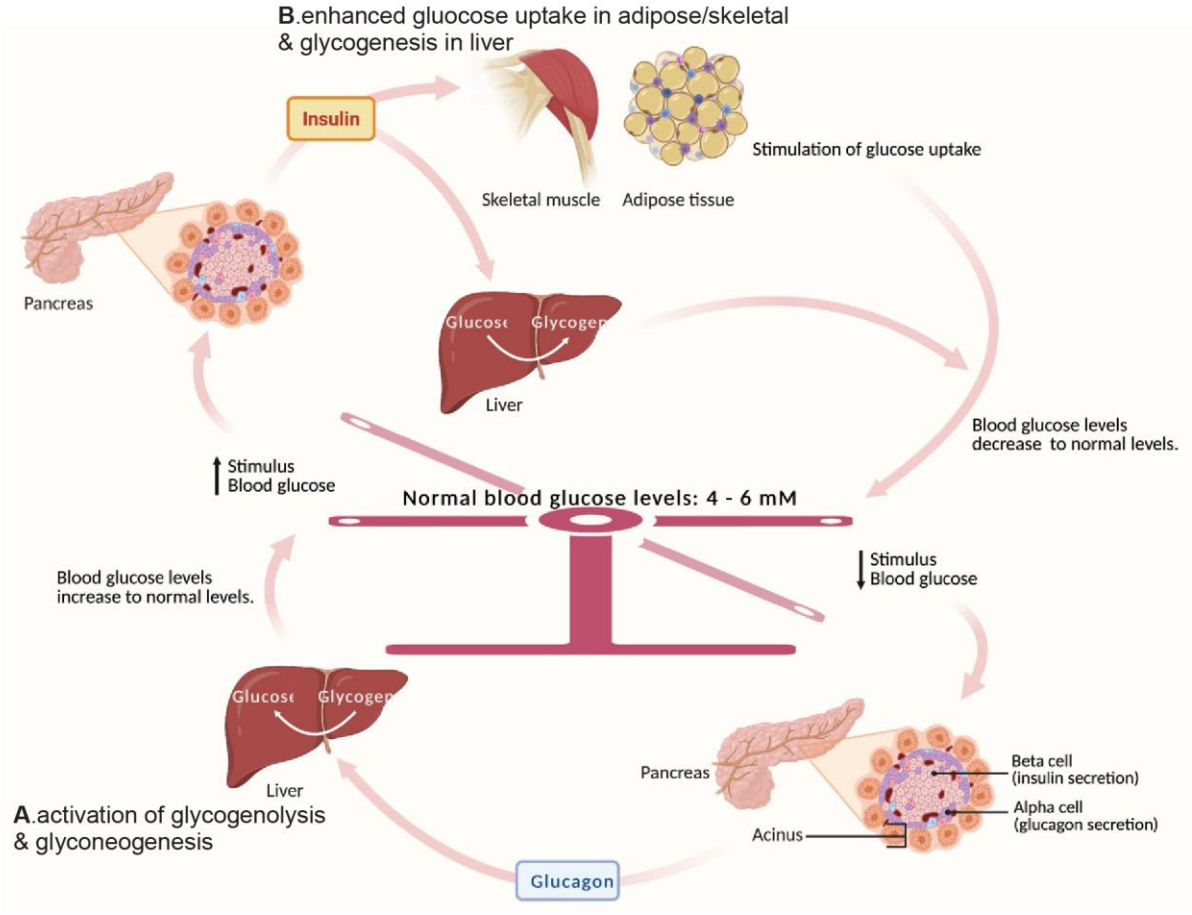

Figure 1-1 Regulation of blood glucose levels by insulin and glucagon

When blood glucose levels are low during fasting, α cells in the pancreas release glucagon to (**A**) increase blood glucose levels *via* activation of glycogenolysis and gluconeogenesis in the liver. In the fed-state, β cells in the pancreas release insulin to (**B**) enhance glucose uptake to insulin-responsive tissues such as muscles and adipose tissues as well as promote glycogenesis in the liver to maintain normal blood glucose levels [1]. *Created in BioRender.com*

1.1.2 Function of β cells

Each β cell in the islets is in contact with at least one capillary and displays polarity with secretion directed to the apical domain towards the vasculature [27,33,34]. Interestingly, recent three-dimensional analysis studies of β cells using 3D two-photon, 3D confocal and 3D block-face serial electron microscopy provide strong evidence that β cells have functional polarity with three distinct domains: **1)** apical domain adjacent to the vasculature, **2)** lateral domain between neighbour cells and **3)** basal region closed to the islet vasculature [34]. Additionally, liprin and glucose transporter type-2 (GLUT-2), known as synaptic scaffold proteins are enriched and distributed in the apical domain and lateral region respectively [27,34].

β cells function as key regulators of glucose homeostasis by coupling rapid glucose sensing, insulin synthesis and insulin secretion upon exposure to external nutrient stimuli **(Figure 1-2)** [13,35]. Excess glucose in the blood enters the β cell through GLUT-2 expressed at the plasma membrane. The increased glucose in the β cell cytosol is rapidly phosphorylated by glucokinase through glycolysis to generate pyruvate, which is the main fuel for the mitochondrial tricarboxylic acid (TCA) cycle. After transporting pyruvate into the mitochondria, the TCA cycle promotes the formation of NADH and $FADH_2$ to activate ATP synthase-dependent respiration *via* increased ATP production. The elevated ATP leads to an increase in the cytosolic ATP/ADP ratio, triggering the closure of plasma membrane ATP-dependent K^+ channels. This induces plasma membrane depolarization and enhances intracellular Ca^{2+} concentration *via* activation of voltage-gated Ca^{2+} channels at the plasma membrane, consequently promoting release and exocytosis of insulin secretory granules **(Figure 1-2)** [19,35,36].

Recent studies described the distinct features of two synaptotagmin protein isoforms such as syt7 and syt9 for insulin biphasic secretory in response to glucose stimulation [37]. Both syt7 and syt9 are known as granule membrane-associated proteins that facilitate the assembly of the SNARE complex *via* fusion between the granules and plasma membranes [37]. In biphasic insulin secretion following glucose stimulation, syt9 has high-affinity Ca^{2+} binding (41 ± 4 mM) that allows rapid release during the first-phase insulin secretion (3-5 minutes). However, due to the low affinity against Ca^{2+} of syt7, the insulin granule with syt7 is released slowly and it allows prolonged insulin release during the second phage in insulin biphasic secretory [37,38].

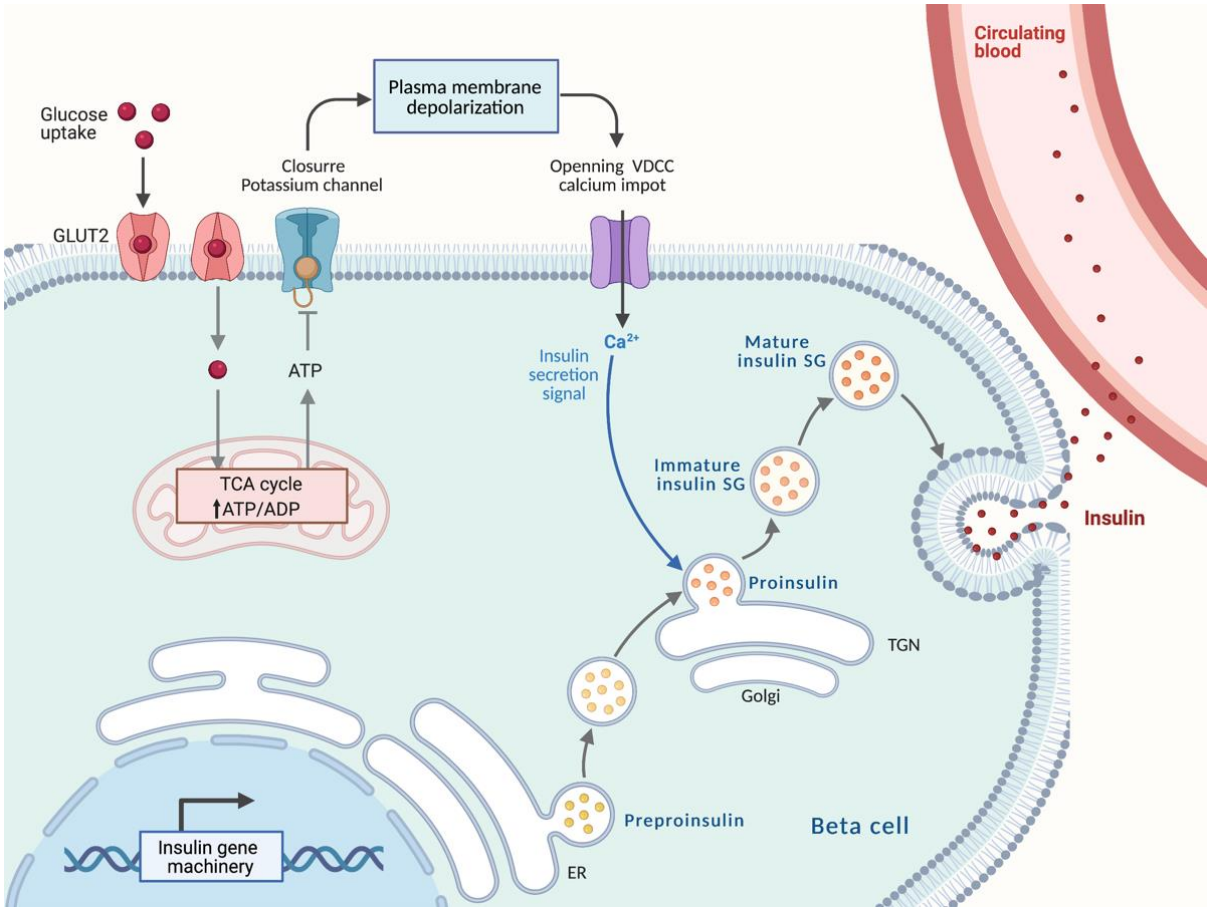

Figure 1-2 Mechanism of glucose-stimulated insulin secretion in pancreatic β cells

Glucose enters the β cells rapidly through glucose transporters and undergoes phosphorylation by glucokinase to produce ATP *via* the TCA cycle in the mitochondria. ATP is then used as fuel to promote depolarization of the plasma membrane by activating K^+ATP channels in the membrane. This promotes the opening of the voltage-gated calcium channels and the influx of extracellular Ca^{2+} and the increased Ca^{2+} acts as the signal for activated insulin secretion *via* exocytosis. *Created in BioRender.com*

1.1.3 Insulin and its action on glucose-mediated metabolism

Insulin is the most dominant anabolic hormone in biological organisms to modulate the metabolism of carbohydrates, lipids, and proteins [1–4]. Insulin gene (*Ins*) expression occurs in insulin-producing β cells through actions of key transcription factors such as *MafA, Pdx1* and *NeuroD1* [5–7]. These transcription factors as well as many components relevant to insulin secretory machinery including glucose transport and insulin processing enzymes allow β cells to maintain their identity. Insulin mRNA is initially translated as preproinsulin composed of A-chain, B-chain and C-chain (C-peptide) which contains a signal sequence, which subsequently is cleaved by activation of a signal peptidase to produce proinsulin in the rough endoplasmic reticulum (RER) **(Figure 1-3)**. In the ER lumen, the properly folded and stabilized proinsulin is linked by 3 disulfide bonds and transits to the Golgi apparatus **(Figure 1-3)**. Proinsulin is the biologically inactive form of insulin thus, sequential processing by active specific ions and enzymes contributes to the formation of the bioactive mature insulin in β cells. This active insulin is exported into the bloodstream in response to external stimuli such as glucose **(Figure 1-3)** [8–11].

Insulin is a peptide hormone composed of 51 amino acids and acts as a key player to modulate energy storage and cell survival of the organism [4,12,13]. Elevated blood glucose concentrations above 5mM stimulate the release of insulin from the pancreatic β cells which enhances peripheral glucose uptake into cells thus, up-regulates glucose-mediated metabolism especially in target tissues such as the liver, adipose tissues, and muscles to facilitate glucose metabolism (**Figure 1-1B**) [2,14,15].

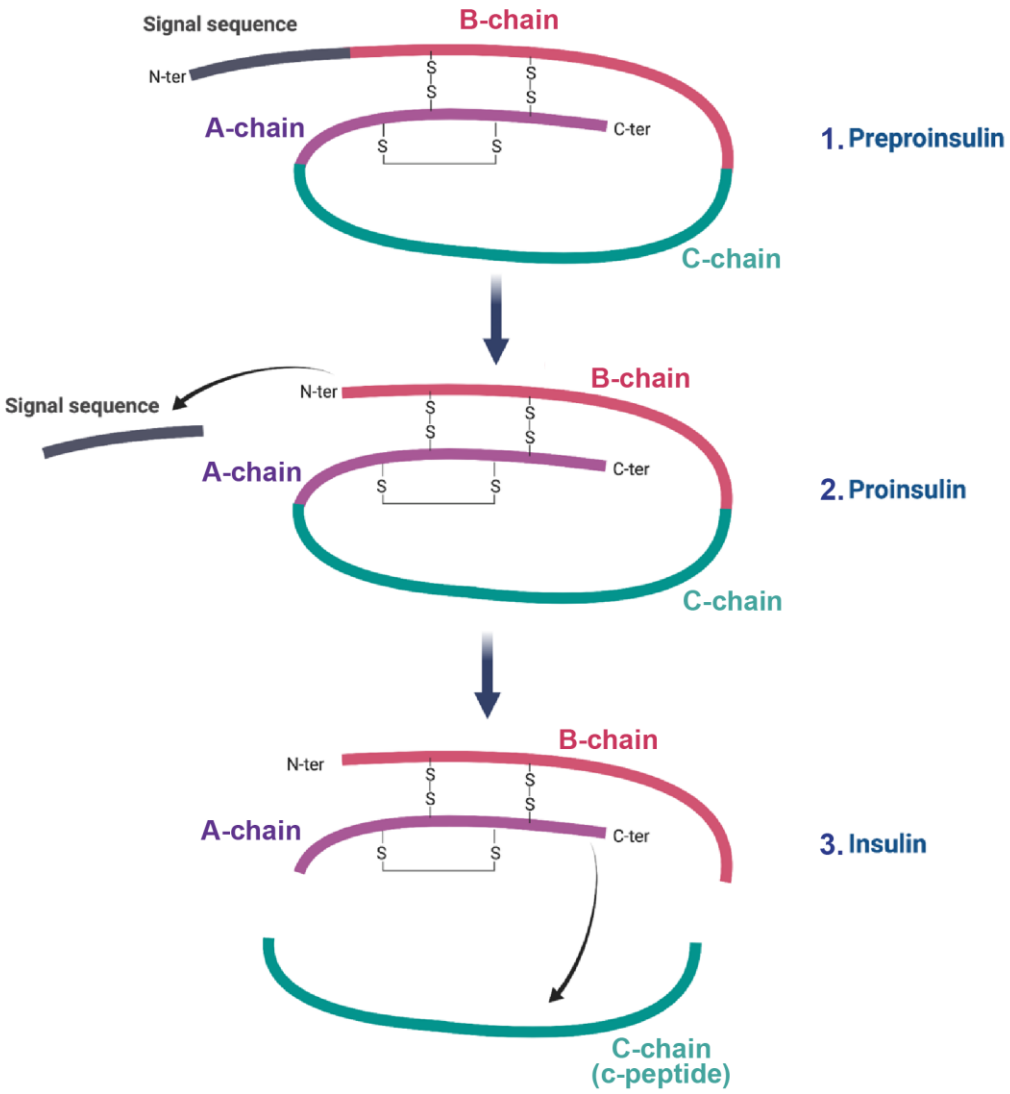

Figure 1-3 Processing of immature insulin into mature insulin

In β cells, insulin is first synthesized as a precursor molecule 1. Preproinsulin. The preproinsulin undergoes subsequential post-translational steps including cleavage of a signal sequence to produce 2. Proinsulin. Next, the folding of proinsulin and stabilization by forming three disulfide bonds between A-chain and B-chain to become the mature 3. Insulin [14,15]. *Created in BioRender.com*

Glucose transporter type-4 (GLUT-4) is the principal glucose transporter, well-known as the insulin-responsive tissues in skeletal muscles and adipose tissues. It is present within small intracellular storage vesicles known as GLUT-4 storage vesicles (GSVs) under low concentrations or the absence of insulin **(Figure 1-4)** [16]. When insulin is secreted from the β cell upon elevated circulating glucose in the blood, the insulin signaling pathway is activated *via* insulin binding to the insulin receptor **(Figure 1-4)** [16,17]. This mobilizes GSVs containing GLUT-4 to translocate to the plasma membrane, allowing glucose uptake into skeletal muscles and adipose tissues for metabolism into glycogen and ATP generation **(Figure 1-4)** [16,17]. Insulin also regulates the recycling of GLUT-4 and GSVs assembly by facilitating GLUT-4 transportation from membranes into the cytosol. Insulin activates the general receptor for 3-phosphoinositides 1 (GRP1) through AKT-mediated phosphorylation, leading to the accumulation of ADP-ribosylation factor 6 (ARF6) for GSV formation [16,17].

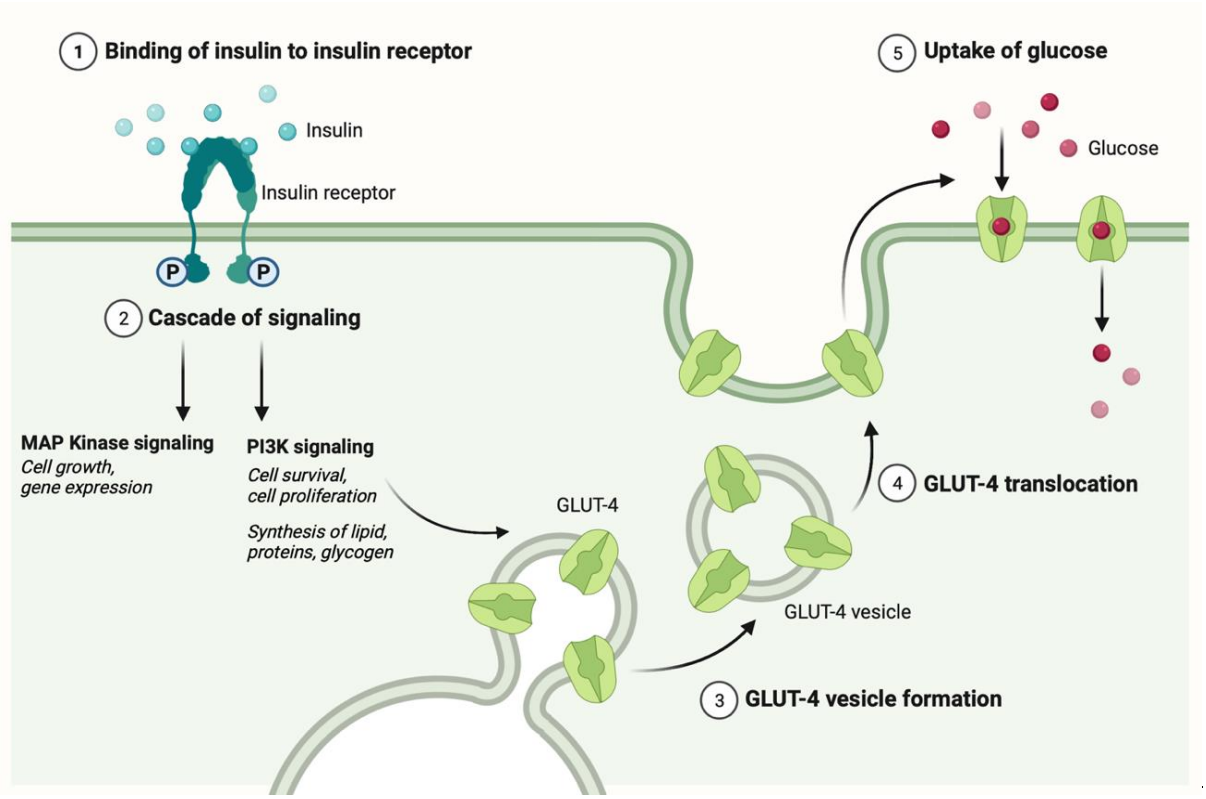

Figure 1-4 Insulin signaling pathway on peripheral tissues

After binding of insulin to the insulin receptor, the receptor is activated by phosphorylation. Activated insulin receptor triggers two major signaling pathways such as MAP kinase and PI3 kinase/AKT signaling pathways. The activated MAP kinase signaling enhances gene expression and cell growth. The activated PI3K/AKT pathway *via* subsequential phosphorylation stimulates the translocation of GLUT-4 to cellular membranes from the cytosolic vesicles, which allows glucose uptake in the cell. Besides PI3K/AKT signaling pathway facilitates glycogen synthesis *via* phosphorylation of glycogen synthase kinase 3 [16,19]. *Created in BioRender.com*

Insulin has an influence on lipid and protein metabolism for overall energy conservation during feeding and fasting states [20]. Insulin enhances additional glucose uptake in adipose tissues to facilitate fatty acid synthesis when glycogen synthesis is saturated due to a high accumulated level of glycogen in the liver (**Figure 1-1B**). Glycogen is a readily mobilizable storage form of glucose and is a very large, branched polymer molecule that can be broken down into glucose to maintain blood glucose homeostasis (**Figure 1-1A**). Indeed, glycogen is essential as the glucose source for the brain during prolonged nutrient deprivation [21]. In the liver, owing to the activation of enzymes such as glucokinase, phosphoglumutase, UDP-glucose pyrophosphorylase, pyrophosphatase, glycogenin and glycogen synthase, glycogen is synthesized as the large branched polymer form from free glucose [18,22]. Insulin inhibits adipose tissue lipolysis by inhibiting intracellular lipase activation, thus reducing fatty acid levels in the circulation [18,23]. It also regulates the rate of protein turnover by increasing protein synthesis in muscles, adipose tissues, liver and decreasing protein degradation in muscles to maintain normal plasma levels of amino acids [24]. Thus, insulin is a well-characterized anabolic hormone that stimulates the synthesis of protein and carbohydrate compounds including glycogen while preventing the degradation of these compounds in insulin-responsive tissues such as the liver, skeletal muscle, and adipose tissues.

1.1.4 Insulin secretory granule biogenesis

Pancreatic β cells exhibit the unique ability to modulate insulin production/release in response to metabolic demand including nutrient starvation or over-nutrition, which demonstrates β cells' adaptive plasticity [39–41]. Insulin biosynthesis under normal glucose conditions accounts for up to 10% of total protein synthesis in β cells [15,42,43]. This capacity can increase up to 50% upon external glucose stimulation for rapid insulin production and release to lower blood glucose [1,19,44]. In β cells, insulin biosynthesis is initiated within the cytosol when insulin mRNA is translated into the precursor, preproinsulin [45,46]. As previously described, preproinsulin is composed of the insulin A-chain, B-chain, C-chain (C-peptide), and the N-terminal signal peptide (**Figure 1-3**). Through the signal peptide, the newly synthesized preproinsulin translocates into the ER where the signal peptide is cleaved by signal peptidase and the molecule is transformed into proinsulin. In the ER lumen, proinsulin undergoes folding and forms its conserved disulfide bonds, upon which, it exits the ER for transit to the Golgi apparatus [10,14,47].

In the trans-Golgi network (TGN), proinsulin is packaged into immature SG, and many other cargo components as well as ions are required to regulate the multiple sequential steps for regulated secretory pathways **(Figure 1-5)** [48–52]. These steps include vesicle budding, sorting of cargo into vesicles (**Figure 1-5A**), trafficking, maturation and processing of immature SGs **(Figure 1-5B)** [47,53–57]. Each β cell contains approximately 5,000 - 10,000 insulin SGs but only a small portion (1 ~ 2 %) from the insulin SG pool is released in response to external stimuli (**Figure 1-5C**) [10,57,58]. The structural and dynamic properties of insulin SGs contribute to β cell function by acting as a signaling hub for insulin maturation processing [59,60]. Recently, the age of SGs has been identified as a limiting factor for SG delivery to the plasma membrane and subsequent release *via* exocytotic events [61,62]. Aged immature SGs that are not released are transported to the lysosomal for degradation through an autophagosome-dependent or -independent manner [63].

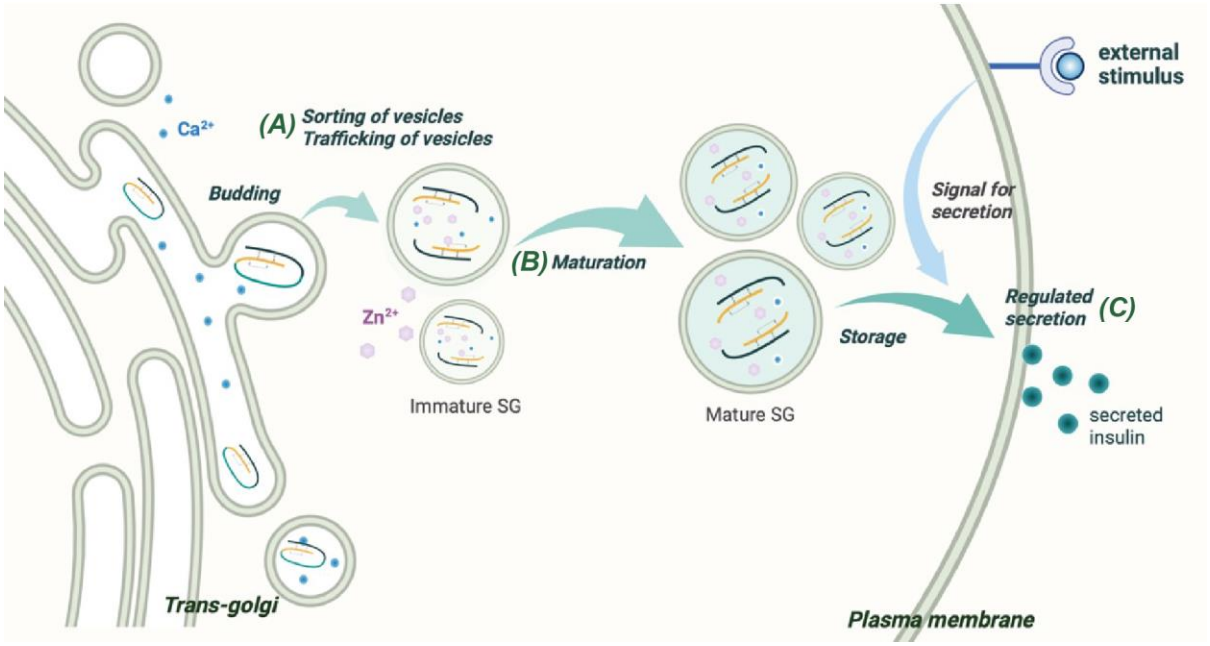

Figure 1-5 Regulated secretory pathway of the insulin secretory granules

After synthesising and folding in the ER, proinsulin is transported to the Trans-Golgi and (**A**) sorted into budding vesicles as immature in SGs. (**B**) The immature SGs undergo multiple steps including a maturation to form dense core granules then, (**C**) release upon exposure to external stimuli [58,64]. *Created in BioRender.com*

There are proposed mechanisms for protein sorting of SGs in β cells [10,53,58,65–67]. One mechanism called '*sorting-by-entry*' proposes that immature SG forms with low pH/high Ca^{2+} driven aggregation and are associated with the TGN membrane or protein-sorting receptors at the TGN lumen [65–67]. After budding from the TGN, immature SG containing proinsulin and processing enzymes are coated with clathrin, which is a key protein in vesicle formation for cellular trafficking pathways [47,68,69]. During the SG maturation process, proinsulin is cleaved by activation of three prohormone convertases PC1/3, PC2 and carboxypeptidase (CPE), converting proinsulin into mature insulin and C-peptide [42,70–72]. The insulin hexamer crystal is then stabilized with Zn^{2+} which accumulates in SGs *via* the zinc transporter, ZnT8. Mature insulin exists in a crystalized hexamer form for storage in SG vesicles [52,73,74]. The '*sorting-by-entry*' occurs at the TGN lumen requiring the interaction of TGN membrane factors and specific proteins [54]. The mechanisms known as '*sorting-by-retention*' and '*sorting-by-exit*' occur within the immature SG after budding from the TGN, and are processes designed to select or eliminate proteins [10,65,75]. Indeed, '*sorting-by-retention*' is a selection process where proteins of the regulated secretory pathway are retained within the maturing granule [10]. In contrast, '*sorting-by-exit*' is the selection of proteins to exit the regulated secretory pathway. The clathrin-coated vesicles may be involved in the transport of unwanted cargo proteins out from granules and into the endosomal pathway, which has two potential destinies either recycling for intracellular regions or subsequent protein degradation for eventual targeting to the lysosome. [76].

1.1.5 Proteins relevant to insulin secretory granule biogenesis

The insulin SG contains a wide range of proteins that coordinate their functions for insulin SG biogenesis, insulin release and glucose homeostasis [47,49,50]. Multiple proteomics studies have revealed a large number of unidentified proteins that are associated with insulin granules [11,77,78].

In addition to proinsulin, the chromogranin-secretogranin protein family including chromogranin A (CgA), chromogranin B (CgB) and VGF (nonacronymic; unrelated to VEGF) are the most abundant molecules in the secretory granule lumen [79–81]. A common feature of CgA and CgB is aggregation at a low pH (pH 5.5) and high Ca^{2+} environment, which are essential for insulin SG biogenesis [49,79,82,83]. CgB is recognized to regulate insulin SG trafficking at the early stage, which is the initial trafficking stage of nascent insulin SG from the TGN [79,83]. And this function is a similar manner to VGF in insulin SG biogenesis [79,81,83]. CgB directly interacts with VGF, whereas there is no interaction of CgA with VGF [84]. In the absence of CgB or VGF, impaired glucose-stimulated insulin release coupled with defective budding of proinsulin-containing granules at the TGN, leads to trafficking delay of newly formed insulin SG, which results in the accumulation of proinsulin-containing granules near the TGN [81,83]. Bearrows et al and Stephens et al showed these data by using a fluorescence probe-based pulse-chase procedure to track nascent proinsulin [81,83]. Hence, these studies demonstrate that CgB and VGF are required for efficient delivery and trafficking of proinsulin into the budding granules toward the plasma membrane, which impacts the capacity of insulin-containing SG for insulin exocytotic release [81,83].

Interestingly, CgA knockout mouse islets display compensatory mechanisms with the increased number of mature SGs along with higher insulin content. They also exhibited alteration of mitochondria dynamics (e.g. increased mitochondrial abundance, volume & elongation) however, the numbers of immature SG were reduced on islets from these KO mice model [85]. Thus, the depletion of CgA subsequently led to enhanced insulin exocytosis and glucose-stimulated insulin secretion *via* triggering mitochondrial ATP synthesis in CgA KO mice [85]. These data indicate that granin proteins contribute to insulin SG biogenesis as critical regulatory factors that impact cargo-mediated trafficking of SG as well as insulin storage for external stimuli-dependent insulin release.

Arfaptin-1, PICK1 (Protein interacting with C-kinase 1) and ICA69 (Islet cell autoantigen of 69kDa) are members of the Arfaptin family and additionally belong to the BAR (Bin/amphiphysin/Rvs)-domain family. Recent studies emphasize the role of BAR-domain-containing proteins and their role as intracellular transport carriers in the regulated secretory pathway [86–88]. Intracellular transport of secretory granules occurs in sequential steps at the TGN [89,90]. **1)** initially, the Golgi membrane bends to form a vesicle-structure, in which step membrane curvature and cytoskeleton rearrangement are required. **2)** Following vesicle formation, the vesicle is pinched off the membrane at the narrow vesicle neck. **3)** The cargo-containing vesicle is detached through the activated scission complex, releasing the vesicle from the TGN for delivery to the target plasma membrane [89,90]. Indeed, the BAR-domain has been shown to facilitate vesicle formation and budding by modulation of membrane curvature-sensing and membrane remodeling for example converting vesicle membranes from a flat to curved morphology [87,89]. Thus, BAR-domain containing proteins are thought to take part in vesicle neck formation at the contact of the vesicle [86,88,90,91]. In addition, BAR-domain containing family members have been reported to interact with small GTPases, which regulate actin cytoskeleton remodeling [89,90].

PICK1 is a cytosolic lipid-binding protein containing the BAR-domain [86,88,91]. Notably, PICK1 forms heteromeric complexes with ICA69, and these heteromeric complexes are present on immature insulin SG near the TGN [88]. However, only the PICK1 molecule resides in mature SGs [88]. Although the function of ICA69 is still unclear due to a scarcity of literature, the N-terminal region of ICA69 is similar to Arfaptin-1's N-terminus that interacts with ARF, a member of the Ras superfamily of small GTPase [48]. Arfaptin-1 is known to act as an important component of the vesicle scission machinery when the SG is detached from the TGN [89]. Arfaptin-1 is required for granule formation at the TGN *via* PKD1 (protein kinase D1) - mediated phosphorylation. Indeed, the phosphorylated Arfaptin-1 facilitates to generate a scission complex between membrane of granules and the TGN following release of phosphorylated Arfaptin-1 [89]. This machinery of scission complex formation *via* Arfaptin-1 regulation thus allows the detachment of granules from the TGN as transport carriers in regulated secretory pathway [89]. In Arfaptin-1 knockdown INS1 cells, despite having abundant insulin granule numbers, most of the granules are distributed throughout the cytoplasm rather than in proximity to the plasma membrane for insulin exocytosis, thus leading to impaired glucose-stimulated insulin secretion [89]. It is possible that the lack of insulin granule proximal to the plasma membranes in Arfaptin-1 knockdown INS1 cells could be explained due to the

granule scission defect at the TGN, which is necessary for functional intracellular transport in insulin SG biogenesis. Consistently, depletion of either PICK1 or ICA69, which prevents the formation of PICK1-ICA69 heteromeric protein complex leads to the loss of insulin secretion, enhanced proinsulin secretion, impaired insulin maturation, and insufficient insulin release, eventually triggering hyperglycemia and the development of diabetes [88,91]. Collectively, these findings reveal the pivotal role of BAR-domain containing proteins in the insulin secretory pathway, and as part of the bigger picture highlights the risk of impaired intracellular trafficking of insulin SG in diabetes pathogenesis.

Similarly to PICK1, High-temperature-Induced Dauer formation domain-containing protein (HID-1) is one of the novel proteins involved in the early stage for the budding reaction of secretory granules at the TGN [8,51]. Interestingly, HID-1 has a unique feature associated with TGN acidification driven by the vacuolar H^+-ATPase, which is responsible to transport H^+ into the granule lumen [8]. The H^+ influx through H^+-ATPase contributes to the intragranular acidic environment, which is required for aggregation of secretory granule proteins and cargo sorting in the regulated secretory pathway near the TGN, which is the initiating site of SG biogenesis [8,49,51]. β cell specific HID-1 knockout mice exhibit impaired insulin secretion with enhanced proinsulin secretion due to a failure to acidify immature SGs due to dysregulated H^+ influx [8]. This in turn prevents homotypic fusion of immature SGs in the maturation process [8]. Moreover, it has been reported that the blockage of homotypic fusion contributes to defected prohormone processing by disturbing SG acidification [92]. Interestingly, using an acidotropic probe to track acidificated insulin SG, less insulin co-localized with the acidotropic agent in HID-1 KO β cells compared to WT cells [8]. Like pancreatic β cells, the absence of HID-1 in neuroendocrine PC12 cells prevents the TGN acidification by abolishment of H^+ influx throughout Golgi-enriched vacuolar H^+-ATPase subunit isoform a2 [51]. It is unclear whether HID-1 interacts with H^+-ATPase subunit isoform a2 directly or indirectly through another partner [51]. Loss of H^+ influx and consequently acidification in these cells impaired the aggregation of soluble cargo proteins and SG formation, and consequently reduced numbers of effective SG in the regulated secretory pathway [51]. These data suggests that HID-1 acts as a key contributor to create a pH gradient in insulin SG lumen by interacting with H^+-ATPase that is necessary for soluble protein aggregation and SG formation in the regulated secretory pathway.

The insulin SG is transported to the cell surface for insulin release to the bloodstream, by microtubule-based movement [93]. Thus, it is not surprising that the cytoskeletal elements including microtubules and actin filaments play a fundamental roles for insulin SG trafficking and insulin secretion upon external nutrient stimuli [94–96]. Myosin 1b, of the well-known Myosin-1 subclass actin-associated sensitive motor family, functions in cell migration, membrane trafficking and vesicle transport [97]. Tokuo and colleagues have described the critical function of myosin 1b as a regulator for insulin SG trafficking from the TGN. Depleted myosin 1b *via* small interfering RNA (siRNA) in rat insulinoma β cells caused impaired glucose-stimulated insulin secretion with concomitant accumulation of SG containing proinsulin as the immature form at the TGN [97]. Interestingly, the authors observed reduced SG numbers in myosin1b depleted cells using a pulse-chase fluorescence-labeling strategy to track newly synthesized SGs [97]. These results provide evidence that myosin 1b is (at least partly) responsible for insulin secretion through regulation of insulin SG docking and fusion near the plasma membranes.

SNARE (soluble N-ethylmaleimide-sensitive factor attachment protein receptor) complexes composed of SNARE-associated proteins such as syntaxin, VAMP2 (Vesicle-Associated Membrane Protein 2) and SNAP25 (synaptosome-associated protein 25kDa) are critical factors regulating Ca^{2+}-dependent insulin exocytotic events, similar to those controlling neurotransmitter release by mediating vesicle fusion with the plasma membranes [98,99]. A recent study reported the role of SNAP23, a SNAP25 isoform that mediates insulin secretion like SNAP25 in pancreatic β cells [99]. Surprisingly, β cell specific SNAP23 KO mice had increased β cell exocytotic events as well as insulin secretion, eventually improving glucose homeostasis [99]. Consistently, SNAP23 depletion led to the increased insulin secretion upon glucose stimulation in both cultured human non-diabetic and T2D islets [99]. Similar to SNAP25, SNAP23 binds to and regulates voltage-gated calcium channels in β cells [53,99]. In contrast to SNAP25, the capacity of SNPA23 as a fusion protein to form excitosome as well as promote insulin exocytosis is low [99]. Therefore it is probable that these isoforms facilitate different rates of insulin release in β cells e.g. SNAP23 mediates slow secretion whereas SNAP25 mediates fast secretion [99]. Furthermore, reduced SNAP25 levels correspond with decreased SNAP25-mediated insulin secretion in islets isolated from T2D human donors while SNAP23 levels were not altered [99]. The authors suggest that a shift toward the slow SNAP23-mediated insulin release from the fast SNAP25-meidated insulin release occurs in islets as they progress into T2D [99]. Owing to the antagonist behavior of SNAP23 to SNAP25-mediated insulin release

in β cells, SNAP23 depletion encourages SNAP25 to bind Ca^{2+} channels faster and longer for granule fusion formation thus increasing insulin release [99].

Overall, the insulin SG together with its soluble cargo proteins and prohormone convertases undergoes restricted sequential procedures including vesicle budding, trafficking, maturation of SGs and selective removal of specific components from the granules such as the clathrin-coat and ICA69 to ensure the insulin SG is delivered to the plasma membrane for release into the bloodstream in response to external nutrient stimuli. Therefore, it is plausible that dysregulation of components associated with insulin granule biogenesis, packaging or secretion may directly or indirectly with their binding partners contribute to dysfunctional β cells and the development of T2D.

1.2 β cells in Type 2 Diabetes

1.2.1 β cell dysfunction in T2D

Obesity-related T2D is a prevalent complex disease, which is characterized by insulin resistance and insufficient insulin secretion due to β cell failure, causing chronic hyperglycaemia and impaired glucose homeostasis **(Figure 1-6)** [36,100–102]. β cell failure in obesity occurs when β cells are unable to compensate for peripheral insulin resistance[3,13,102]. Normally, increased insulin resistance leads to compensation of β cells through expansion of β cell mass, enhanced insulin biosynthesis and insulin exocytosis to fulfil the high demand for insulin [102–104]. However, in some genetically predisposed individuals, prolonged insulin resistance leads to β cell stress and impaired glucose tolerance, culminating in β cell failure **(Figure 1-6)**.

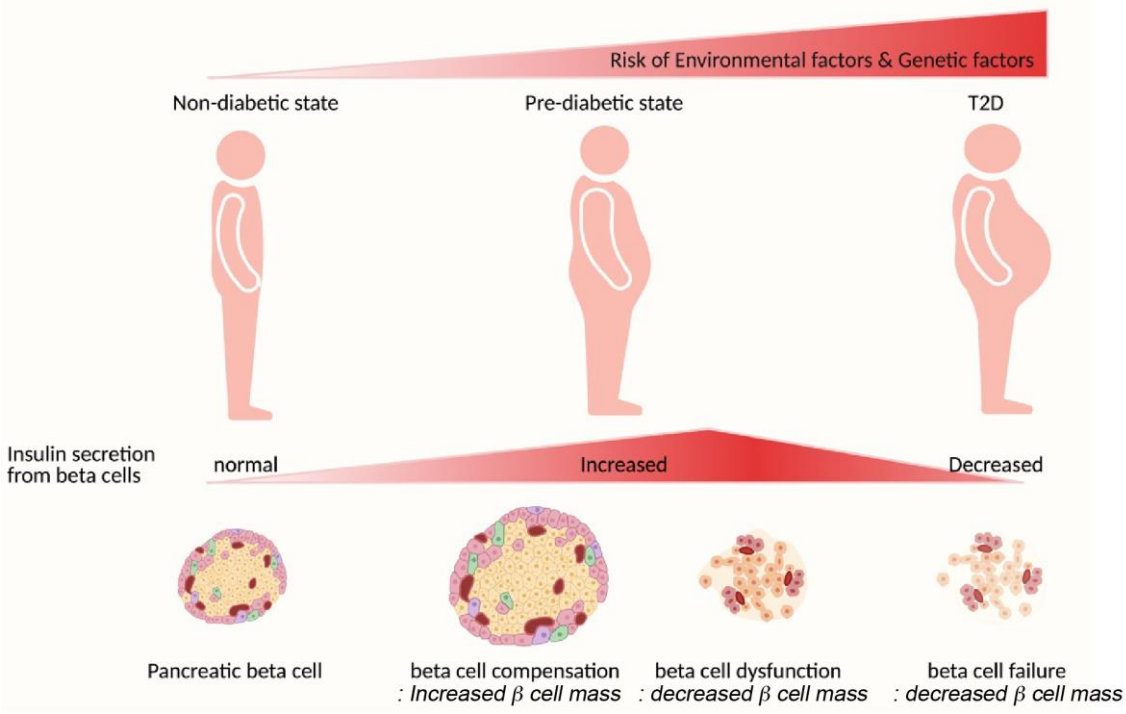

Figure 1-6 Pancreatic β cell failure and development of type 2 diabetes

Environmental risk factors such as over-nutrition and lack of physical activity as well as genetic risk factors affect insulin secretion from β cells. Initially β cell compensation occurs in response to insulin resistance; however, due to the high demand for insulin over time, β cells become dysfunctional. Consequently, β cell failure occurs and type 2 diabetes develops over time [102]. *Created in BioRender.com*

Mechanistically, β cell compensation in response to insulin resistance is reported to occur through increased β cell mass coupled with enhanced β cell function, as a result of increased nutrient supply in the circulation such as glucose/fatty acid and insulin/growth factor signaling [103,105,106]. Indeed, increased fatty acid acts as the critical stimulant for β cell mass expansion *via* enhanced glucagon-like peptide-1 (GLP-1) signaling [105,106]. In addition to its function in β cell mass expansion, GLP-1 also acts as a survival factor by regulating multiple pathways that lead to enhanced β cell proliferation [107,108]. The upregulated insulin gene expression is also required for β cell compensation and this increased insulin gene expression occurs through the regulation of signaling proteins that act as transcription factors such as Pdx1, MafA and Beta2/NeuroD [14,102].

However, the compensation process in β cells can become defective due to the combination of genetic and environmental risk factors [109,110]. Failure of β cell compensation results in dysfunctional β cells through multiple mechanisms including mitochondrial dysfunction, oxidative stress, ER stress, dysregulation of the glycerolipid /FFA (Free fatty acids) cycle and glucolipotoxicity all of which are associated with early progression of T2D [13,57,102,109,110]. Sustained hyperglycemia accelerates β cell dysfunction causing the loss of β cell mass and finally, β cell failure, which occurs in the late stages of T2D progression [102,111,112]. Normal levels of glucose and FFA are not harmful to β cells [14,113]. However, exposure to sustained elevation of hyperglycemia and hyperlipidemia in β cells facilitates changes in cellular energy metabolism *via* alteration of enzyme activities and expression of key transcription factors that regulate insulin secretion [102,103,113,114]. For instance, a combination of saturated fatty acids with high glucose has synergistic effects on apoptotic cell death in rat insulinoma β cells and human islet β cells [113]. Additionally, chronic stimulation with glucose and fatty acids facilitates increased mitochondrial membrane potential and causes excess mitochondrial-derived byproducts of oxidative phosphorylation (oxphos), reactive oxygen species (ROS) that promote the activation of uncoupling proteins [115,116]. Physiologically, β cells have high rates of oxphos to generate ATP fulfilling the increased energy demand required for stimulated insulin production and release [19,117]. Interestingly, β cells have low levels of antioxidant enzymes, which feature is necessary to clear the excess ROS [118,119]. Increased levels of ROS causes oxidative stress, which is well characterized to disturb insulin secretion [40,41,120]. Uncoupling protein 2 (UCP2), a mitochondrial inner membrane protein, has been shown to defend against accumulated oxidative stress by regulating uncoupled proton flux within the

mitochondria in β cells [116,121]. Activated UCP2 induces a significant increase of UCP2-mediated proton leak when there are elevated ROS products [121,122]. The enhanced proton leak disturbs ATP synthesis by abolishment of the proton gradient at the mitochondrial membrane and consequently prevents membrane depolarization by inactivating ATP-dependent K^+ channels and blocking of Ca^{2+} influx into the cytosol for insulin secretion [116,121,122]. This mechanism, thereby, leads to impaired insulin secretion characteristic of β cell dysfunction [116,121,122]. The glycerolipid/FFA cycle not only plays an important role in the β cell compensation process by inducing greater insulin secretion without increased glucose oxidation but also acts as a protective mechanism from damaging processes such as increased mitochondrial membrane potential and excessive ROS production [102,123]. Thus, elevated and prolonged dysregulation of the FFA cycle contributes to β cell failure in T2D [113,119,120].

A state of hyperproinsulinemia, where there is an elevated circulating proinsulin and therefore an elevated proinsulin/insulin ratio in the blood, is a key hallmark of T2D [100,124–126]. Increased proinsulin secretion is thus thought to be a consequence of β cell dysfunction [100,124,126,127]. In an obesity-linked diabetic mouse model (obese 6J $^{db/db}$ mice), there is a significant increase in proinsulin synthesis with enlargement of rough endoplasmic reticulum and Golgi apparatus, accompanying a reduction of mature secretory granules in response to the chronic hyperglycaemia [43]. In this case, in contrast to normal β cell function, newly synthesized proinsulin is not completely processed to insulin and C-peptide, leading to increased secretion of proinsulin, which results in a higher proinsulin/insulin ratio in the blood [124,126,128].

Overall, chronic hyperglycemia facilitates the excessive prolonged demand for insulin biosynthesis in the ER. It thus can lead to the accumulation of misfolded proteins as well as increased ER stress, which initiates β cell death and ultimately results in T2D [129,130]. As evidence of this, in the Akita mouse model which has a mutation of the *Ins2* gene, there is enhanced ER stress due to increased misfolded mutant proinsulin, leading to β cell death and glucose intolerance [71,131].

1.2.2 β cell de-differentiation and β cell failure in T2D

In general, T2D is characterized by dysfunctional β cells and the reduction of β cell mass in the human diabetic pancreas, which results from enhanced β cell death and decreased β cell survival [100,104,128,149,150]. However, in comparison to the marked reduction of functional β cell mass in T2D patients and in T2D rodent islets, β cell death rate is relatively low [124,151,152], suggesting that β cell death is not the main contributor to loss of β cell mass. Recent studies have proposed an alternative mechanism for the loss of β cell mass, suggesting that β cell de-differentiation might be associated with the failure of β cell function, promoting T2D progression [14,153].

During the process of β cell differentiation from embryonic stem cells to insulin-secreting mature β cells, gene expression programs including specific transcription factors and β cell identity genes are required for the generation of functional β cells **(Figure 1-7)** [152,153]. Interestingly, some rodent islet studies highlight the importance of β cell differentiation and its functional roles in response to external glucose stimulation to maintain glucose homeostasis [154,155]. Indeed, β cell-enriched genes relevant to β cell identity (e.g. *Ins1, Ins2, MafA, Glut2, Neurod1, Pdx1, Nkx6.1*), as well as metabolic genes promoting the insulin secretory pathway (including transport of ions or electron-related genes) (e.g. Kir6.2, Sur1) and insulin secretory granules processing and exocytosis-related genes (Pcsk1, Pcsk2, Snap25), are up-regulated under glucose stimulation [6,152,154–156].

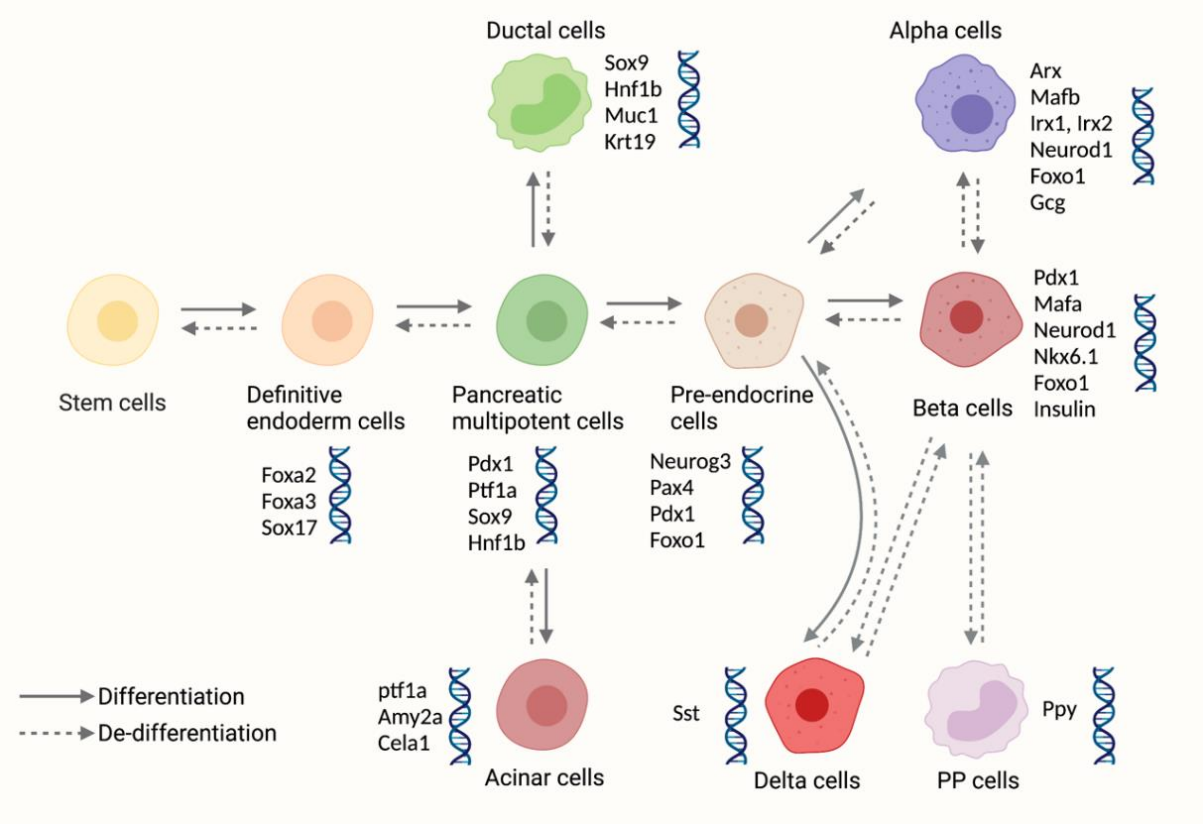

Figure 1-7 Process of pancreatic β cell differentiation from human stem cell

The process of β cell differentiation is regulated by the activation/repression of specific transcription factors that drive the transition from a stem cell to a mature β cell during embryonic development [152]. *Created in BioRender.com*

Several studies using isolated islets from human and rodent models have provided great insight into the mechanisms of β cell de-differentiation, which involves: **1)** suppressed expression of β cell-enriched genes and transcriptional factors for insulin expression **2)** enhanced expression of β cell-disallowed genes (e.g. *AldH1, HK2, LdhA, Mct1, Myc*3) [149,150,157–159]. Thus, β cell de-differentiation may be a potential adaptive mechanism against cell death under stress-induced hyperglycemia, which can contribute to restored functional β cells following re-differentiation to become mature insulin-secreting β cells once again.

1.2.3 Degradation of insulin-containing secretory granules and β cells in T2D

To ensure an adequate supply of hormones required for glucose homeostasis, endocrine cells including β cells finely regulate hormone biosynthesis, storage, secretion, and degradation. Pancreatic β cells have the essential nutrient-sensing machinery system to control glucose homeostasis under physiological conditions. In addition to this crucial feature, β cells have another key characteristic termed, 'β cell plasticity', which allows these cells to adapt to chronic glycemic changes, from starvation to overnutrition, and to produce insulin appropriately depending on the metabolic demand [40,41,132]. Generally, a tight relationship is present between autophagy and nutrient conditions and this relationship promotes functional autophagic processes, which are important for intracellular homeostasis as well as cell growth and development [41,132–135].

Autophagy is a catabolic process for lysosome-mediated protein degradation, which removes damaged cellular materials including organelles and promotes their recycling for cellular homeostasis [133,136]. Autophagy, known as 'self-eating' or 'self-consumption', acts as a fundamental regulator in energy metabolism by removing cytosolic materials destined for proteolysis [137,138]. These digested molecules can be subsequently recycled to generate ATP or essential cellular components [137–139]. Autophagy has several subtypes including macroautophagy, microautophagy, chaperone-mediated autophagy and crinophagy, which are categorized depending on how cellular materials are delivered to lysosomes for intracellular digestion [134,139,140]. The linked relationship between autophagy and nutrients as fuel to produce ATP is critical to adapt to metabolically challenged circumstances and maintain energy homeostasis [136,141]. In limited-nutrient conditions, many mammalian cells adapt by enhancing macroautophagy as a survival strategy to cope with nutrient depletion and to manage energy homeostasis [141]. However in pancreatic β cells, undernutrition suppresses macroautophagy while triggering protein kinase D regulated lysosomal degradation of insulin granules, so that starved β cells are able to adapt to a lack of nutrients and survive [63,141].

In nutrient-depleted human embryonic kidney (HEK) 293 and INS1 cells, Goginashvili and colleagues observed differential expression of microtubule-associated protein 1 light chain 3 B (LC3B), a central protein and marker in the autophagic vesicle-mediated pathway. Upon growth media starvation of HEK 293 cells, LC3B, tagged with green fluorescent protein (GFP), expression was increased, whereas this increase was not observed in INS1 cells [141].

Interestingly, there was a reduction of newly generated secretory granules containing proinsulin, proximal to the Golgi, in nutrient-depleted INS1 cells; however, this effect was partially restored after treatment with lysosomal inhibitors such as Pepstatin A or E-64 [141]. Based on this result, the authors postulated that β cells trigger the stress-induced nascent insulin granule degradation (SINGD) *via* a lysosomal-dependent pathway during prolonged starvation [141].

During the normal fed state, the newly formed insulin secretory granules transport towards release but upon nutrient-depleted circumstances, these insulin granules undergo the lysosomal degradation route to reduce unwanted insulin release [63]. Hence, SINGD, the macroautophagy-independent lysosomal degradation pathway, might be a beneficial strategy in pancreatic β cells that prevents insulin release by down-regulating autophagy and maintaining low levels of insulin secretion to overcome metabolic circumstances such as starvation [63,141,142]. However, the SINGD pathway is a potentially controversial mechanism to control insulin homeostasis in β cells as the SINGD is enhanced, *via* activation of mTORC1, in diabetic conditions, leading to the loss of insulin and β cell failure [63].

In contrast to the downregulation of autophagy observed in SINGD pathway, there are controversial observations for enhanced autophagy in INS1 cells cultured with FFA [143–146]. INS1 cells cultured with 0.4mM palmitate for 14 hours exhibit up-regulated autophagy by the formation of expanded autophagic cargo and by increasing the autophagy tracking pathway of autophagic cargo[144]. This study emphasized that enhanced autophagy is considered a protective response to restore β cell function as well as avoid β cell death during sustained insulin resistance, which can occur in compensating β cells during pre-diabetes [133,143,146]. However, treatment of INS1 cells, exposed to overnutrition conditions with the autophagy-inhibitor 3-methylademine, thus inhibiting dysregulated autophagy, led to the accumulation of ubiquitinated intracellular components including damaged organelles resulting in β cell dysfunction [120]. Additionally, studies in diabetic and non-diabetic mouse model have reported the link between altered autophagic activity and pancreatic β cell function in T2D [133,142,146]. Therefore, dysregulated autophagic function in β cells is associated with metabolic diseases such as obesity and diabetes [147,148].

Emerging evidence has highlighted the crucial role of autophagy regulation in metabolically challenged β cells at different timepoints in T2D progression. [63,134,147]. Depending on the metabolic-challenge, autophagy levels can be increased or decreased to maintain β cell function during cell stress that is associated with the development of T2D [63,147]. Mouse islet studies showed that reduced autophagy activity led to enhanced glucose intolerance with impaired insulin secretion in autophagy-deficient mutant mice that lacked β cell *Atg7* , a gene necessary for autophagic pathways [133]. The *Atg7* KO autophagy-deficient mice displayed enhanced β cell death with increased levels of cleaved caspase-3 under high-fat diet conditions [133]. The increased cleaved caspase 3 levels could account for β cell failure and even β cell loss due to dysregulated autophagy activity in *Atg7*-deficient mouse models including β cell specific *Atg7* KO mice and *Atg7* knockdown mice *via* adeno-associated virus shRNA against *Atg7* [133,146]. Also, the accumulation of autophagic vacuoles and autophagosome with enhanced cell death has been observed in islets isolated from T2D patients [147].

1.3 Vacuolar protein sorting – associated protein 41

As described in Section 1.1.4, insulin is packaged and released as concentrated secretory granules, which are the membrane-bounded components on regulated secretory pathways. Like pancreatic β cells, exocrine, neuroendocrine, and neuronal cells are also well-known as professional secretory cells in regulated secretory processes [65,160,161]. In these cells, most of the similar proteins and molecules described in section 1.1.5 are involved in the release of synthesized proteins in response to external stimuli, especially in neuroendocrine cells and β cells [81,162]. Additionally, for exocytosis of synthesized neuropeptides or hormones (e.g., insulin), similar processes including the formation of secretory granules, sorting from the TGN and intracellular transport to the destination of their targeting occur on neuroendocrine cells or β cells, respectively [65,92,163]. A recent study of secretory granules on mouse neuroendocrine PC12 cells suggests that a cytosolic component named vacuolar protein sorting-associated protein 41 (VPS41) involved in the intracellular transports of membrane-bounded vesicles is a critical factor in regulated secretory processes [164,165]. However, the exact mechanism of VPS41 on β cells is not fully understood. Thus, that led to the question of whether the VPS41 could affect regulated insulin secretory pathways on β cells such as insulin release upon external stimuli, the capacity of insulin storage, and subsequently regulation of glucose homeostasis. It should be noted that the results on the βVPS41 KO mouse model presented in the current thesis are novel and first *in vivo* results, which address the function of a vacuolar protein sorting-associated protein 41 on β cells.

VPS41 is known as a cytosolic component of the HOPS (homotypic fusion and protein sorting) complex [166–169]. The HOPS complex is known as an intracellular mediator for membrane fusion at endosomes, vacuoles and lysosomes in the endo-lysosomal pathway [169,170]. In addition to the HOPS complex, the CORVET (class C-core vacuole/endosome tethering) complex plays a similar role in the endo-lysosomal pathway [171,172] (**Figure 1-8**). HOPS and CORVET complexes have similar structures, and they share the same subunits such as class C proteins including VPS11, VPS16, VPS18 and VPS33. However, they function at different stages in endo-lysosomal pathways *via* interaction with two different small Rab GTPases, Rab5 and Rab7 [166,171–173] (**Figure 1-8**). Except for four class C proteins within HOPS and CORVET, the specific subunits including VPS3, VPS8, VPS39 and VPS41 are compartments of HOPS or CORVET complexes, thereby these specific subunits allow interactions with Rab GTPases

through their specific Rab-GTP binding sites [173]. Indeed, HOPS has two Rab7-binding subunits, VPS39 and VPS41, instead, CORVET has VPS3 and VPS8 as Rab5-binding subunits [167,171,174] **(Figure 1-8)**.

Within specific subunits of the HOPS complex, Rab-GTP binding sites enable HOPS to bind with late endosomes or MVB (multivesicular bodies), *via* Rab7 membrane-tethering; therefore, VPS41 as the subunit of the HOPS complex acts as a regulator for cargo trafficking in the endosomal pathway as well as autophagosome-lysosome pathway **(Figure 1-8)** [166,175,176]. Furthermore, VPS41, as a component of HOPS, has a critical role in regulating the endocytic pathway, thus the depletion of VPS41 causes defective HOPS-dependent trafficking of endocytic cargo to the lysosomes [168,173,177,178].

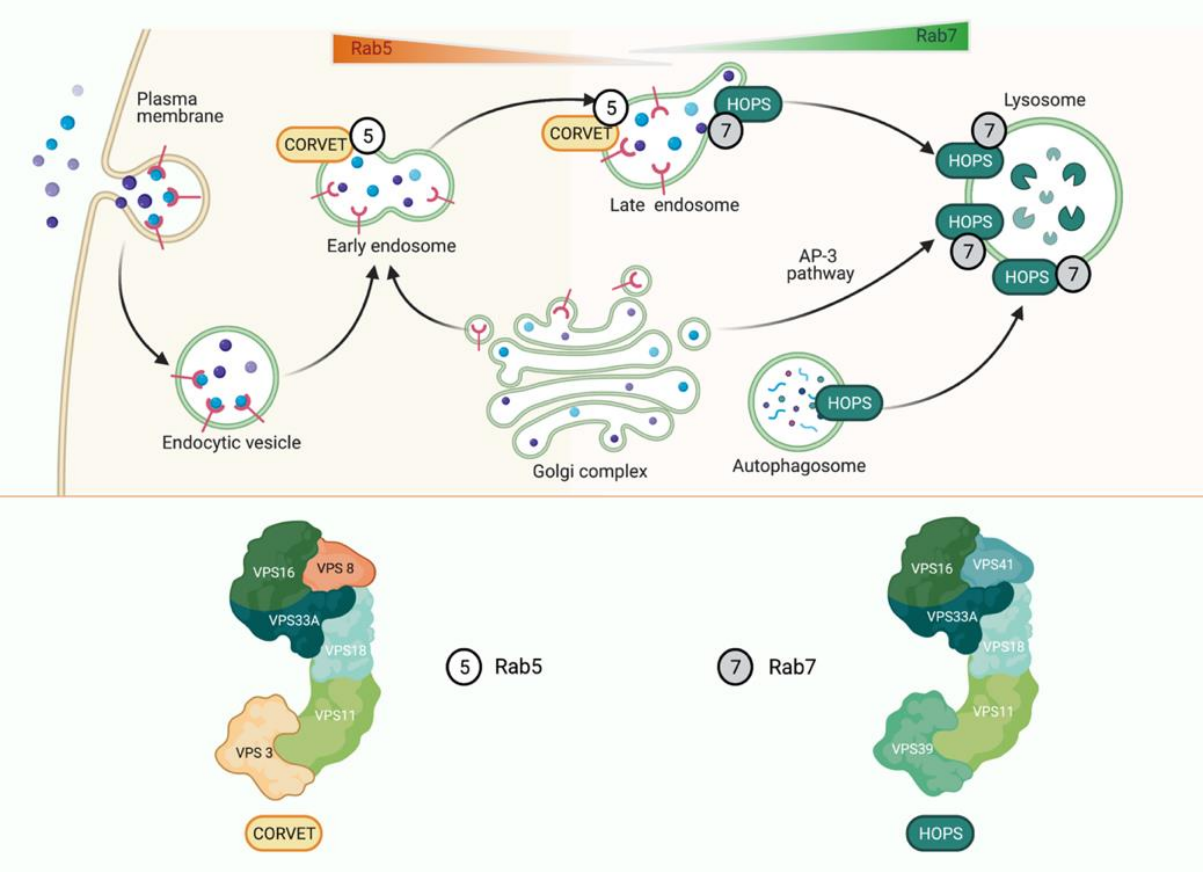

Figure 1-8 Function of CORVET and HOPS complex in endo-lysosomal pathways

In the early endosome pathway, CORVET interacts with the small GTPase Rab5 for endosome-endosome fusion. At the late endosome pathway, HOPS promotes vesicle fusion by interaction with Rab7. HOPS is also responsible for the fusion of autophagosomes with lysosomes. Additionally, Golgi-derived adaptor protein 3 (AP-3) mediates vesicle transport directly to the lysosomes in a HOPS-dependent manner [171]. *Created in BioRender.com*

Rab7 has multiple effectors such as RILP (Rab-interacting lysosomal protein) and WDR91 (WD repeat-containing protein 91) that have important roles in Rab7-dependent endo-lysosomal pathways [178,179]. Lysosome-mediated pathways are critical mechanisms to ensure the appropriate removal of aggregated proteins and damaged/aged organelles [134]. Lin and colleagues described the interaction of VPS41 with the N-terminus of RILP, a downstream effector protein of Rab7, by recruiting the dynein-dynactin motor to Rab7-containing late endosomes [178]. Indeed, RILP interacts with HOPS via the C-terminus of VPS41 [178]. RILP enables the recruitment of HOPS subunits except for VPS33 to the vesicular membranes, unlike Rab7 [178]. This mechanism allows RILP to act as a late endosomal integrator by interacting with Rab7 and the C-terminus of VPS41 to coordinate the activity of Rab7-HOPS and stabilize the complex, eventually facilitating membrane fusion to late endosomal membranes [175,178].

Moreover, Rab7 and RILP are involved in epidermal growth factor receptor (EGFR) endocytosis by regulating multiple post-translational modifications including tyrosine and serine/threonine phosphorylation, ubiquitylation and acetylation [178,180,181]. In general, VPS41, as a component of the HOPS, has a major role in regulating vacuolar fusion events between lysosomes with late endosomes and autophagosomes [166,168].

VPS41 has also been reported to mediate fusion of AP-3 (adaptor protein-3)-coated vesicles and transport of these vesicles from the TGN to the lysosome directly [182–186]. Then, how does VPS41 regulate AP-3 mediated vesicles fusion and transport in AP-3 mediated pathway? In yeast, there are two types of vesicle-mediated transport, the carboxypeptidase Y (CPY) pathway and the alkaline phosphatase (ALP) pathway, as the major and the bypass route, respectively [182,183]. In the ALP pathway, VPS41 is required to form AP-3-coated vesicles for the selective trafficking of proteins between organelles in secretory systems. Within the domain of VPS41 (**Figure 1-9**), the N-terminus WD40 region enables binding with Apl5, a subunit of AP-3 or highly curved-membranes *via* its amphipathic lipid-packing sensor (ALPS) motif (Angers & Merz, 2009; Cabrera et al., 2010).

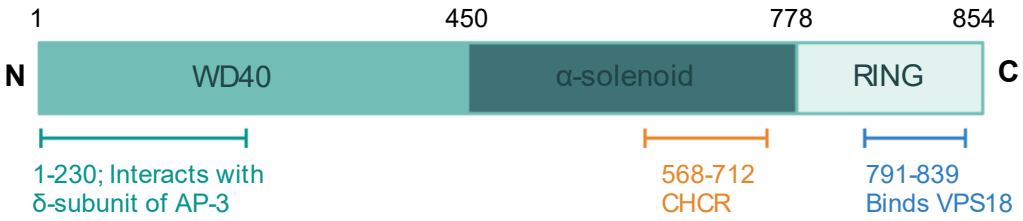

Figure 1-9 Domain of VPS41 protein

VPS41 contains specific regions relevant to its binding/interacting with different components such as adaptor protein-3 or VPS18. *Created with BioRender.com*

Interestingly, the ALPS motif functions as a sensor for binding to curved membranes and contains the vacuolar casein kinase yck3 phosphorylation site [187,188]. Cabrera and colleagues described that yck3-mediated phosphorylation of the VPS41 ALPS motif is responsible for determining the fate between different transport pathways for vacuole fusion [187]. When the ALPS motif of VPS41 recognizes highly curved endosome membranes, the amphipathic helix structure of the ALPS motif inserts into the hydrophobic lipid bilayer

between roughly packed lipids on late endosomes [187]. Consequently, it leads to the embedded binding site of Apl5, a subunit of AP-3 by interrupting the binding between AP-3 and VPS41 [184,187]. At less curved vacuole membranes, the VPS41-ALPS motif allows binding to AP-3 vesicles through the exposed binding site of Apl5, of VPS41, by yck3–mediated phosphorylation, indicating that yck3-activated VPS41 phosphorylation is required for the AP-3 mediated vesicle fusion pathway from the TGN [187]. Inhibition of VPS41 phosphorylation prevents AP-3 mediated vesicle fusion and causes the accumulation of VPS41 at the endosomes [187].

Pols and colleagues suggested that VPS41 is responsible for transporting lysosomal membrane proteins from the TGN to lysosomes as the independent role of HOPS. [189]. Using the lysosome membrane marker, lysosome-associated membrane protein (LAMP1), and TGN membrane marker such as TGN38 or TGN46, they performed immuno-electron microscopy and identified that VPS41 distributes in the membranes of late endosomes and lysosomes on β cells [189]. Furthermore, immuno-EM images in live cells confirmed that newly synthesized LAMP1 vesicles exit the Golgi/TGN and late endosome areas, providing evidence for the direct transport of LAMP from the TGN to late endosomes [189]. Surprisingly, VPS41 depletion leads to dysregulation in the LAMP transport pathway from the TGN to late endosome that results in the accumulation of LAMP cargo vesicles; whereas, knockdown of the VPS39 subunit, or one of class-C core subunits, VPS18, did not [189] . Therefore, VPS41, as part of the HOPS complex, is required for vesicle-mediated movement towards lysosomes, which is a HOPS-dependent function.

However, there is now emerging evidence suggesting a HOPS-independent role for VPS41 in the regulated secretory pathway [164,190,191]. VPS41 has recently been identified as a novel protein modulating movement of secretory granules in regulated secretory pathways [164,190,191]. Asensio and colleagues described VPS41 as influencing the regulated secretion of peptide hormones and neuropeptides in neuroendocrine cells independently of the HOPS complex (**Figure 1-10**) (Asensio et al., 2013). VPS41 knockdown lead to impaired regulated secretion of peptide hormones such as atrial natriuretic factor (ANF) in mammalian neuroendocrine cells [164]. In contrast, knockdown of other C-core subunits, VPS11 and VPS18, and another specific subunit, VPS39, showed no effect [168,190], thus supporting the evidence that VPS41 has a specific HOPS-independent function in regulated secretory pathways (Asensio et al., 2013).

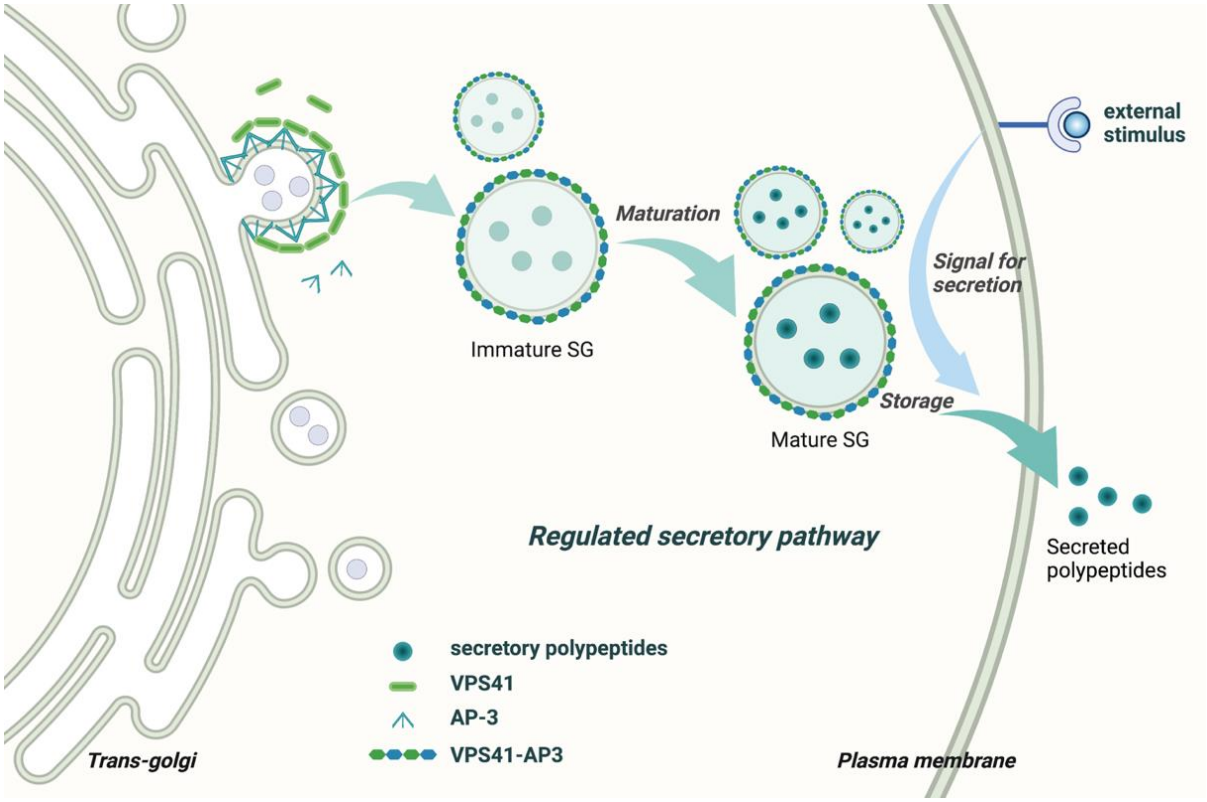

Figure 1-10 VPS41 interaction with AP-3 in regulated secretory pathway

In regulated secretory cells such as neuroendocrine cells, VPS41, independent of HOPS, is required for polypeptide secretion by forming secretory granules via interaction with AP-3 directly at the TGN. *Created in BioRender.com*

VPS41 can form a lattice structure, which allows it to act as a coat protein by interacting with AP-3 complex on secretory granules (**Figure 1-10**) [164]. As described above, AP-3 is known to be involved in vesicle trafficking from endosomes and the TGN [164,192]. Indeed, AP-3 is located mainly in endosomes and it has been thought to function in the lysosomal targeting pathway by the formation of lysosome-related organelles and transport hydrolases [192–194]. However, AP-3 existing Golgi complex enables an alternative pathway from the TGN by the formation of regulated secretory vesicles [164]. In neuroendocrine PC12 cells, AP-3 knockdown with AP-3 α subunit siRNA leads to the dysregulated secretory pathway of SgII (secretogranin II), which is a chromogranin family member of neuroendocrine secretory proteins [192]. Dysregulation of the SgII pathways was due to a defect in the membrane composition of secretory vesicles and changed membrane properties at the TGN [192].

In particular, loss of AP-3 altered the distribution of synaptotagmin I, a major Ca^{2+} sensor for regulated exocytosis toward lighter fractions rather than those containing secretory vesicle cargo, thus causing defective regulated secretion [192]. Notably, PC12 cells lacking AP-3 exhibited rapid release of SgII after budding from the TGN compared to control cells [192]. Hence, this study supports the alternative role of AP-3 in secretory vesicle sorting within the TGN rather than the lysosomal targeting pathway [192]. Consistent with the impaired regulated release of neuropeptides, mutant mice lacking AP-3 have shown dysregulated release of peptide hormones, e.g. increased basal release of both glucagon and insulin from pancreatic islet cells [195]. Hence, the compiling evidence suggests AP-3 interaction with VPS41 contributes to VPS41 function as a key mediator in the regulated secretory pathway.

Recently it has been reported that patients diagnosed with a complex neurological disorder with ataxia and dystonia have heterozygous variants (S285P and R662*) in *VPS41* [190]. These two VPS41 variants are **1)** $VPS41^{S285P}$: a missense variant in the WD domain (**Figure 1-9**), and **2)** $VPS41^{R662*}$: a nonsense variant in the CHCR (Clathrin heavy chain repeat, **Figure 1-9**) domain resulting in a premature stop-codon [190]. The CHCR domain of VPS41 is considered the binding region to VPS18, that leads to the formation of HOPS complex (**Figure 1-9**). In isolated patient fibroblasts, Reini and colleagues showed that all VPS41 variants failed to form the functional HOPS complex [190]. Thus, this loss of functional HOPS due to VPS41 variants leads to dysregulated vesicle trafficking such as defective HOPS-dependent late endosome-lysosome fusion [190]. Additionally, $VPS41^{R662*}$ transfection did not rescue the dysregulated endocytic events of VPS41 KO HeLa cells that results from the failure of HOPS complex formation [190]. Transfection of HeLa VPS41 KO cells with $VPS41^{S285P}$ also failed to restore HOPS function, even though $VPS41^{S285P}$ can bind to other HOPS components and enables HOPS complex formation [190]. It is possible that $VPS41^{S285P}$ mutation does not allow for the formation of the functional HOPS complex due to the serine to proline switch causing protein misfolding [190]. Notably, the authors emphasized that the $VPS41^{S285P}$ variant retains the VPS41 HOPS-independent role for normal regulated secretion in response to stimuli while displaying the dysregulated HOPS-dependent endocytosis and autophagy pathways (VPS41 KO PC12 cells expressing $VPS41^{S285P}$) [190]. Therefore, the S285P variant in *VPS41* could be used to distinguish between HOPS-dependent and HOPS-independent function.

Recent evidence suggests the importance of VPS41 function in regulated secretory pathways. Some VPS41 variants associated with T2D such as T294M and R843H have been also reported in human GWAS by T2D exome sequence analysis [196,197]. Moreover, *VPS41* gene expression analysis has shown a significant reduction of mRNA level in the BTBR mouse strain, a diabetes-susceptible model compared to the B6 diabetes-resistant model [198]. However, the mechanism of VPS41 in how to regulate the insulin regulatory pathway on β cells has been unrevealed.

1.3.1 Aims

This thesis investigates the role of VPS41 as a key component for insulin SG biogenesis that contributes to the regulation of glucose homeostasis and insulin storage capacity in insulin-secreting/producing β cells using *in vitro* and *in vivo* model. Thereby, the aims of the present thesis were to identify fundamental roles of VPS41 relevant to insulin machinery under chronical deleted (**Chapter II**) and acute deleted (**Chapter III**) circumstances in rat insulinoma β cells, and to characterize the functional consequence of β cell specific deletion of VPS41 on glucose homeostasis in mice (**Chapter IV**).

2 Chapter II: Effect of Chronic VPS41 Deletion on INS1 Cells

2.1 Introduction

Insulin is produced by pancreatic β cells and is stored within the insulin secretory granules (SGs) [4,47]. Many molecules including membrane and soluble proteins, and ions, are located within the insulin SGs and are a part of the secretory machinery required for insulin release [10,47,199]. Insulin SGs form from the TGN through vesicle budding as immature SGs [66]. This immature SG subsequently undergoes multiple steps to become a mature SG. Hence, insulin SG biogenesis, involving many regulators, is a critical component of the insulin secretory pathway [57,199,200]. However, the mechanism detailing the specific functions of the molecular components regulating insulin SG biogenesis remains poorly understood.

VPS41 is well-defined as a subunit of the homotypic fusion and vacuole protein sorting (HOPS) complex and characterized as a coordinator in the tethering/fusion of TGN-derived vesicles with the vacuole/lysosome [166,169,174]. In addition to HOPS-dependent function as part of that complex, VPS41 has been recently identified as a regulator in trafficking pathways of synthesized proteins by the formation of coat-structures relevant to regulated secretory pathways of small molecules [164]. Asensio firstly demonstrated that VPS41 and its interacting protein, adaptor protein-3 (AP-3) complex are required for the biogenesis of SGs as cytosolic components in neuroendocrine PC12 cells and neurons [164]. The lack of VPS41 thus led to defects of neuroendocrine secretion in PC12 cells [164,190]. Like neuroendocrine PC12 cells, pancreatic β cells also possess the regulated secretory machinery including the biosynthesis, storage, and release of secretory protein hormones such as insulin [55,201]. Besides, GWAS of VPS41 in human and rodent models revealed that *VPS41* gene expression is relevant to the risk of T2D development [196–198]. For example, mRNA levels of VPS41 in islets are lower in the diabetes susceptible BTBR mice, compared to the diabetes-resistant C57BL/6J mice [198]. Together these findings suggest that VPS41 plays a central role in the insulin SGs biogenesis as a coat protein together with AP-3 complex on pancreatic β cells. However, it is not fully understood if VPS41 is essential for the formation of insulin SGs, insulin release as well as insulin storage within the SGs on pancreatic β cells.

The aim of my thesis is to investigate the potential role of VPS41 on insulin SG biogenies. In this chapter, I investigated the role of chronic deletion of VPS41 on β cell function. Specifically, I compared insulin secretion, insulin content and total proteomic composition of VPS41 KO and WT INS1 cells.

2.2 Materials and Methods

2.2.1 Cell culture

The rat insulinoma cell line, INS1 cells were cultured at 37°C and 5% CO_2 conditions in RPMI 1640 Medium (Gibco™, #11875093) containing 11mM glucose, 2.05mM L-Glutamine, 10% Fetal Bovine Serum (Gibco™, #10099-141), 10mM HEPES (Thermo Scientific, #7365-45-9), 1mM Sodium Pyruvate (Sigma-Aldrich, #P5280), 0.05mM 2-β-mercaptoethanol (Sigma-Aldrich, #M6250) and 1% penicillin-streptomycin (Gibco™, #15070063). VPS41 KO and HA-VPS41 rescue INS1 including WT cells were kindly provided by Associate Professor Cedric S. Asensio (University of Denver, USA). All cell lines were regularly tested for mycoplasma contamination.

2.2.2 Western blotting

INS1 cells were lysed in RIPA buffer containing the protease inhibitor cocktail (Roche, #11697498001). Protein lysates (25µg) were loaded onto 10% SDS-PAGE and proteins were transferred onto PVDF membrane at 100 V for 1 hour (Bio-Rad, #1620177) then, the membranes were blocked with 5% Skim Milk in TBS-T (TBS, 50mM Tris-HCl at pH 7.4, 150mM NaCl + 0.1% Tween 20). Membranes were then incubated with primary antibodies overnight at 4°C (**List of antibodies**) and the following day after washing with TBS-T, the membranes were incubated with appropriate secondary antibodies for 1 hr at room temperature. The chemiluminescence was detected using Immobilon Western HRP Substrates (Merck, #WBKLS0500) and the ChemiDoc™MP Imaging System (Bio-rad) was used for imaging membranes. Densitometry was performed using ImageJ software and protein levels normalized to appropriate housekeeping protein, β-actin as a loading control.

Insulin protein expression, from INS1 cell lysates, was detected and quantified following a modified Western blotting assay [202] . Briefly, INS1 cells were lysed in SDS lysis buffer (75 mM Tris-HCl at pH 6.8, 1% SDS, 10% glycerol, 2.5% sucrose), boiled at 95°C for 5 minutes and sonicated with 90% of power, 3 seconds on and off for 24 seconds. Protein concentrations were determined using BCA protein assay (ThermoFisher Scientific, #23225) according to the manufacturer's instructions. Loading volumes were standardized by the addition of SDS lysis buffer and 4X sample buffer (277.8mM Tris-HCl pH6.8, 44.4% glycerol, 4.4% LDS, 0.02% bromophenol blue, Bio-Rad, #1610747). These mixtures were then boiled

at 95°C for 5 minutes. Proinsulin and insulin were analysed using SDS-PAGE under non-reducing conditions (as described below) to preserve the intermolecular disulfide bonds of insulin.

Proteins (25µg) were separated on a 4-12% gradient gel (Invitrogen™, #NW04120) at 100V for 1 hour with MES-SDS (Invitrogen™, #NP0002) running buffer (50mM MES, 50mM Tris Base, 0.1% SDS, pH7.3). After gel-electrophoresis, the separated proteins on the gel were transferred to PVDF membrane using a modified transfer buffer (25mM Tris-HCl at pH 8.3, 192mM Glycine, 0.05% SDS, 20% methanol). Between transfer and primary antibody incubation, the Okita et al method described extra steps to optimize insulin detection, which are as follows [202]. After transfer, membranes were soaked with a pre-blocking buffer (1% skim milk, 0.1% BSA in PBS-T (PBS, 10mM Na_2HPO_4, 1.8mM KH_2PO_4, 137mM NaCl, 2.7mM KCl at pH 7.4 + 0.1% Tween 20) for 5 minutes, briefly washing with PBS-T, and incubated in 0.2% GA (glutaraldehyde, Sigma-Aldrich., #G5882) in PBS-T (PBS + 0.1% Tween 20) for 15 minutes. Following these additional steps, membranes were washed three times with PBS-T, incubated in standard blocking buffer (5% skim milk in TBS-T, TBS + 0.1% Tween 20) for 30 minutes, and incubated with the anti-insulin (Santa Cruz, #SC-8033) and anti-proinsulin (Hybridoma Bank, #GS-9A8) as the primary antibodies, respectively overnight at 4°C. The following day, membranes were probed with the appropriate secondary antibody (@Mouse IgGK BP-HRP, Santa Cruz, #SC-516102) and chemiluminescence was detected using Immobilon Western HRP Substrates (Merck, #WBKLS0500).

2.2.3 Immunofluorescence assay

1.5 X 10^5 INS1 cells/well were seeded on coverslips in a 6-well plate and incubated at 37°C and 5% CO_2 overnight to attach on coverslips. Then, cells were washed with PBS and fixed with 4% PFA (Electron Microscopy Sciences, #15710) for 20 minutes at room temperature. After washing with PBS 3 times, cells were permeabilized with 0.1% SDS for 5 minutes at room temperature. The fixed and permeabilized cells were further washed with PBS and 3x with ICC buffer (0.1% BSA, 0.01% Sodium Azide in PBS), and non-specific proteins were then blocked with blocking buffer (Dako Protein serum-free Ready-to-use, #X0909) for 1 hour at room temperature. The coverslips were then incubated with appropriate primary antibodies (**List of antibodies**) at 4°C overnight. Upon additional washing with ICC buffer, the cells were incubated with Fluor-conjugated secondary antibodies (**List of antibodies**, 1:500

in diluent buffer, Dako Antibody Dilunet, #S0809) for 1 hour at room temperature under dark conditions. The coverslips were mounted with ProLong™ Diamond Antifade Mountant with DAPI (Invitrogen™, #P36962). All fluorescence images on slides were captured on a confocal microscope (Leica, SP8 confocal).

2.2.4 Glucose-stimulated insulin secretion assay

After cell counting by using a hemocytometer with trypan blue stained INS1 cell suspension, cells were seeded at 2 X 10^5 cells per each well in a 6-well and incubated with the complete media containing 2.8mM glucose 24 hours prior then, stimulated Krebs buffer (10mM HEPES, 0.1% fatty-acid free BSA, pH 7.4) supplemented with 2.8mM glucose 1 hour prior and maintained with 5% CO_2 at 37°C. Cells were stimulated in 1mL Krebs buffer supplemented with stimulatory condition (16.7mM glucose) or basal glucose (2.8mM) in Krebs buffer for 1 hour. The secreted insulin, total cellular insulin content and DNA content were analyzed using HTRF assay (Cisbio, #62IN2PEH) and DNA picoGreen assay (Invitrogen™, #P11495) respectively.

For insulin measurements such as insulin secretion and insulin content, the supernatant was collected from each well then, cells were collected in lysis buffer (100mM Tris, 300mM NaCl, 10mM NaF, 2mM Na_3VO_4 and protease inhibitor). HTRF was used serial standard solutions of insulin for a nine-point standard curve with concentrations: 0, 0.078, 0.156, 0.312, 0.625, 1.25, 2.5, 5 and 10 ng/ml. Supernatant and lysates were diluted with Milli-Q water at 1:5 for the supernatant and 1:500 for the lysates, respectively. 10 µl of standard or samples were loaded into a 384-well plate (Corning, #3824BC) then, 10 µl of Cryptate antibody and XL655 antibody mixture was added per a well directly. After incubation at room temp for 5 hours, the plate was read using Magellan software on Microplate Reader (Infinite F200 PRO, Tecan) with two fluorescent reading methods, 620 nm and 665 nm.

DNA content from cell lysates was measured using a Quant-iT™ PicoGreen™ dsDNS assay kit (Invitrogen™, #P11495) according to the manufacturer's instructions. The DNA assay used a nine-point standard curve with concentrations: 0, 0.039, 0.078, 0.156, 0.312, 0.625, 1.25, 2.5 and 5.0 ng/ml. 20 µl of diluted cell lysates in Milli-Q water as 1:200 was loaded into a 96-well plate (Greiner Bio-One, #655209) with standard solutions. Then, 100 µl of 1X PicoGreen in 1X TE buffer (Life Technologies, #P11496, 200mM Tris-HCl, 20mM EDTA, pH7.5) was added into each well-containing sample or standard solutions directly and

incubated in the dark at room temp for 5 minutes before reading at 485 nm excitation and 535 nm emission on a FLUOstar Omega Microplate Reader (BMG LABTECH).

2.2.5 Preparation of Label-Free Quantitative-proteomics samples

Two biological replicates from WT and VPS41 KO INS1 cell lines were prepared for label-free quantitative proteomics analysis. Each 10 cm culture plate with approximately 80% cell confluency was washed with PBS gently 3 times and all liquids were completely removed. Cells were then lysed with 4% SDC lysis buffer (4% Sodium deoxycholate, 100 mM Tris-HCl pH 8.0) for protein extraction. Extracted proteins were boiled at 95°C for 10min, followed by sonication (QSonica-Q800, 4°C for 10 minutes, 95% power). The protein extracts were centrifugated at 18,000 g for 10 min at 4°C, and the supernatant was collected into a new tube for digestion and further analysis. Protein concentrations were quantified by the BCA assay (Pierce™ BCA® Protein Assay Kits and Reagents, Thermo Scientific, #23225) and approximately 800µg of protein, for each sample, was reduced and alkylated by the addition of DTT and IAA for 30 minutes at room temperature. After protein digestion with trypsin (Sigma-Aldrich) at a ratio of 1:50 at 37°C, peptides were diluted by the addition of an equal volume of ethyl acetate. LC-MS/MS and spectra analysis was performed as described in proteomics analysis by Harney et al. [203].

For comparative proteome analysis of WT and VPS41 KO INS1 cells, the LFQ (Label-free quantification) proteomic approach was applied using MaxQuant (version 2.0.3.0) followed by data analysis with Perseus software (version 1.6.15.0), R package (version 4.1.1) and R studio. MaxQuant is the most widely used application for analyzing proteomics data. Perseus is a software framework used for data annotation and statistical analysis of proteomics data obtained through high–resolution Mass Spectrometry. The 'Rattus norvegicus' UniProt Proteome (Proteome ID: UP000002494) was used.

2.2.6 Statistical analysis

Statistical analyses were performed using GraphPad Prism 9 software using student's t-test, One-way ANOVA or Two-way ANOVA followed by Tukey's or Šídák's multiple comparisons tests (specified in figure legends). Data were presented as mean ± SEM.

2.3 Results

2.3.1 Characterization of WT and VPS41KO INS1 cells

2.3.1.1 Validation of VPS41 on INS1 cells

To examine the role of VPS41 in insulin-secreting β cells, VPS41 KO INS1 cells were generated using the CRISPR/Cas9 system. The rescue INS1 cells were generated by lentiviral expressing of the full-length VPS41 (N-terminal HA-tagged VPS41) into the VPS41 KO cells. These stable cell lines were generated were kind gifts from our collaborator, Associate Professor Cedric S. Asensio (University of Denver, USA).

Depletion of VPS41 was validated using a western blotting assay. As expected, VPS41 KO cells had significantly lower levels of VPS41 protein, while HA-VPS41 rescue INS1 cells exhibited restored VPS41 protein expression (**Figure 2-1A & B**). Furthermore, the HA tag was detected only in the rescue INS1 cells expressing N-terminal HA-tagged VPS41 (**Figure 2-1A**). Notably, endogenous insulin protein levels were significantly reduced in VPS41 KO INS1 cells compared to WT cells (mean insulin ± SEM = [KO: **0.097** ± **0.008**] vs [WT: **1.000** ± **0.089**]) ($p < 0.0005$) (**Figure 2-1C & E**), however, endogenous proinsulin protein levels were not different between WT and VPS41 KO INS1 cells (mean proinsulin ± SEM = [KO: **0.680** ± **0.132**] vs [WT: **1.000** ± **0.208**]) ($p = 0.264$) (**Figure 2-1C & D**). Therefore, the proinsulin-to-insulin ratio of the KO cells is significantly higher than that of the WT cells (**Figure 2-1F**).

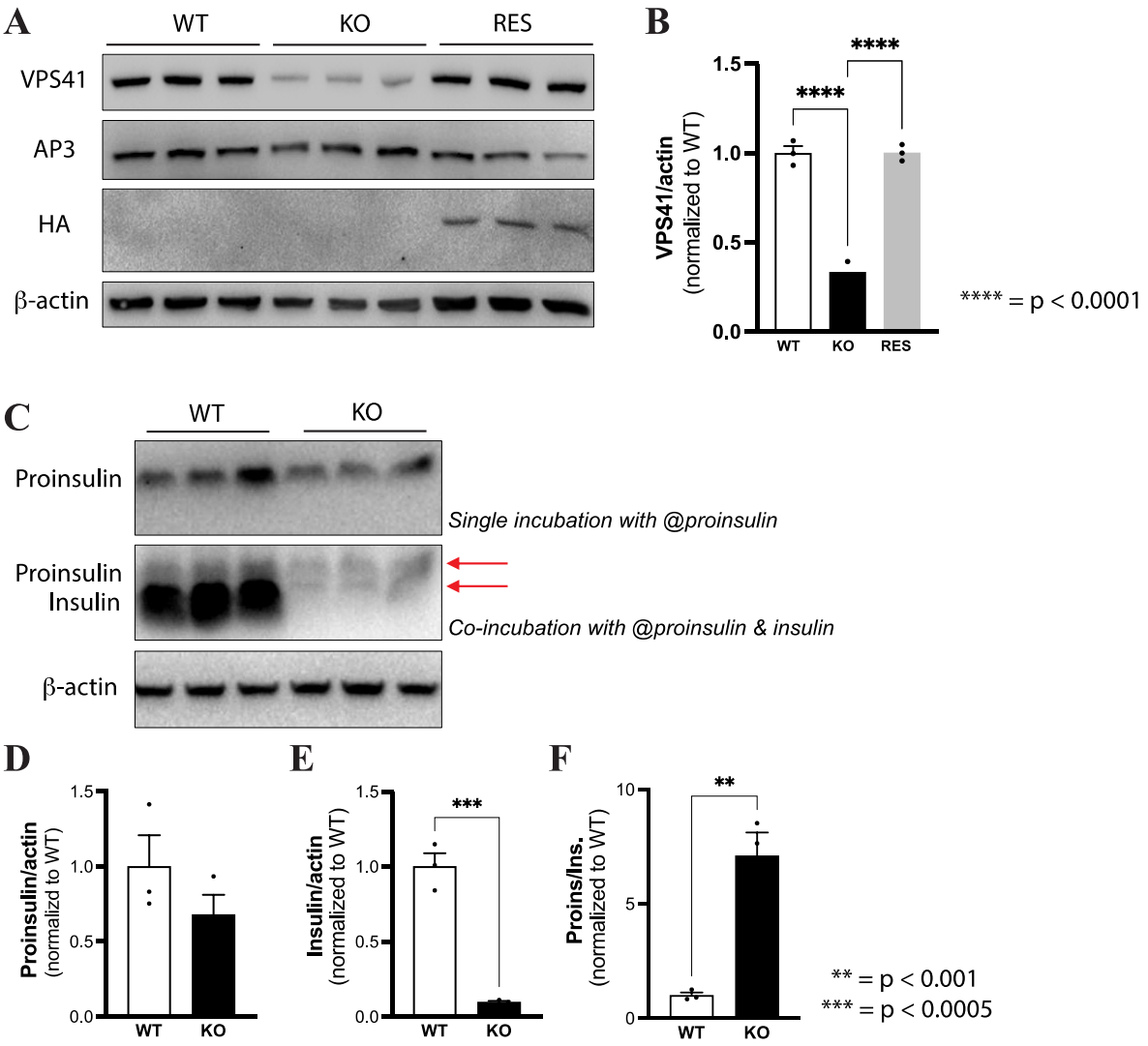

Figure 2-1 VPS41 Protein Expression and insulin expression in WT, VPS41 KO and Rescue INS1 cells

(A) Protein expression of VPS41, AP-3, HA and β-actin, from WT, KO and Rescue INS1 cell lysates, was detected by Western blotting assay. (B) Band intensity of VPS41 versus β-actin were quantified using ImageJ software and normalized to WT INS1. RES indicated Rescue INS1 cells (C) Proinsulin and insulin protein levels in WT and VPS41 KO INS1 cells were detected and quantified following a modified Western blotting assay [202]. Band intensities of (D) proinsulin versus β-actin and (E) insulin versus β-actin were quantified using ImageJ software and normalized to WT INS1. (F) The ratio of proinsulin over insulin. All the data were presented as mean ± SEM. ** $p < 0.005$, *** $p < 0.0005$ and **** $p < 0.0001$ by using One-way ANOVA with Šídák's multiple comparisons test (B) and student t-test (D, E and F).

Next, I examined the intracellular distribution of insulin SG in VPS41 KO INS1 cells by performing immunofluorescence staining using the anti-insulin antibody. It is important to note that the anti-insulin antibody (Guinea Pig anti-insulin pre-diluted, DAKO, #A0564) used for immunostaining on this thesis reacts with mature insulin as well as immature proinsulin.

Upon culturing control WT INS1 cells with standard culturing conditions 11mM glucose, the majority of cells were insulin-positive, and these insulin-positive granules distributed broadly throughout the cytoplasm and cell periphery regions (**Figure 2-2A top**). In contrast, very few insulin-positive cells were observed in VPS41 KO INS1 cells (**Figure 2-2A middle**). However, HA-VPS41 rescue INS1 cells displayed restoration of insulin-positive cells (**Figure 2-2A bottom**), which didn't reach levels present in WT INS1 cells (mean of relative insulin intensity ± SEM = [WT: **9.18** ± **0.86**] vs [KO: **1.44** ± **0.31**] ($p < 0.0001$) or [WT: **9.18** ± **0.86**] vs [HA-VPS41 rescue: **5.45** ± **0.60**] ($p < 0.0005$)) (**Figure 2-2B**) thus, indicating VPS41 loss leads to the reduction of insulin-containing secretory granules.

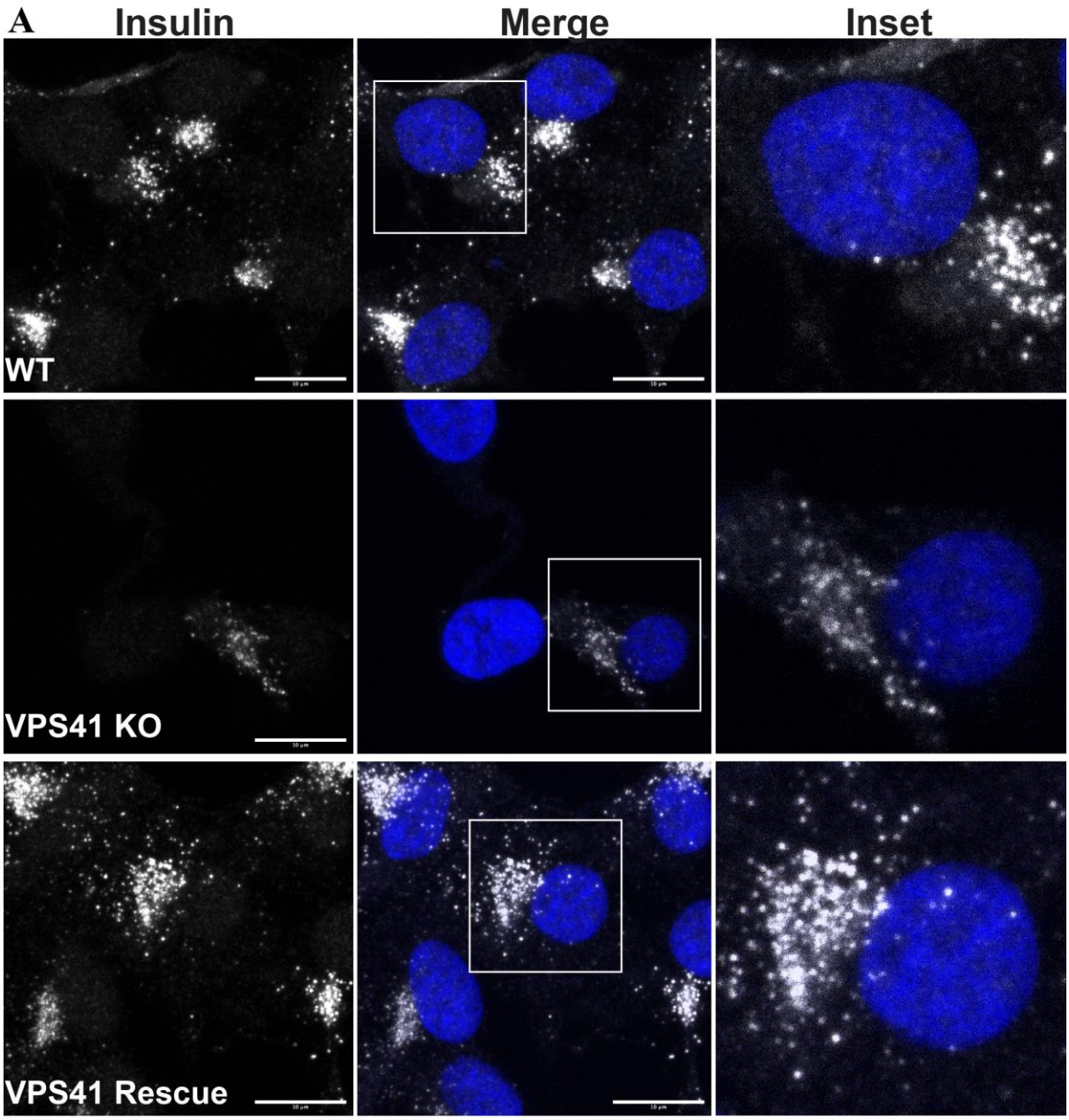
A
Insulin
Merge
Inset
WT
VPS41 KO
VPS41 Rescue

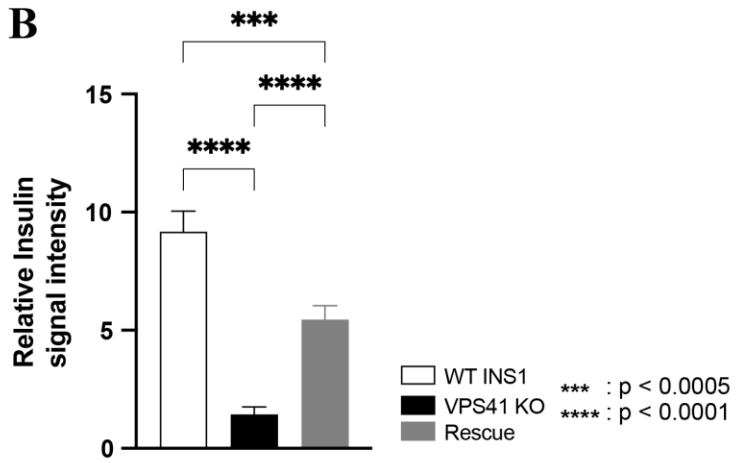

Figure 2-2 Immunofluorescence images of insulin staining in WT, VPS41 KO and HA-VPS41 rescue INS1 cells

(A) Insulin (gray) immunostaining merged with DAPI (blue) in WT, VPS41 KO and HA-Rescue INS1 cells. These representative fluorescence images were obtained using confocal microscopy and a scale bar indicates 10μm. (B) The relative immunofluorescence intensities of insulin were quantified using Image J software and presented as mean ± SEM. *** $p < 0.0005$ and **** $p < 0.0001$ by using One-way ANOVA with Tukey's multiple comparisons test.

Taken together, western blotting assay (**Figure 2-1**) and immunofluorescence staining data (**Figure 2-2**) shows that depletion of VPS41 in INS1 cells results in a dramatic loss of insulin while not much-changed proinsulin protein (**Figure 2-1C& D**).

2.3.1.2 Glucose-stimulated insulin secretion and insulin content in INS1 cells

The significant reduction of insulin protein and insulin SGs in VPS41 KO INS1 cells led to further examine the functional role of VPS41 on β cell insulin secretion. To do this, glucose-stimulation insulin secretion (GSIS) assays were performed. The total cellular DNA content was measured for the normalization of secreted insulin in INS1 cells. Insulin release in response to high glucose stimulation (16.7mM) was significantly increased both in WT and rescue INS1 cells compared to low glucose stimulation (2.8mM); however, the secreted insulin in rescue cells was less than WT's (**Figure 2-3A & C**). Both WT and rescue INS1 cells exhibited similar levels of insulin secretion upon basal conditions (2.8mM low glucose) while VPS41 KO cells had significantly impaired insulin secretion with insulin release almost abolished. Indeed, this defective insulin secretion was shown regardless of basal and high glucose stimulation (**Figure 2-3A & C**). Total DNA content was measured by DNA picoGreen assay and used for normalization of secreted insulin on INS1 cells. Although the same cell numbers of each cell line for the seeding on a plate after cell counting by using a hemocytometer, the DNA content was significantly increased in VPS41 KO INS1 cells (**Figure 2-3B**). It could be due to the different rates of cell growth depending on VPS41 presence in INS1 cells however, the growth rate was not evaluated in this thesis. Even after correction of DNA content, the secreted insulin was blunted in VPS41 KO cells while WT and rescue INS1 cells exhibited glucose-response insulin secretion (**Figure 2-3C**).

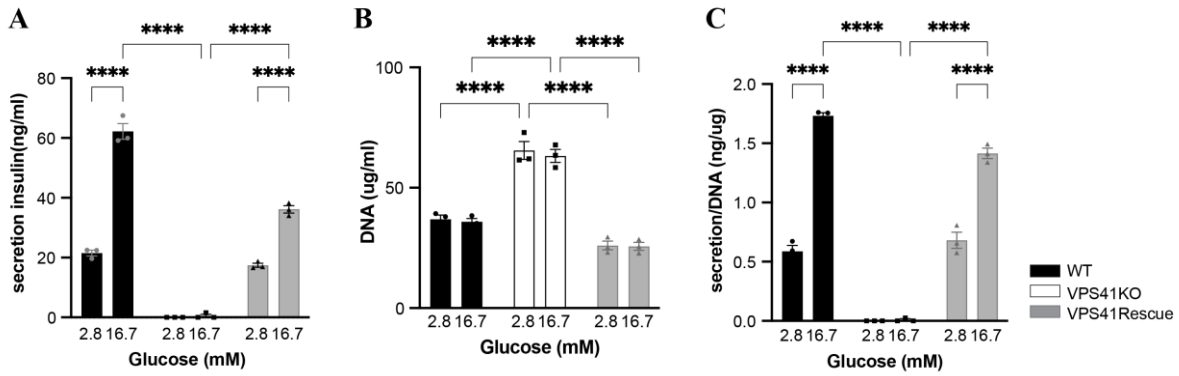

Figure 2-3 Glucose-stimulated insulin secretion in INS1 cells

(A) Low (2.8mM) or high (16.7mM) glucose-stimulated insulin secretion, (B) DNA content and (C) the normalized insulin secretion by DNA content on WT, VPS41 KO and rescue INS1 cells. All data were presented as mean ± SEM, **** $p < 0.0001$ by using Two-way ANOVA with Tukey's multiple comparison tests.

Consistent with immunoblotting and immunostaining results showing decreased endogenous insulin protein expression (**Figure 2-1~2-2**), I also observed defective cellular insulin storage with a considerable reduction in VPS41 KO INS1 cells relative to WT and rescue VPS41 INS1 cells (**Figure 2-4A**). The insulin content measured by HTRF assay was shown similar levels of cellular insulin on them (**Figure 2-4A**), although there was a difference between WT and rescue INS1 cells on immunostaining with insulin (**Figure 2-2**). It could be due to the different specificity to detect endogenous insulin on INS1 cells by performing different assays.

As well, the normalized insulin content by DNA content (**Figure 2-4B**) was shown as the same indicator as insufficient insulin storage in VPS41KO INS1 cells (mean insulin content /DNA ± SEM = [KO: **0.11** ± **0.02**] vs [WT: **14.06** ± **0.75**] ($p < 0.0001$) or [KO: **0.11** ± **0.02**] vs [Rescue: **19.70** ± **0.83**] ($p < 0.0001$)) (**Figure 2-4C**).

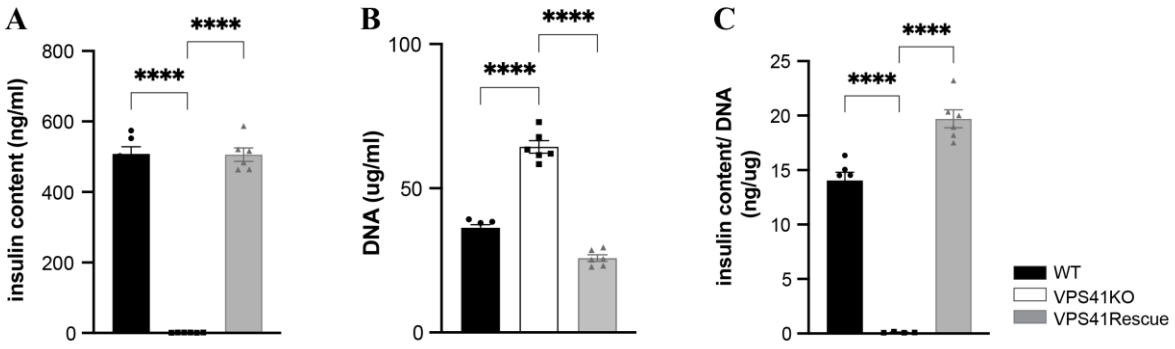

Figure 2-4 Total cellular insulin content in INS1 cells

(A) Total cellular insulin content, (B) DNA content and (C) the normalized insulin content by DNA on WT, VPS41 KO and rescue INS1 cells. All data were presented as mean ± SEM, **** $p < 0.0001$ by using One-way ANOVA with Tukey's multiple comparison tests.

Therefore, chronically VPS41-depleted INS1 cells displayed a severe reduction in cellular insulin content as well as significantly impaired glucose-stimulated insulin secretion upon external stimuli, suggesting VPS41 is required for insulin storage and regulated insulin secretion in INS1 cells.

2.3.2 Proteomics analysis on WT and VPS41 KO INS1 cells

This section of proteomics analysis used a limited sample size (two biological replicates of each cell line) as the main purpose of this analysis was preliminary proteomics of VPS41 KO INS1 cells for further experimental designs to investigate the functional role of VPS41 role on β cells.

To gain some insight into potential mechanisms for the loss of insulin in VPS41 KO INS1 cells, I performed proteomics analysis based on a label-free quantification (LFQ). The mass spectrometry-based proteomics provided protein profile and quantification data, allowing a detailed comparative analysis of enrichment pathways between WT INS1 and VPS41 KO INS1 cells.

2.3.2.1 Differential analysis of identified proteins on WT and VPS41 KO INS1 Cells

MaxQuant analysis identified and quantified approximately 6000 proteins in individual WT and VPS41 KO INS1 cells. The output was further analyzed using Perseus, R package and R studio, allowing analysis of quantitative protein abundance data. The original data matrix from MaxQuant was performed by data preparation, filtering, normalization, and imputation of missing values as well as statistical analysis (**Figure 2-5**). Proteins were annotated with Gene Ontology terms from Uniprot and subsequently, used for functional annotated pathways of the identified proteins. In general, parameter values in MaxQuant were their default values without changes unless explicitly mentioned and the LFQ intensities of single cells from the original MaxQuant output were used for further analysis. Furthermore, a Benjamini-Hochberg FDR of 5% was performed to minimize errors in multiple hypothesis testing.

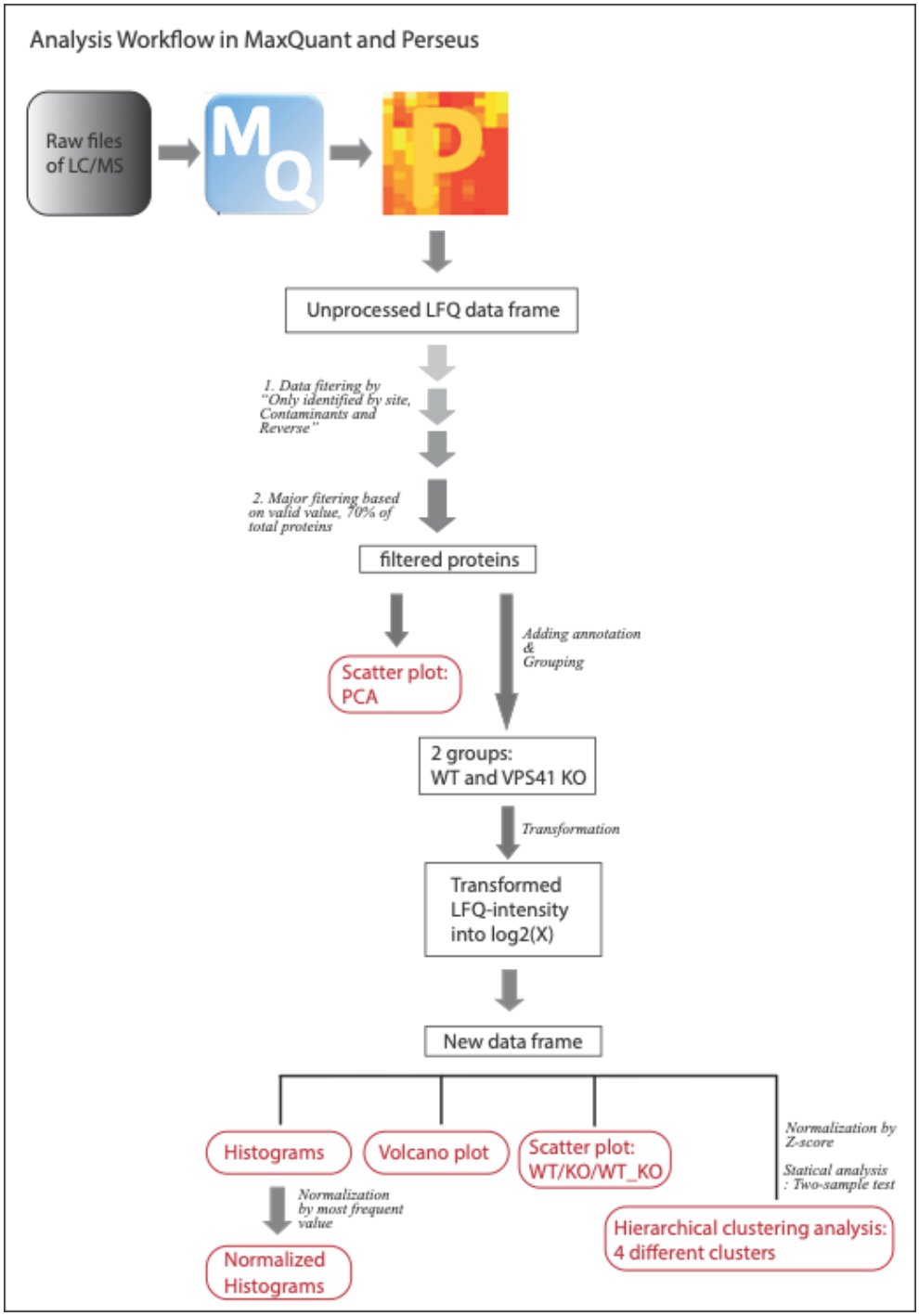

Figure 2-5 Workflow of Label-free quantification analysis on WT and VPS41 KO INS1 cells

A label-free quantification (LFQ) approach was used for the detection and quantification of abundant proteins on WT and VPS41 KO INS1 cells. The raw file of LC/MS on WT and VPS41 KO INS1 cells was processed using MaxQuant (version 2.0.3.0) using the default setting. The original data frame from MaxQuant was further analyzed using Perseus (version 1.6.15.0), R package (version 4.1.1) and R studio following pre-processing of data including filtering and normalization of LFQ intensities. The LFQ-intensity values were transformed into log2 for further visualization of results including histograms, volcano plot, scatter plots and Hierarchical clustering analysis.

2.3.2.2 Pre-processing of data – filtering and normalization of LFQ intensities

The data frame of identified proteins was filtered on missing values by setting the threshold for the allowed number of missing values per condition since some of the proteins are not quantified in all replicates and only quantified in a single replicate. After filtering by 'Reverse sequences' and 'Only identified by site', the number of identified proteins per sample was approximately 4800 (4897 and 4798) and 4600 (4665 and 4679) and in biological replicated WT and VPS41 KO INS1 cells, respectively (**Figure 2-6**).

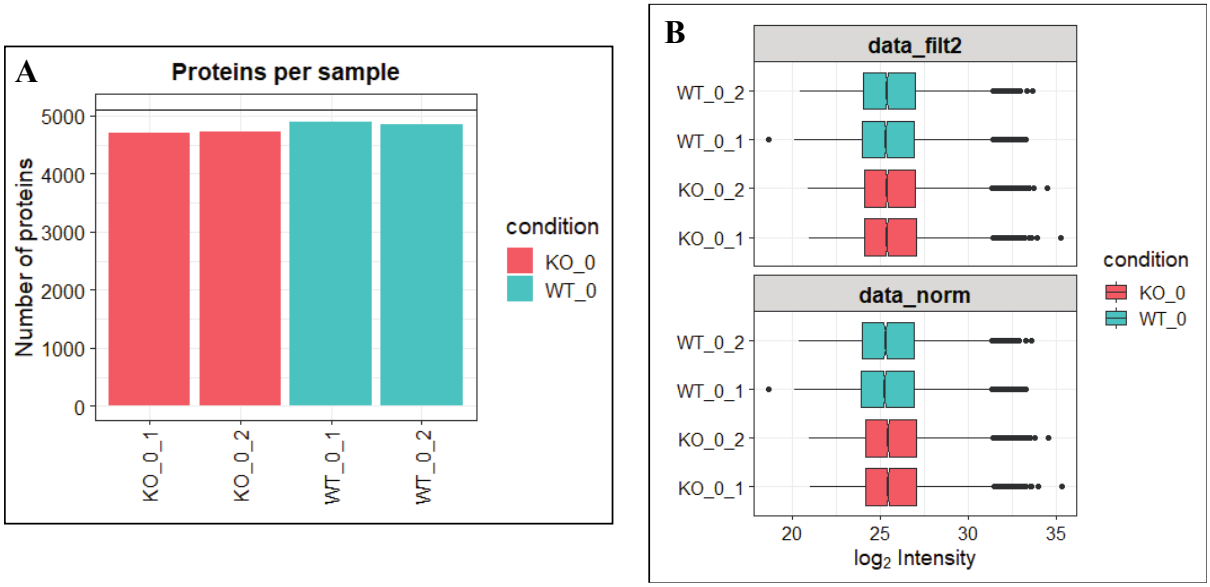

Figure 2-6 Bar-plot of the number of identified proteins (A) and visualized boxplots (B)

(A) The number of identified proteins after filtering by 'reverse sequences' and 'only identified by site'. (B) Visualized boxplots for all filtered samples before (top) and after (bottom) normalization.

The data (**Figure 2-6A**), before and after normalization, were visualized by boxplots (**Figure 2-6B**). To reduce systematic biases in mass spectrometry-based data due to many potential risk factors such as experimental and technical processing, normalization was carried out before statistical analysis.

The remaining missing values in the original data frame could be imputed since data can be missing if proteins are not quantified in specific conditions, indicating that proteins are below the detection limit in specific conditions which will be usual in proteomics samples with high proportions of missing values. However, simple imputations based on the observed data can sometimes overestimate abundance values leading to biased results. To decide whether missing values need to be imputed in the matrix for further processing, I evaluated the missing values using the imputation option, the common procedure, implemented in the Perseus and R package (**Figure 2-7A**). Default parameters were defined so that the missing values are replaced by random numbers drawn from a normal distribution of 1.8 standard deviations down shift and with a width of 0.3 of each sample. The imputation effect on the distribution was visualized with a before-imputation plot (**Figure 2-7B**).

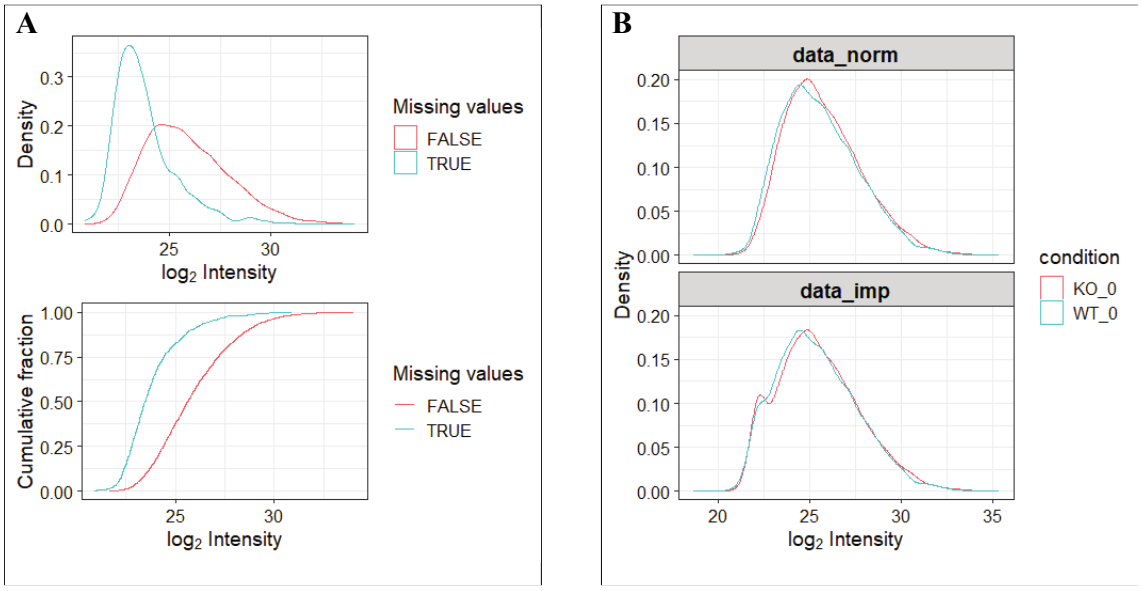

Figure 2-7 Density plots (A) and intensity distribution plots (B)

The density plots with or without missing values (A) and the data plots of intensity distributions before and after imputation (B).

Next, histograms for all LFQ intensity columns of total identified proteins on WT and VPS41 KO INS1 cells were generated. Histograms depicting the LFQ intensities of the identified proteins on WT and VPS41 KO INS1 cells displayed mostly normal distribution pattern before/after normalization by most frequent values (**Figure 2-8A & B**). However, histograms of the LFQ intensities after imputations showed non-normal distributions with skewed fatter tails (**Figure 2-8C**). Based on these analyses, approaches without imputation were used to improve quantitative proteomics data analysis.

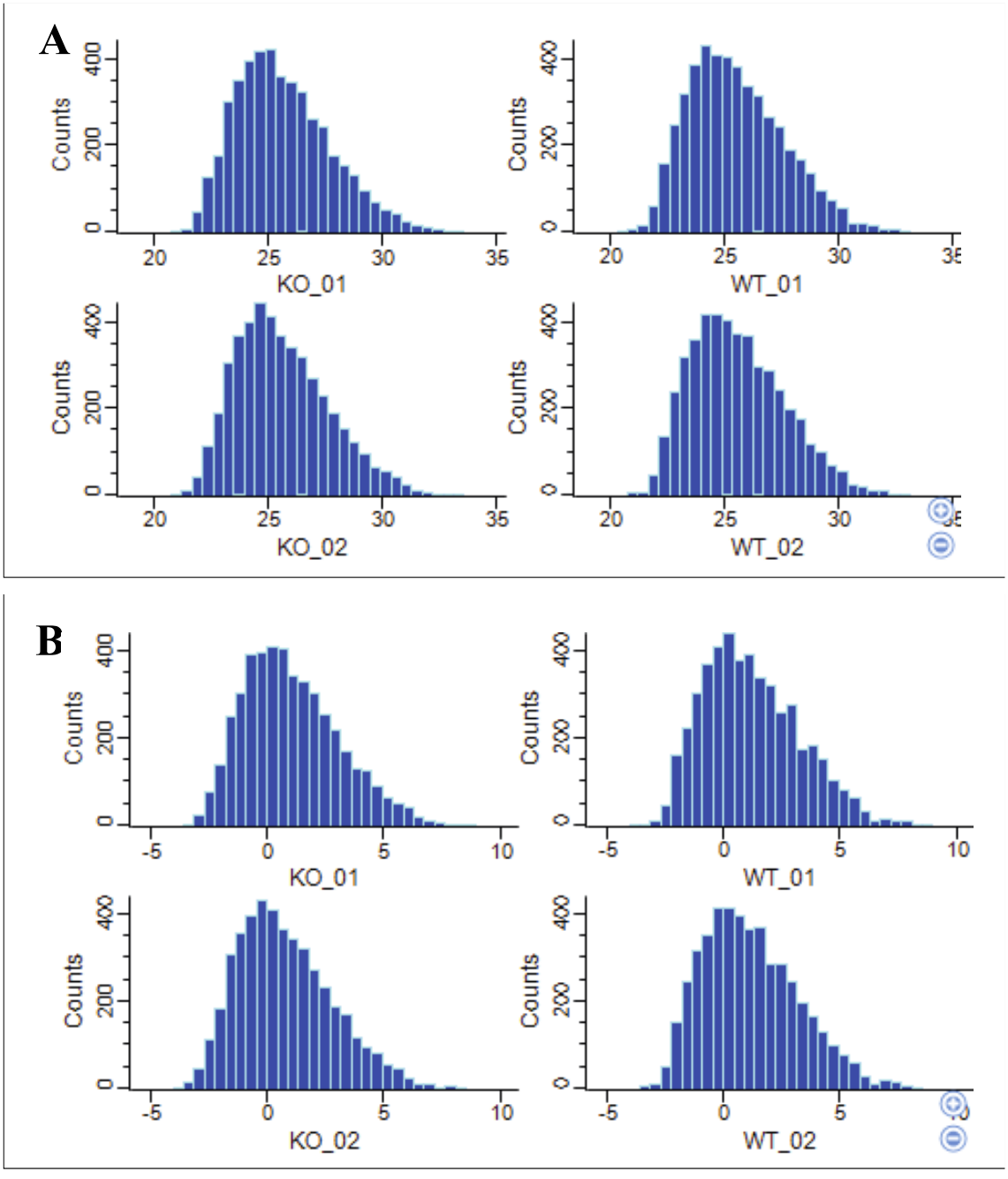

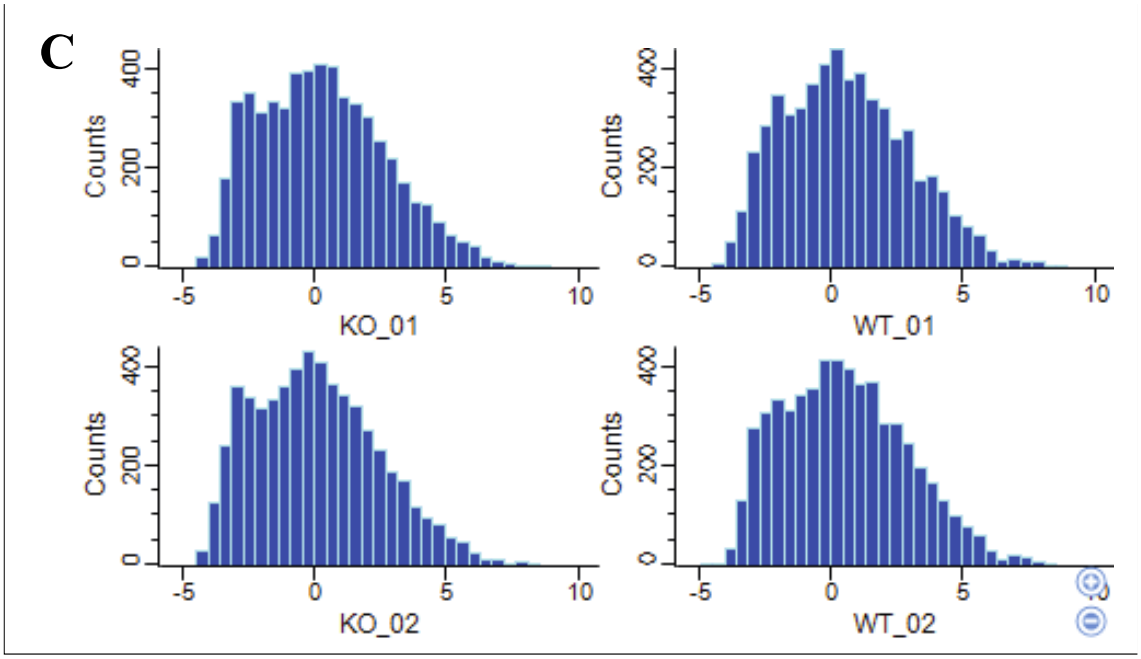

Figure 2-8 Histograms of LFQ intensity counts on WT and VPS41 KO INS1 cells

(A) Histograms showing LFQ intensity counts of total identified proteins. (B) Histograms showing LFQ intensity counts of total identified proteins after subtracting normalization by most frequent values. (C) Histograms showing LFQ intensity counts of total identified proteins after normalization followed by missing value imputations.

2.3.2.3 Visualization of MS-based data in WT and VPS41 KO INS1 cells

Principal component analysis (PCA) led to the clear grouping of individual biological replicates into different principal components (PCs). Indeed, WT and VPS41 KO INS1 cells were separated in PC1, which accounted for 85.1% of the total variation (**Figure 2-9**).

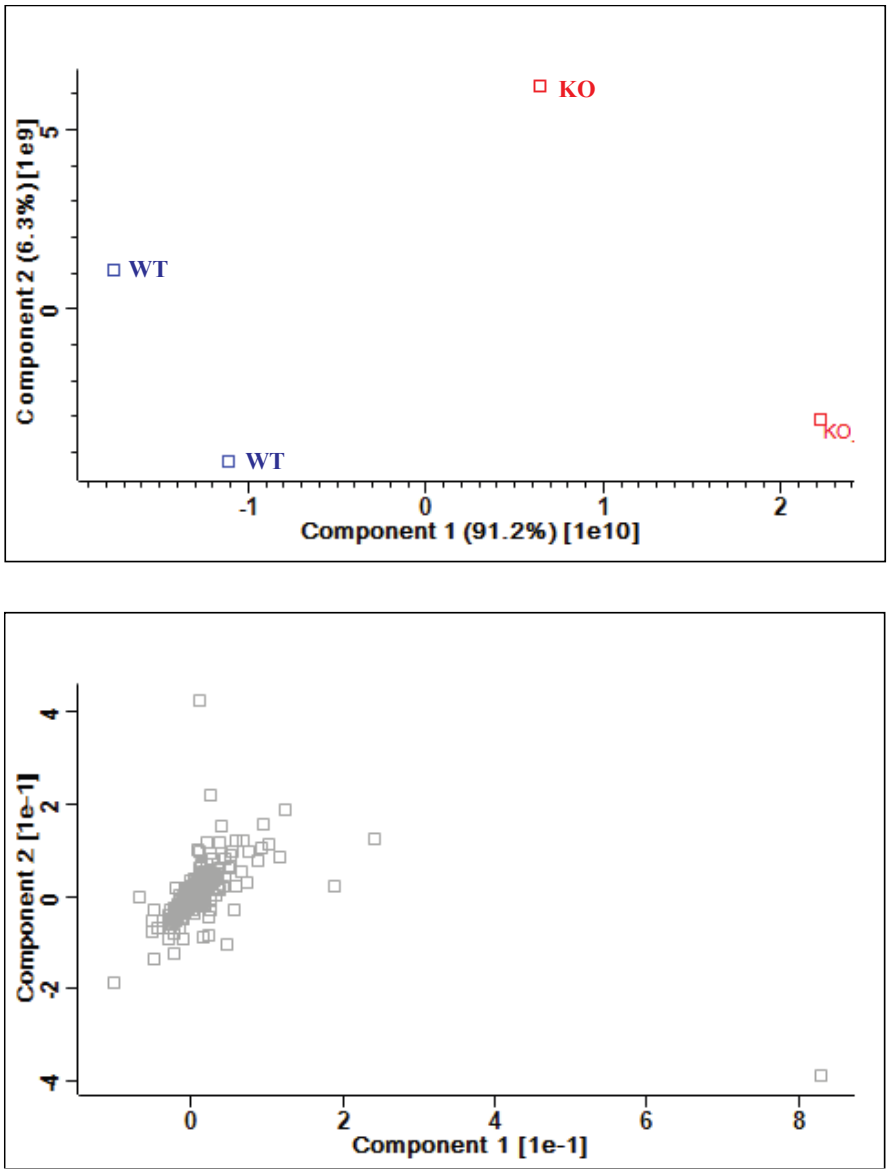

Figure 2-9 Principal component analysis of WT and VPS41 KO INS1 cells

Scatter plots with density-estimation were generated to confirm the reproducibility of the label-free protein quantification between biological replicate groups, accounting for the high degree of Pearson correlation coefficient between biological replicates (WT Replicate1-WT Replicate2, $\mathbf{R^2 = 0.992}$ and KO Replicate1-KO Replicate2, $\mathbf{R^2 = 0.987}$, respectively), while less correlation from different samples between WT and KO ($\mathbf{R^2 = 0.912}$, **Figure 2-10**).

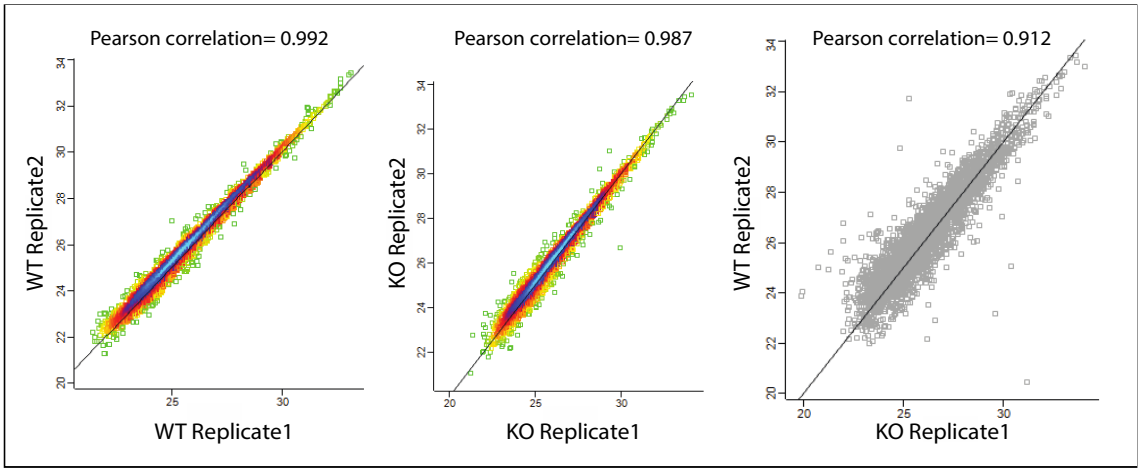

Figure 2-10 Scatter plots of WT and VPS41 KO INS1 cells

Scatter plots of WT Replicate1-2/ VPS41 KO Replicate 1-2/ WT Replicate2-VPS41 Replicate1 INS1 cells.

As described previously, the HOPS complex is composed of 4 cytosolic class C-core subunits VPS11, VPS16, VPS18, VPS33, and 2 specific subunits VPS39 and VPS41. I thus evaluated the LFQ intensities of the single subunits including VPS41 within the HOPS complex before identifying differential proteins or enrichment proteins on WT and VPS41 KO INS1 cells. Except for VPS41, similar levels of quantified LFQ intensities were observed on WT and VPS41 KO INS1 cells (**Figure 2-11**). LFQ-VPS41 on KO repeated biological (and technical replicate) samples was not observed while LFQ-VPS41 on WT INS1 cells was observed in abundant levels with similar values to other HOPS subunits (**Figure 2-11**).

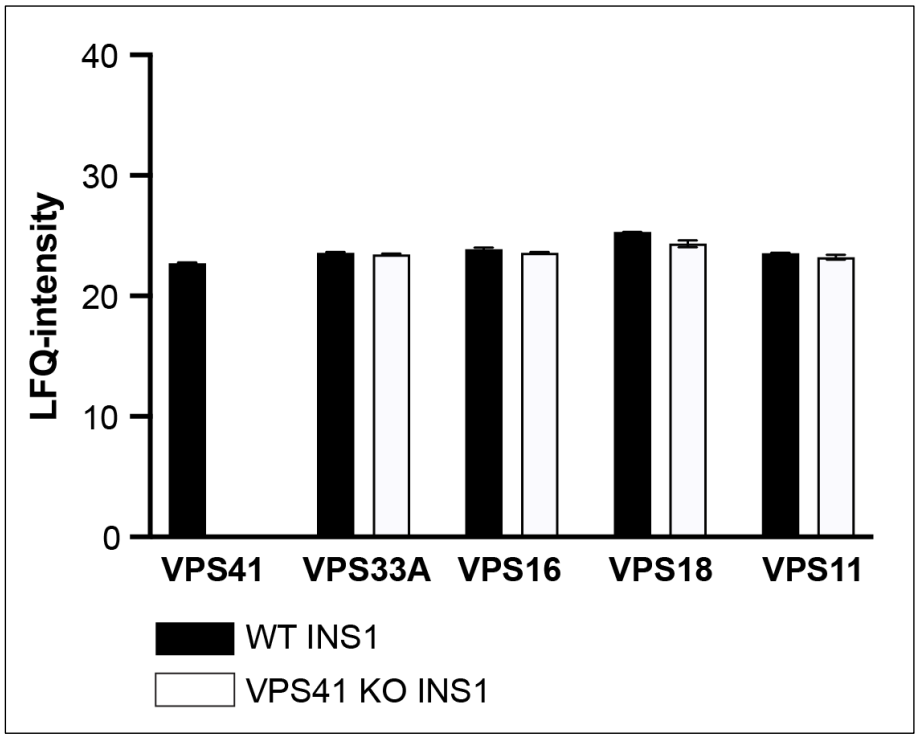

Figure 2-11 LFQ-intensities of the HOPS complex single subunits

LFQ intensities for each subunit of the HOPS complex. The HOPS complex is composed of 4 cytosolic class C-core subunits including VPS33, VPS16, VPS18 and VPS11 together with specific subunits. The LFQ intensities of VPS41 and the C-core subunits of HOPS complex were quantified on WT and VPS41 KO INS1 cells. The data were presented as mean ± SD.

Next, I performed a comparative DEP (Differential Enrichment analysis of Proteomics data) to identify differential proteins or differential enrichment proteins between WT and VPS41 KO INS1 cells. LFQ-based volcano plots showed the fold change of expressed proteins and significant differences were assessed by Student's t-test. Adjusted p-value and log2 fold change were defined as $p < 0.05$ and 1 as significant, respectively (**Figure 2-12**). Indeed, the bar plots of interest proteins associated with β cell properties suggest that β cells could lose β cell features relevant to insulin machinery under VPS41-depleted circumstances. Expression of β cell-disallowed genes such as *Ldha*, *Ldhb* and *HK1* were significantly enhanced in VPS41 KO INS1 cells, while β cell-identity genes including *Ins2* and *Pdx1* were reduced (**Figure 2-13**). Notably, the level of LFQ-*Ins1* was not considerably different between WT and VPS41 KO INS1 cells; however, that of LFQ-*Ins2* was not quantified at all on VSP41 KO INS1 cells as the expressed *Ins2* was not detected on these KO INS1 cells.

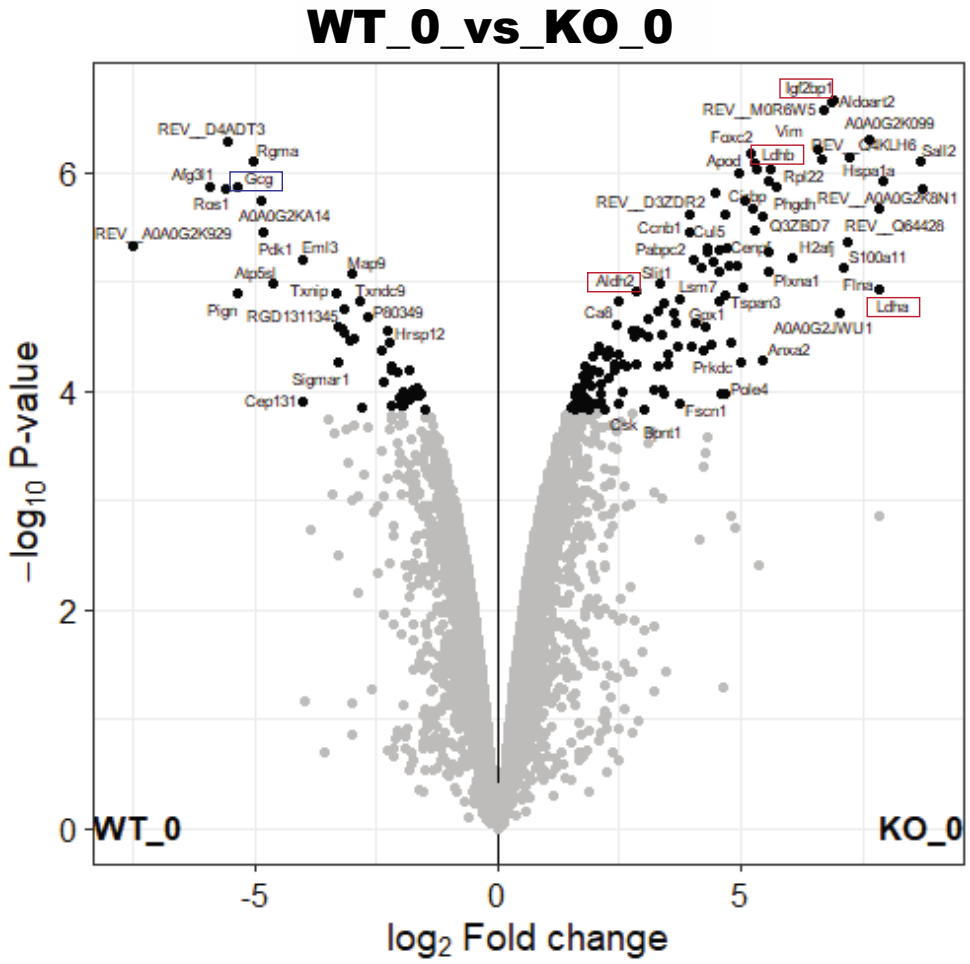

Figure 2-12 Volcano plot of WT and VPS41 KO INS1 cells

Volcano plots to visualize comparison between WT and VPS41 KO INS1 cells.

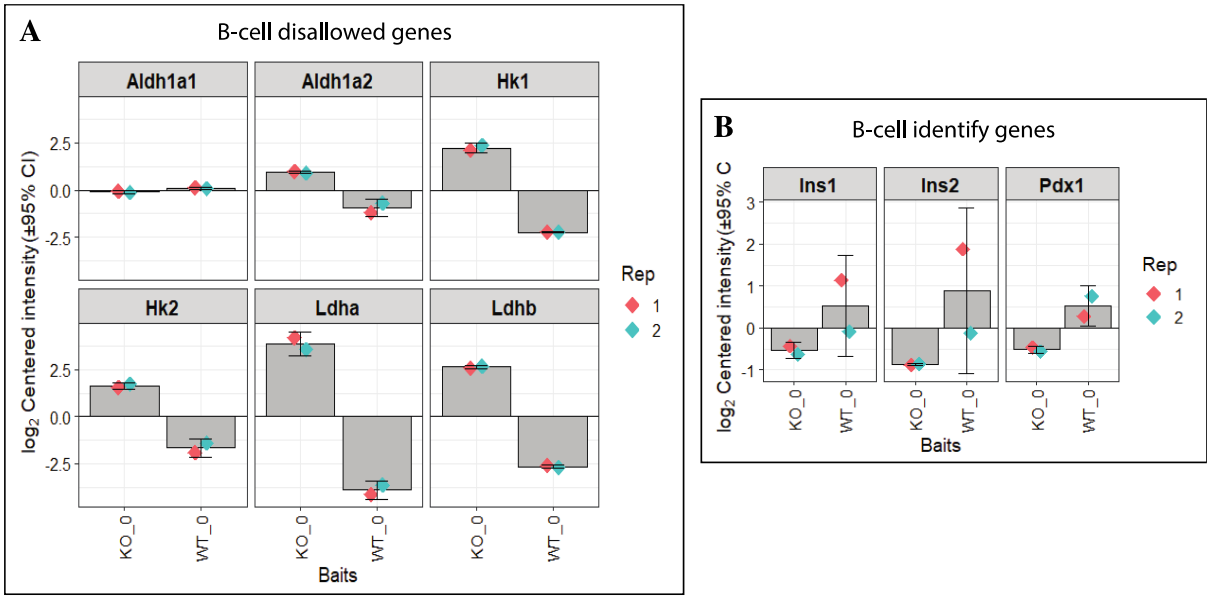

Figure 2-13 LFQ intensities of proteins associated with β cell de-differentiation and identity

(A) Bar-plots displaying LFQ intensities of single proteins of special interest associated with β cell de-differentiation and (B) β cell identity. The data were presented as mean ± SD.

Hierarchical clustering analysis (HCL) of the quantified proteins was carried out to identify the protein groups with similar expression patterns. For the HCL, LFQ intensities were transformed into log2 LFQ intensities, and then Z-score normalization and a two-sample test of the data (1283 proteins) were performed. The HCL data was grouped into four major clusters (**Figure 2-14A**).

I next assessed the enrichment of unique groups in the identified proteins using annotated Gene Ontology pathways. As expected, VPS41 KO INS1 cells were less enriched for β cell function-associated gene ontology (GO) terms, including insulin processing and secretion including insulin SG biogenesis and vesicle-mediated transport proteins, whereas proteins associated with ubiquitin-mediated proteolysis were more enriched in these cells compared to the WT INS1 cells (**Figure 2-14A**). Importantly, both prohormone convertases PC1/3 and PC2, which (encoded by the *PCSK1* and *PCSK2* genes, respectively) facilitate proinsulin processing, were expressed significantly less on VPS41 KO INS1 cells (**Figure 2-14B**), suggesting that VPS41 depletion contributes to dysfunctional β cells exhibiting impaired insulin processing and secretion.

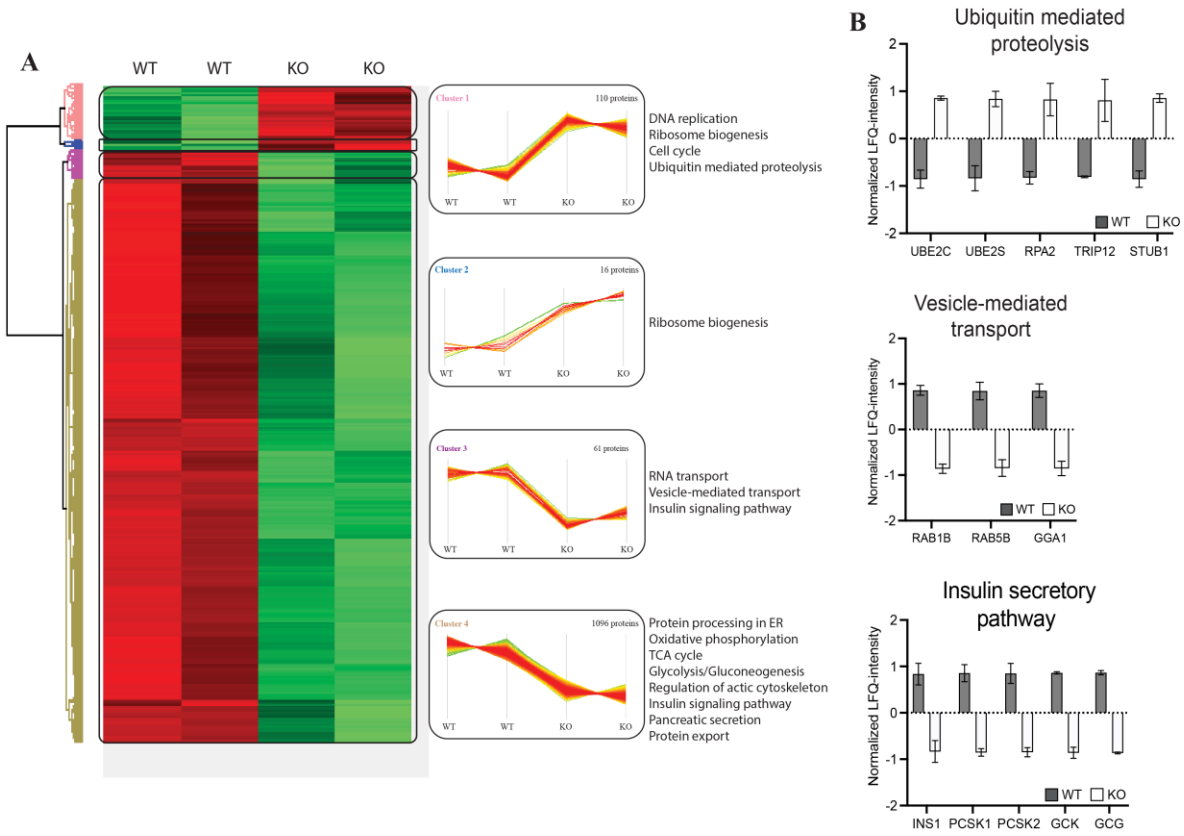

Figure 2-14 Hierarchical clustering analysis and visualized bar-plots of selected clusters

(A) A visualized heatmap of hierarchical clustering analysis (HCL) of the quantified proteins and line plots of proteins with enriched pathways in unique clusters of proteins. (B) Visualized bar plots of a single protein associated with special interest pathways from select clusters.

Hence, INS1 cells that lack VPS41 have reduced expression of proteins associated with β cell function especially, the insulin secretory pathway. Taken together, the proteomics data together with our *in vitro* results on WT and VPS41 KO INS1 cells provides strong evidence of impaired β cell function under chronic VPS41-deficiency.

2.4 Discussion

To investigate the role of endogenous VPS41 in insulin-producing pancreatic β cells CRISPR/Cas9 genome editing system was used to generate VPS41 KO INS1 cells. I characterized β cell function e.g., insulin storage and insulin secretion on these VPS41 KO INS1 cells comparing their phenotype to WT and VPS41 rescue INS1 cells. I observed marked reduction in insulin protein levels using Western blotting assay (**Figure 2-1**), reduced numbers of insulin-positive cells by IF (**Figure 2-2**) as well as total insulin content by HTRF assay on VPS41 KO INS1 cells (**Figure 2-4A & C**). Additionally, VPS41 KO INS1 cells had impaired insulin secretion with significantly blunted secretion in response to high glucose while VPS41 rescue cells had restored insulin secretion (**Figure 2-3A & C**). However, proinsulin protein levels were comparable to WT INS1 cells by evaluating the western blotting assay (**Figure 2-1C**). Thus, it could be informative to measure insulin mRNA levels to assess whether the loss of VPS41 impacts proinsulin synthesis in INS1 cells. To address this possibility, insulin mRNA levels would be measured by RT-qPCR in the cells lacking VPS41. However, so far, VPS41 has not been identified to act as a transcriptional factor for gene expression including *insulin* expression. It has been reported that the pool of VPS41 resides near the TGN [164,189,191]. Additionally, our collaborator, Associate Professor Cedric Asensio, (University of Denver) revealed that VPS41 plays a role in the budding of regulated secretory granules at the TGN in neuroendocrine cells [164]. These neuroendocrine cells, PC12 are specialized cells similar to endocrine cells, that produce and release neuropeptide hormones in response to external signals thus, regulate target cell functions [164].

The granins are highly expressed in both neuroendocrine and endocrine cells including pancreatic β cells and are well-known as critical factors to regulate SG formation through aggregating with TGN membrane under a typical luminal environment (acidic and high $Ca2^{+}$) of the TGN [4,9,163]. In particular, this tendency of self-aggregation at low pH/high $Ca2^{+}$ conditions allows them to act as a regulator of SG budding at the TGN [49,163]. The absence of CgB, a member of the granins family led to a defect of insulin secretion not affecting biosynthesis of insulin SG [204] on isolated mouse islets, while the impaired proinsulin processing was observed together with an altered composition of SG proteins and its density on CgB depleted INS1 cells through siRNA-mediated transfection [83]. In agreement with the phenotypes on β cell specific-CgB KO mouse islets, there were insignificant differences in protein levels of proinsulin between WT and VPS41 KO INS1 cells (**Figure 2-1**) however, VPS41 KO INS1

cells exhibited a remarkable reduction of insulin SGs (**Figure 2-2**), total cellular insulin content (**Figure 2-4A & C**) as well as secreted insulin exposed to external stimuli such as glucose (**Figure 2-3A & C**).

The mechanism whereby VPS41 deletion leads to β cell dysfunction is not clear. In collaboration with the Asensio group at the University of Denver, we have shown that deletion of VPS41 in INS1 cells leads to reduced numbers of SG containing insulin, shown by Electron Microscopy analysis of thin sections obtained from WT and VPS41 KO INS1 cells [191], whereas insulin packaging was not affected in the VPS41 KO INS1 cells [191]. Furthermore, our collaborators applied the retention using selective hooks (RUSH) system, which is a useful methodology tool that tracks movement of proteins within the cells, to monitor fluorescent-vesicles trafficking upon biotin addition at the secretory pathway [191]. The strategy of the RUSH system utilizes the different affinity of the protein complex composed of interest proteins, streptavidin binding peptide (SBP) and a fluorescent protein (eGFP) against the initial donor and the acceptor compartment according to the presence or absence of biotin. Without biotin, the protein complex is retained within the donor compartment; however, upon biotin addition, the complex is released into the acceptor compartment enabling the study of protein trafficking [191,205,206]. Thus, by applying the RUSH system using specific markers such as SG marker (MPY-GFP-SBP) and transmembrane marker (phogrin-GFP-SBP), they examined whether the VPS41 loss would cause a budding/sorting defect of SG from the TGN, consequently leading to reduced numbers of insulin SG in VPS41 KO INS1 cells. It was observed that VPS41 lack did not affect budding kinetics and sorting; however, transmembrane protein composition and SG density changed [191]. Indeed, the altered composition of SG transmembrane as well as granule density could affect the maintaining of SG stability, thus leading to decreased insulin secretion and impaired insulin storage capacity, therefore physiologically there is limited bioactive insulin available for release.

Overall, decreased insulin secretion and poor storage of the mature insulin SG in the absence of VPS41 in INS1 cells led us to hypothesize that the loss of VPS41 leads to enhanced SG degradation. However, VPS41 KO INS1 cells via chronical deletion of *VPS41* might be not suitable to examine the precise mechanisms relevant to β cell feature. The results associated with phenotypes on VPS41 KO INS1 cells indicate that VPS41 KO INS1 cells lose β cell identity and may have been de-differentiated. In the present thesis, the upstream regulation of *VPS41* expression was not investigated thus, the role of *VPS41* in development of β cell

differentiation still remains to be studied. However, I observed significant changes of genes associated with β cell identity such as *Pdx1*, *Ins1* and *Ins2* on VPS41 KO INS1 cells using proteomics analysis. It is tempting to expect a strong correlation between activated transcription factors e.g., *Pdx1* and *VPS41* expression for β cell development and maturation. Hence, I propose that chronically depleted *VPS41* expression contributes to altered β cell state such as de-differentiation, consequently leading to deficiency of insulin storage in pancreatic β cells. The proteomics analysis on INS1 cells revealed the enrichment expression of β cell-disallowed genes however, suppression of β cell-identify genes associated with regulated insulin secretory pathways in the absence of VPS41 (**Figure 2-12 ~ 2-14**).

Unlike β cell death as the clear outcome in T1D due to the autoimmune destruction of β cells [207], T2D is characterised as a complex metabolic disorder due to dysfunctional β cell, eventually leading to a reduction in β cell mass and defective glucose homeostasis in response to external stimuli (**Figure 1-6**)[151,208]. In addition to β cell death such as apoptosis, it has been recently reported that β cell de-differentiation contributes to the loss of β cell mass, which is strongly associated with the failure of β cell, leading to T2D progression [150,151]. Foxo1 (Forehead box protein 1) is well-defined as the core transcription factor to maintain β cell integrity, which inhibits β cell proliferation *via* suppression of *Pdx1*[150,152]. *In vivo* study in mice with β cell specific Foxo1 KO thus revealed that Foxo1 determines β cell fate as the transcription factor through suppression of gene expression associated with insulin synthesis under metabolic stress circumstances, while there were insignificant changes of apoptotic cell death using caspase-3 activity or TUNEL assay on these KO mice [150]. Although the present thesis has not investigated the upstream regulation of *VPS41* or whether VPS41 gene affects the expression of specific genes required for β cell identity like *Foxo1*, I observed a significant reduction of insulin in β cells in the absence of VPS41. As well, I observed a significant suppression of genes associated with insulin secretory machinery such as those involved in vesicle-mediated transport and insulin maturation such as *PCSK1* or *PCSK2* on VPS41 KO INS1 cells (**Figure 2-13 & 2-14**). Additionally, at the levels of LFQ-*Ins1* and LFQ-*Ins2*, LFQ-*Ins1* levels were not significantly different between the WT and VPS41 KO INS1 cells, but VPS41 KO INS1 cells exhibited significantly less quantified LFQ-*Ins2*. Previous KO experiments with NOD (non-obese diabetic) mice revealed that the lack of *Ins2* leads to insulin deficiency, accelerating the development of T1D in this model while, in contrast, there was no remarkable reduction of insulin content in mice lacking *Ins1* [209].

In addition to the Foxo1-mediated pathway, the loss of active UPR (unfolded protein response) under chronic hyperglycemia leads to β cell de-differentiation by regulating cytokine release as well as inflammatory gene expression *in vivo* [155]. The accumulation of unfolded/misfolded proteins is characterized as the hallmark of β cell dysfunction and failure (**Figure 1-6**) [130]. Thus, adaptive UPR allows for the reduction of oxidative stress and apoptosis, eventually maintaining β cell identity [155]. Although changes in UPR genes expression were not examined in this chapter, proteins related to ubiquitin-mediated proteolysis were abundant in VPS41 KO INS1 cells (**Figure 2-14B**), which suggests that the absence of VPS41 can affect UPR through upregulation of proteolysis to remove unfolded/damaged proteins on β cells. From 4 cluster groups identifying proteins between WT and VPS41 KO IN1 cells, I also observed the reduction of proteins associated with the regulation of the actin cytoskeleton in VPS41 KO INS1 cells. This data raises questions as to whether VPS41 depletion affects the regulation of the actin cytoskeleton leading to mis-transported insulin SG, and consequently a dysfunctional insulin secretory pathway in β cells. This proteomics result thus provides evidence that chronic VPS41-deficiency is related to impaired β cell function, which is consistent with VPS41 KO INS1 cells phenotype I observed *in vitro*.

Altogether, my findings in the current chapter suggest that VPS41 is required for insulin secretory pathways in pancreatic β cells; however, the underlying mechanisms of how VPS41 mediates these functions in β cell remains unknown. Therefore, I decided to employ siRNA-mediated VPS41 knock-down (KD) strategies in INS1 cells as a secondary method to VPS41 KO mice used in the following chapter.

3 Chapter III: Effect of Acute VPS41 Depletion on INS1 Cells

3.1 Introduction

In Chapter II, the findings revealed that chronic deletion of VPS41 in INS1 cells leads to β cell dysfunction. I observed a marked reduction in insulin SG content and blunted GSIS in VPS41 KO INS1 cells (**Figure 2-1 ~ 2-3**). However, the specific cellular mechanisms underlying these phenotypes are not yet clear. The proteomic changes observed in **Figure 2-14** suggest a likelihood that chronic VPS41 deletion has led to dramatic cellular changes, such that over an extended period of time has resulted in a loss of β cell identity. For this reason, I believe that this model is not appropriate to study the immediate effect of VPS41 deletion. Therefore, in this chapter, I will use VPS41 knockdown (KD) cells to interrogate the potential mechanism for the loss of insulin in the acute system. To do that, I utilized siRNA-mediated KD of VPS41 on INS1 cells.

In this chapter, I first characterized phenotypes of VPS41 KD INS1 cells to understand the functional consequences of VPS41 deletion. The LFQ analysis on INS1 cells exhibited an abundance of ubiquitin-mediated proteolysis as well as down-regulated insulin secretory pathway in the absence of VPS41 (**Figure 2-14**), which suggests that the loss of insulin as the major phenotypes on VPS41 KO INS1 cells (**Figure 2-1, 2-2 & 2-4**) could be due to enhanced insulin degradation. To identify the mechanisms underlying the loss of insulin in VPS41-depleted β cells, I thus examined if the loss of insulin in the absence of VPS41 is associated with enhanced protein degradation pathways in INS1 cells.

3.2 Materials and Methods

3.2.1 Cell culture and treatment of pharmacological reagents

INS1 cell culture conditions including the completed medium were described in section 2.2.1. For pharmacological reagents treatment to examine their effects for restored insulin through inhibition of protein degradation pathways, INS1 cells were cultured with the completed RPMI 1640 media containing different types of inhibitors including chloroquine (Sigma-Aldrich, #C6628), MG132 (Sigma-Aldrich, #M8699), NH_4Cl (Sigma-Aldrich, #326372) and E-64 (Sigma-Aldrich, #E3132), respectively on VPS41 KD and control INS1 cells. Except for MG132, other inhibitors including CQ, NH_4Cl, and E-64 are water soluble, a DMSO negative control was thus used as MG132 was dissolved in DMSO.

3.2.2 Transfection assay

For the generation of VPS41 KD cells, parental WT INS1 cells, between passages 10 and 20, were used for small interfering RNA (siRNA) - mediated oligomer transfection. siRNA against the rat VPS41 (ThermoFisher Scientific, #4390771) was transfected using Lipofectamine 2000 (Invitrogen™, #11668019) or RNAiMAX (Invitrogen™, #13778075) transfection reagent according to manufacturer's protocols to achieve final siRNA concentrations of 25 or 50 pmol in cells seeded on 12-well or 6-well plates respectively. Non-targeting siRNA was used as a control (ThermoFisher Scientific, #4390843). Cells were harvested at 24-, 48-, 72- or 92-hours post-transfection for protein extraction to validate VPS41 KD efficiency *via* western blotting assay before performing further assays including glucose-stimulated insulin secretion assay and immunofluorescence assay.

For GFP-tagged proinsulin plasmid-mediated transfection assay, 1 X 10^5 cells per well of WT and VPS41 KO were seeded on coverslips in a 6-well plate. On transfection day, 70% confluence cells were transfected with proinsulin-msGFP (Addgene, #160466) or msGFP plasmid (Addgene, #135301) using Lipofectamine 2000 (InvitrogenTM, #11668019) transfection reagent according to the manufacture's protocol.

3.2.3 Isolation of plasmids and restriction digest analysis

pQE-60NA-proinsulin-msGFP2 (Addgene, #160466) and pQE-60NA-msGFP2 (Addgene, #135301) were purchased from Addgene. Both plasmids' backbone is pQE-60NA and insert genes are proinsulin-msGFP2 and msGFP2, respectively (**Figure 3-1**). After receiving bacterial stabs of the plasmids, I carried out inoculation, amplification, and purification of the plasmid. The bacterial stab-formed plasmids were grown in Luria-Bertani (LB) broth (Invitrogen^{TM}, #12795-027) containing 100 μg/ml ampicillin overnight to amplify. To obtain high-quality and concentrated plasmids from the bacterial culture, I then performed a plasmid purification assay following HiPure Plasmid kit (Invitrogen^{TM}, #K210007) instructions.

A

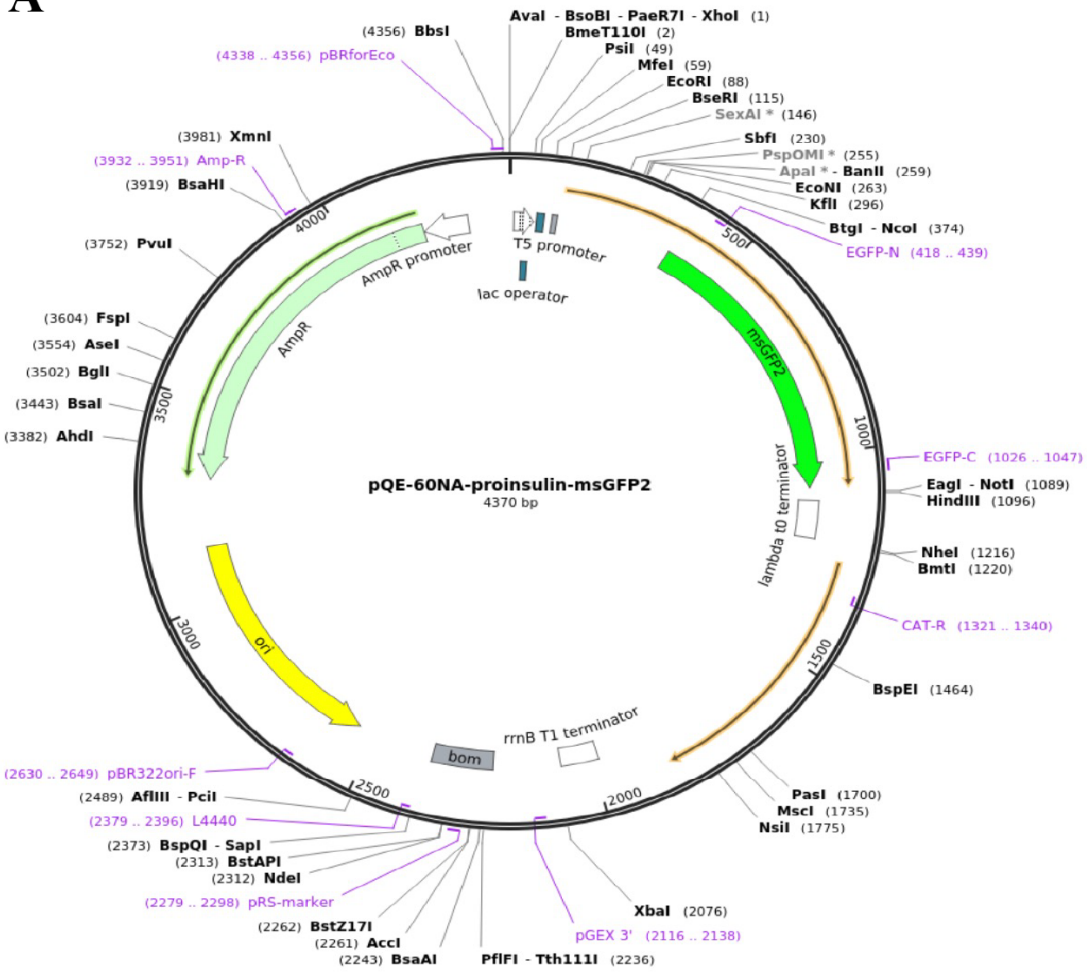
pQE-60NA-proinsulin-msGFP2
4370 bp
AvaI - BsoBI - PaeR7I - XhoI (1)
BmeT110I (2)
PsiI (49)
MfeI (59)
EcoRI (88)
BseRI (115)
SexAI * (146)
SbfI (230)
PspOMI * (255)
ApaI * - BanII (259)
EcoNI (263)
KflI (296)
BtgI - NcoI (374)
EGFP-N (418 .. 439)
EGFP-C (1026 .. 1047)
EagI - NotI (1089)
HindIII (1096)
NheI (1216)
BmtI (1220)
CAT-R (1321 .. 1340)
BspEI (1464)
PasI (1700)
MscI (1735)
NsiI (1775)
XbaI (2076)
pGEX 3' (2116 .. 2138)
PflFI - Tth111I (2236)
BsaAI (2243)
AccI (2261)
BstZ17I (2262)
pRS-marker (2279 .. 2298)
NdeI (2312)
BstAPI (2313)
BspQI - SapI (2373)
L4440 (2379 .. 2396)
AflIII - PciI (2489)
pBR322ori-F (2630 .. 2649)
BbsI (4356)
pBRforEco (4338 .. 4356)
Amp-R (3932 .. 3951)
XmnI (3981)
BsaHI (3919)
PvuI (3752)
FspI (3604)
AseI (3554)
BglI (3502)
BsaI (3443)
AhdI (3382)
T5 promoter
lac operator
AmpR promoter
AmpR
msGFP2
lambda t0 terminator
rrnB T1 terminator
bom
ori
500
1000
1500
2000
2500
3000
3500
4000

B

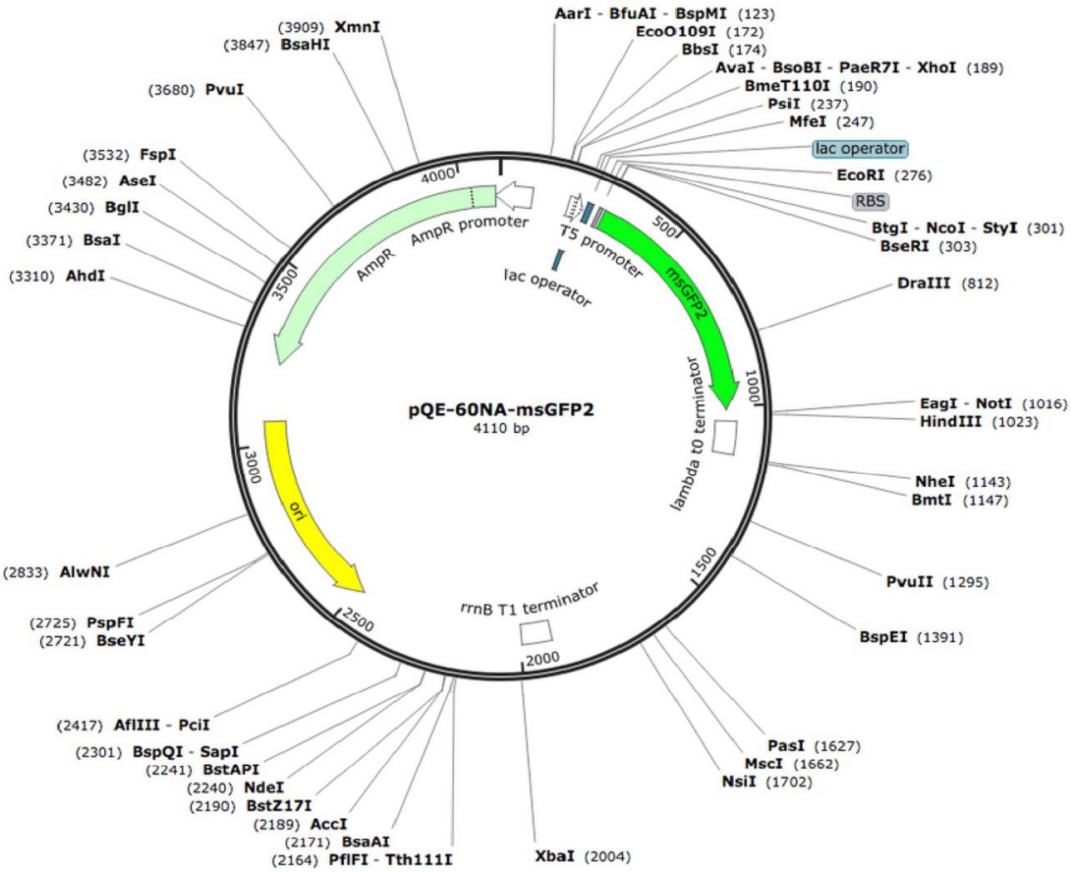

Figure 3-1 Full sequence maps of plasmids

(A) Full sequence maps of pQE-60NA-proinsulin-msGFP2 (Addgene, #160466) and (B) pQE-60NA-msGFP2 (Addgene, #135301) provided by Addgene. Both vector backbones are pQE-60NA and insert genes are proinsulin-msGFP2 and msGFP2, respectively.

Before beginning further experiments including transfection assay on culture INS1 cells, the isolated plasmids were verified by restriction enzyme digest analysis and Sanger sequencing. Based on plasmid maps from Addgene (**Figure 3-1**), I selected two unique restriction endonucleases, *EcoRI* (NEB, #R0101S) and *XbaI* (NEB, #R0145S) for plasmid digest reaction. 1 μg of plasmid with 1 unit of each restriction enzyme, appropriate 10 X reaction buffer and MQ-water was adjusted 50 μl as total reaction volume, then incubated at 37°C. Following a double-digest reaction, the cleaved DNA fragments of plasmids were analyzed on 1.5 % agarose (Bioline, #BIO-41025) gel electrophoresis at 100 V for 1 hour.

Based on the Restriction Analyzer tool (https://molbiotools.com/restrictionanalyzer.php) and plasmid maps (**Figure 3-1**), I expected fragment patterns on a gel (**Figure 3-2A**), which allows me to verify if cloned plasmids contain appropriate backbone and insert sizes.

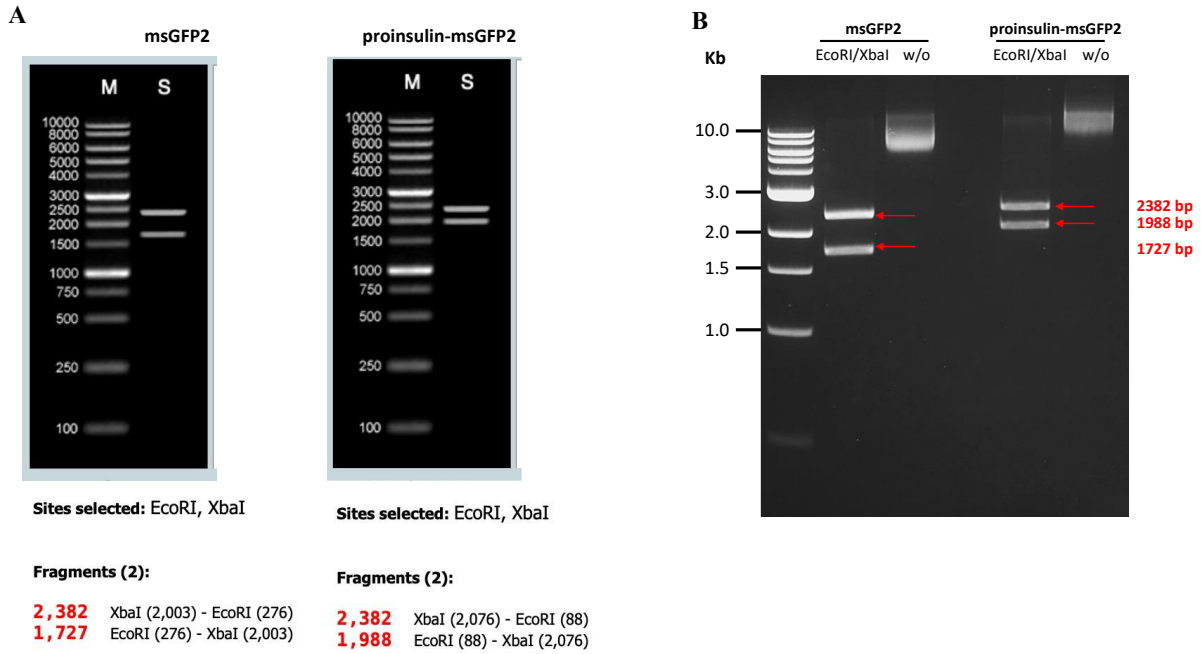

Figure 3-2 Confirmation of cloned proinsulin-msGFP2 and msGFP2 by restriction digest

(A) Expected sizes of cleaved DNA products after digestion with restriction enzymes, *EcoRI* and *XbaI*. Images were generated using the Restriction Analyzer tool. (B) Restriction digest reactions, with/without *EcoR1 and XbaI* were run on agarose gels and the cleaved DNA fragments observed.

For Sanger sequencing analysis of the cloned plasmids from bacterial culture, I used the following primers:

Proinsulin_msGFP2_Forward: 5'- TAGATTCAATTGTGAGCGGATAACAATTTC -3'.

Proinsulin_msGFP2_Reverse: 5'- TGAGGTCATTACTGGATCTATCAACAGGA -3'.

msGFP2_Forward: 5'- TCAATTGTGAGCGGATAACAATTTCACAC -3'.

msGFP2_Reverse: 5'- TGAGGTCATTACTGGATCTATCAACAGGA -3'.

The mixtures with 40 ng of plasmid and 3.2 pmol of primer were analyzed by Sanger sequencing (Sanger Sequencing Service at Garvan Molecular Genetics, Australia) and verified that the cloned plasmid sequences completely agreed with the reference sequences from Addgene (Addgene, #160466 & #135301).

3.2.4 Western blotting

Following transfection with siRNA (negative control or VPS41 siRNA) on INS1 cells, Western blotting assays were performed as described in section 2.2.2.

3.2.5 Immunofluorescence assay

Following transfection with siRNA (negative control or VPS41 siRNA) on INS1 cells, Immunofluorescence assays were performed as described in section 2.2.3.

3.2.6 Glucose-stimulated insulin secretion assay

After 96 hours of transfection with siRNA (negative control or VPS41 siRNA) on INS1 cells, glucose-stimulated insulin secretion assays were performed as described in section 2.2.4. Briefly, at 96 hours after transfection, cells were cultured at low glucose (2.8mM) to achieve baseline for insulin secretion by reducing metabolism, then the cells were exposed to different glucose concentrations either 2.8 or 16.7mM in KRB buffer for 1 hour. Insulin secretion was measured using HTRF assay.

3.2.7 Preparation of LFQ samples and LFQ proteomics analysis

After 48 hours of transfection of 50 pmol siRNA (negative control or VPS41 siRNA), three biological replicates from control and VPS41 KD INS1 cell lines were prepared for label-free quantitative proteomics analysis. LFQ proteomics samples were prepared as described in section 2.2.5. For comparative proteome analysis of control and VPS41 KD INS1 cells, LFQ proteomics analysis was applied using MaxQuant (version 2.0.3.0) followed by data analysis with Perseus software (version 1.6.15.0), R package (version 4.1.1) and R studio.

3.2.8 Statistical analysis

Statistical analyses were performed using GraphPad Prism 9 software using student's t-test, One-way ANOVA or Two-way ANOVA followed by Tukey's comparisons tests (specified in figure legends). Data were presented as mean ± SEM or mean ± SD depending on independent experiment numbers (specified in figure legends).

3.3 Results

3.3.1 Characterization of VPS41 KD INS1 cells

3.3.1.1 Optimization of VPS41 KD in INS1 cells

To investigate VPS41 function in β cells, I used the small siRNA oligomer to transiently deplete endogenous VPS41 in WT INS1 cells. Firstly, I identified the optimized knockdown conditions following transfection with siRNA. To do that, I transfected INS1 cells with different amounts of VPS41 siRNA and non-targeting siRNA (25 ~ 100 pmol) and evaluated expression levels of endogenous VPS41 along with the housekeeping protein, β-actin at different time points post-transfection in a dose and time-dependent manner. Protein extracts from transfected cells were resolved on SDS-PAGE and immunoblotted to determine VPS41 protein expression levels. VPS41 protein levels were quantified using ImageJ software. VPS41 siRNA (50 pmol) had a high KD efficiency with a 90% reduction of endogenous VPS41 (**Figure 3-3A & B**). But endogenous VPS41 levels in INS1 cells transfected with 50 pmol of the non-targeting siRNA were not much changed (**Figure 3-3C & D**). 100 pmol of siRNA was not suitable due to the reduction of the housekeeping protein, β-actin on control siRAN-treated INS1 cells (**Figure 3-3C**), indicating that 100 pmol of siRNA at 96 hours post-transfection can induce cellular damage. Thus, 25 and 50 pmol of siRNA for 48 and 72 hours were selected for further experiments to investigate VPS41 KD effects on INS1 cells.

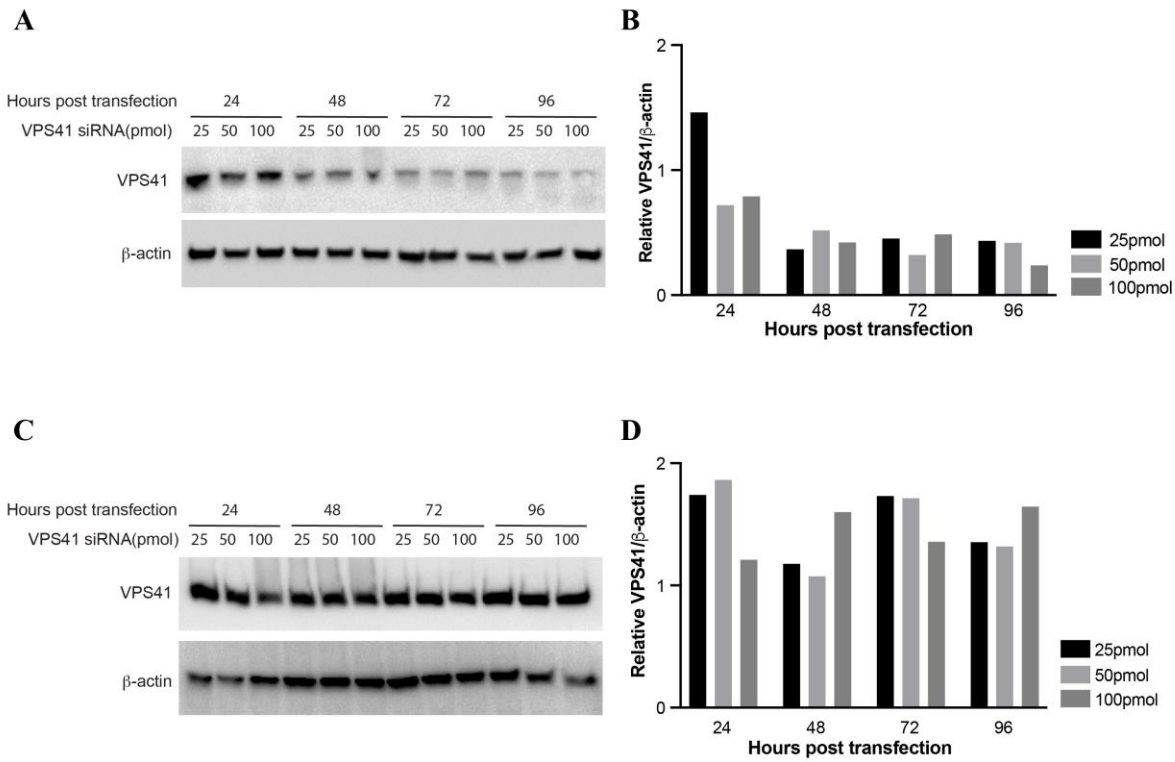

Figure 3-3 VPS41 expression in INS1 cells transfected with VPS41 or non-targeting siRNA

INS1 cells transfected with (A & B) VPS41, or (C & D) non-targeting control siRNA (25 - 100 pmol) were lysed at 24-, 48-, 72- and 96-hours post-transfection. VPS41 and β-actin protein expression in transfected INS1 cells at the indicated times were examined using Western blotting. The relative densitometry of VPS41 protein levels (B & D) was quantified with ImageJ software.

I further optimized the experimental design by testing different transfection methods such as forward, reverse, or dual transfection *via* forward following reverse transfection to examine whether transfection methods affect VPS41 knockdown efficiency. WT INS1 cells were treated with 50 pmol siRNA following the three different transfection procedures and then lysed at 96 hours post-transfection. By Western blot, I observed a significant reduction of endogenous VPS41 in KD INS1 cells; however, no significant differences among the transfection procedures were observed (**Figure 3-4A**). Consistent with the data from VPS41 KO INS1 cell lysates (**Figure 2-1C**), transient deletion of VPS41 *via* siRNA led to a significant decrease in the level of endogenous insulin protein (**Figure 3-4A**, insulin after cutting (pro)insulin std.). Like VPS41 siRNA transfection, the different transfection procedures did not affect insulin levels, suggesting that the transfection method does not significantly affect endogenous levels of VPS41 and insulin in VPS41 KD INS1 cells (**Figure 3-4A**). Thus, I selected the forward transfection method for further experiments.

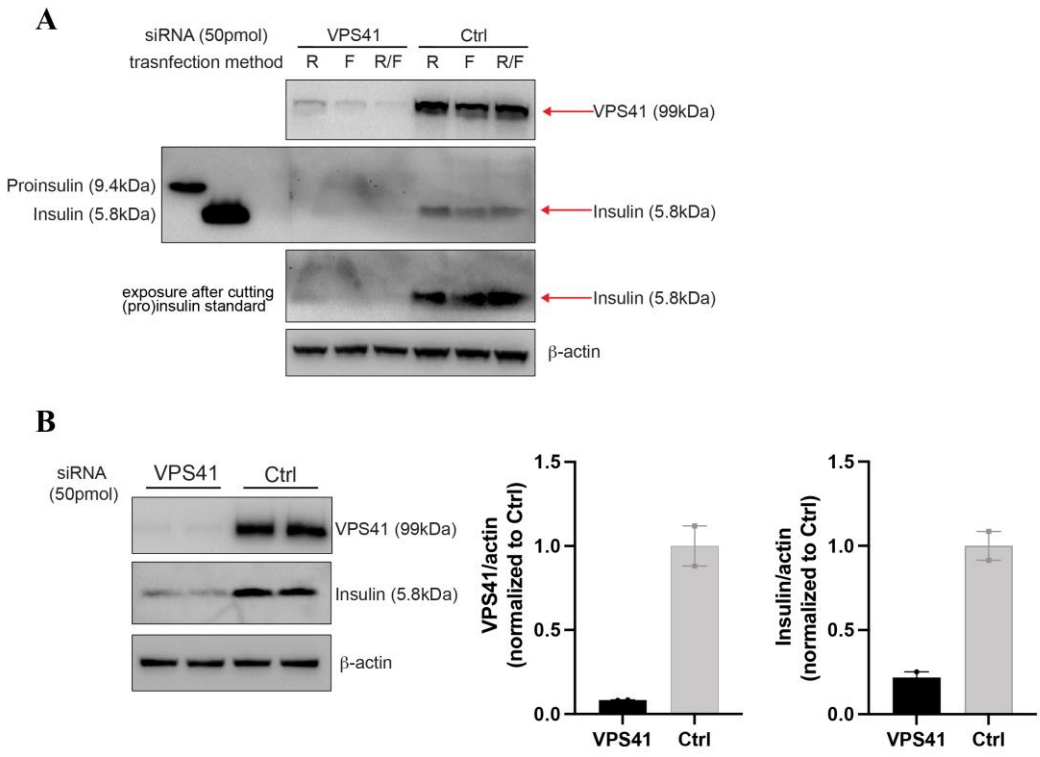

Figure 3-4 VPS41 and insulin expression in INS1 cells transfected with VPS41 and control siRNA

VPS41 and insulin expression in WT INS1 cells post-transfection with VPS41 or non-targeting control siRNA. WT INS1 cells were treated with 50 pmol of siRNA and lysed at 96 hours post-transfection. (A) Reverse (R), forward (F) or double-transfection (R/F) methods were trialed for VPS41 knock-down in WT INS1 cells. Human proinsulin and insulin protein expression were used as standard markers to confirm the expressed insulin in lysates. Proinsulin (300 ng) and insulin (4 μg) standards were used. (B) After protein extraction from the forward transfected INS1 cells, the protein expression intensities of

VPS41 and insulin were quantified by ImageJ software. All the data were presented as mean ± SD from independent experiments and the blot images (B) were from one of the independent experiments.

To confirm if VPS41 KD led to a dramatic reduction of insulin expression in INS1 cells (**Figure 3-4B**), I performed replicate experiments by forward transfection with 50 pmol of VPS41 or nontargeting control siRNA in WT INS1 cells. VPS41 and insulin protein expression levels were determined 96 hours post-transfection by Western blot. As before, VPS41 protein expression was reduced by 90% in VPS41 KD INS1 cells compared to control INS1 cells (**Figure 3-4B**). Consistent with the previous result (**Figure 3-4A**), VPS41 KD cells showed a significant reduction of insulin levels, having 40% less insulin compared to control cells (**Figure 3-4B**). This data indicates that transient VPS41 depletion affects endogenous insulin levels in INS1 cells, suggesting VPS41 function in β cells is intimately connected to insulin protein levels.

3.3.1.2 Glucose-stimulated insulin secretion in VPS41 KD INS1 cells

In vitro characterization of VPS41 KO INS1 cells revealed that chronic VPS41 deletion decreases insulin storage and impairs insulin secretion upon external glucose stimulation in INS1 cells (**Figure 2-3**). To examine the effect of acute depletion of VPS41 on β cell function, I performed GSIS on control siRNA or VPS41 siRNA transfected cells. No significant differences in insulin secretion were observed between VPS41 KD and control INS1 cells exposed to 2.8mM glucose (mean of secretion insulin ± SEM = [2.8mM VPS41KD: **6.42** ± **0.85**] vs [2.8mM Ctrl: **7.81** ± **1.22**]) (**Figure 3-5A**). Like control INS1 cells, VPS41 KD INS1 cells exhibited an approximately 2-fold increase in the insulin secretory response to 16.7 mM glucose stimulation (mean of secretion insulin ± SEM = [2.8mM VPS41KD: **6.42** ± **0.85**] vs [16.7mM VPS41KD: **19.62** ± **3.01**] ($p < 0.05$)) (**Figure 3-5A & C**). Before normalization, VPS41 KO INS1 cells exhibited defective insulin release with significantly reduced secretion under high glucose stimulation (**Figure 2-4B & C**), whereas VPS41 KD INS1 cells did not (**Figure 3-5A**). However, the observed increase in insulin secretion at 16.7mM glucose was insignificant after normalization to DNA content in VPS41 KD INS1 cells (mean of secretion insulin over DNA ± SEM = [2.8mM VPS41KD: **0.13** ± **0.03**] vs [16.7mM VPS41KD: **0.35** ± **0.03**]) (**Figure 3-5C**). The cellular DNA content was measured by DNA picoGreen assay, which was used to normalize secreted insulin on VPS41 KD and control INS1 cells (mean of

DNA ± SEM = [2.8mM VPS41KD: **57.42** ± **7.01**] vs [16.7mM VPS41KD: **56.35** ± **7.21**] vs [2.8mM Ctrl: **60.88** ± **7.76**] vs [16.7mM Ctrl: **65.33** ± **6.89**]) (**Figure 3-5B**).

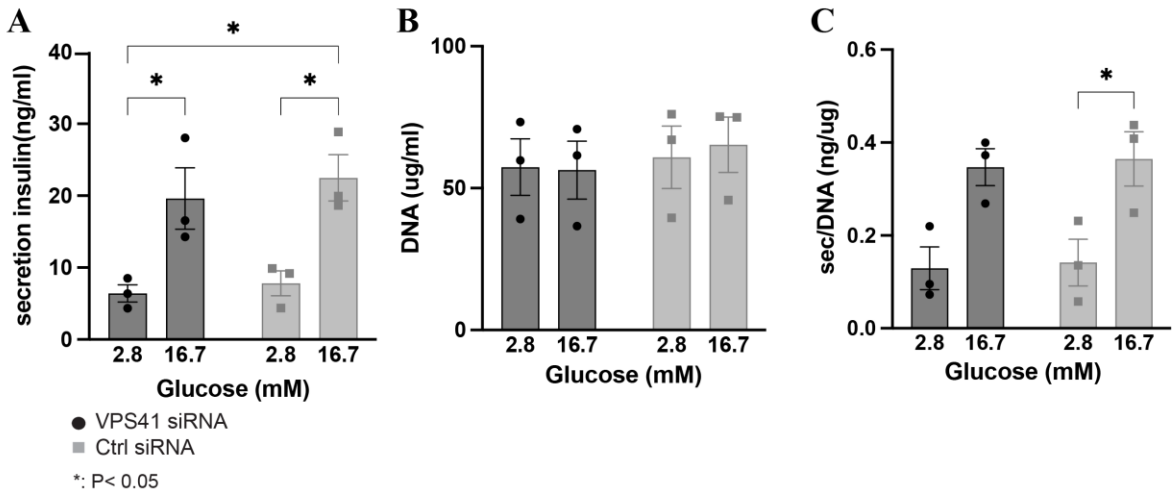

Figure 3-5 Glucose-stimulated insulin secretion in VPS41 KD and control INS1 cells

At 96 hours post-forward transfection with VPS41 or non-targeting siRNA (50 pmol), GSIS was performed. (A) The secreted insulin was measured by HTRF assay following exposure to either 2.8 or 16.7 mM glucose for 1 hour after the achievement of the baseline for insulin secretion. (B) DNA content was measured by DNA picoGreen assay after cell lysis. (C) Secreted insulin was normalized to DNA content. Each value represented the average (3 biological replicates per condition) from individual independent experiments (experiment numbers = 3) and presented as mean ± SEM & *: $p < 0.05$ by using Two-way ANOVA

3.3.1.3 Insulin content in VPS41 KD INS1 cells

Insulin content in the INS1 VPS41 KD and control cells was measured by HTRF assay 96 hours post-transfection. VPS41 KD led to a reduction in insulin content compared to the control (mean of insulin content ± SEM = [VPS41KD: **657.33** ± **58.77**] vs [Ctrl: **1179.37** ± **177.82**]) (**Figure 3-6A**). The decrease in insulin content was significant in VPS41 KD INS1 cells after normalization with DNA content (mean of insulin content over DNA ± SEM = [VPS41KD: **10.08** ± **0.37**] vs [Ctrl: **14.04** ± **1.14**] ($p < 0.05$)) (**Figure 3-6C**).

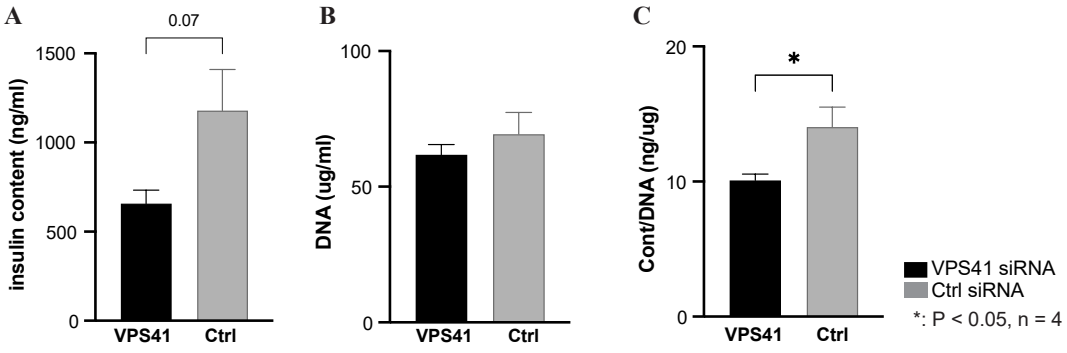

Figure 3-6 Insulin content in INS1 cells after transfection with VPS41 or non-targeting control siRNA

At 96 hours post-transfection with 25pmol VPS41 or non-targeting control siRNA, insulin content in the VPS41 KD and control cells was measured by HTRF assay. (A) Insulin content displayed before normalization with DNA content. (B) DNA content of cell lysates was measured using a DNA picoGreen assay. (C) Insulin content was normalized by DNA content. All the data from replicated independent experiments were presented as mean ± SEM & *: $p < 0.05$ by using unpaired t-test.

3.3.1.4 Distribution of insulin SGs in VPS41 KD INS1 cells

Next, immunofluorescence assays were performed to examine the distribution of insulin SGs containing insulin and proinsulin in INS1 VPS41 KD and control cells. At 96 hours post-transfection, WT INS1 cells were fixed with 4% PFA and immunostained for insulin (DAKO, #A0564). While the majority of insulin accumulated at perinuclear regions in control cells, there was a significant reduction of insulin-positive cells in VPS41 KD INS1 cells (**Figure 3-7**). The quantification of the insulin staining in VPS41 KD cells showed approximately 55% reduction compared to control INS1 cells (mean of relative insulin fluorescence intensity ± SEM = [VPS41si: **0.465** ± **0.056**] vs [Ctrl si: **1.000** ± **0.130**] ($p < 0.01$)) (**Figure 3-7B**).

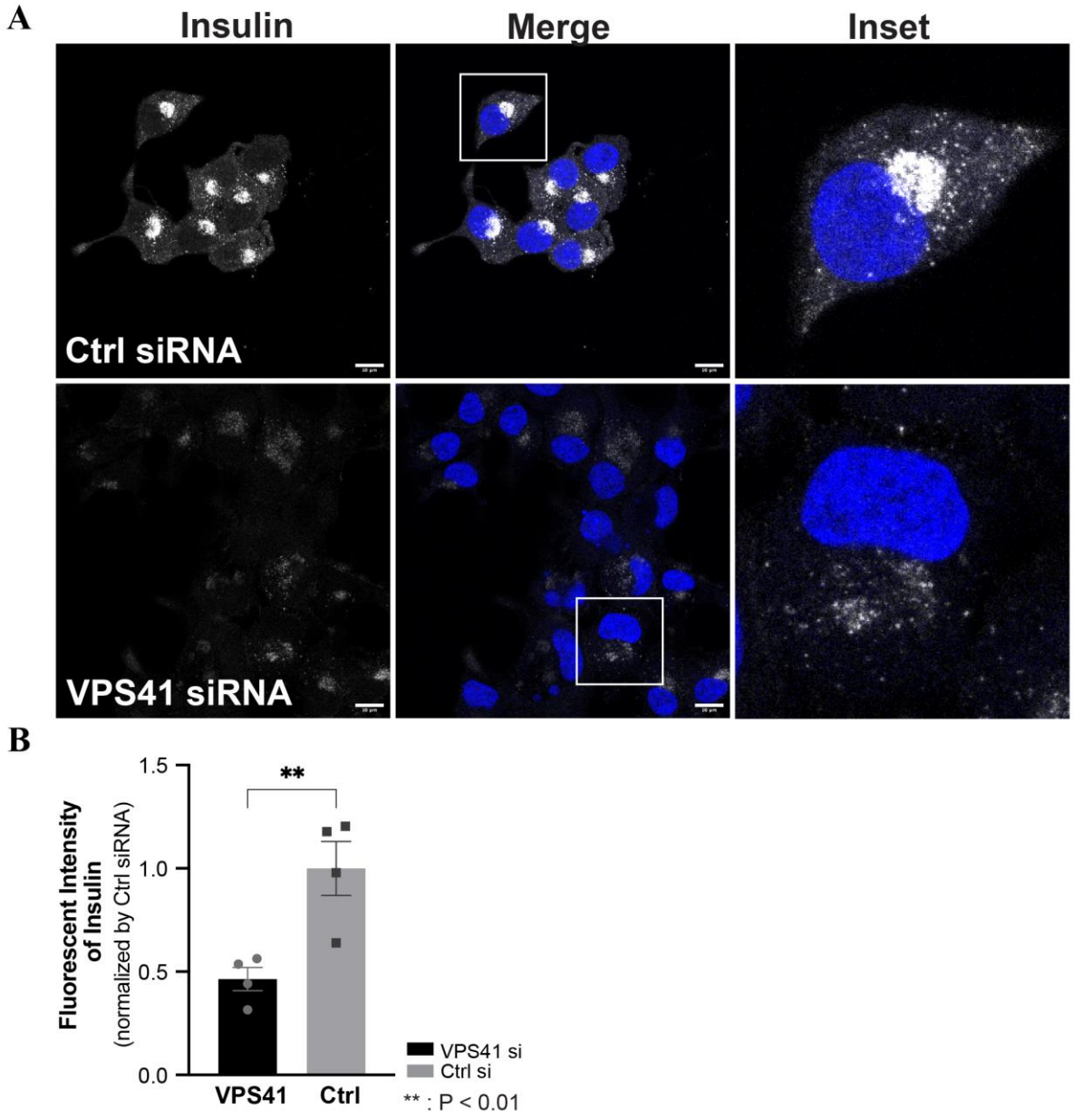

Figure 3-7 Representative immunofluorescence images of insulin and quantified insulin intensity in control and VPS41 KD INS1 cells

INS1 cells were fixed at 96 hours following transfection with 25pmol VPS41 or non-targeting control siRNA. (A) Insulin (grey) immunostaining was shown merged with DAPI (blue). (B) Relative fluorescence intensity of insulin from fluorescence microscopy images was quantified using ImageJ software and then normalized by the value of control siRNA. All the data were presented as mean ± SEM from replicated independent experiments (n=4) & ** $p < 0.01$ using t-test. The scale bar indicates 10μm.

To examine the distribution of immature SGs, immunofluorescent staining was performed using an anti-proinsulin antibody. It is important to note that the anti-insulin antibody (Guinea Pig anti-insulin pre-diluted, DAKO, #A0564) used for immunostaining in this thesis reacts with mature insulin as well as immature proinsulin while the anti-proinsulin antibody (Hybridoma Bank, #GS-9A8) specifically recognizes proinsulin. In the previous chapter, I confirmed the down-regulated trend of proinsulin protein in the absence of VPS41 on INS1 cells compared to WT INS1 cells by performing a western blotting assay (**Figure 2-1C**). The immunostaining against anti-proinsulin antibody also revealed the reduction of proinsulin intensity on VPS41 KD INS1 cells rather than proinsulin build-up (mean of proinsulin intensity ± SEM = [VPS41 si: **0.530 ± 0.015**] vs [Ctrl si: **1.000 ± 0.025**] ($p < 0.0001$)) (**Figure 3-8**), suggesting that the depletion of VPS41 also affects loss of immature as well as mature insulin on β cells.

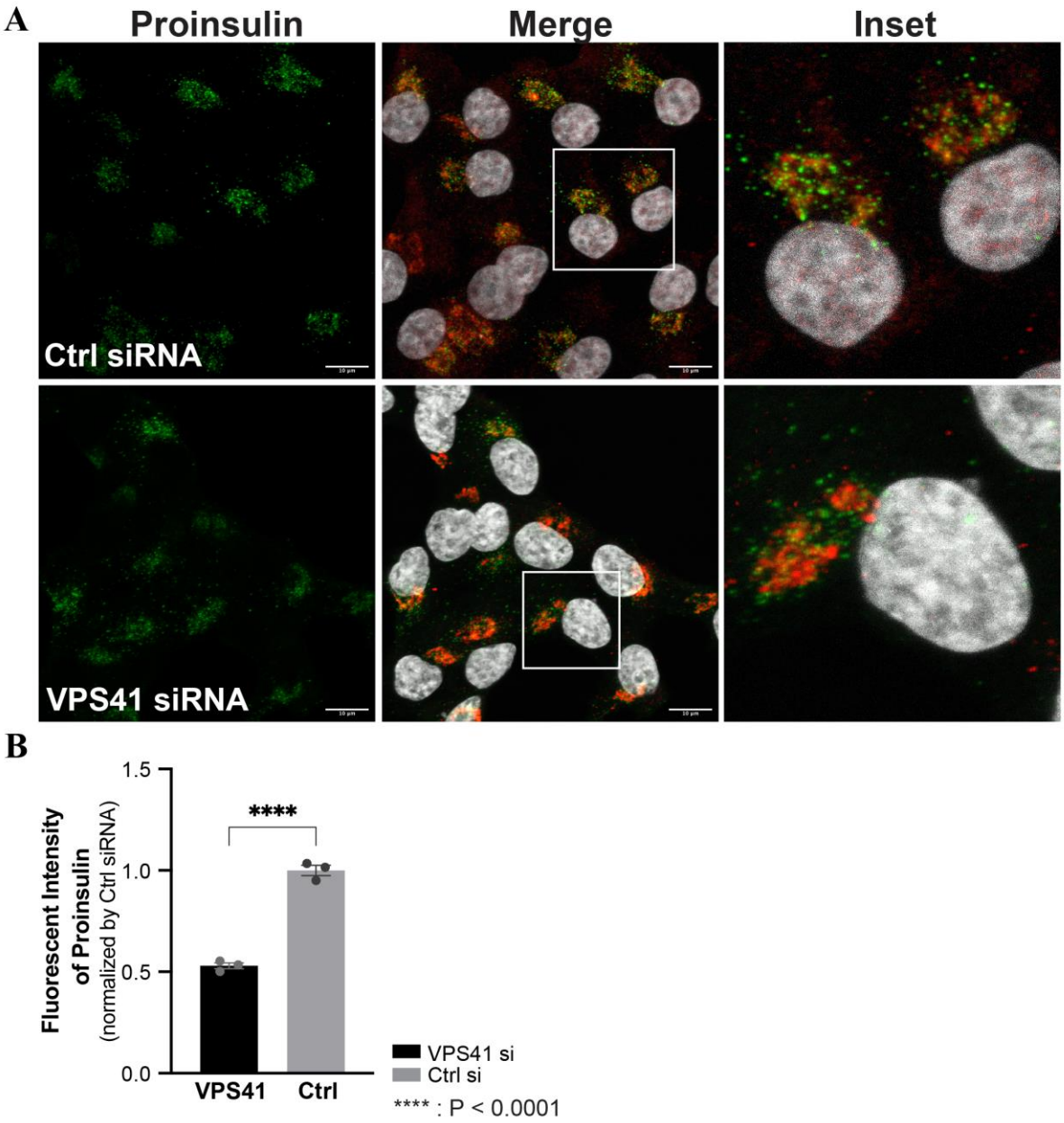

Figure 3-8 Proinsulin staining in control and VPS41 KD INS1 cells

INS1 cells were fixed at 96 hours following transfection with 25pmol non-targeting control (top) or VPS41 siRNA (bottom). (A) Proinsulin (green) immunostaining was shown merged with DAPI (grey) and TGN38 (red). The scale bar indicates 10μm. (B) The relative fluorescence intensity of proinsulin from fluorescence microscopy images was quantified using ImageJ software and then normalized by the value of control siRNA. All the data were presented as mean ± SEM from replicated independent experiments (n=3), **** $p < 0.0001$ using t-test.

3.3.1.5 Label-free quantification (LFQ) proteomic analysis on VPS41 KD INS1 cells

Next, LFQ mass spectrometry analysis was performed to investigate upregulated or downregulated proteins and their relevant pathways on VPS41 KD INS1 cells. The HCL analysis of the quantified proteins and GO term analysis revealed that the proteins relative to intracellular transports or membrane-bounded vesicles were down-regulated on VPS41 KD INS1 cells compared to control cells (**Figure 3-9**). However, I did observe no significant differences for β cell identity genes such as insulin processing (*Pdx1*, *PCSK1* and *PCSK2*) or β cell-disallowed genes including *Ldha*, *Ldhb* and *HK1*. Interestingly, these phenotypes are clearly different between VPS41 KD and VPS41 KO since KO cells *via* chronic *VPS41* gene deletion exhibited a remarkable reduction of proteins related to β cell function, especially β cell identity gene expression (**Figure 2-13 & 2-14**).

Indeed, the Gene Ontology (GO) enrichment analysis provided knowledge of the biological domains with specialized three aspects such as molecular function, biological process, and cellular component between VPS41 KD and control INS1 cells (**Figure 3-10**). Primarily, protein transport activity or intracellular protein transport processing was identified as the enrichment pathways on control cells despite their down-regulation on VPS41 KD INS1 cells (**Figure 3-10B**).

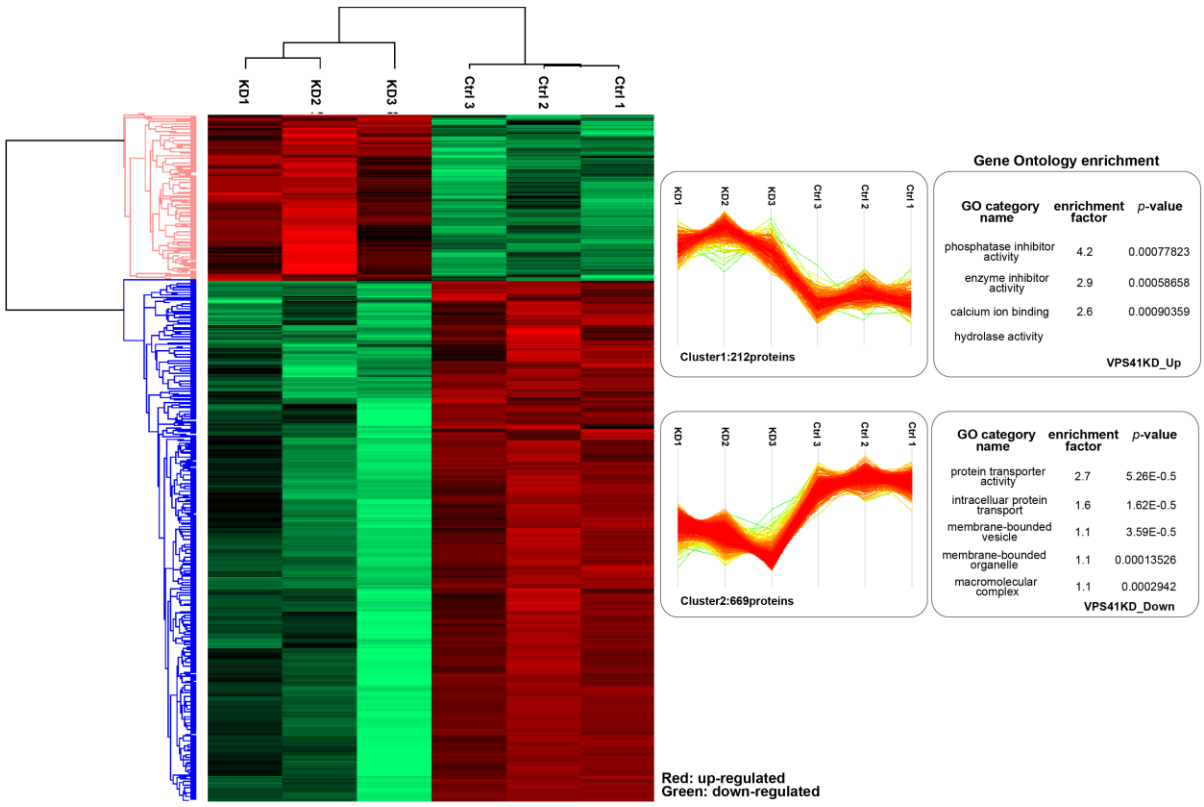

Figure 3-9 The visualized heatmap of significantly regulated proteins on VPS41 KD and control INS1 cells

INS1 cells were lysates at 48 hours following transfection with VPS41 siRNA (KD) or negative control siRNA (Ctrl) for LFQ mass spectrometry analysis. Gene ontology (GO) analysis shows enriched pathways with enrichment factors on VPS41 KD or control INS1 cells.

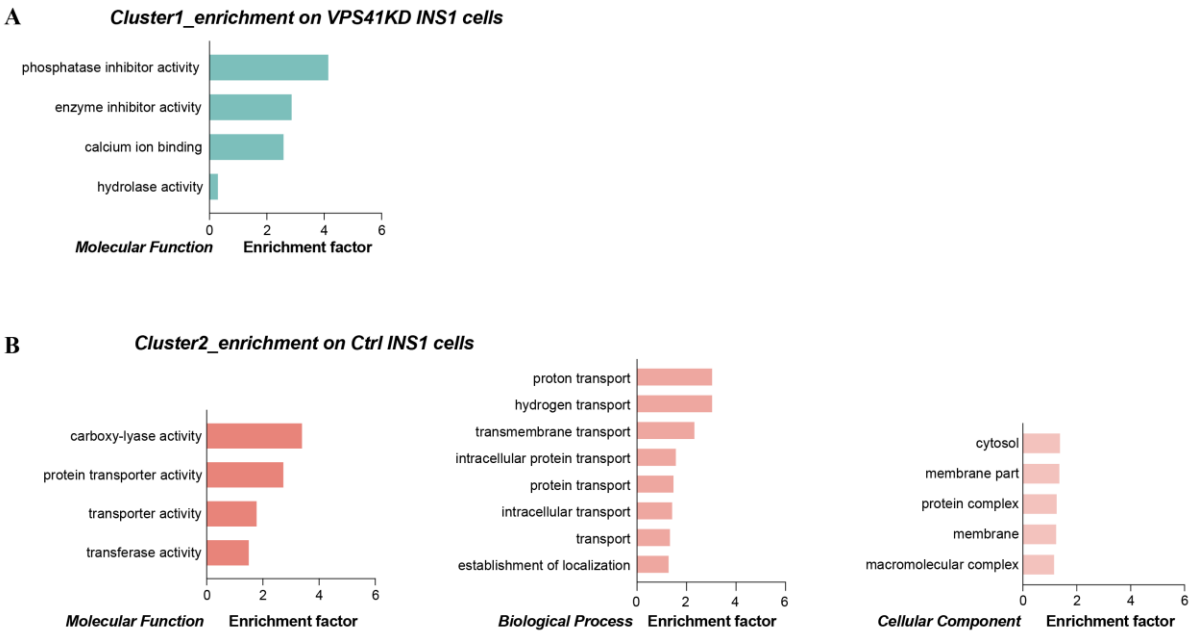

Figure 3-10 Gene ontology enrichment analysis on VPS41 KD and control INS1 cells

Gene ontology enrichment analysis shows the functional annotation of proteins with GO term in Cluster 1 (**A**, up-regulated pathways on VPS41 KD INS1 cells) and Cluster 2 (**B**, up-regulated pathways on control INS1 cells).

The normalized log2 LFQ intensity also showed that *Pdx1*, *PCSK1* and *PCSK2* associated with β cell features were not significantly altered while the remarkable reduction of *VPS41* or *Insulin-1* was observed on VPS41 KD INS1 cells (**Figure 3-11**).

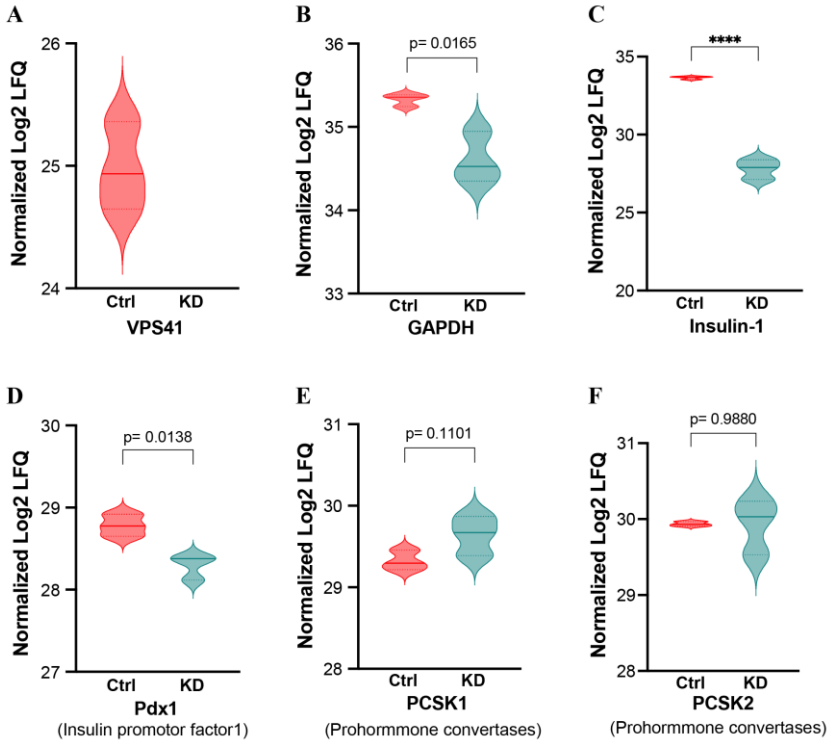

Figure 3-11 LFQ intensities of proteins associated with β cell features

Violin plots display LFQ intensities of single proteins of special interest associated with β cell feature (C, D, E, F), VPS41 (A) as well as housekeeping protein (B). Data were represented as mean ± SEM, **** $p < 0.0001$ by using an unpaired t-test.

3.3.2 The effect of inhibiting protein degradation pathways to restore insulin content in VPS41 KD INS1 cells

Like VPS41 KO INS1 cells, VPS41 KD INS1 cells have an abnormal phenotype of reduced insulin content. However, the link between dysfunctional VPS41 *via* chronic or acute gene deletion, and loss of insulin storage within INS1 cells remains a core question to understanding VPS41 function in β cells. Decreased insulin content could be due to a defect in insulin processing, but it could also result from enhanced insulin degradation. VPS41 is known as a cytosolic-resident protein and a vesicle-sorting membrane component involved in protein trafficking pathways [164,198,210]. In this light, deficient VPS41 in insulin-producing β cells could not directly affect proinsulin protein synthesis through *INS* gene transcription in the nucleus or preproinsulin mRNA translation in the ER due to VPS41's intracellular localization (being related to its function). Additionally, it has been reported that VPS41 functions as a sorting protein of secretory granules and forms coat-structures with AP-3 via direct interaction on the granule membranes [164,191]. Therefore, it led to hypothesis that insulin granules may be shunted to proteasome-mediated degradation or delivery to the lysosome through cellular protein degradation pathways in β cells that lack VPS41 (**Figure 3-12**).

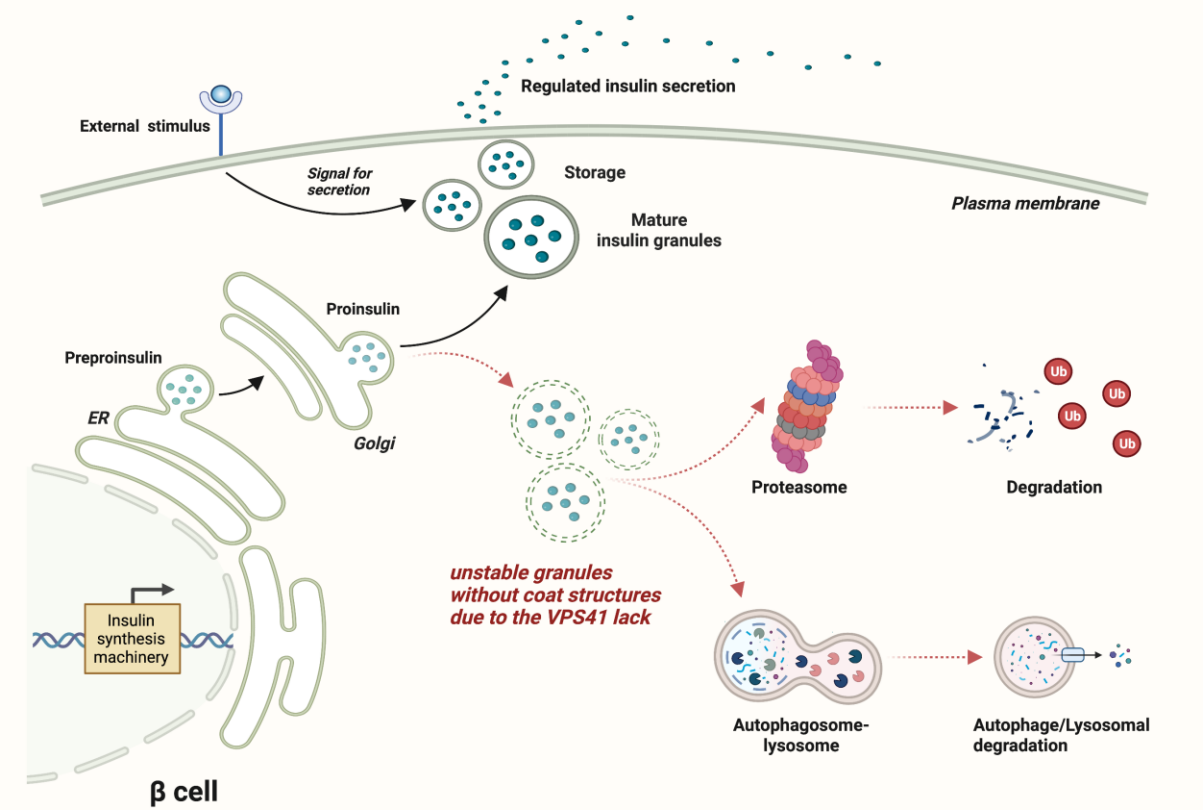

Figure 3-12 Possible model of insulin granules degradation in the absence of VPS41 in pancreatic β cells

In the absence of VPS41, the budding vesicle is unable to form coat structures on insulin granule membranes, consequently the granules are delivered to protein degradation pathways including proteosome-mediated degradation or lysosome degradation. VPS41-depleted β cells have significantly decreased insulin storage capacity which could result in dysfunctional β cells. *Created in BioRender.com*

To test the hypothesis that the lack of VPS41 results in enhanced insulin granules degradation in INS1 cells, I first examined poly-ubiquitinated protein expression on WT and VPS41 KO INS1 cells under normal culture conditions of 11mM glucose.

Ubiquitinated protein expression was significantly higher in VPS41 KO INS1 cells than WT INS1 cells (mean poly-ubi protein ± SEM = [WT: **1.00** ± **0.06**] vs [KO: **1.70** ± **0.01**]) ($p < 0.05$)) (**Figure 3-13**). Cell treatment with MG132 (10μM), a proteasome inhibitor, led to the accumulation of poly-ubiquitinated proteins in both WT and VPS41 KO INS1 cells due to the inhibition of proteasomal degradation of ubiquitin-tagged proteins (mean poly-ubi protein ± SEM = [WT: **1.00** ± **0.06**] vs [KO: **1.70** ± **0.01**] ($p < 0.05$) or [KO_MG: **2.00** ± **0.11**] ($p < 0.005$)) (**Figure 3-13**). Consistently, and importantly, the hierarchical clustering analysis of the proteomic data revealed enriched protein clusters associated with ubiquitin-mediated proteolysis pathways in VPS41 KO INS1 cells (**Figure 2-14B**).

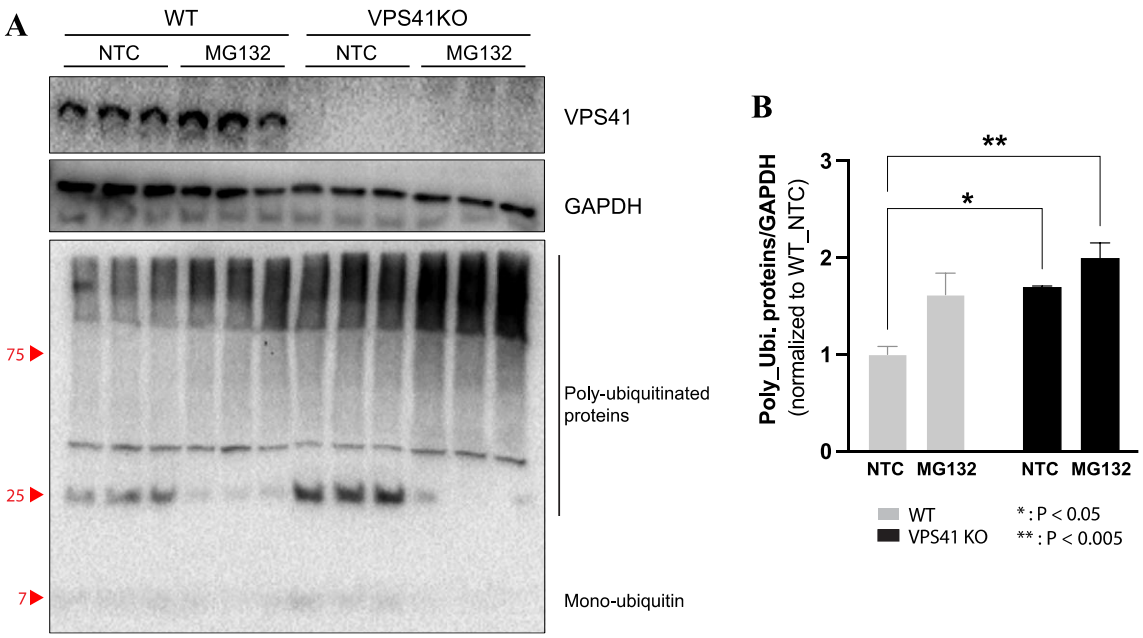

Figure 3-13 Expression of poly-ubiquitinated proteins in WT and VPS41 KO INS1 cells treated with or without MG132

(A) WT and VPS41 KO INS1 cells, cultured with normal conditions, were treated with MG132 (10μM) for 4 hours and the cells lysed. Protein extracts (25ug) were run on SDS-PAGE and immunoblotted for poly-ubiquitinated proteins. (B) The intensity values of poly-ubiquitinated protein levels were quantified using Image J software and normalized against non-treated WT INS1 (WT_NTC) cells. The data were presented as mean ± SEM, *: $p < 0.05$ & **: $p < 0.005$ by using two-way ANOVA.

To examine whether the loss of insulin content is due to enhanced protein degradation in the absence of VPS41 in INS1 cells, protein degradation pathways were inhibited using different types of pharmacological inhibitors including chloroquine (CQ), MG132, E-64 and NH_4Cl. I performed several optimized experiments to establish the correct dose and time of inhibitor treatments on INS1 cells. The details of each inhibitor were emphasized and described in Appendix.

Upon protein degradation pathway inhibition, VPS41 and insulin proteins expression was evaluated in VPS41 KD and control INS1 cells by performing the western blotting assay. Consistently, VPS41 siRNA transfection of the INS1 cells led to reduced expression of VPS41, which was approximately 50% decrease of control cells (mean VPS41/actin ± SEM = [NTC VPS41si: **0.439** ± **0.034**] [DMSO VPS41si: **0.575** ± **0.128**] [CQ VPS41si: **0.473** ± **0.117**] [MG132 VPS41si: **0.537** ± **0.089**] [E64 VPS41si: **0.650** ± **0.114**] [NH_4Cl VPS41si: **0.595** ± **0.080**] vs [NTC Ctrl si: **1.000** ± **0.145**] ($p < 0.05$) or [DMSO Ctrl si: **1.190** ± **0.215**] ($p < 0.005$)) (**Figure 3-14A & B**). VPS41 KD led to reduced endogenous insulin levels in both non-treated and DMSO negative control, compared to insulin expression in control INS1 cells (mean insulin/actin ± SEM = [NTC VPS41si: **0.590** ± **0.229**] [DMSO VPS41si: **0.385** ± **0.083**] vs [NTC Ctrl si: **1.000** ± **0.156**] [DMSO Ctrl si: **0.999** ± **0.089**]). Reduced insulin expression was restored when protein degradation pathways were inhibited in VPS41 KD INS1 cells, however showing a statistically significant difference only on CQ-treated or E-64 treated KD INS1 cells compared to untreated VPS41 KD INS1 cells (mean insulin/actin ± SEM = [CQ VPS41si: **1.292** ± **0.095**] [E-64 VPS41si: **1.354** ± **0.014**] vs [NTC VPS41si: **0.590** ± **0.229**]) (**Figure 3-14A &C**). The degree of insulin expression rescue was different depending on the protein degradation pathways inhibited in the KD INS1 cells; however, lysosomal inhibitors, CQ and E-64, more effectively restored endogenous insulin expression compared to the other inhibitors (**Figure 3-14**). These findings indicated that insulin is shunted to protein degradation pathways, especially the lysosomal-mediated degradation pathway instead of being targeted into the regulated secretory pathway in INS1 cells that lack VPS41.

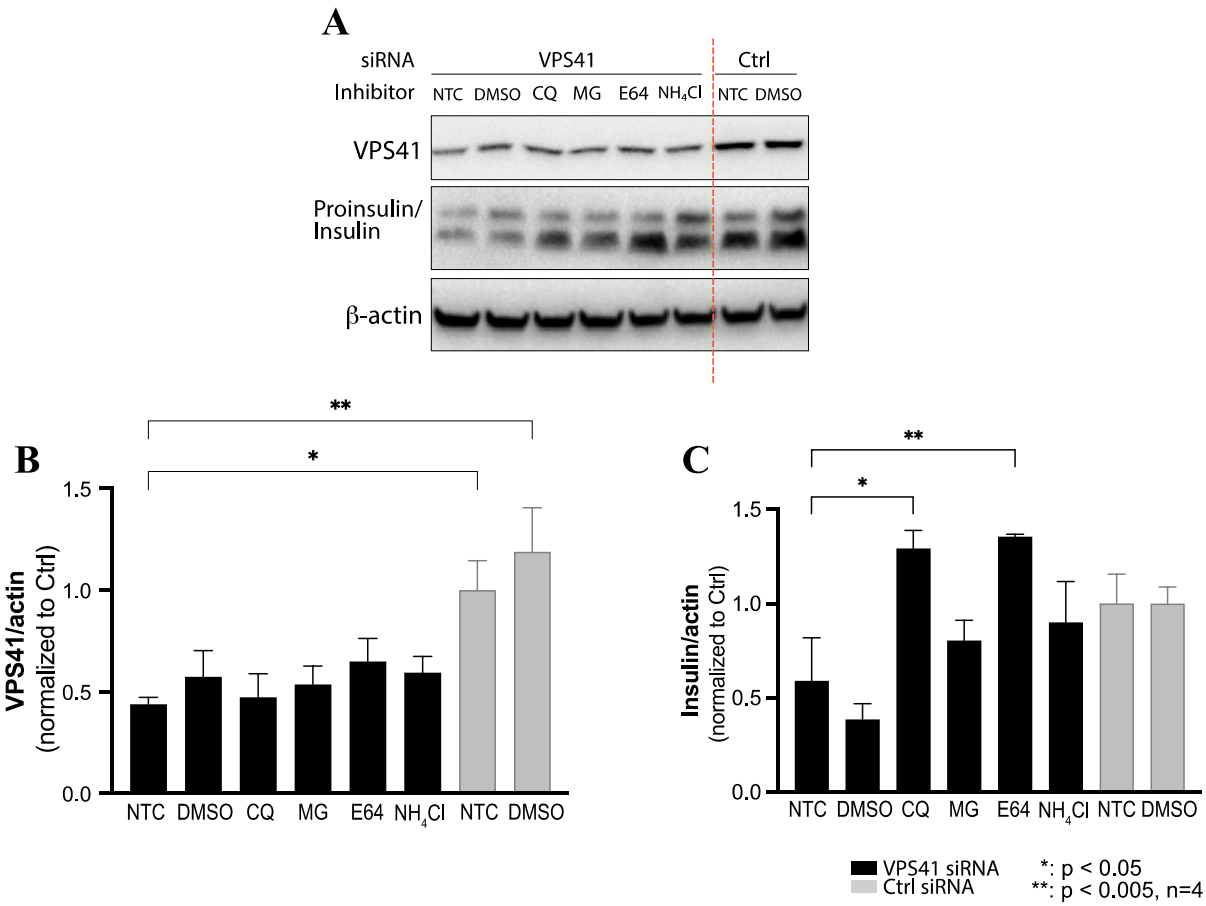

Figure 3-14 VPS41 and insulin expression in INS1 cells treated with inhibitors of protein degradation

INS1 cells were treated with different protein degradation inhibitors including CQ, MG132, E-64 and NH_4Cl, then transfected with VPS41 or non-targeting control siRNA. (A) At 24 hours post-transfection, cells were lysed with SDS lysis buffer, the protein extracts were resolved on SDS-PAGE and the protein expression of VPS41, and insulin was examined by immunoblotting. (B) The intensity values of VPS41 and (C) insulin protein bands were quantified using Image J software. The pool quantified results of VPS41, and insulin protein expression were obtained from independent experiments (n=4). All the data were presented as mean ± SEM, *: $p < 0.05$ & **: $p < 0.005$ by using One-way ANOVA.

3.3.3 Distribution of insulin granules following proinsulin-GFP transfection in INS1 cells

INS1 cells that lack VPS41 either transiently or chronically have significantly decreased insulin content causing them to be dysfunctional β cells. As described earlier, I hypothesized that deficient VPS41 alters insulin granules' storage capacity through enhanced insulin degradation, or the absence of VPS41 on INS1 cells could impair insulin processing thereby reducing insulin expression in INS1 cells. To study the latter hypothesis and possible mechanisms, I transiently transfected exogenous proinsulin encoding photostable GFP (green fluorescent protein) (Addgene, #160466, **Figure 3-1**) in INS1 cells to evaluate the processing of newly synthesized insulin by monitoring GFP expression in transfected cells. In addition, immunofluorescence studies of GFP-tagged proinsulin movement are a useful strategy to study insulin trafficking.

To optimize the transfection efficiency of exogenous proinsulin-GFP and minimize an overloaded GFP effect, different amounts of plasmid were transfected into INS1 cells. Proinsulin-GFP transfection causes the overexpression of proinsulin in the WT cells, which could impact the ability to obtain consistent immunofluorescence images. WT INS1 cells were cultured in complete RPMI containing 11mM glucose for 48 hours after transfection, fixed with 4% PFA and mounted with DAPI. Differing DNA concentrations did not significantly affect the proinsulin staining localization in the transfected cells. Indeed, the majority of the proinsulin-tagged GFP is localized to the perinuclear region regardless of transfected GFP-proinsulin DNA concentrations (**Figure 3-15**).

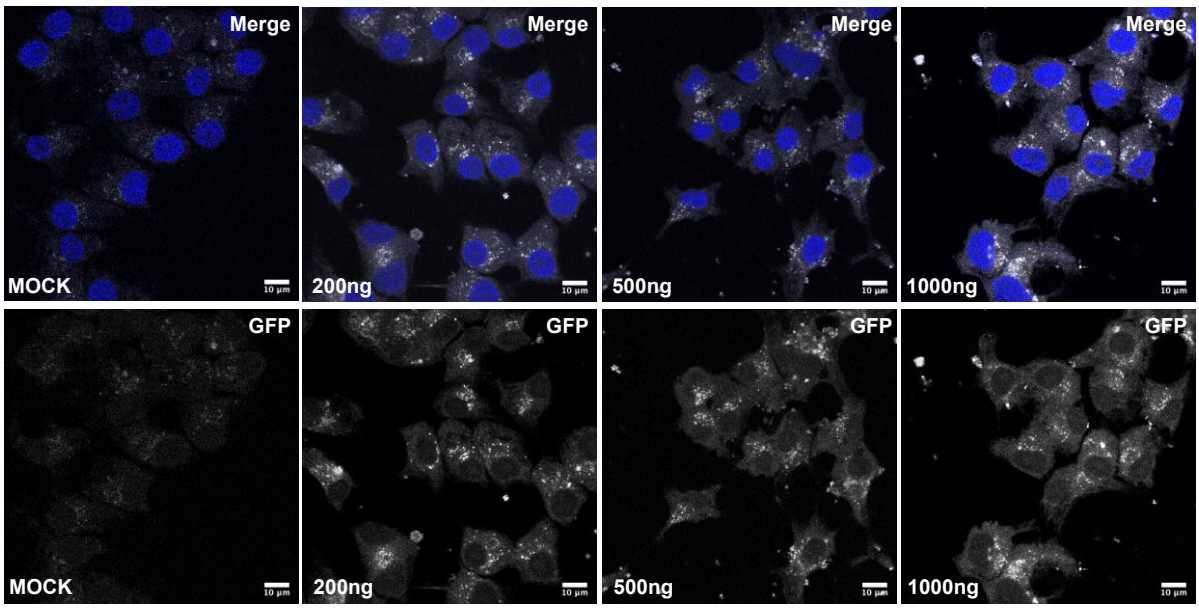

Figure 3-15 GFP-tagged proinsulin immunofluorescence images in WT INS1 cells

WT INS1 cells were transfected with GFP-tagged proinsulin construct, with indicated amounts using Lipofectamine 2000 transfection reagent. Cells were fixed with 4% PFA and were mounted with DAPI (blue). GFP (gray) fluorescence images were captured on a confocal microscope. Scale bar indicates 10μm.

To examine whether loss of VPS41 impairs insulin processing in INS1 cells, both WT and VPS41 KO INS1 cells were transfected with GFP-tagged proinsulin. By monitoring the subcellular localisation of exogenous proinsulin by the GFP tag, the role of VPS41 on insulin processing could be determined. VPS41 KO INS1 cells did not express GFP-tagged proinsulin post-transfection (**Figure 3-16B**) while in WT INS1 cells, the GFP-tagged proinsulin and insulin expression were observed in the perinuclear region (**Figure 3-16A**). Consistent with this observation, the proteomics analysis revealed that VPS41KO on INS1 cells have down-regulated β cell-identity genes such as *Ins2* and *Pdx1* (**Figure 2-13**) and less-enriched expression proteins associated with insulin secretory machinery such as insulin SG biogenesis and vesicle-mediated transport proteins (**Figure 2-14**).

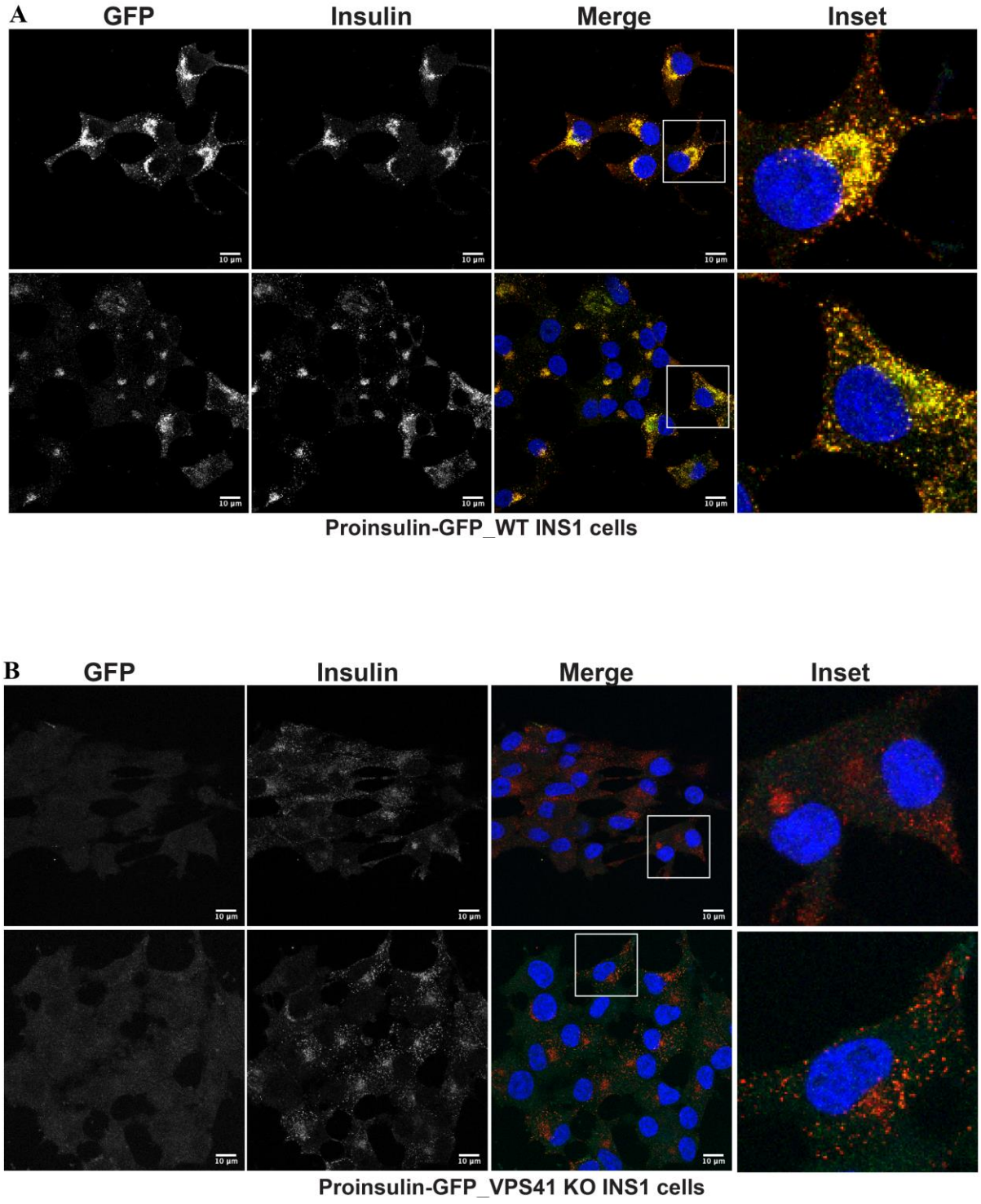

Figure 3-16 GFP-tagged proinsulin and insulin immunofluorescence staining in GFP-tagged proinsulin transfected WT and VPS41 KO INS1 cells

(A) WT ISN1 and (B) VPS41 KO INS1 cells were fixed on coverslips at 48 hours after transfection with GFP-tagged proinsulin. GFP fluorescence (green at merge) and insulin fluorescence (red at merge) images. All fluorescent images were captured on confocal microscope. The Scale bar indicates 10µm.

Collectively, the immunofluorescence studies of proinsulin subcellular localization in VSP41 KD cells (**Figure 3-8**) and of GFP-tagged proinsulin in VPS41 KO INS1 cells (**Figure 3-16B**), as well as the proteomics analysis on VPS41 KO INS1 cells (**Figure 2-13 & 2-14)**, show VPS41 lack impairs the ability of cells to express proinsulin. It is likely that these phenotypes are due to the downregulation of β cell-identified genes such as *Ins1*, *Ins2* and *Pdx1* on VPS41-depleted INS1 cells.

3.3.4 Adaptor-protein 3 complexes in VPS41-depleted INS1 cells

Inhibition of proteolysis by pharmacological inhibitors, especially CQ and E-64, restored insulin expression to endogenous protein levels in VPS41 KD cells (**Figure 3-14**). Thus, reduced insulin content in VPS41 KD INS1 cells is strongly correlated with enhanced lysosomal proteolysis; however, the mechanism of how insulin granules are selectively degraded instead of being targeted to the regulated secretory pathway in VPS41 deficient cells is unclear.

VPS41 is required for the transport of secretory granules including insulin granules and the trafficking of lysosomal membrane proteins [165,183,189,191]. VPS41's interaction with AP-3, a cytosolic component in forming coat structures in membrane-bounded vesicles, has been reported to be essential for both these functions of VPS41 [164,182]. Thus, I propose that in the absence of VPS41, AP-3-mediated insulin granules transport towards proteolysis rather than the regulated secretory pathways on INS1 cells.

Endogenous AP-3 protein expression was not different amongst WT, VPS41 KO and rescue INS1 cells despite the marked reduction of endogenous insulin in VPS41 KO cell lysates (**Figure 2-1A**). In addition, the endogenous levels of proteins including LAMP1 and LC3A/B which are involved in autophagy-lysosome-mediated proteolysis were not significantly different regardless of VPS41 KD (**Figure 3-17**). However, the endogenous CgA known as a cargo protein of insulin SGs [49,211], exhibited a time-dependent reduction following VPS41 KD in INS1 cells (**Figure 3-17**). This suggests that the membrane-bounded insulin SGs containing insulin as well as CgA could be the target for the trafficking into the proteolysis in the absence of VPS41. Based on these results, I monitored the distribution of AP-3 complexes together with subcellular compartments relevant to proteolysis. The result would provide evidence that the membrane-bounded granules containing insulin are transported into the proteolysis upon the lack of VPS41. Hence, this can be the possible answer for poor insulin storage in VPS41-deficient pancreatic β cells.

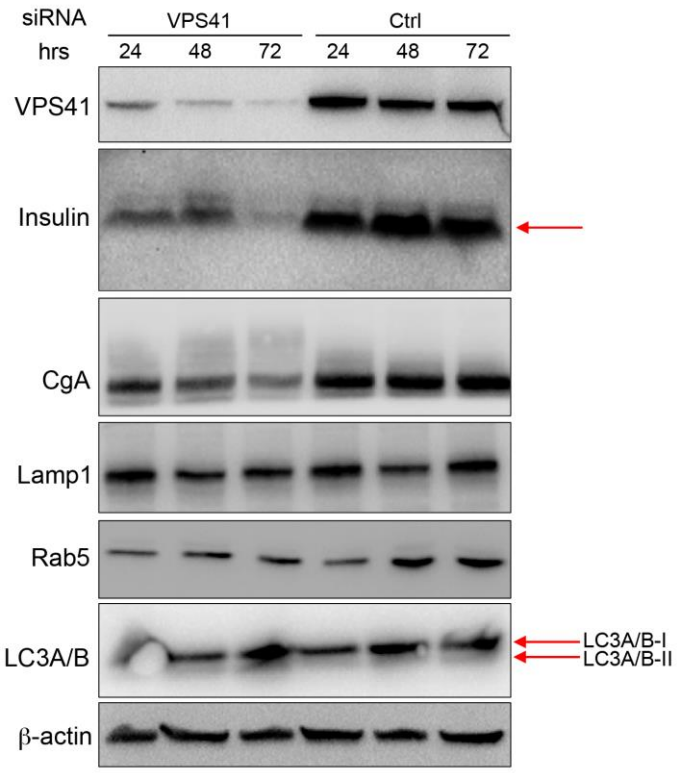

Figure 3-17 Expression of proteins relevant to autophagy-lysosomal mediated proteolysis and insulin secretory granules in WT control and VPS41 KD INS1 cells

WT INS1 cells were transiently transfected with VPS41 or non-targeting control siRNA (50 pmol). Cells were lysed with SDS-lysis buffer at the indicated time points. Protein extracts (25µg) were resolved on SDS-PAGE and immunoblotted for proteins involved in autophagy-lysosomal mediated proteolysis and insulin secretory granules.

To do that, I examined co-localization of AP-3 complexes with several components including the trans-Golgi marker TGN38, SG marker CgA, lysosomal marker LAMP1, autophagosomal marker LC3A/B and endosome marker Rab5A by performing the immunofluorescence assay. Co-staining with CgA or LC3A/B and the correlation analysis between AP-3 using Pearson's coefficient revealed that the majority of AP-3 was co-localized with CgA with predominant localization around the peri-nuclear region, while AP-3 staining did not overlap with LC3A/B, the autophagosomal marker in WT INS1 cells (mean of Pearson's coefficient ± SEM = [AP-3 × CgA: **0.718** ± **0.048**] vs [AP-3 × LC3A/B: **0.442** ± **0.039**] ($p < 0.005$)) (**Figure 3-18**). These data suggest AP-3 complexes facilitate the trafficking of vesicles towards the regulated secretory pathway instead of proteolysis in WT INS1 cells under steady-state conditions.

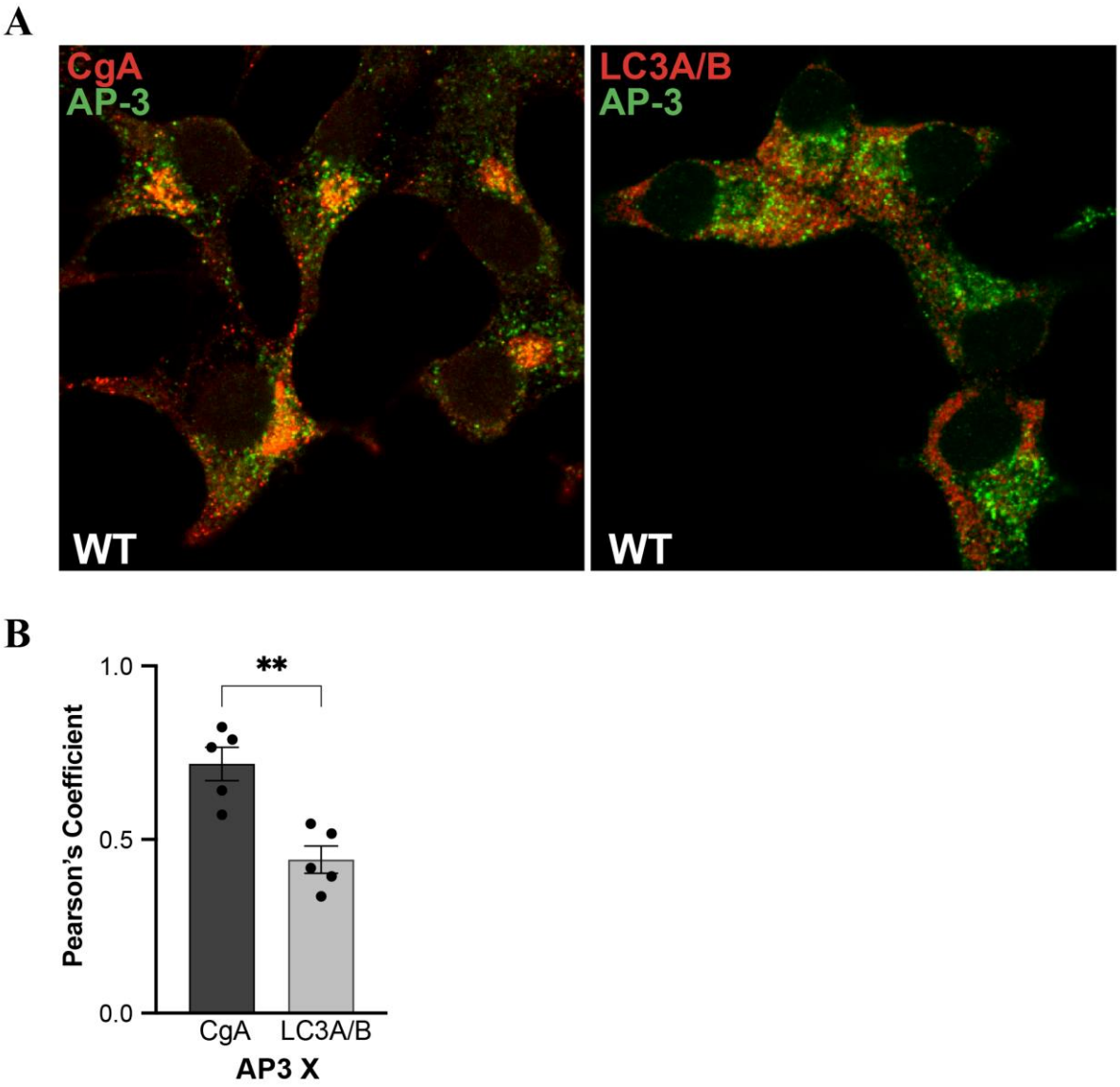

Figure 3-18 Immunofluorescence co-staining of AP-3 with CgA and LC3A/B in WT INS1 cells

(A) AP-3 was co-stained with CgA, an SG marker or LC3A/B, an autophagosomal marker in WT INS1 cells. AP-3 fluorescence (green), CgA fluorescence (red) and LC3A/B fluorescence (red). The fluorescence images were captured on a confocal microscope. (B) Pearson's coefficient of correlation between AP-3 and CgA versus AP-3 and LC3A/B was analyzed by Image J software. Data were presented as mean ± SEM and comparisons were made using unpaired t-test & **: $p < 0.005$.

Next, to get further insights into the potential role that AP-3 may play in vesicle transport in the absence of VPS41, the subcellular localization of AP-3 on INS1 cells were examined by immunostaining with an antibody that recognizes the δ subunit of AP-3 together with markers of specialized secretory pathways, e.g., insulin, CgA (SG marker), Rab5 (early-endosome marker) and LAMP1 (lysosome-related marker) (**Figure 3-19**) at 48 hours following transfection with siRNA. In control INS1 cells, AP-3 displayed a punctate pattern across the cytoplasm but most of the AP3 was accumulated in the perinuclear region, likely within the Golgi complex (**Figure 3-19**). In VPS41 KD cells, the distribution of AP-3 was spread out more toward the cell periphery (**Figure 3-19**). Further, in control cells, AP-3 was co-localized with insulin in the perinuclear region, however this co-localization was markedly diminished in VPS41 KD cells probably due to the extensive loss of insulin SGs combined with the redistribution of AP-3 throughout the cell periphery as indicated by Pearson's coefficient of correlation between AP-3 and insulin (mean of Pearson's coefficient ± SEM = [Ctrl siRNA of AP-3 × Insulin: **0.604** ± **0.019**] vs [VPS41 siRNA of AP-3 × Insulin: **0.373** ± **0.041**] ($p < 0.0005$)) (**Figure 3-19A**). The distribution of LAMP1 and Rab5 also showed clear differences between control and VPS41 KD INS1 cells (**Figure 3-19C & D**). In control cells, LAMP1 was detected across the plasma membrane as well as the perinuclear region where it co-localized with AP-3. However, like AP-3, in the absence of VPS41, LAMP1 became redistributed from the plasma membrane and the perinuclear area and spread throughout the cell cytoplasm, which was analyzed by Pearson's coefficient of correlation using Image J software (mean of Pearson's coefficient ± SEM = [Ctrl siRNA of AP-3 × LAMP1: **0.446** ± **0.068**] vs [VPS41 siRNA of AP-3 × LAMP1: **0.646** ± **0.019**] ($p < 0.05$)) (**Figure 3-19C**). Similarly, Rab5 was redistributed from the perinuclear area in control cells toward the cell periphery following the deletion of VPS41 although there was no significant difference between control and KD INS1 cells (**Figure 3-19D**).

A

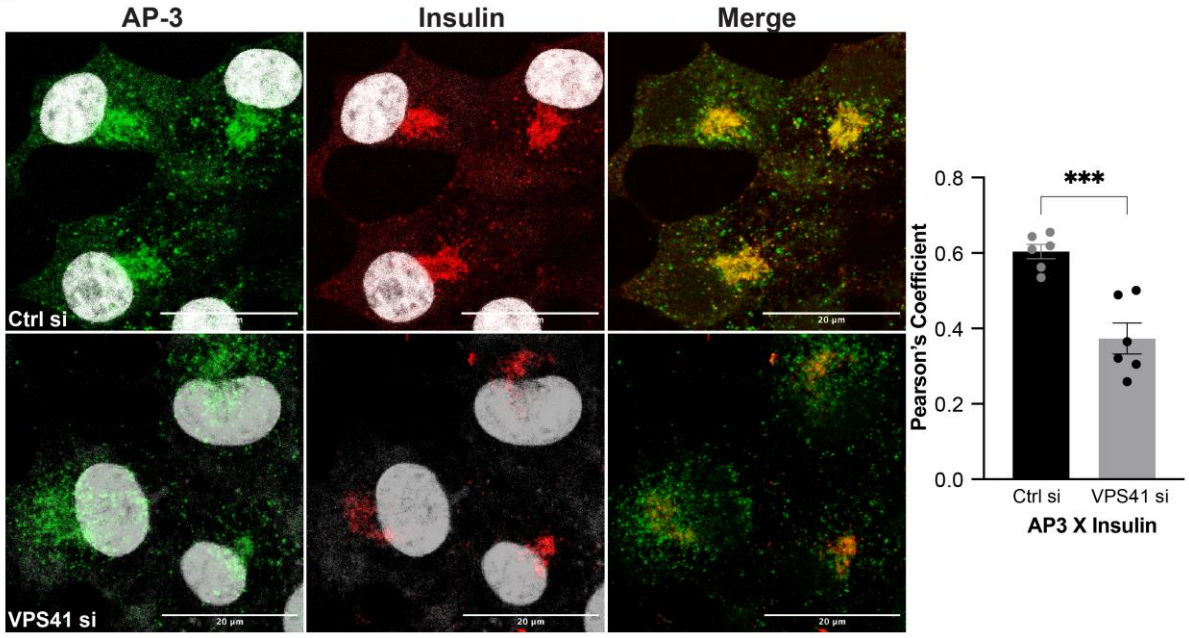
AP-3
Insulin
Merge
Ctrl si
VPS41 si
20 µm
***
Pearson's Coefficient
0.8
0.6
0.4
0.2
0.0
Ctrl si
VPS41 si
AP3 X Insulin

B

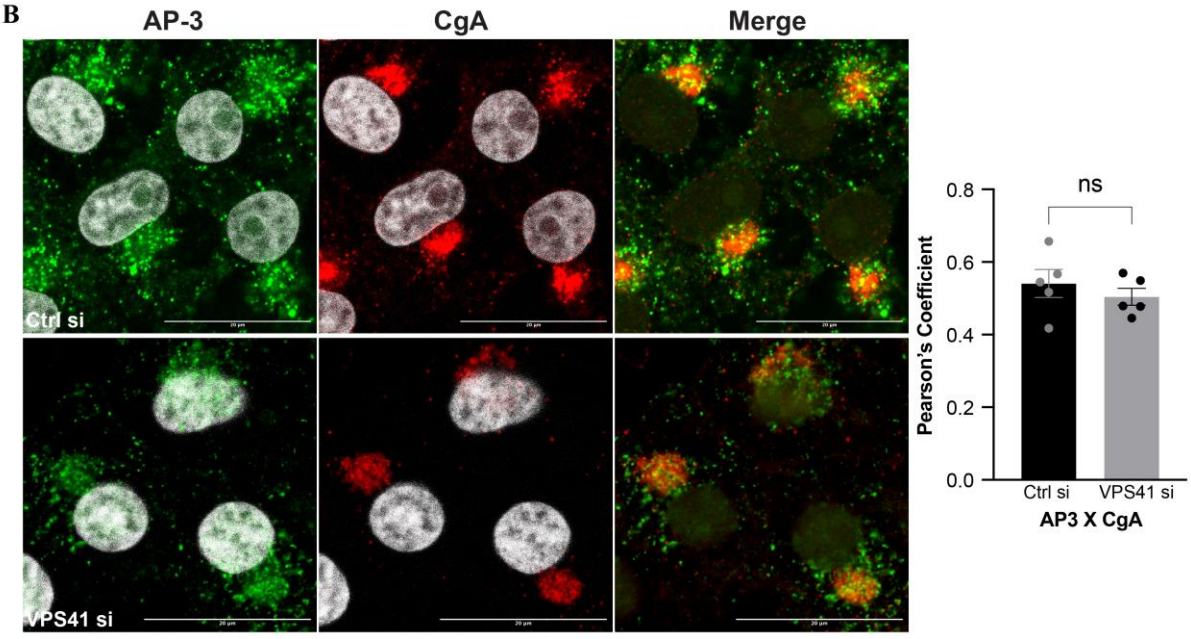
AP-3
CgA
Merge
Ctrl si
VPS41 si
ns
Pearson's Coefficient
0.8
0.6
0.4
0.2
0.0
Ctrl si
VPS41 si
AP3 X CgA

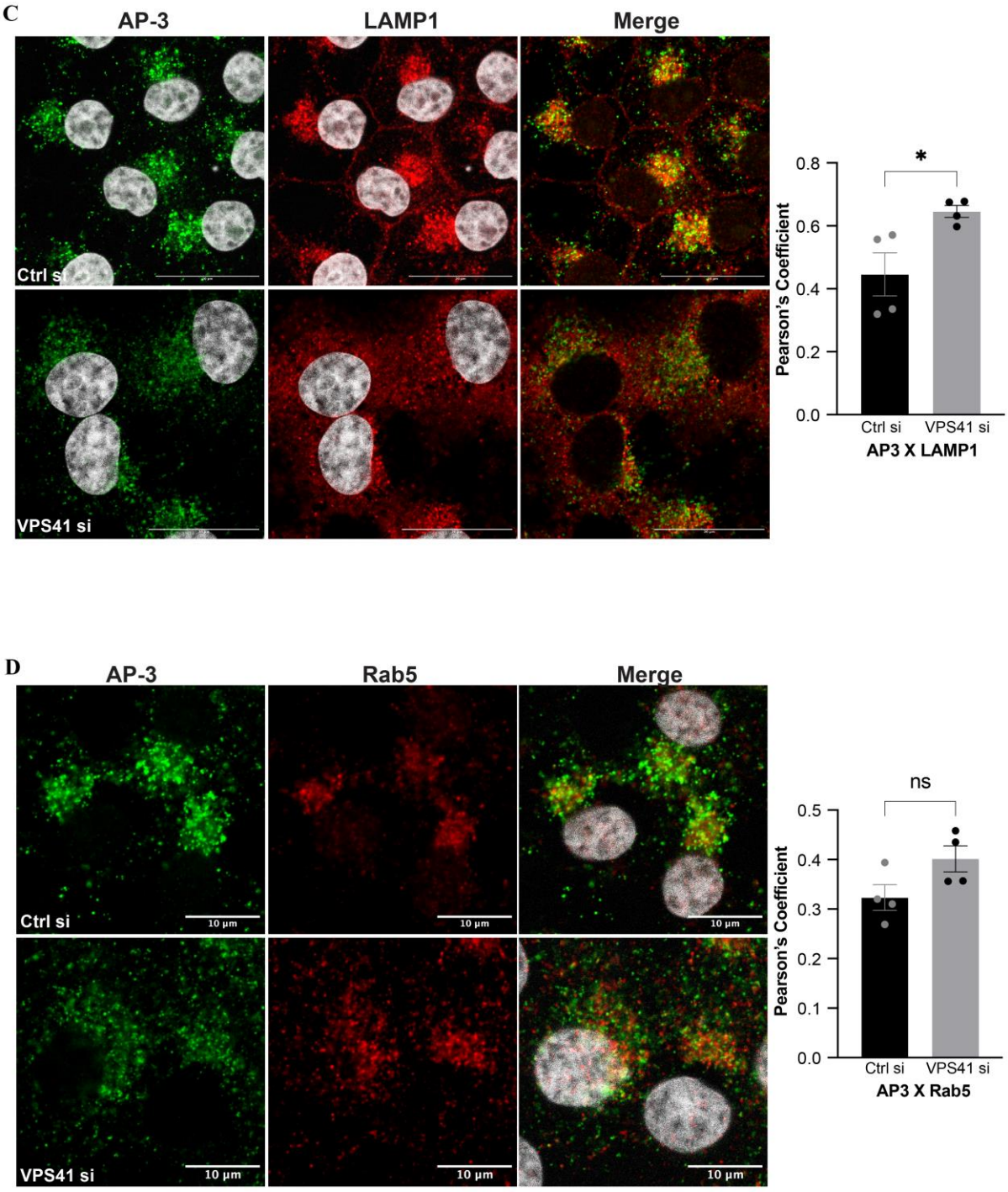

Figure 3-19 Immunofluorescence images of co-staining AP-3 with insulin, CgA, LAMP1 and Rab5 in control and VPS41 KD INS1 cells

INS1 cells were transfected with VPS41 or non-targeting control siRNA. At 48 hours post-transfection, cells were fixed with 4% PFA, and they were co-stained with anti-AP-3 and anti-Insulin (A), anti-CgA (B) anti-LAMP1 (C) anti-Rab5 (D) respectively. All fluorescence images of AP-3 (green), CgA (red), LAMP1(red) and Rab5 (red) were captured on a confocal microscope. The scale bars indicate 20µm (A, B, C) or 10µm (D). Pearson's coefficient of correlation between AP-3 and insulin (A), CgA (B), LAMP1 (C), Rab5 (D) was analyzed by Image J software. Data were presented as mean ± SEM and comparisons were made using unpaired t-test & * $p < 0.05$, *** $p < 0.0005$.

3.4 Discussion

To investigate the precise mechanisms underlying the lack of insulin content in the absence of VPS41 in pancreatic β cells, I acutely deleted VPS41 through siRNA-mediated KD in INS1 cells. Characterization of the VPS41 KD INS1 cells showed the same impaired insulin secretory machinery phenotype presented in the VPS41 KO INS1 cells. Indeed, I observed that reduced levels of VPS41 via either KD or KO in INS1 cells causes a significant decrease in endogenous insulin protein expression (**Figure2-1 & 3-4 & 3-5**), while endogenous proinsulin levels were unchanged when in cells depleted of VPS41 (**Figure 2-1, 3-1 & Appendix Figure 1**). Endogenous proinsulin was still expressed 72 hours following VPS41 KD transfection but, endogenous insulin was completely diminished (**Appendix Figure 1**). Thus, it is unlikely that a defect in insulin processing *via* proinsulin conversion enzymes could be a primary cause for the reduced intracellular insulin content in VPS41 KD INS1 cells. If the process of insulin maturation was delayed or impaired due to a defect in the conversion process of proinsulin through prohormone convertases, PC1/3 & PC2, the proportion of less proinsulin, would be increased. PC1/3 and PC2 prohormone convertases are well-known as the distinct members of proprotein convertases that act mainly within the insulin maturation process in the regulated secretory pathway [71,212]. Impairment in the conversion process to mature and bioactive insulin within dense-core granules as a result of defective PC1/3 or PC2 leads to hyperproinsulinemia, a hallmark of β cell dysfunction in T2D [71,124]. Iida and colleagues identified that a defect in proinsulin processing is linked to impaired maturation of the proinsulin processing enzymes on ER Ca^{2+}ATPase pump (SERCA2, sarcoendoplasmic reticulum Ca^{2+} ATPase -2 pump) deficient pancreatic β cells using KO mice and INS1 cells [213]. The loss of SERCA2 led to a defect of proinsulin trafficking between the ER and Golgi, showing an accumulation of proinsulin in the intermediate region between the ER and Golgi or cis-Golgi [213]. Consequently, it was demonstrated to be linked to impaired maturation of proinsulin via reduced active forms of proinsulin processing enzymes by Western blotting [213]. However, I did not observe a significant difference in proinsulin protein expression by Western blotting (**Figure 3-14 & Appendix Figure 1**) or proinsulin build-up by immunostaining with anti-proinsulin antibody (**Figure 3-8**) in VPS41 KD INS1 cells. In agreement with this, there were insignificant differences in protein levels of proinsulin between WT and VPS41 KO INS1 cells (**Figure 2-1 & 2-3**). Immunostaining against insulin as well as proinsulin however revealed reduced insulin SGs in VPS41 KD INS1 cells (**Figure 3-7 & 3-8**). Although a dramatic reduction of insulin (**Figure 3-4, 3-6 & 3-7**) was observed along with a reduced tendency of proinsulin

(**Figure 3-8**), defective insulin processing by prohormone convertases such as PC1/3 and PC2 would not be the main cause of loss of insulin on VPS41 KD INS1 cells. Indeed, LFQ analysis revealed a significant decrease in key proteins involved in insulin processing including Pdx1, PC1/3 and PC2 on VPS41 KO INS1 cells (**Figure 2-13 & 2-14**) however, the differences in these proteins were not significant on VPS41 KD INS1 cells (**Figure 3-11**). Rather, the pathways related to protein vesicle transports were downregulated on VPS41 KD cells compared to the control (**Figure 3-10**).

To examine β cell function on INS1 cells in the absence of VPS41, GSIS assay was performed. The result revealed that VPS41 KD cells still secreted insulin upon high glucose (16.7mM) stimulation before normalization of the data (**Figure 3-5A**). I considered that a subpopulation of non-transfected cells could still be present in the VPS41 KD transfected cells and release insulin upon high glucose stimulatory conditions. However, after normalizing insulin secretion to DNA content, the secreted insulin levels were insignificant following comparison by Two-way ANOVA analysis (**Figure 3-5C**). Hence, the loss of insulin both in VPS41 KO and KD INS1 cells via chronic and acute VPS41 deletion was observed then consequently, leading to impaired insulin secretion. But VPS41 KD would be closed defective transport of secretory granules containing insulin on β cells while VPS41 KO might lose β cell identity along with downregulated β cell identity genes (**Figure 2-13 & 2-14**) as well as non-expression of exogenous GFP tagged proinsulin (**Figure 3-16**).

As described earlier, VPS41 serves as one of the sorting proteins of large-dense core vesicles by forming coat structures near the TGN in the regulated secretory pathway on neuroendocrine PC12 cells [164]. It is thus possible that un-coated insulin granules, due to the absence of VPS41, undergo protein degradation, which causes the lack of insulin granules in VPS41 KD INS1 cells (**Figure 3-13**). In the previous chapter, the proteomics analysis also suggested the enrichment of proteins relevant to proteolysis in VPS41 KO INS1 cells compared to WT INS1 cells (**Figure 2-14B**). Enhanced expression of poly-ubiquitinated proteins was observed in VPS41 KO INS1 cells, that ubiquitinated proteins were also accumulated following pharmacological treatment with MG132 to prevent intracellular proteolysis of ubiquitinated proteins (**Figure 3-14**).

Insulin is packaged into secretory granules, which is the fundamental unit for insulin storage in pancreatic β cells. The regulation of insulin production, secretion and intracellular degradation are critical to maintain optimal levels of insulin in β cells. Distinct mechanisms

exist with several factors regulating the balance between them. Indeed, short-term (<4h) simulation with glucose increases proinsulin synthesis *via* enhanced translation so protein levels are replenished upon rapidly lost insulin. Prolonged glucose stimulation (>12h) additionally increases preproinsulin gene transcription to meet the increased insulin demand. Further to the time of glucose stimulation, different glucose threshold concentrations contribute to optimal insulin levels within β cells by facilitating insulin production (2-4mM glucose) or enhanced insulin secretion (4-6mM) [41,214], thus restocking insulin storage in β cells *via* continuous insulin production even under non-stimulated circumstances. In addition to the regulation of insulin production or secretion in response to external stimuli such as glucose, intracellular degradation of insulin is considered another contributor to maintaining insulin granules as functional units in β cells [132,215]. Insulin is continuously degraded as it has an estimated half-life (3~5 days) in granules thus, aged insulin granules undergo intracellular digestion instead of exocytosis by the regulated secretory pathway [62,216,217]. Intracellular degradation of insulin is up-regulated under normal conditions due to little demand for insulin secretion while the rate of insulin degradation is down-regulated in response to external stimuli to fulfil the high demand for insulin secretion. Thereby, the degradation of intracellular insulin maintains insulin content at optimal levels in β cells. Autophagy has several subtypes depending on how cellular targeting materials are transported into lysosomes for proteolysis such as macroautophagy, microautophagy, chaperone-mediated autophagy, and crinophagy [132,139]. The loss of autophagy on mouse islets (βAtg7 KO mice) results in defective insulin secretion and hyperglycemia together with enhanced ER stress [140,218]. The functional autophagy and acidification of lysosomes are required for the degradation of insulin granules for balanced insulin granules in β cells [219]. However, nutrient conditions such as duration of metabolic stress or shortage of nutrients affect this degradation of insulin granules in β cells [134,141,144]. However, the lack of VPS41 led to the reduction of insulin on INS1 cells despite culturing with normal completed cell culture conditions, not metabolic stress such as nutrient starvation or FFA cultured conditions. In addition to the insulin reduction, CgA known as a compartment of insulin SGs in the regulated secretory pathway was reduced in a time-dependent manner following transfection with siRNA of VPS41 on INS1 cells (**Figure 3-17**), which suggests insulin SG as functional units on β cells could be the target for degradation in the absence of VPS41 (**Figure 3-17**).

Therefore, I tested the hypothesis of whether poor insulin storage correlates with enhanced proteolysis in INS1 cells upon deficient VPS41 circumstances. Pharmacological reagents that prevent intracellular protein degradation through different mechanisms were selected. The ubiquitin-proteasome mediated degradation pathway and lysosomal-mediated degradation pathway are well-known proteolytic pathways that contribute to cellular homeostasis and physiological function by regulation of target protein turnover e.g. removing unwanted or misfolded proteins [220,221]. MG132 was used to inhibit the ubiquitin-proteasome mediated degradation pathway [120,222]. CQ and NH_4Cl are both inhibitors of the lysosomal-mediated degradation pathway but they act to inhibit degradation at different steps during the pathway. CQ prevents the fusion of the autophagosome-lysosome leading to increased levels of lysosomal pH thereby, blocking the degradation of autophagic-mediated protein degradation and causing accumulation of aggregated autophagosomes within the lysosome [220,223,224]. E-64 is a natural compound that specifically inhibits lysosomal cysteine protease activity [225,226].

Inhibiting protein degradation restored endogenous insulin expression in VPS41 KD INS1 cells compared to non-treated VPS41 KD INS1 cells (**Figure 3-14**). Surprisingly, lysosomal-mediated proteolytic inhibitors, CQ and E-64, exhibited more efficient insulin rescue among the different inhibitors (**Figure 3-14**). Thus, these results indicate that the reduction of insulin is strongly correlated with enhanced proteolysis, especially through the lysosomal-mediated pathway in the absence of VPS41 in INS1 cells.

Recently Rab7 interacting lysosomal protein (RILP) has been reported to be associated with lysosomal degradation of proinsulin in both mouse and rat β cell lines (MIN6 and INS1 cells, respectively), and isolated mouse islets [227]. Indeed, overexpression of RILP strongly correlates with dysfunctional β cells and the development of T2D progression along with reduced numbers of immature SGs containing proinsulin and significantly induces the lysosomal-mediated degradation of proinsulin, which finally causes defective insulin secretory pathway [227]. Despite regulation of the lysosomal-mediated proteolysis for insulin SGs on both RILP-dependent and VPS41-dependent pathways, VPS41-mediated regulation of insulin SG could be the target for insulin rather than proinsulin in the absence of VPS41. Thus, the data suggests the insulin granules as uncoated structure forms in the absence of VPS41 might undergo lysosomal proteolysis rather than insulin storage or release in the regulated secretory pathway on pancreatic β cells. So, how are insulin granules selectively shunted to proteolytic pathways under VPS41 deficient circumstances in INS1 cells?

VSP41 role in forming the secretory granule's coat-structure is dependent on its binding with the adaptor protein AP-3. Adaptor protein complexes are involved in vesicular-mediated transport of newly synthesized protein between cellular compartments including the Golgi complex, endosomes, lysosomes, and plasma membrane [56,228–230]. Indeed, it has been revealed that adaptor complexes play a role in the selection of cargo molecules and vesicle budding. Several types of adaptor protein complexes, AP-1, AP-2, AP-3, AP-4, and AP-5, each with distinct intracellular localizations and functions are involved in the trafficking steps of distinct membrane proteins in mammalian cells [230]. Like endocrine β cells, neuroendocrine cells release newly synthesized proteins through a regulated secretory pathway. In neuroendocrine cells, VPS41 functions as a sorting protein through the formation of coat-structures together with AP-3 [164,182,183].

AP-3 could form coat structures *via* binding with VPS41 in regulated secretory pathway [164,192] as well as select cargo for its trafficking [229,231]. Thus, this ability of AP-3 led to the possibility that insulin granules undergo AP-3 complex-mediated trafficking towards proteolysis as the alternative pathway through interacting with other subcellular components in VPS41-depleted INS1 cells. To test this possibility, I examined the co-localization of AP-3 complexes with components including Insulin, CgA, LAMP1, LC3A/B, and Rab5A by immunostaining (**Figure 3-18 & 3-19**). It was observed different patterns of distribution of AP-3 and these markers in VPS41 KD INS1 cells (**Figure 3-19**) compared to control cells. The lysosome-mediated marker, LAMP1 was detected in surface area as well as peri-nuclear in control cells while the co-localization with LAMP1 and AP-3 was distributed through the cytoplasm in VPS41 KD INS1 cells (**Figure 3-19C**). In addition, the accumulated Rab5 together with AP-3 was observed in the perinuclear region in control INS1 cells however, this accumulated pattern between Rab5 and AP-3 was disrupted in VPS41 KD INS1 cells (**Figure 3-19D**). The organelles related to proteolysis such as LAMP could exist throughout the cytoplasm however, AP-3-mediated vesicles may have already cleared via lysosome-regulated proteolysis in the absence of VPS41.

In the present chapter, all findings provide that the lack of VPS41 *via* siRNA-mediated acute deletion causes poor insulin storage due to enhanced lysosomal-mediated proteolysis of insulin SGs, which consequently leads to defected insulin secretion on β cells.

4 Chapter IV: Characterization of β cell specific VPS41 Deletion Mice

4.1 Introduction

Based on the *in vitro* studies, both chronic and acute deletion of VPS41 caused an abnormal phenotype of dysregulated glucose-stimulated insulin secretion and loss of cellular insulin content in INS1 cells. Although VPS41 has been researched in several different cellular contexts, an *in vivo* model has not been investigated to understand its role in pancreatic β cells. Here, for the first time, the role of VPS41 in regulating whole-body glucose homeostasis is demonstrated using β cell specific VPS41 KO mice.

VPS41 gene expression studies suggest that *VPS41* expression is associated with the risk of T2D in rodent models [190,191,198]. Hence, *in vivo* studies of β cell specific VPS41 KO could provide fundamental evidence for the physiological function of VPS41 in β cells and in regulating whole-body glucose homeostasis. The specific aims of Chapter IV are:

1. To generate β cell specific VPS41 KO mouse using Cre-Lox genetic techniques.
2. Characterize the phenotypes of control and β cell specific VPS41 KO mice
3. To examine the role of VPS41 to regulate glucose homeostasis by performing *ex vivo* experiments on isolated mouse islets from control and β cell specific VPS41 KO mice

4.2 Materials and Methods

4.2.1 Mouse housing and diet

Mice were housed at the Laboratory Animal Services Facility, Bosch Institute, University of Sydney, Australia and transferred to the Charles Perkins Centre, University of Sydney where all experimental procedures were performed. Mice were housed in cages, controlled under a 12-hour light and dark cycle with free access to water and a standard laboratory chow (calories: 13% fat, 65% carbohydrates, 22% protein) diet (Gordon's Speciality Stock Feeds, Yanderra, New South Wales, Australia).

4.2.2 Generation of β cell specific VPS41 KO mouse line

To investigate the *in vivo* role of VPS41 in pancreatic β cells, we used a conditional gene-targeting approach by '*Cre-Lox technology*' to generate mice with selective depletion of VPS41 in pancreatic β cells [232,233]. Cre recombinase has specific enzyme activity that recognizes loxP sites in the genome, leading to on-target effects through the deletion of loxP-flanked target genes by excision, flipping or translocation in a tissue-specific manner [191,232,233]. VPS41-floxed mice were generated by first introducing two lox sites into the mouse VPS41 gene. Then, VPS41-floxed mice were crossed with mice expressing Cre recombinase under the control of the insulin 1 gene promoter (**Figure 4-1**). All mice were on a C57BL/6J genetic background (**Figure 4-1**). Initial characterization was performed on gender-mixed mice. Age-matched VPS41 floxed/floxed, VPS41 floxed/ + and Ins1-Cre mice were used as controls.

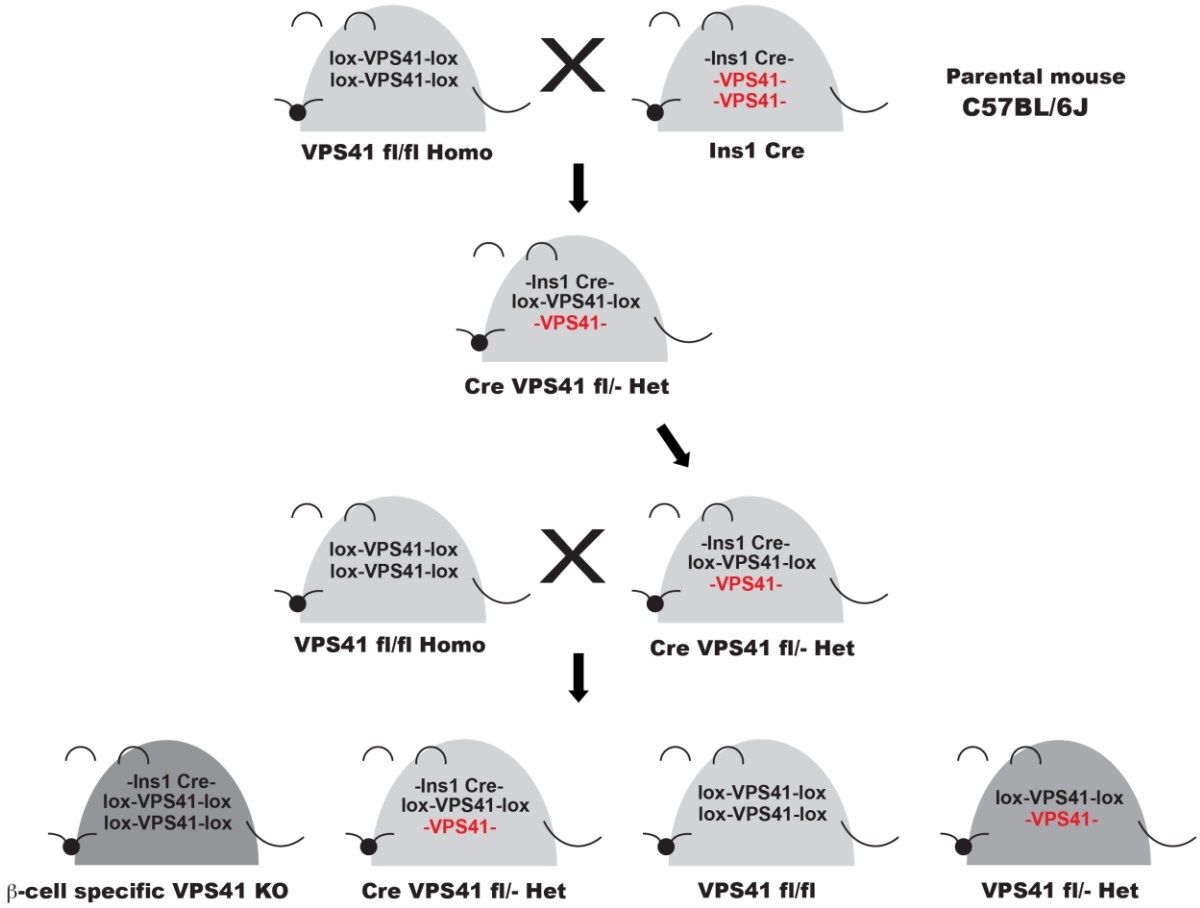

Figure 4-1 Schematic diagram depicting the generation of β cell-specific VPS41 KO mice

4.2.3 Intraperitoneal and oral glucose tolerance test

Mice were fasted for 5 hours and then analyzed by EcohMRI (Magnetic Resonance Imaging) to calculate a dose of 2mg/kg glucose to lean mass prior to the intraperitoneal glucose tolerance test [191] (IP-GTT) or oral glucose tolerance test (OGTT). The age-matched mice were weighed for whole-body mass and the EchoMRI was used for lean and fat mass measurements. Mice were tail tipped for basal blood glucose and insulin measurement and then, injected with a 25% glucose solution in injectable water via intraperitoneal route or oral gavage. The blood samples were collected from a tipped tail and measured immediately using a glucometer (Accu-Chek Performa, Roche) with Accu-Check Performa Strips (#RDS48874020) at the indicated time points during the IP-GTT or OGTT and then, subsequently measure circulating insulin levels at the corresponding time points.

4.2.4 *Insulin ELISA assay*

Circulating plasma insulin levels in the blood were measured by insulin ELISA kit (Crystal Chem, #90080) pre- and post-glucose administration for IP-GTT and OGTT. Blood samples from the tipped tail were transferred into a 96-well insulin ELISA kit and the blood insulin levels were determined by the kit's insulin standard following the manufacturer's instructions. The fluorescent signal was measured using a plate reader (FLUOstar Omega microplate reader).

4.2.5 *Mouse intraperitoneal insulin tolerance test*

To calculate the volume of insulin administration for the intraperitoneal insulin tolerance test (IP-ITT), age-matched mice (10-week-old) were weighed for whole-body mass and an EchoMRI was performed for lean and fat mass measurements. Humalog U-100 Insulin (1/400 dilution in saline) was injected into the intraperitoneal cavity of the mice. Following the intraperitoneal injection of insulin (0.5 U/kg), the blood samples were collected from a tipped tail and measured immediately using a glucometer (Accu-check Performa, Roche) at the indicated different time points during the IP-ITT.

4.2.6 *Mouse islets isolation*

For *ex vivo* experiments, 15-week-old mice were euthanatized by cervical dislocation. The islets from the mice were isolated after injecting 2 ml of Liberase TM (Roche, #5401127001) in HBSS (Gibco™, #14065056) into the common bile duct. Perfused pancreata were digested at 37°C in a shaking water bath for 13 minutes. After 2 washes with HBSS (1% BSA), the digested pancreases were filtered through 2 layers of sterile gauze into a new tube to remove undigested tissue. Following a centrifugation step at 500g for 3 minutes, the pellet was resuspended in 10 ml of Histopaque 1119 (Sigma-Aldrich, #11191) followed by the slow addition of 6ml of Histopaque 1077 (Sigma-Aldrich, #10771) and 6 ml of HBSS wash buffer to separate the islets by gradient centrifugation at 1000 g for 20 minutes with no breaks for deceleration. Islets were collected from the interface between the HBSS wash buffer and Histopaque 1077 using a pasture pipette. After picking islets from the interfaced solutions under a microscope, the islets were washed twice with HBSS (1% BSA) and were allowed to culture in RPMI 1640 complete media containing 10% FBS and 1% penicillin/streptomycin for overnight recovery.

4.2.7 *Glucose-stimulated insulin secretion assay*

To measure the insulin secretion of the isolated mouse islets, GSIS assay was performed. After recovery with RPMI 1640 completed media, the mouse islets were incubated at basal conditions i.e., 1 ml Krebs buffer (20mM HEPES, pH 7.4; 119 mM NaCl; 4.75 mM KCl, 2.54 mM $CaCl_2$; 1.2 mM $MgSO_4$; 1.18 mM KH_2PO_4; 5 mM $NaHCO_3$) containing BSA (0.125%, Sigma-Aldrich, #A7030) and glucose (2.8mM) for 1 hour at 37°C. The mouse islets were then exposed to low or high glucose conditions (2.8 mM or 16.7 mM, respectively) at 37°C for 1 hour. At the end of 1 hour incubation, media was collected for measurement of secreted insulin then, the islets were lysed with islet lysis buffer (pH 7.4, 100mM Tris-HCl, 300mM NaCl, 10mM NaF containing protease/phosphatase inhibitors) and collected for measurement of cellular insulin content. The levels of secreted insulin, intra-cellular insulin content and total DNA content were analyzed using HTRF assay (Cisbio, #62IN2PEH) and DNA picoGreen assay (Invitrogen™, #P11495), respectively. Secreted insulin and total insulin content were normalized to DNA content and presented as a fold-over basal-stimulated secretion. HTRF assay and DNA picoGreen Assay were performed as described in section 2.2.4.

4.2.8 *Immunocytochemistry*

Whole pancreases from 15-week-old mice were embedded with paraffin and sectioned. Section slides were deparaffinized and rehydrated in a sequential manner: 2x 100% xylene rinses, 1x 50% xylene, 50% ethanol, 1x 100% ethanol, 1x 95% ethanol, 1x 80% ethanol, 1x 75% ethanol, 1x 50% ethanol and 1x distilled water. Slides were further washed 3x with wash buffer (0.1% BSA, 0.01 Sodium Azide in PBS) for 3 minutes each. Section slides were blocked with a blocking buffer (Dako, #X0909) to block non-specific staining for 1 hour at room temperature. Slides were incubated with primary antibodies at 4°C overnight in a humidified chamber. The following day, slides were washed with wash buffer and incubated with fluor-conjugated secondary antibodies (1:500 in diluent buffer, Dako, #S0809) for 1 hour at room temperature in the dark. After 2x washes with wash buffer and 2x washes with PBS, the slides were dried for 5 minutes at room temperature and mounted with ProLong™ Diamond Antifade Mountant with DAPI (Invitrogen™, #P36962). Immunofluorescence images were captured on confocal microscope (Leica, SP8 confocal).

4.2.9 Western blotting

To validate β cell-specific deletion of VPS41 in mice, different tissues including islet, brain, hypothalamus, and liver were dissected from age-matched (15-week-old) mice. The appropriate amount of ice-cold RIPA (100µl) lysis buffer (10mM Tris-HCl pH 8.0, 1mM EDTA, 0.5mM EGTA, 1% Triton X-100, 0.1% Sodium Deoxycholate, 0.1% SDS, 140mM NaCl) containing protease inhibitor cocktail (Roche, #11697498001) was added into the piece of tissues on ice. Following sonication with 95% power for 24 seconds with a 3-second interval between each sonication, the tissue samples containing lysis buffer were centrifugated at 14,000 g for 15 min at 4°C, and the supernatant was collected into a new tube for BCA assay and Western blotting. Western blotting was performed as described in section 2.2.2.

4.2.10 Statistical analysis

Statistical analyses were performed using GraphPad Prism 9 software using student's t-test, One-way ANOVA or Two-way ANOVA followed by Tukey's comparisons tests (specified in figure legends). *Data were presented as mean ± SEM or mean ± SD (specified in figure legends) due to the limited mouse sample numbers affected by COVID-19 lockdown over 2020/2021.*

4.3 Results

4.3.1 Validation of VPS41 KO in βVPS41 KO mice

VPS41 KO was confirmed in β cells by using SDS-PAGE in lysates collected from different tissues in age-matched mice. VPS41 protein expression was detected in many tissues since VPS41 gene expression is prevalent in different types of cells and tissues as mentioned above; however, VPS41 expression was depleted in isolated pancreatic islets. Western blots analysis revealed a significant decrease in VPS41 protein expression in isolated islets from β cell-specific VPS41 KO mice (mean VPS41/GAPDH ± SEM = [WT islet: **1.000** ± **0.121**] vs [KO islet: **0.161** ± **0.041**] ($p < 0.005$)) (**Figure 4-2**). Low levels of VPS41 expression in βVPS41 KO islets were observed, which is thought to be the expression of VPS41 in a small number of non-β cells including α, δ, and pancreatic polypeptide cells in the islets. The reduced GAPDH in islets compared to other tissues may simply reflect that as a proportion of total protein, there is less GAPDH in islets. This is perhaps unsurprising considering a large amount of protein in islets is insulin and other storage hormones.

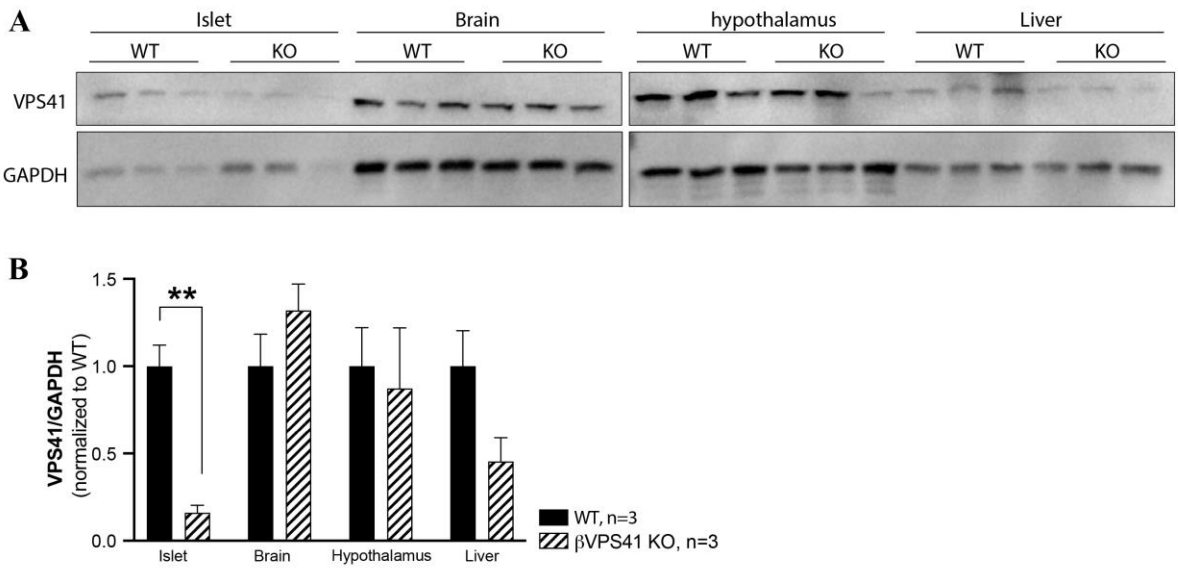

Figure 4-2 VPS41 expression in βVPS41 KO mouse tissues

(A) Protein extracts from various tissues in age-matched (15-week-old) βVPS41 KO mice were run on SDS-PAGE and immunoblotted for VPS41 and the housekeeping protein, GAPDH. (B) The intensity values of VPS41/GAPDH protein bands were quantified using Image J software and normalized to WT. The data presented as mean ± SEM. ** $p < 0.005$ by Two-way ANOVA with Tukey's multiple comparisons test.

4.3.2 Physiological metabolic phenotypes of β VPS41 KO mice

4.3.2.1 Body composition of 8-week-old mice

8-week-old βVPS41 KO mice showed no alterations in body composition phenotype including fat, lean mass, and total body weight on a normal chow diet compared to age-matched littermate controls (**Figure 4-3**).

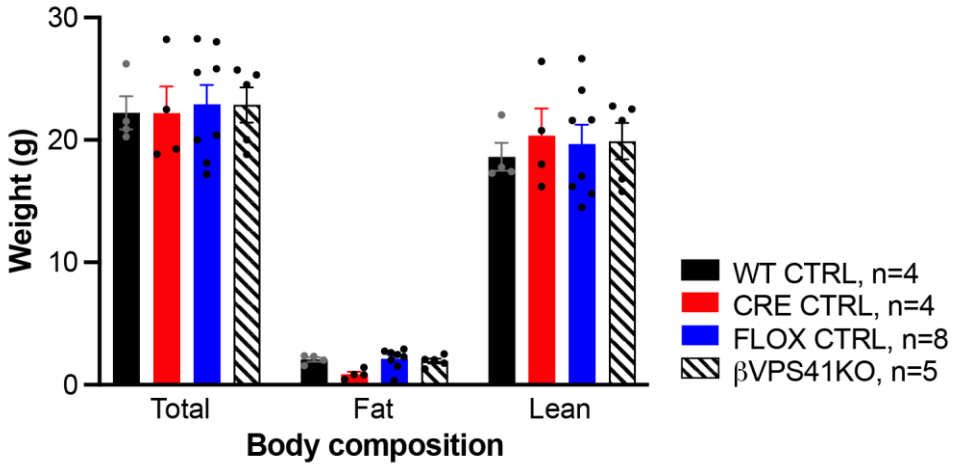

Figure 4-3 Body composition of 8-week-old βVPS41 KO mice

All age-matched and gender-mixed mice were fed a standard chow diet. 8-week-old mice were weighed for whole-body mass and an Echo MRI was performed to measure lean and fat mass.

4.3.2.2 Fasting insulin, Fasting glucose, IP-GTT and iAUC of IP-GTT in 8-week-old β VPS41 KO mice

After 5 hours fasting, plasma insulin was measured using an insulin ELISA kit (Crystal Chem, #90080). βVPS41 KO mice had significantly decreased plasma insulin levels compared to control including WT, Cre and Flox (mean fasting insulin ± SEM = [KO:**0.019** ± **0.009**] vs [WT: **0.222** ± **0.019**] ($p < 0.0005$) or [Cre: **0.225** ± **0.066**] ($p < 0.005$) or [Flox: **0.339** ± **0.040**] ($p < 0.0001$)) (**Figure 4-4A**). Next, fasting glucose concentrations of blood samples from tipped mouse tails were measured using a glucometer. 8-week-old βVPS41 KO mice had fasting hyperglycemia with significantly higher blood glucose concentrations compared to control mice, which demonstrates that βVPS41 KO mice are diabetic (mean fasting glucose ± SEM = [KO: **26.43** ± **3.42**] vs [WT: **10.30** ± **0.74**] ($p < 0.0005$) or [Cre: **9.95** ± **2.05**] ($p < 0.005$) or [Flox: **10.35** ± **0.87**] ($p < 0.0005$)) (**Figure 4-4B**).

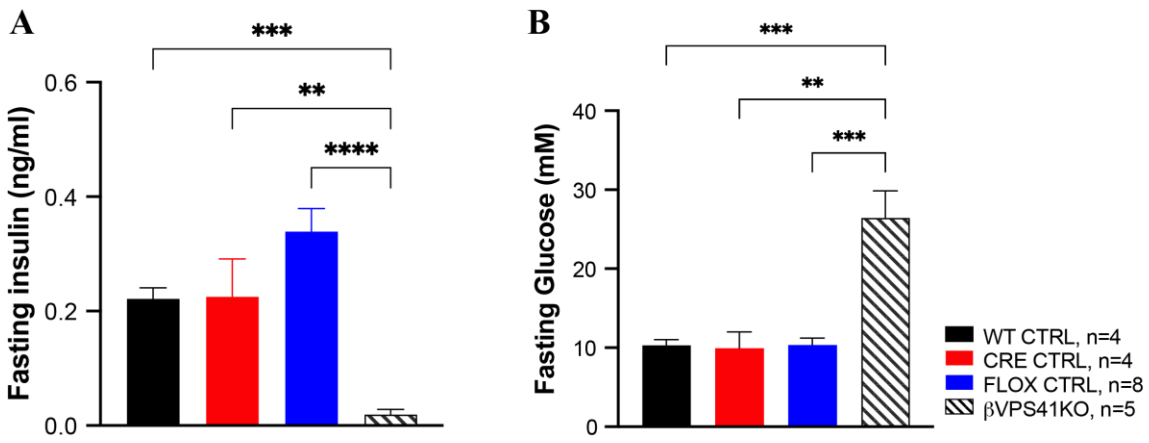

Figure 4-4 Fasting insulin and fasting glucose concentrations in 8-week-old βVPS41 KO mice

After 5 hours-fasting, the blood samples were collected from tipped tail. (A) The fasting insulin was analyzed using insulin ELISA kit. (B) The fasting glucose was measured by a glucometer. Data represented mean ± SEM, ** $p < 0.005$, *** $p < 0.0005$ & **** $p < 0.0001$ by One-way ANOVA with Tukey's multiple comparisons test.

To determine if βVPS41 KO mice have disturbances in glucose metabolism compared to age-matched controls, an intraperitoneal glucose tolerance test (IP-GTT) was performed to monitor the clearance of glucose from the body after IP glucose administration. For each GTT time point, the control groups including WT, Cre and Flox mice showed a similar pattern, leading to reduced blood glucose levels over two hours (**Figure 4-5A**). However, βVPS41 KO mice exhibited severe hyperglycemia with maximum levels of blood glucose (**Figure 4-5A**) and they could be underestimated values due to the detection limit of the glucometer (Accu-Chek Performa, 35mM). Interestingly, the beginning fasting glucose levels were significantly elevated in the βVPS41 mice compared to control mice (**Figure 4-5A**), showing different baselines of fasting blood glucose in each group by different genotypes. The area under the curve (AUC) of the glucose tolerance test (GTT) is widely used as the index to estimate the total changed blood glucose and diagnose impaired glucose tolerance [234–236]. I applied the incremental area under the curve (iAUC) of GTT by subtracting baseline values to minimize the variations in basal fasting blood glucose levels between individuals depending on genotypes. However, no significant differences in quantified iAUC of GTT were observed between βVPS41 KO mice and the control groups (mean iAUC ± SEM = [KO: **509.500 ± 147.754**] vs [WT: **492.00 ± 55.500**] or [Cre: **421.533 ± 25.680**] or [Flox: **623.856 ± 56.130**] (**Figure 4-5B**).

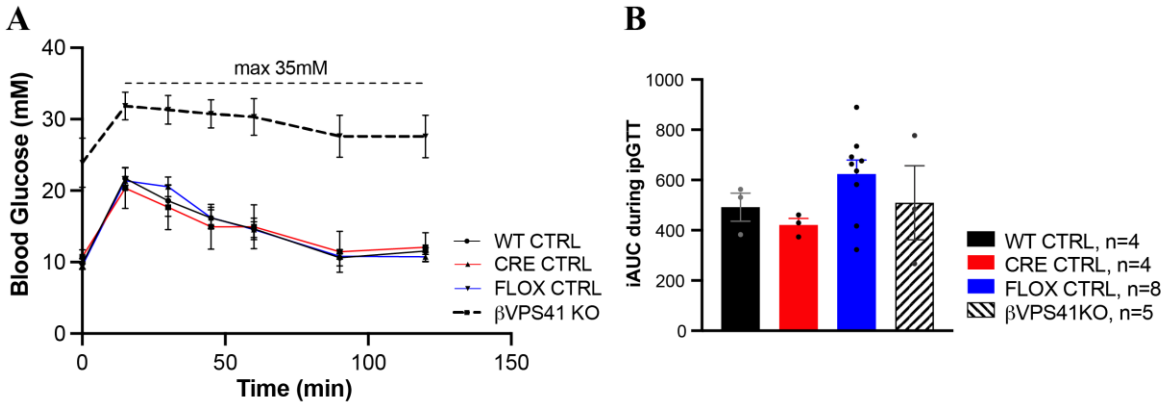

Figure 4-5 Regulation of glucose homeostasis during the IP-GTT and iAUC in 8-week-old βVPS41 KO mice

(A) After 5 hours fasting, blood samples were collected from the tipped tail at the indicated time points and the blood glucose was measured by a glucometer. (B) The quantified iAUC of the glucose tolerance test. Data represented means ± SEM. Data were analyzed by Two-way ANOVA with Tukey's multiple comparisons test but there was no significance.

4.3.2.3 Body composition of 15-week-old βVPS41 KO mice

15-week-old βVPS41 KO mice had no phenotypic differences in body composition, including fat mass and lean mass in the absence of VPS41 (**Figure 4-6A**). The control mice including WT, Cre and Flox and βVPS41 KO mice had slight weight gain on a normal chow diet (**Figure 4-6B**). All mice were fed a standard laboratory chow diet (calories: 13% fat, 65% carbohydrate, 22% protein).

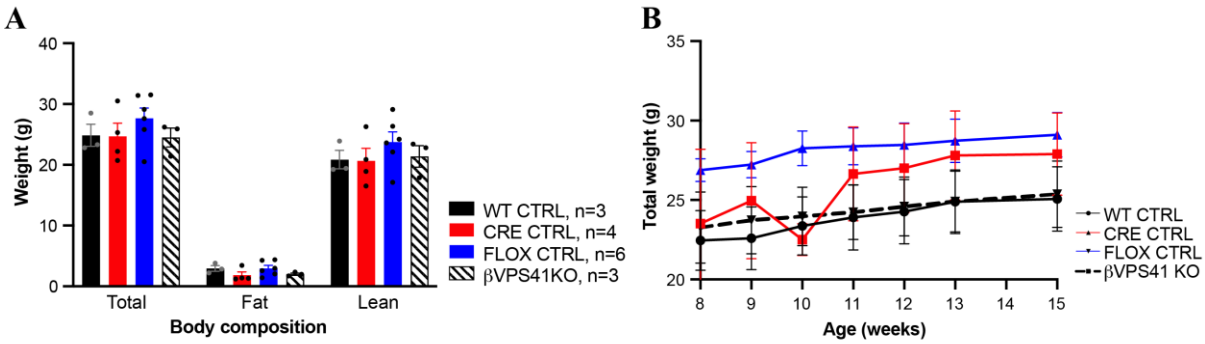

Figure 4-6 Body composition of 15-week-old βVPS41 KO mice and body weight over time

Age-matched and gender-mixed mice were fed a standard chow diet. (A) 15-week-old mice were weighed for whole-body mass and an Echo MRI was performed for lean and fat mass measurement. (B) The change of body weight over time.

4.3.2.4 Insulin ELISAs for 15-week-old βVPS41 KO mice

WT control mice appear to have significantly enhanced insulin secretion at 15 minutes following the glucose administration (Mean of insulin ± SEM = [WT at 0 min: **0.222** ± **0.019**] vs [WT at 15 min: **0.387** ± **0.042**] ($p < 0.005$)), while both Cre and Flox control mice have shown slightly increased insulin secretion (Mean of insulin ± SEM = [Cre at 0 min: **0.225** ± **0.066**] vs [Cre at 15 min: **0.255** ± **0.041**] or [Flox at 0 min: **0.339** ± **0.040**] vs [Flox at 15 min: **0.395** ± **0.048**]). Consistent with the insulin ELISA data of 8-week-old βVPS41 KO mice (**Figure 4-4A**), 15-week-old βVPS41 KO mice had statistically less insulin secretion compared with age–matched littermate controls at fasting. Besides, βVPS41 KO mice did not display insulin secretion upon post-administration of glucose at 15 minutes (Mean of insulin ± SEM = [KO at 0 min: **0.019** ± **0.009**] vs [KO at 15 min: **0.012** ± **0.008**]) (**Figure 4-7**).

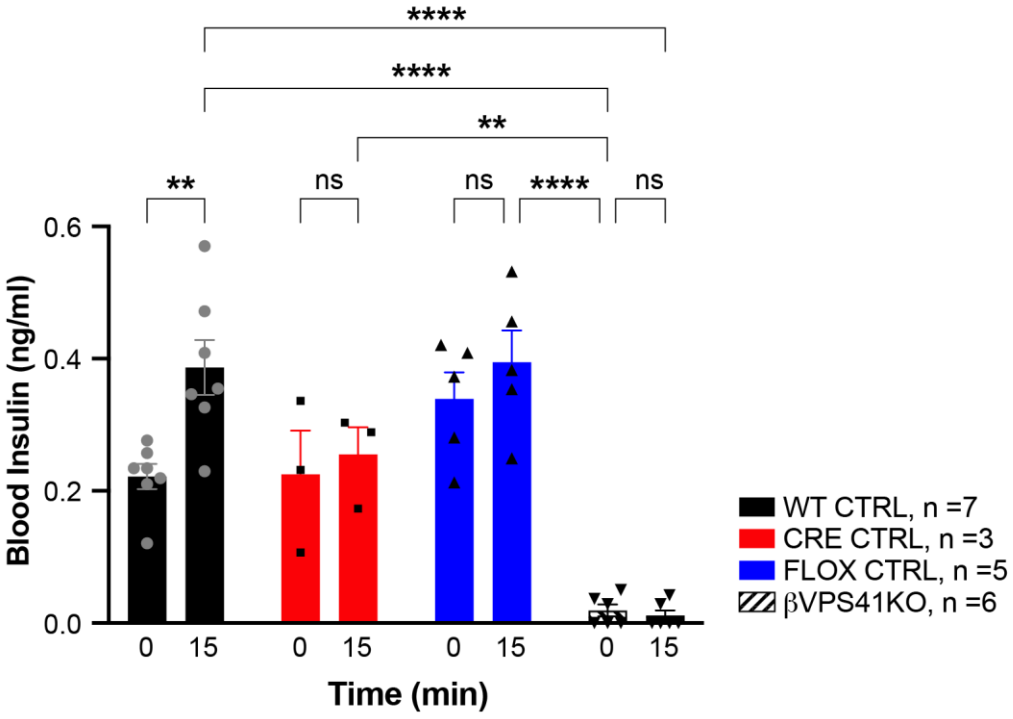

Figure 4-7 Insulin ELISA for 15-week-old βVPS41 KO mice

After IP of glucose administration, at 0 and 15 minutes, the blood was collected from the tipped tail. By Insulin ELISA kit, the blood samples were analyzed along with insulin standards. Data represented mean ± SEM. ** $p < 0.005$ & **** $p < 0.0001$ by Two-way ANOVA with Tukey's multiple comparisons test.

4.3.2.5 Fasting glucose, IP-GTT and iAUC of IP-GTT in 15-week-old βVPS41 KO mice

Consistent with the data from 8-week-old βVPS41 KO mice, 15-week-old mice had enhanced glucose concentrations after 5 hours fasting, a 3-fold increase compared to the 3 mouse control groups (mean fasting glucose ± SEM = [KO: **29.500** ± **2.193**] vs [WT: **10.633** ± **0.970**] or [Cre: **10.850** ± **1.150**] or [Flox: **10.800** ± **0.381**] ($p < 0.0001$)) (**Figure 4-8**). The 15-week-old βVPS41 KO mice exhibited a slight increase in blood glucose with severe fasting hyperglycemia compared with 8-week-old KO mice (mean fasting glucose ± SEM = [15wk KO: **29.500** ± **2.193**] vs [8wk KO: **26.443** ± **3.418**]) (**Figure 4-8 & 4-4B**). However, there were no changes in fasting glucose between 8 weeks to 15 weeks in the control groups (mean fasting glucose ± SEM = [8wk WT: **10.30** ± **0.74**] vs [15wk WT: **10.6** ± **1.0**] or [8wk Cre: **9.95** ± **2.05**] vs [15wk Cre: **10.9** ± **1.20**] or [8wk Flox: **10.35** ± **0.87**] vs [15wk Flox: **10.8** ± **0.4**]) (**Figure 4-4B & 4-8**).

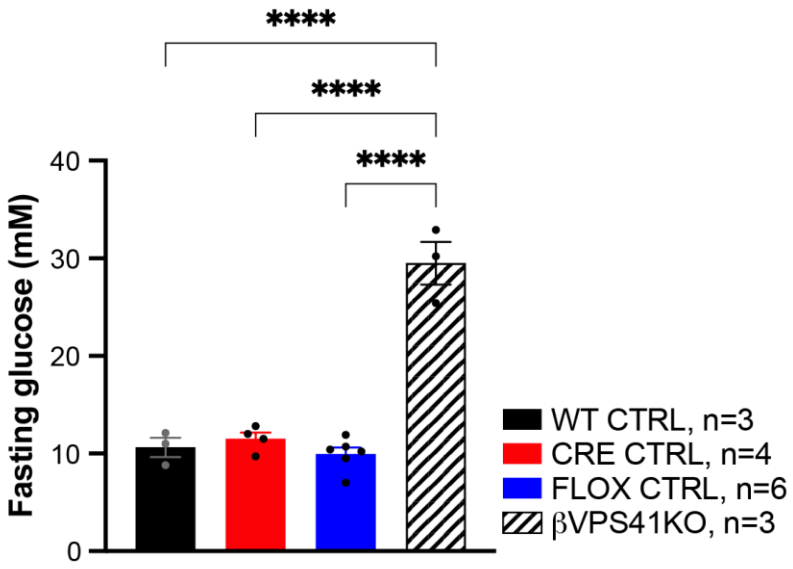

Figure 4-8 Fasting glucose levels in 15-week-old βVPS41 KO mice

After 5 hours fasting, blood samples were collected from the tipped tail and blood glucose was measured by a glucometer. Data represented mean ± SEM, **** $p < 0.0001$ by One-way ANOVA with Tukey's multiple comparisons test.

The measured blood glucose concentrations at 8-week-old βVPS41 KO mice during IP-GTT exhibited maximum values above the detection limit (approximately 35mM) of the glucometer (**Figure 4-5A**). Thus, the blood was diluted in a normal saline solution at a 1:1 ratio

and then read using the glucometer to estimate the measurement of glucose in 15-week-old VPS41 KO mice during the IP-GTT. Finally, the glucose concentrations were displayed as values multiplied by the dilution ratio in **Figure 4-9A**. During IP-GTT after administration of glucose, βVPS41 KO mice exhibited the clearance of glucose however, they showed characteristics of severe diabetes due to a higher baseline of blood glucose (**Figure 4-9A**). βVPS41 KO mice had a significant increase in the iAUC of glucose tolerance test compared with age-matched controls (mean iAUC of IP-GTT ± SEM = [KO: **2209.333** ± **212.558**] vs [WT: **523.033** ± **58.273**] or [Cre: **852.325** ± **377.611**] or [Flox: **664.517** ± **103.889**] ($p < 0.005$)) (**Figure 4-9B**).

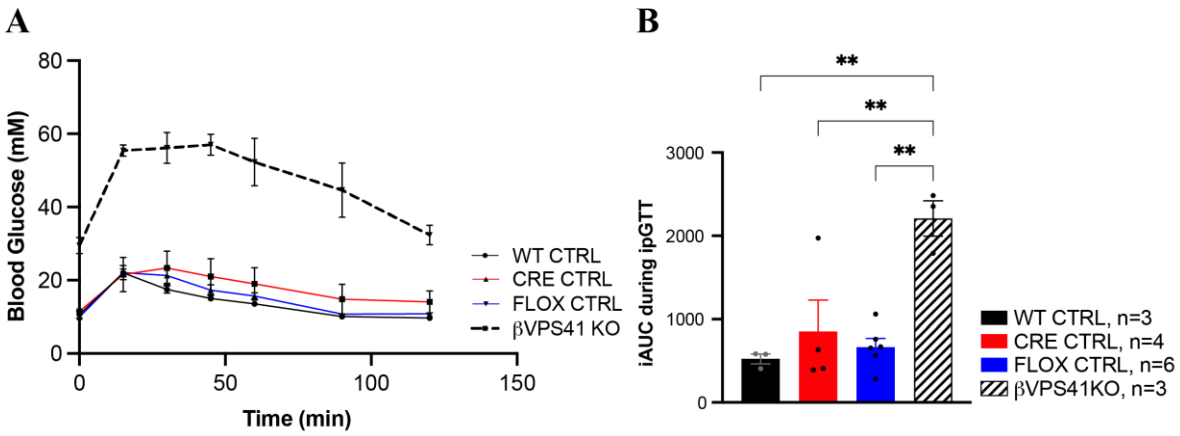

Figure 4-9 Regulation of glucose homeostasis during an IP-GTT and iAUC in 15-week-old βVPS41 KO mice

(A) After 5 hours fasting, the blood samples were collected from the tipped tail at the indicated time points and the blood glucose was measured by a glucometer. (B) The iAUC of IP-GTT. Data represented mean ± SEM, ** $p < 0.005$ by One-way ANOVA with Tukey's multiple comparisons test.

The glucose homeostasis results from 8- and 15-week-old βVPS41 KO mice (**Figure 4-5 & 4-9**) demonstrates that VPS41 is critical in the maintenance of glucose homeostasis *in vivo*.

4.3.3 Ex vivo functional characterization of β VPS41 KO mice

4.3.3.1 Glucose-stimulated insulin secretion in isolated islets

To determine the potential role of VPS41 in regulating insulin secretion, GSIS was performed using size-matched and same no. of islets (~ 5 islets/ per mouse) from 15-week-old mice. Based on phenotype results of 8 and 15-week control mice including WT, Cre and Flox, we did not observe abnormal changes depending on their genotypes. Thus, WT, Cre and Flox control mice were combined and then used as the control groups.

βVPS41 KO islets secreted significantly less insulin compared with control islets upon exposure of glucose (mean secreted insulin per 5 islets ± SEM = [2.8mM Ctrl: **18.042** ± **4.994**] vs [16.7mM Ctrl: **27.403** ± **6.618**] & [2.8mM KO: **0.003** ± **0.003**] vs [16.7mM KO: **0.563** ± **0.277**]) (**Figure 4-10A**). I also observed a substantial reduction in insulin secretion at high glucose stimulation when adjusted for total DNA content in the βVPS41 KO islets compared to controls (mean insulin/DNA ± SEM =[16.7mM Ctrl: **10.684** ± **2.248**] vs [16.7mM KO: **0.193**± **0.097**] & [2.8mM Ctrl: **5.795** ± **1.481**] vs [2.8mM KO: **0.003** ± **0.003**]) (**Figure 4-10D**) although there was no statistical difference on total DNA content measured by DNA picoGreen assay (mean total DNA ± SEM =[Ctrl: **2.718** ± **0.240**] vs [KO: **2.489** ± **0.257**]) (**Figure 4-10C**). Regardless of external glucose concentrations, the secreted insulin from βVPS41 KO islets was blunt compared to WT islets (mean insulin/DNA ± SEM = [2.8mM KO: **0.003** ± **0.003**] & [16.7mM KO: **0.193**± **0.097**] (**Figure 4-10D**) this thus led to a question of whether impaired glucose-stimulated insulin secretion on βVPS41 KO islets is due to defective insulin storage in islets. Therefore, the total insulin content was measured from the same isolated islets by DNA picoGreen assay.

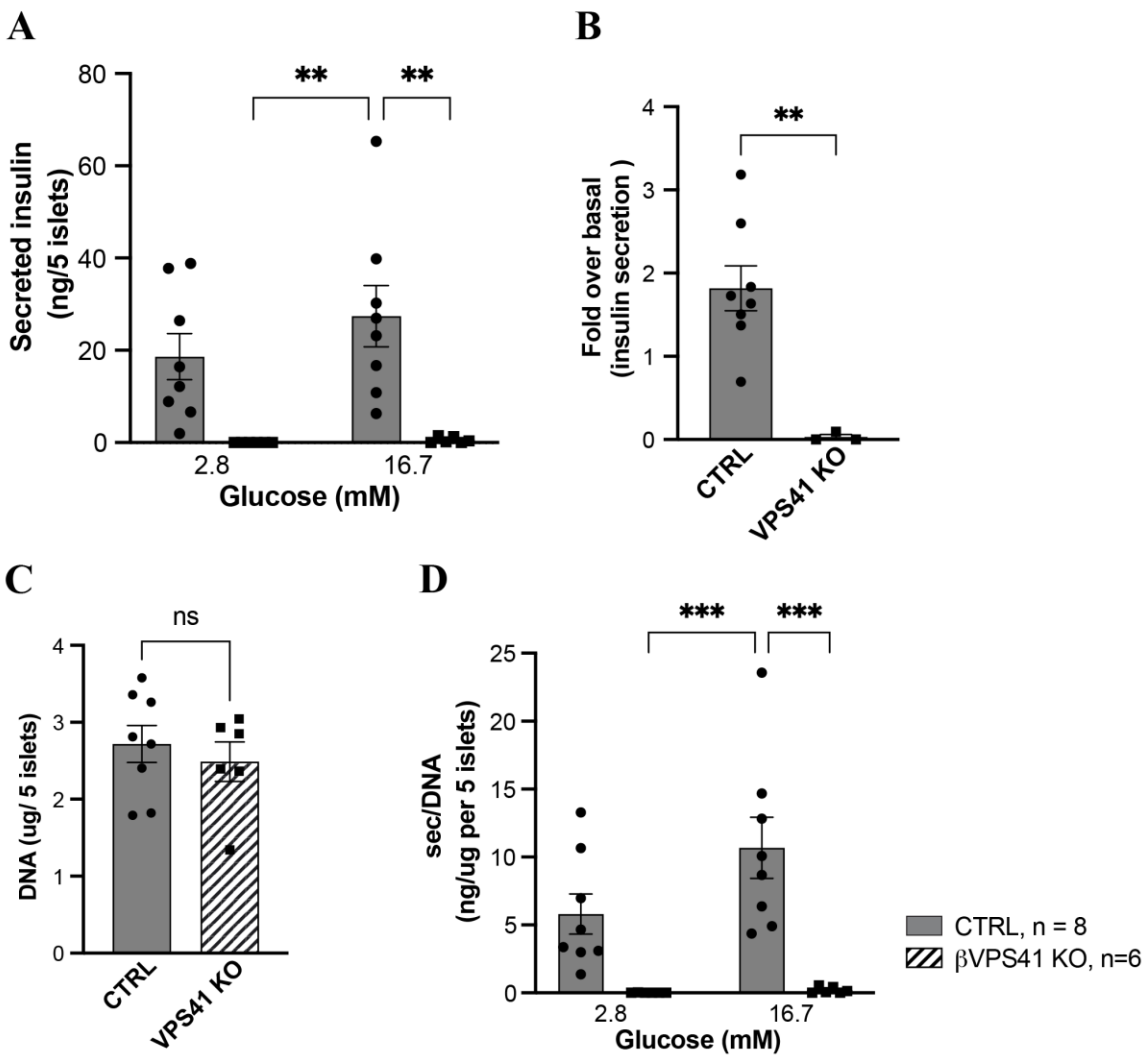

Figure 4-10 Glucose-stimulated insulin secretion in isolated βVPS41 KO islets

Isolated islets from WT, Cre and Flox mice were combined as controls. Size-matched islets were selected for GSIS assay. (A) Glucose-simulated insulin secretion and (B) its fold change. (C) DNA content analyzed by DNA picoGreen assay and (D) Insulin secretion from isolated mouse islets was normalized to DNA content. Data were represented mean ± SEM, ** $p < 0.005$ & *** $p < 0.0005$ by Two-way ANOVA with Šídák's multiple comparisons test (A), unpaired t-test (B & C) and Two-way ANOVA with Tukey's multiple comparisons test (D).

4.3.3.2 Insulin content in isolated β VPS41 KO islets

The total insulin content in islets was normalized to the total DNA content of islets (**Figure 4-11**). Like VPS41 KD and KO INS1 cells, βVPS41 KO islets had significantly less total insulin content compared to littermate controls (mean insulin content per 5 islets ± SEM = [Ctrl: **808.690** ± **87.506**] vs [KO: **442.233** ± **66.849**] ($p < 0.005$)) (**Figure 4-11C**). Collectively, these data demonstrate that VPS41 has a key role in insulin storage in β cells both *in vivo* and *in vitro*.

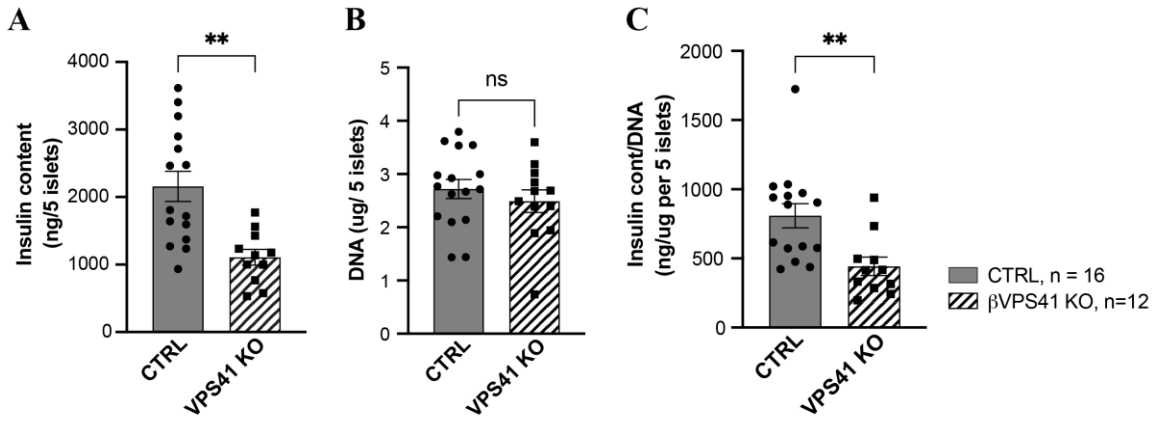

Figure 4-11 Insulin content in isolated βVPS41 KO islets

Size-matched isolated islets were selected and combined from 15-week-old WT, Cre and Flox mice as controls. (A) Insulin content was measured by HTRF assay and (B) DNA content was measured by DNA picoGreen assay. (C) The insulin content was normalized to DNA content. Data presented as mean ± SEM, ** $p < 0.005$ by unpaired t-test.

4.3.4 In vivo metabolic phenotypes of VPS41 Het KO male & female mice

4.3.4.1 Body composition

In this section, I examined *in vivo* metabolic phenotypes of βVPS41 Het mice and sex-specific differences in diabetes risk in βVPS41 Het and KO mice. βVPS41 Het KO and age-matched littermates (10 weeks old) were fed a standard chow diet. No major differences in total mass or body composition were observed between βVPS41 Het and KO mice compared to controls (**Figure 4-12**). However, female mice in control, Het and KO groups all exhibited increased body fat percentage compared to the male control group (mean % of fat/lean mass ± SEM = [male Ctrl: **6.125** ± **0.510**] vs [female Ctrl: **10.614** ± **0.897**] ($p < 0.005$) or [female Het: **12.115** ± **1.004**] ($p < 0.0001$) or [female KO: **11.406** ± **1.214**] ($p < 0.0005$)) (**Figure 4-12D**).

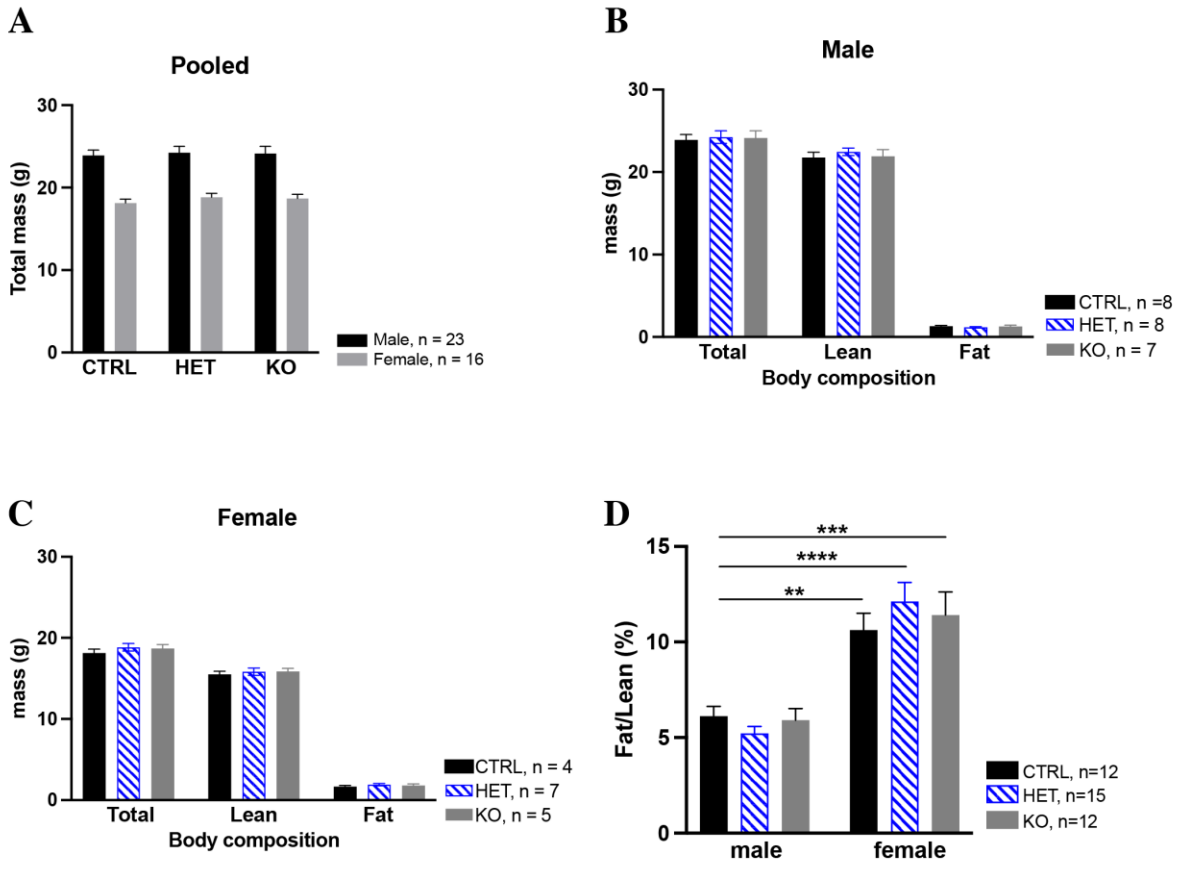

Figure 4-12 Body composition between sexes

HET, KO and age-matched control mice were fed a standard chow diet (A). Body composition parameters of total, lean and fat mass were measured in age-matched males (B) and females (C). For measurement of lean and fat mass, Eco MRI was used. (D) Fat mass as a percentage of lean mass. Data presented as mean ± SEM and ** $p < 0.005$, *** $p < 0.0005$, **** $p < 0.0001$ by ANOVA (D).

4.3.4.2 OGTT, AUC of OGTT and fasting glucose, OGTT and iAUC of OGTT of male and female Het and KO mice

In order to observe the maximal insulin response during the glucose tolerance test, in this section, oral glucose tolerance tests (OGTT) were performed. Age-matched (10 weeks old) mice fasted for 5 hours before oral administration of glucose. During the OGTT, blood glucose concentrations were measured from tipped tails at the indicated time points.

Consistent with the IP-GTT data (**Figures 4-4 & 4-9**), male KO mice had impaired glucose tolerance compared to Het mice and control groups through the course of the experiment (**Figure 4-13B**). Notably, male KO mice exhibited higher blood glucose levels over the course of the OGTT, and at time 0 after fasting for 5 hours. But female KO mice did not. Especially, the blood glucose levels in female KO mice increased sharply and peaked at 15 minutes after glucose administration however, they had trended towards reduced circulating glucose through all time periods (**Figure 4-13C)**. The glucose tolerance as indicated by incremental AUC (iAUC) revealed that HET mice were not different to controls regardless of sex. Overall, there were no marked differences of quantified data from the iAUC in male Het or female Het mice when comparing with each relevant control (mean iAUC of OGTT ± SEM = [male HET: **11.888** ± **2.296**] vs [male Ctrl: **10.070** ± **0.656**] or [female HET: **9.629** ± **0.499**] vs [female Ctrl: **8.550** ± **0.558**]) (**Figure 4-13B & C**).

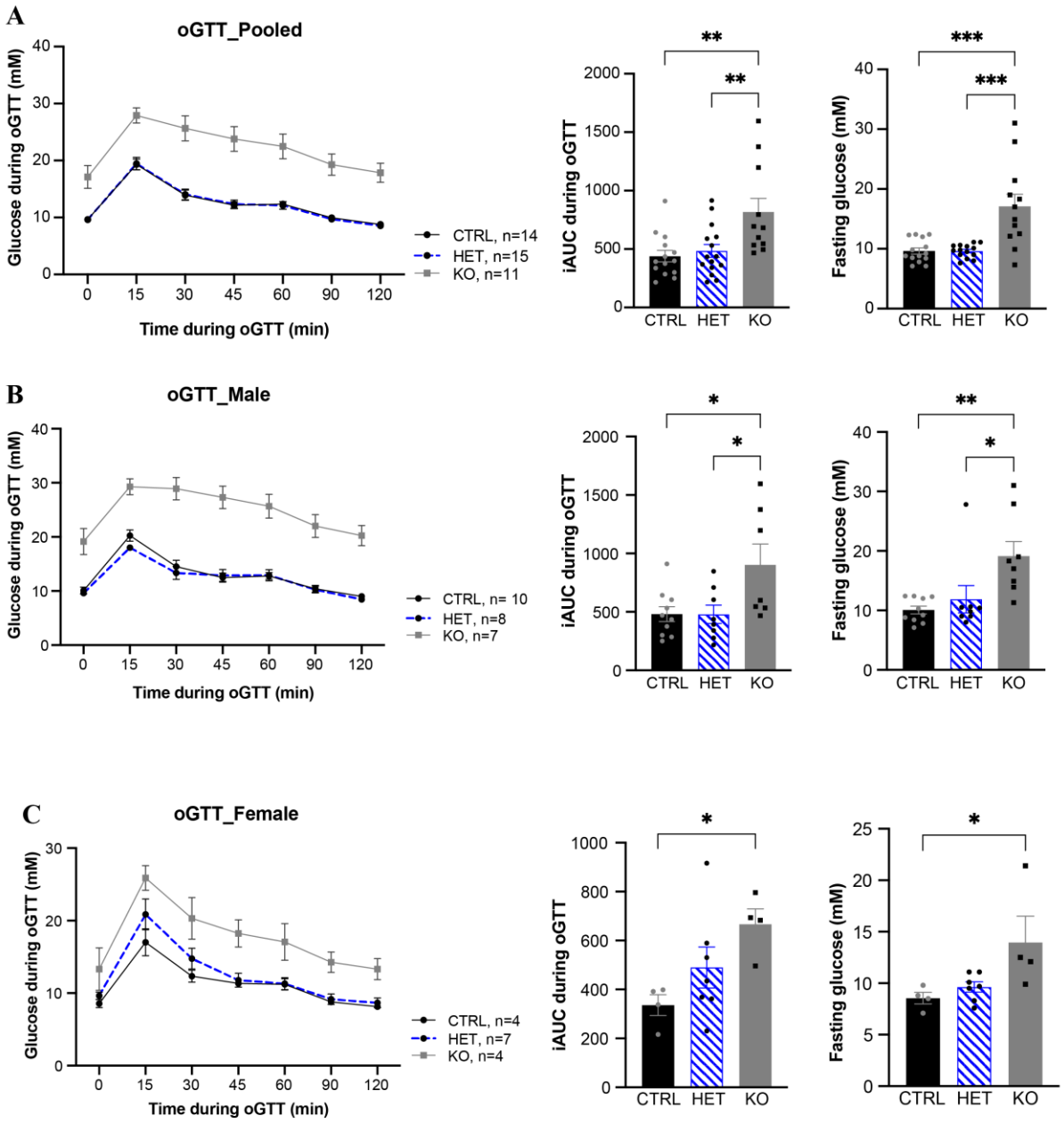

Figure 4-13 Regulation of glucose homeostasis in male and female mice

Het, KO and age-matched (10-week) control mice were fed a standard chow diet (A). After 5 hours fasting, blood samples were collected from the tipped tail at the indicated time points and blood glucose was measured by a glucometer. The age-matched males (B) and females (C) were displayed as control, Het and KO. Data presented as mean ± SEM. * $p < 0.05$, ** $p < 0.005$ & *** $p < 0.0005$ by One-way ANOVA with Tukey's multiple comparisons test.

Slight differences in glucose disposal were also observed at early time points of OGTT between male and female mice (**Figure 4-13B & C**), thus, glucose concentrations at 15, 30 and 45 minutes were directly compared (**Figure 4-14**). Except for the male KO mice, male Het mice, female Het and female KO groups experienced reduced circulating glucose concentration over time-returning towards normal glucose levels like control groups (**Figure 4-14)**.

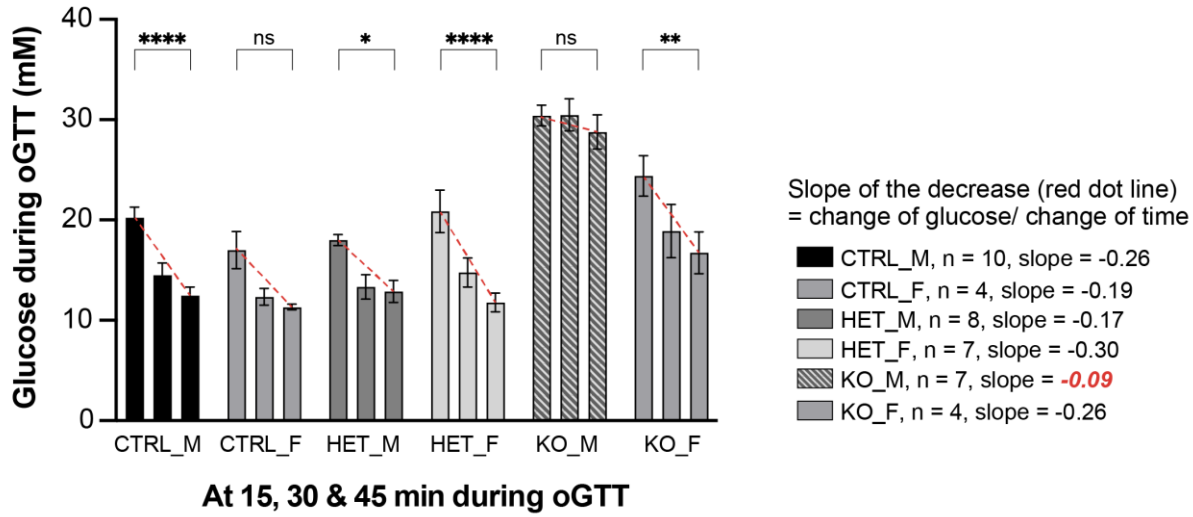

Figure 4-14 Changed glucose levels at 15, 30 and 45 min during OGTT on Control, Het and KO mice

Blood glucose concentrations at 15, 30 and 45 minutes during the OGTT on aged-matched Control, Het and KO mice. The red dot line indicated a slope of the decrease in blood glucose during the indicated times. Data presented as mean ± SEM. * $p < 0.05$, ** $p < 0.005$ & **** $p < 0.000.1$ by Two-way ANOVA with Tukey's multiple comparisons test.

4.3.4.3 Insulin Levels in Blood on Mice

Circulating insulin was measured using insulin ELISA assay (Crystal Chem, #90080) at time 0 under fasting conditions and 15 minutes after oral administration of glucose in age-matched mice. As expected, insulin levels were slightly enhanced at 15 minutes post-administration compared to fasting insulin for both control and Het mice (**Figure 4-15**). Male KO mice appeared non-responsive to glucose administration, showing similar insulin levels to fasting insulin levels (mean insulin ± SEM = [0 minutes male KO: **0.33** ± **0.09**] vs [15 minutes male KO: **0.36** ± **0.09**] (p = 0.84)) (**Figure 4-15B**). Female KO mice, however, had enhanced but not statistically significant circulating insulin levels at 15 minutes (mean insulin ± SEM = [0 minutes female KO: **0.20** ± **0.07**] vs [15 minutes female KO: **0.34** ± **0.17**] (p = 0.49)) (**Figure 4-15C**).

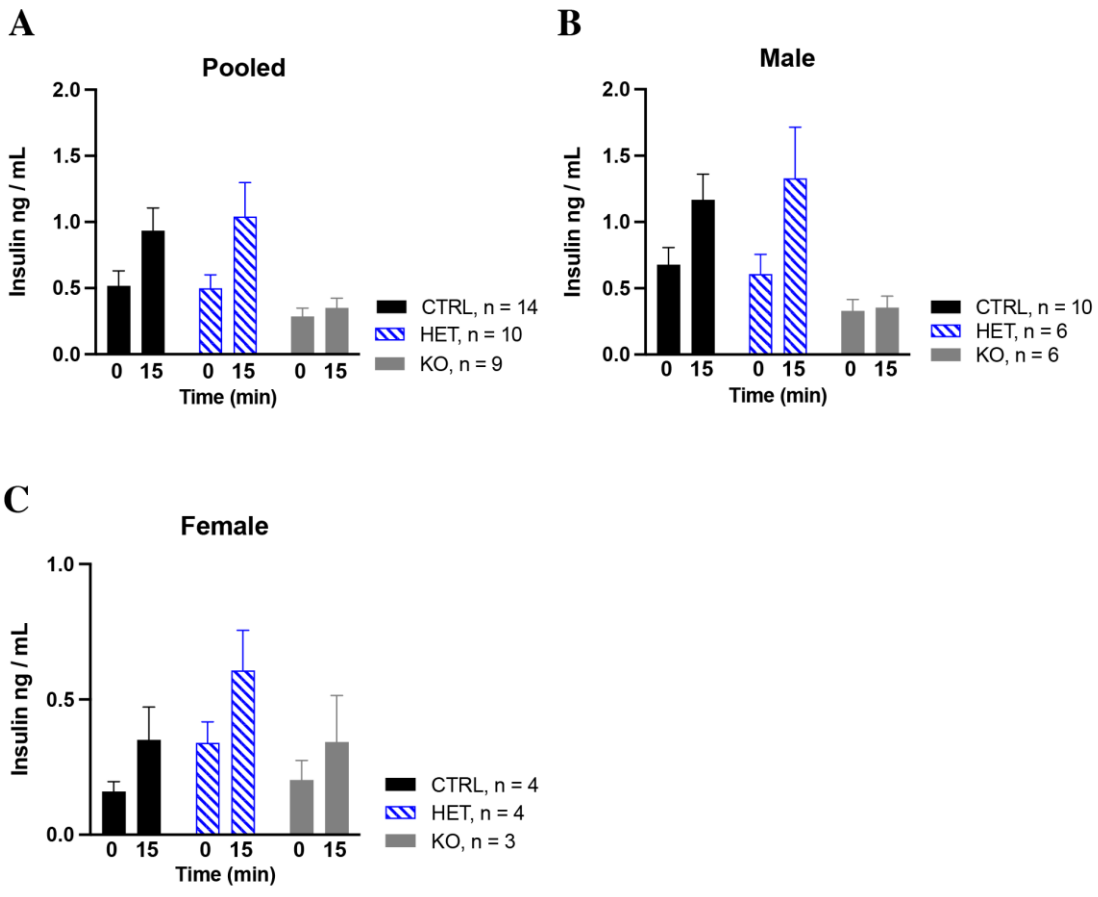

Figure 4-15 Gender differences on blood insulin concentrations at 0 and 15 minutes during OGTT

Circulating insulin levels at 0 and 15 minutes during the OGTT was measured using insulin ELISA kit (Crystal Chem, #90080). (A) Pooled (total n=33), (B) male (total n=22) and (C) female (total n=11) were displayed as control, Het and KO. Data were presented as mean ± SEM and analyzed by Two-way ANOVA with Tukey's multiple comparisons test but there was no significance.

4.3.4.4 Whole Body Insulin Action between Male and Female βVPS41 Mice

Regrettably, ITT on in-vivo mouse model was not obtained proper sample numbers due to COVID-19 shutdown over 2020/2021.

To evaluate the insulin sensitivity of insulin-responsive tissues, an intraperitoneal insulin tolerance test (IP-ITT) was performed in age-matched mice (10-week-olds). By monitoring endogenous glucose levels over time during the ITT, the rate of insulin action in insulin-responsive tissues can be determined. Age-matched mice fasted for 5 hours, and their endogenous glucose levels were measured at the indicated time points over 2 hours before and after the administration of human insulin.

Both male and female KO mice exhibited significantly higher endogenous glucose levels even at time 0, before insulin administration (baseline) (mean glucose concentration ± SD = [0 min male KO: **19.163** ± **2.426**] & [0 min female KO: **13.975** ± **2.540**]. During the ITT, the iAUC of glucose was higher in KO mice (mean iAUC of ITT ± SD = [male KO: **902.114** ± **178.359**] & [female KO: **667.325** ± **62.449**]), while control and Het mice had similarly quantified iAUC during the ITT (mean iAUC of ITT ± SD = [male Ctrl: **480.920** ± **63.708**] & [male Het: **478.525** ± **78.255**] or [female Ctrl: **336.400** ± **42.371**] & [female Het: **490.314** ± **83.797**]) (**Figure 4-16**). The insulin sensitivity was statistically different in KO mice only when compared to the pooled mix-gender control (mean iAUC of ITT ± SD = [pool Ctrl: **439.269** ± **49.531**] vs [pool KO: **816.736** ± **117.675**] ($p < 0.05$)) (**Figure 4-16A**) since the number of mice available for the ITT experiment was not enough for statistical comparison (**Figure 4-16**).

In this thesis, there was a lack of statistical power to interpret for risk of developing T2D by gender in the βVPS41 KO mouse model due to the limited mouse numbers depending on sex or genotypes. However, *in vivo* phenotypes of β cell VPS41 KO mouse demonstrate that VPS41 deletion contributes to dysregulated whole-body glucose homeostasis and there could exist a gender-based role of VPS41 in the risk of developing hyperglycaemia in a mouse model.

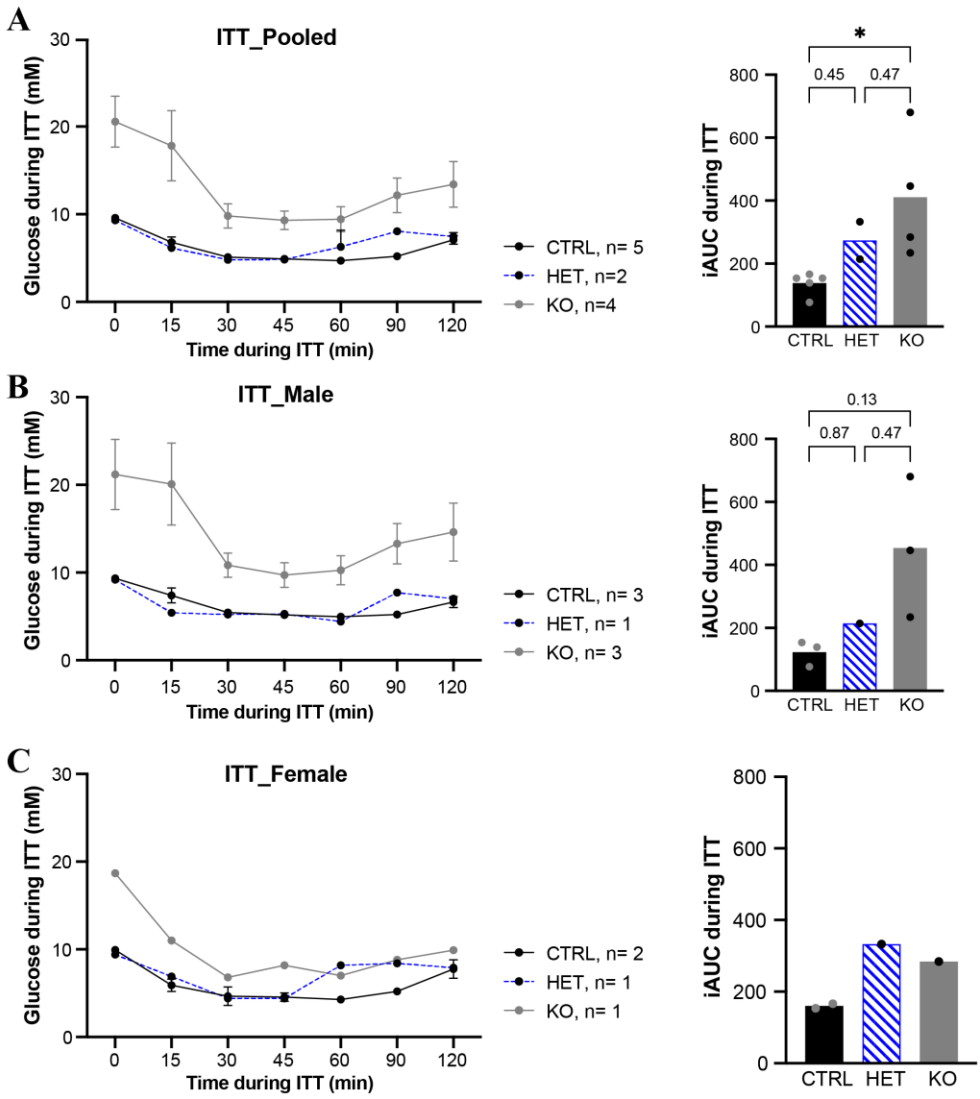

Figure 4-16 Gender differences in blood glucose levels during ITT in Het, KO and control mice

Blood glucose levels were measured at the indicated time points during ITT in age-matched mice. Age-matched (10-week) mice were used as the control group (n=5) Het (n=2), KO (n=4) mice. Pooled (A), male (B) and female (C) were displayed as control, Het and KO. Data presented as mean ± SD. * $p < 0.05$ by One-way ANOVA with Tukey's multiple comparisons test (A).

4.3.4.5 Insulin and Glucagon Expression in Male and Female β VPS41 KO Pancreata

Insulin levels in the whole pancreata of individual mice from each littermate were examined by performing immunofluorescence staining on paraffin-embedded pancreas sections. Insulin levels were slightly reduced in pancreata from βVPS41 KO mice while no marked alteration in glucagon levels was observed between them (**Figure 4-17**). Besides, there was no effect on islet architecture between WT and βVPS41 KO mice.

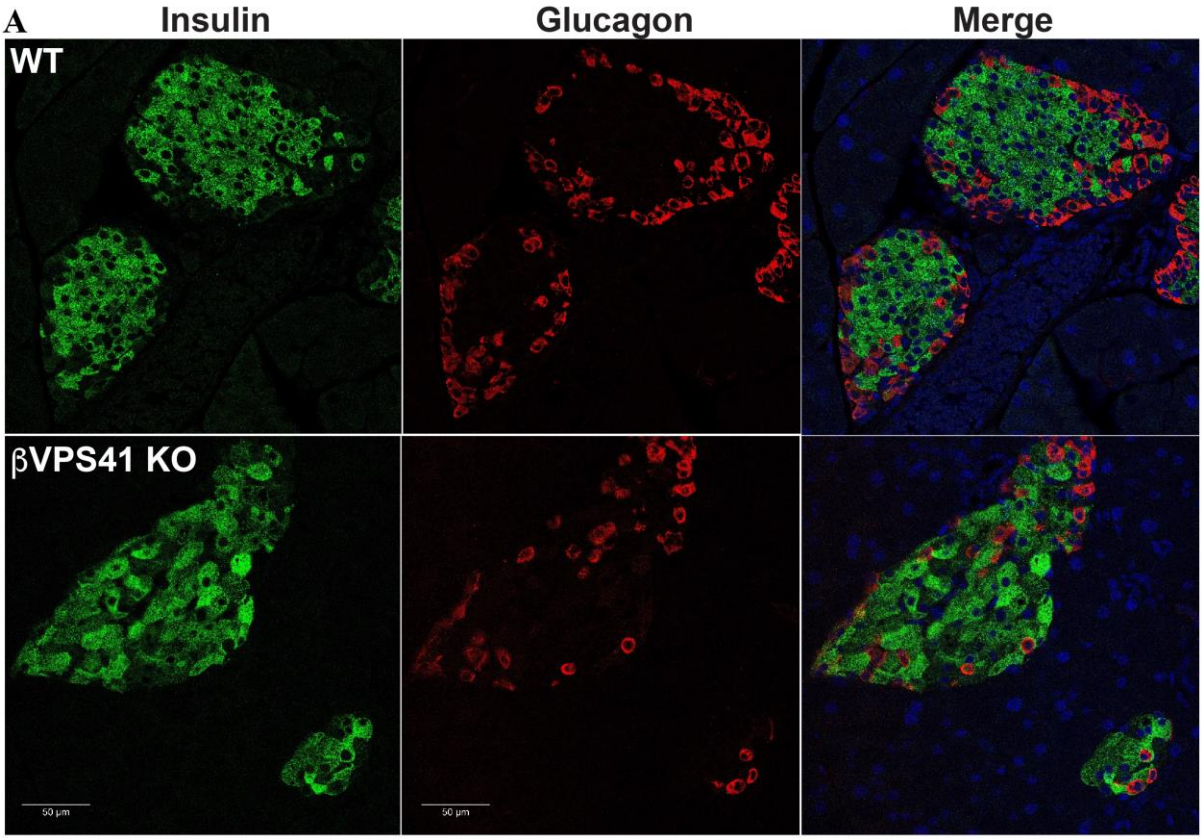

Figure 4-17 Insulin and Glucagon staining in whole pancreas slices from WT and βVPS41 KO mice

Pancreas slices were stained for insulin (green) and glucagon (red). (A) Whole pancreata were obtained from age-matched (15-week) WT (top) and VPS41 KO (bottom) male mice. The scale bar indicates 50µm.

4.3.5 *Ex vivo* characterization of βVPS41 Male & Female mice

4.3.5.1 Glucose-stimulated insulin secretion on isolated islets

To characterize β cell function in female and male mice lacking β cell VPS41, islets from age-matched mice (10 weeks) were isolated and GSIS assays were performed *ex vivo*. Except for male KO mice, all genotypes secreted insulin in response to high glucose (16.7mM) (mean at 16.7/2.8mM ± SD = [male KO: **1.09** ± **0.33**] vs [male Ctrl: **5.55** ± **1.90**] [male Het: **6.43** ± **1.82**] [female Ctrl: **2.70** ± **1.75**] [female Het: **2.47** ± **0.75**] [female KO: **3.91** ± **1.62**]) (**Figure 4-18A ~ C**). To further analyse sex differences, insulin levels at basal glucose (2.8mM) conditions were measured and male KO mice had the highest levels of insulin at basal glucose (mean basal insulin ± SD = [male KO: **12.56** ± **1.88**] vs [male Ctrl: **3.44** ± **0.94**] ($p < 0.0001$)) (**Figure 4-18A**). Surprisingly, this insulin level in male KO was approximately 4-fold higher than that of female KO upon basal conditions (mean basal insulin ± SD = [male KO: **12.56** ± **1.88**] vs [female KO: **3.40** ± **2.04**] ($p < 0.0005$)) (**Figure 4-18C**).

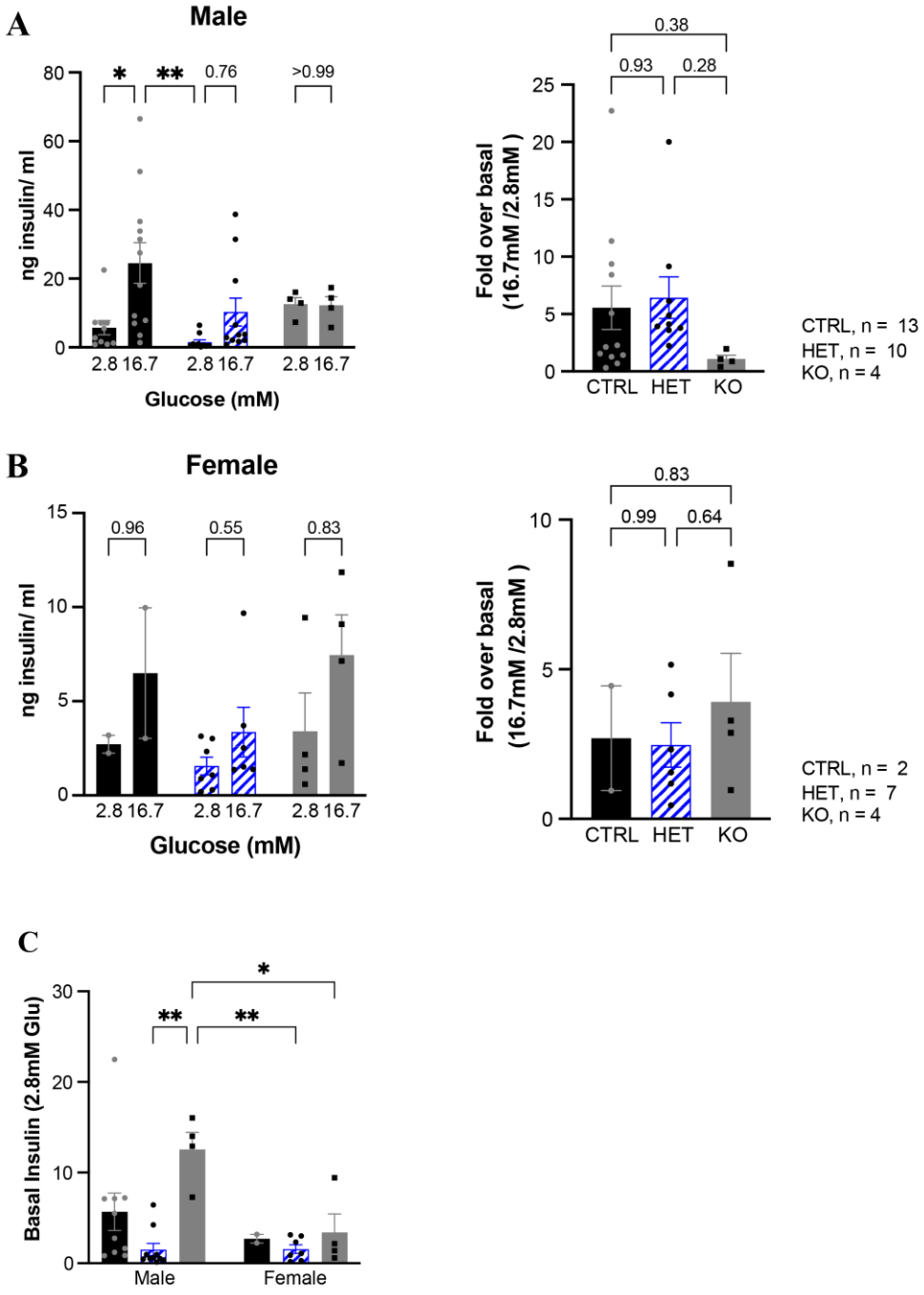

Figure 4-18 Glucose-stimulated insulin secretion in isolated islets of male and female βVPS41 KO mice

Islets were isolated from male and female β VPS41 KO mouse (10 weeks) pancreases. Size-matched islets were selected, and insulin secretion was measured by HTRF assay. Glucose-simulated insulin secretion and its fold over basal of male (A) and female (B). (C) Basal insulin at 2.8mM glucose in male and female mice. Data were presented by mean ± SD. * $p < 0.05$ & ** $p < 0.005$ by Two-way ANOVA (A-left, B-left and C) or One-way ANOVA with Tukey's multiple comparison test (A-right and B-right).

4.4 Summary

In this chapter, we generated β cell-specific VPS41 KO (βVPS41 KO) mice using the Cre-Lox technology to the role of VPS41 in glucose homeostasis *in vivo*. Metabolic phenotypes of glucose regulation in these mice were examined by performing glucose tolerance tests and measuring circulating insulin concentrations. Notably, blood glucose levels were significantly increased during the glucose tolerance test but also prior to glucose administration in βVPS41 KO mice, compared to control mice (**Figure 4-5, 4-9 & 4-13**). Indeed βVPS41 KO mice were hyperglycemic at the 5 hours-fasting state, time 0, (**Figure 4-4B, 4-8 & 4-13**) and their glucose levels significantly increased post-administration of glucose. These data indicate that βVPS41 KO mice exhibit dysregulated whole-body glucose homeostasis. Importantly, the circulating insulin before and 15 minutes post glucose administration during the IP-GTT in 15-week-old βVPS41 KO mice was markedly reduced regardless of fasting or fed state (**Figure 4-7**), showing that βVPS41 KO mice were hyperglycemia with dysregulated glucose homeostasis.

By performing glucose-stimulated insulin secretion assays *ex vivo*, I observed that βVPS41 KO mice had a marked decrease in islet insulin content with an 85% reduction in content compared to control islets (**Figure 4-11**). Consistent with previous VPS41 KO (**Figure 2-2**) and KD INS1 cells (**Figure 3-7**), the immunofluorescence staining of whole pancreas sections exhibited a reduction in insulin levels on βVPS41 KO mouse islets compared to WT (**Figure 4-17**). The pancreas staining images also revealed no obvious alteration or defects in the islet architecture on βVPS41 KO mice compared to WT. Besides, the electron microscopy (EM) images of isolated islets from βVPS41 KO mice indicated the reduction of insulin granules exhibiting a few dense cores surrounded by a grey halo (**Figure 4-19B**). But WT contains large numbers of a dense black core surrounded by a white halo, which is recognized as insulin granules (**Figure 4-19A**).

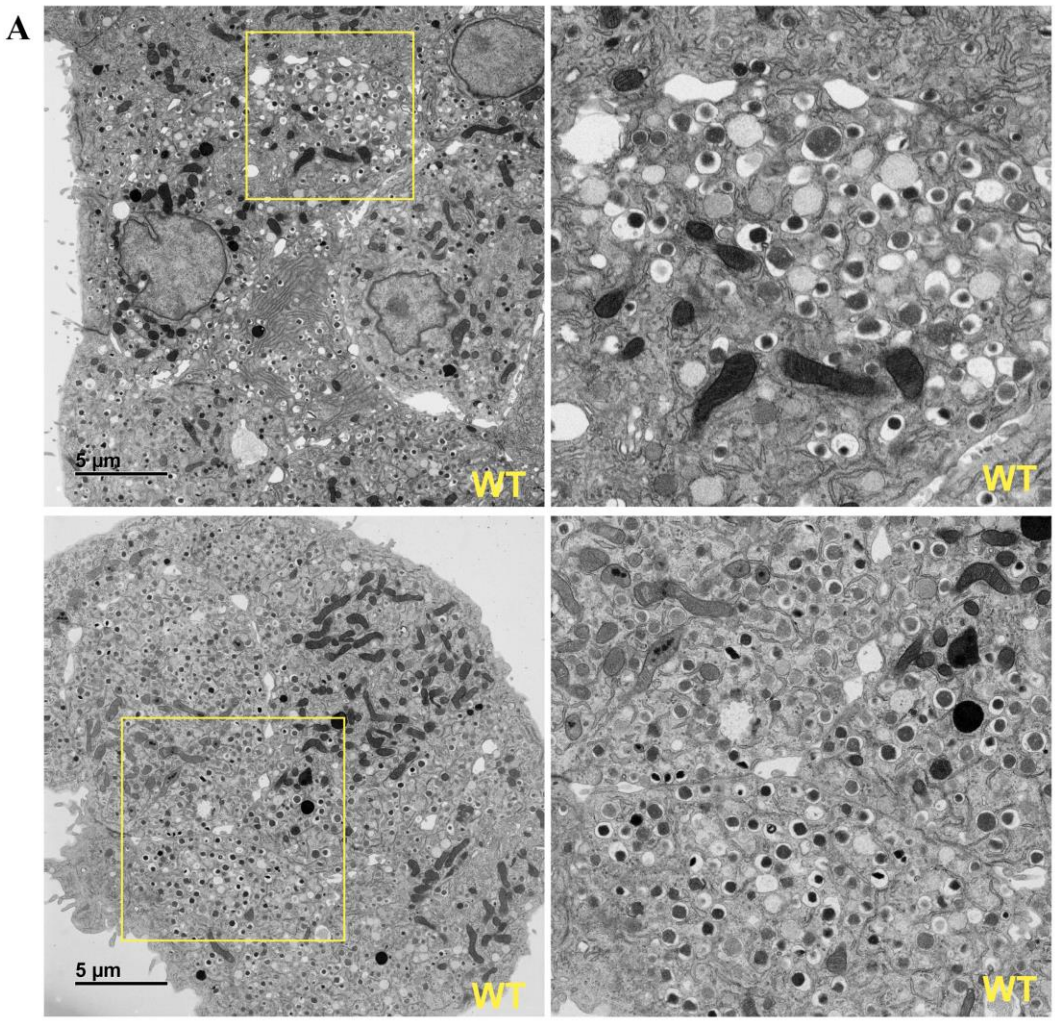
A
5 µm
WT
WT
5 µm
WT
WT

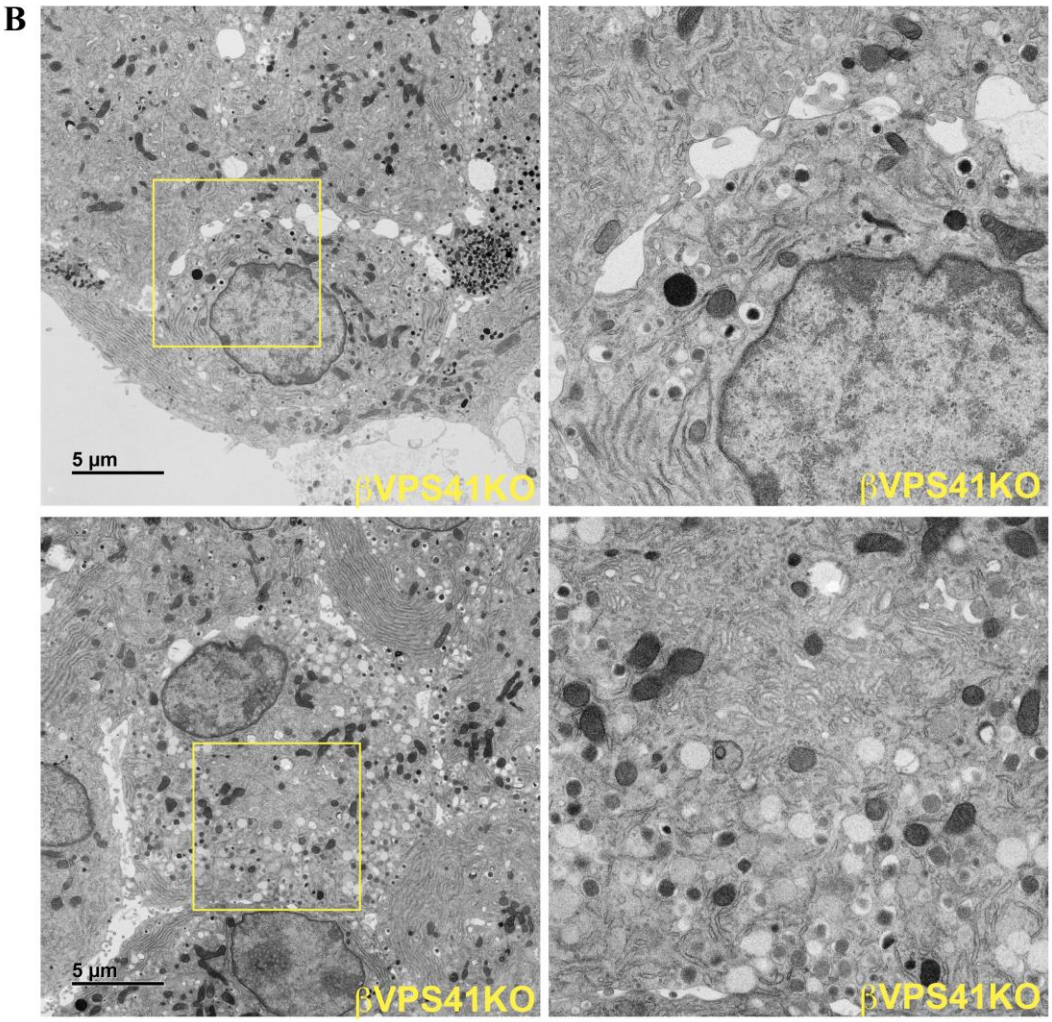

Figure 4-19 Representative electron microscopy (EM) images of isolated islets from the 15-week-old age-matched (A) WT and (B) VPS41 KO mice

Each EM image was captured from 3 biological replicates. Scale bar, 5uM. (https://diabetesjournals.org/diabetes/article/70/2/436/39475/Pancreatic-Cell-Specific-Deletion-of-VPS41-Causes)

In addition to reduced insulin content, βVPS41 KO islets had impaired GSIS (**Figure 4-10**), consistent with plasma insulin levels post-glucose administration in βVPS41 mice (**Figure 4-7**).

To determine if there is gender dependency on VPS41's role in glucose homeostasis, I compare the phenotypes of male and female KO mice. During the OGTT, male KO mice exhibited severe phenotypes of hyperglycemia and impaired glucose tolerance (**Figure 4-13B & C**) and nonresponsive insulin secretion post-glucose administration with circulating insulin plasma levels being similar pre- and post-glucose administration (**Figure 4-15B & C**). The Glucose tolerance test is a well-defined tool in rodent research to investigate whole-body glucose metabolism *in vivo* [234,237]. There are various variables to impact on measured glucose levels e.g., time of fasting, glucose load and route of glucose administration in mice [234,237]. It has been reported that oral glucose delivery in mice allows to better glucose tolerance than I.P. (intraperitoneal) injection due to lower glucose excursion and enhanced insulin response [234,237,238]. Indeed, I.P. injection partially bypasses the gastrointestinal tract, which plays a major role in the control of glucose homeostasis through regulation of incretin hormones including GLP-1 (glucagon-like peptide-1) or GIP (glucose-dependent inhibitory peptide) [237]. Small et al examined the insulin response by measurement of circulating insulin and incretin hormones, e.g., GIP and GLP-1 following glucose administration of oral delivery or I.P. injection [237]. Surprisingly, plasma levels of insulin, C-peptide as well as active GIP were elevated after oral glucose administration, but they were abolished following I.P. injection [237]. These results showed the differences in whole-body glucose handling in mice depending on routes of glucose administration such as oral delivery or I.P. injection for glucose tolerance test. In the βVPS41 KO mouse model, both female and male KO mice had glucose intolerance through the course of the OGTT, consistent with the IP-GTT. The severe fasting hyperglycemia, the hallmark of T2D was observed in male KO mice more than in female KO mice during the OGTT.

Overall, the results from the β cell specific VPS41 KO mice provide the existence of severe diabetic phenotypes such as hyperglycemia and non-responding insulin secretion upon external stimuli. The findings revealed a novel role of VPS41 as a regulator of whole-body glucose homeostasis in mice with VPS41 gene deletion in β cells. Thus, mice with a conditional deletion of VPS41 in β cells develop diabetes as a result of dysregulated whole-body glucose homeostasis that stems from significantly reduced insulin content and secretion in β cells. However, the mice numbers were quite limited to interpret the risk of developing T2D in β cell

specific VPS41 KO mouse model by gender in this thesis. Therefore, further study might be required on whether the risk of developing T2D in this mouse model is sex-dependent with male mice being at risk.

5 Chapter V: Final Summary

Accumulating evidence from both T2D mouse model and T2D patient studies indicate that abnormal phenotypes of islet β cells for the insulin secretory pathway including insulin SG biogenesis and insulin granule storage is implicated in T2D progression[157,199,239,240]. In healthy islet β cells, insulin content is maintained in a bioactive form within SGs for secretion to meet metabolic demand [47,55,57,241]. However, during the progression of T2D, insulin pools in the SGs diminish due to defective insulin synthesis and β cell failure, accompanied by loss of β cell identity [149]. Deficient insulin levels finally lead to dysregulated glycemic control, the hallmark of T2D.

After synthesized in the ER, insulin is stored in SGs, which are small membrane-bound vesicle structures defined as the functional unit for insulin storage [47,76,242]. Many molecules including soluble proteins, ions, transmembrane proteins, and membrane-associated proteins are involved in the formation of insulin SG [49,50,199]. Hence, the coordinated activity of insulin SG membrane-associated proteins and/or their interactions with specific molecules has high potential to determine the fate of insulin in β cells. This thesis identifies VPS41 as a key player in the secretory granule pathway in β cells. VPS41, a subunit of the HOPS complex, functions as a regulator for vesicle-mediated trafficking through interaction with Rab7 in the endo-lysosomal pathway [166,178,179]. In addition to its role in the HOPS component, a role for VPS41 regulating secretion of synthesized proteins such as neuropeptides in neurons has recently been shown [164,165]. Furthermore, VPS41 is required for the direct trafficking of TGN-derived vesicles into lysosome [189] (**Figure 1-9**). Indeed, the alkaline phosphatase (ALP) pathway is a bypass delivery route of vesicle proteins in yeast, which requires VPS41 and AP-3 interaction for the formation of coated vesicles that allows for selective trafficking to target destinations [182,183].

VPS41 regulates insulin storage in β cells both in vitro and in vivo.

The findings presented in this thesis show VPS41 deficiency results in poor insulin storage, and decreased insulin secretion in β cells *in vitro* and *in vivo*. These abnormal phenotypes could be caused by several possible reasons such as impaired insulin synthesis, loss of β cell identity or defective β cell insulin storage [6,14,78,151].

VPS41 is a cytosolic protein and a pool of VPS41 localizes near the TGN [189,243]. So far, VPS41 has not been identified as a transcriptional factor regulating gene expression of proteins involved in insulin synthesis, including insulin. Consistent with this idea, endogenous proinsulin protein levels were not significantly different in the absence of VPS41 expression (**Figure 2-1, 3-15 & Appendix Figure1**); however, endogenous insulin levels (**Figure 2-1, 3-4, 3-6 & 3-14**) and CgA protein expression (**Figure 3-17**), which is a marker of insulin granules, were decreased in VPS41-depleted INS1 cells. These data suggest that defects in insulin synthesis are not the major cause of impaired insulin secretion in the absence of VPS41 on INS1 cells. Our collaborators, Cedric S. Asensio (University of Denver, USA) observed no effects on insulin packaging or defects in vesicle movement from the TGN in VPS41 KO INS1 cells, compared to WT INS1 cell [191], which suggests that the impaired insulin secretion in β cells is also not due to dysregulated of SG packaging or vesicle budding in the absence of VPS41. However, reduced numbers of insulin granules in β cells were observed in the absence of VPS41 (data not shown in this thesis), which eventually leads to defective insulin exocytosis.

To identify and quantify proteins that are important to the insulin-regulated secretory pathways in β cells, label-free quantification mass spectrometry analysis in WT and VPS41 KO INS1 cells was performed. Interestingly, proteomics analysis of VPS41 KO INS1 cells showed enhanced expression of β cell-disallowed genes and suppression of β cell-specific genes (**Figure 2-13**), suggesting that chronic VPS41 deletion could cause β cell de-differentiation with the concomitant loss of β cell identity. The hierarchical clustering analysis on VPS41 KO INS1 cells has revealed a significant reduction of proteins associated with insulin secretory machinery, including vesicle-mediated transport and insulin maturation processing (**Figure 2-14**). Furthermore, VPS41 KO INS1 cells were unable to express insulin after transfection with a GFP-tagged proinsulin construct (**Figure 3-16B**), suggesting that chronic deletion of VPS41 causes the loss of β cell identity. Therefore, I chose to study acute deletion of VPS41, via siRNA-mediated strategy, to investigate the mechanisms whereby lack

of VPS41 decreases insulin secretion and reduces insulin storage in β cells. Like VPS41 KO INS1 cells, the impaired insulin secretory machinery phenotype with a lack of insulin was observed in siRNA-mediated VPS41 KD INS1 cells (**Figure 3-4 ~ 3-11**).

In addition to cell-based *in vitro* studies, we generated a β cell-specific VPS41 KO mouse model to examine the role of VPS41 in pancreatic β cells *in vivo*. There are many *in vivo* and *in vitro* studies describing the strong connection between a loss/defect among intracellular compartments involved in insulin SG biogenesis and defected insulin release upon cellular stimulation on pancreatic β cells [49,50,199,211]. Among several cytosolic proteins, VPS10 has been reported as the essential protein for vesicle trafficking through interacting with cargo proteins in SG biogenesis like VPS41, and Sorcs1 is a member of VPS10 family [244]. Like Sorcs1 KO mice, we observed that mice with the specific deletion of VPS41 in β cells exhibit diabetic phenotypes together with fasting hyperglycemia and glucose intolerance (**Figure 4-4, 4-5, 4-8 & 4-9**). However, the degree of phenotypes related to dysfunctional β cells are different between these KO mouse models. *Ex vivo* studies using isolated islets from KO mice revealed that βVPS41 KO islets exhibited a massive reduction of insulin content as well as defective insulin secretion (**Figure 4-10, 4-11 & 4-18**), while there were no differences between WT and Sorcs1 KO islets for total insulin content and insulin secretion upon cellular stimulation e.g., 16.7mM glucose [244].

However, the insulin content in Sorcs1 KO islets was reduced under metabolic stress such as prolonged FFA, which leads to the defected insulin secretion in Sorcs1 KO mice [244]. Kebede et al thus indicated that the function of Sorcs1 in SG biogenesis is required to replenish insulin SGs on pancreatic β cells under metabolic stress circumstances. But poor storage of insulin SGs and marked reduction of insulin content present as abnormal phenotypes on VPS41-depleted β cells *via* acute or chronic VPS41 deleted systems *in vivo* and *in vitro* models even under ordinary circumstances. Furthermore, whole pancreas sections from βVPS41 mice were stained with an anti-insulin antibody to examine insulin levels revealing a reduction in insulin levels but no change in glucagon expression (**Figure 4-17**). Despite many black dense cores on WT islets, the EM images of βVPS41 also exhibited few dense cores, which are recognized as insulin granules in islets (**Figure 4-19**). Hence, our findings revealed VPS41 as a key player to regulate whole-body glucose homeostasis using a conditional gene deletion mouse model as a diabetic model.

In animal models of type 2 diabetes, males exhibit more severe diabetic phenotypes than females for example, Zucker diabetic fatty (ZDF) rat [245,246], the Akita mouse [127] and the mice with diabetes induced by treatment with streptozotocin [247]. The sex differences in T2D and obesity are also observed in humans with different prevalence as male is predominantly in diabetes [248–250]. Indeed, Mauvais-Jarvis' group reviewed gender-based differences in diabetes to identify underlying mechanisms of genes and/or environmental factors using animal models by focusing on pancreatic β cell function [250–253]. It could be due to different reactions of islets from males and females under stress conditions. However, recent studies on animal models provide evidence that gonadal hormones such as estradiol or testosterone are critical factors for β cell function [250,254,255]. Especially, testosterone facilitates glucose-stimulated insulin secretion in male mice lacking androgen receptors in β cells through the action of androgen receptors, leading to the improvement of β cell function in males [254]. On the high-fat diet-induced T2D model, treatment of testosterone in C57BL6J male mice also improved glucose homeostasis [255]. However, insulin resistance was increased in the liver on testosterone treated in this mouse model along with increased FOXO1 and decreased p-AKT, both levels are indicators for tissue insulin responsiveness [255].

In the current thesis, gender studies of βVPS41 mice presented minor VPS41-dependent sex differences for the risk of developing hyperglycemia. Compared to female KO mice, the age-matched male KO mice exhibited severe glucose intolerance with glucose levels not returning to normal during the GTT (**Figure 4-13**). However, the insulin resistance during ITT was not completely interpreted as whether sex differences exist due to the lack of statistical power (**Figure 4-16**). It is important to note that *in vivo* results for young female mice were not presented in this thesis to fully understand VPS41-dependent gender differences in the progression to T2D. Further studies are necessary including young female mice. Several animal and human clinical studies indicate a strong correlation between estrogen deficiency and metabolic disorder [249,256–258]. Insulin-responsive tissues such as muscle, adipose tissue, and liver are critical in maintaining glucose homeostasis [18,23]. Indeed, estrogen is known as a regulator to control glucose levels in these tissues through estrogen-mediated signaling [249,256,258]. Estrogen not only facilitates glucose uptake in muscle but also suppress glucose production in the liver via the activation of estrogen receptor, which both contribute to the improvement of insulin sensitivity in these insulin-responsive tissues to coordinate glucose homeostasis [249,258]. As βVPS41 mice develop severe hyperglycemia in an age–dependent manner along with dysregulated glucose homeostasis (**Figure 4-5, 4-9 & 4-13**), young female

βVPS41 mice thus might provide evidence of whether sex steroid hormones such as estrogen are crucial factors determining T2D progression. It is possible that gender differences in insulin-responsive tissues determine the degree of T2D. However, in this thesis, I did not examine whether these insulin-responsive tissues could be affected by the absence of VPS41 in pancreatic β cells and, if so, to what extent, depending on gender. However, glucose-stimulated insulin secretion, storage, and subcellular localization in islets were studied on βVPS41 KO mice. Performing GSIS assays on isolated islets *ex vivo*, it was revealed that βVPS41 KO islets from both females and males displayed impaired glucose-stimulated insulin secretion upon high glucose treatment (**Figure 4-10 & 4-18**). Interestingly, basal insulin levels in KO males were extremely high (**Figure 4-18C)**. Hence, further examination of insulin-responsive tissues in βVPS41 mice is important to identify the impact of gender on T2D progression in the absence of VPS41.

AP-3-coated SGs containing insulin undergo proteolysis in the absence of VPS41.

: A proposed mechanism of poor insulin storage in VPS41-depleted β cells

Chronic and acute deletion of VPS41 *in vitro* resulted in phenotypic abnormalities of reduced insulin secretion and storage capacity in INS1 and β cells Similarly, *in vivo* VPS41 absence led to a significant reduction in insulin content, defective insulin release culminating in β cell failure. Interestingly, genes involved in proteolysis were up-regulated in the proteomics analysis of VPS41 KO INS1 cells (**Figure 2-14B**) and enhanced expression of poly-ubiquitinated proteins in these cells were observed by Western blot (**Figure 3-13**). Thus, I hypothesized that SGs containing insulin undergo proteolysis through intracellular protein degradation pathways in VPS41-depleted β cells as the mechanism accounting for reduced insulin storage (**Figure 3-12**). To examine if this is the mechanism whereby insulin content is reduced, protein degradation pathways were inhibited by pharmacological reagents targeting different pathways in VPS41 KD INS1 cells. Surprisingly, inhibiting protein degradation restored endogenous insulin levels in VPS41 KD INS1 cells (**Figure 3-14**). Lysosomal inhibitors CQ and E-64 were especially effective in rescuing insulin expression (**Figure 3-14**).

The next question that arose was how insulin granules degrade selectively in the absence of VPS41 in INS1 cells. According to what is reported in the literature, VPS41 interaction with the AP-3 complex is essential for vesicular transport from the TGN to organelles [164,182]. Both VPS41 (**Figure 1-9 & 1-10**) and AP-3 each have motifs for direct binding and formation of coat structures [164,183]. I proposed that VPS41 and AP-3 (interaction) -mediated formation of coat structures in insulin granules could be essential in determining the fate of insulin granules in β cells. Direct interaction of VPS41 and the AP-3 complex to form coat structures in insulin granules was not studied in this thesis; however, the intracellular distribution of specific markers involved in autophagosome-lysosome mediated proteolysis such as LAMP1, LC3A/B and the AP-3 complex was changed in VPS41-depleted INS1 cells compared to control INS1 cells (**Figure 3-19**). It is not fully understood whether this mechanism could be a selective process only for large and dense-core vesicles such as insulin SGs or if it could occur also during the transport of membrane-bounded organelles via the constitutive secretion pathway, another parallel pathway from the TGN to the plasma membrane. Further studies are required including isolating insulin secretory granules associated with VPS41-AP-3 complex within the insulin SGs transport system.

The underlying mechanism of reduced insulin SGs in VPS41-depleted INS1 cells could be proposed together with AP-3 function to form coated structures for vesicular transport through the secretory pathway. VPS41 is required for trafficking TGN-derived vesicle cargo to its target destination and has a role in vesicle budding [182,189]. VPS41 associates with the AP-3 complex by binding to its delta subunit, (Apl5 in yeast) [164,182,184]. Thus, the formation of VPS41-AP-3 coat structures on insulin SGs might allow for the regulated secretory pathway to occur (**Figure 5-1A**). It is established that AP-3 is a key regulator for vesicle transport from the TGN to the lysosome [182,185,231]. Thus, in the absence of VPS41, AP-3 coated insulin SGs could be shunted to autophagosome-lysosome mediated proteolysis leading to low numbers of insulin granules in β cells (**Figure 5-1B**). Hence, VPS41-depleted β cells exhibit defective insulin release upon external glucose stimuli that contributes to dysregulated glucose homeostasis (**Figure 5-1B**).

To understand the function and effect of the VPS41 and AP-3 interaction on the insulin secretory pathway following glucose stimulation, a β cell line expressing a mutant VPS41 lacking the AP-3 binding region (**Figure 1-10**) will be generated. Further studies will also include examining protein-protein interactions, which are core for understanding the mechanisms and regulation of biological systems. For example, protein-protein interactions are essential for cellular signaling pathways, the formation of enzymatic complexes and the regulation of cell metabolism [259–262]. Co-immunoprecipitation followed by mass spectrometry-based proteomics has emerged as a powerful approach to map protein-protein interaction and would be applied to this study [260–262]. Hence, together with the findings presented in this thesis, identifying protein-protein interactions that are associated with the VPS41 -AP-3 complex using a proteomics approach would increase our understanding of the mechanism regulating insulin SGs in β cells.

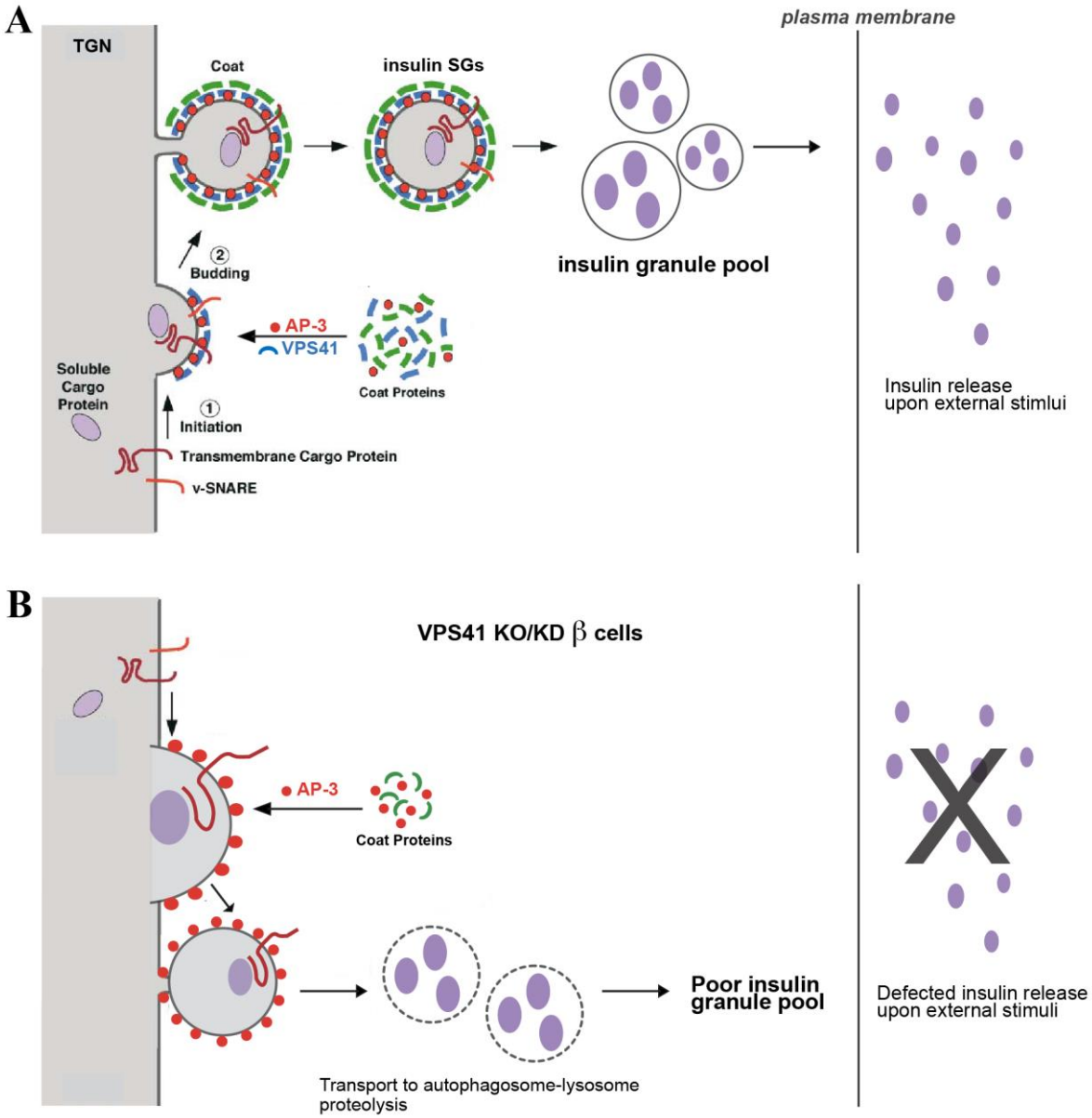

Figure 5-1 Proposed mechanism of poor insulin storage in VPS41-depleted β cells

(A)After coat assembly at the TGN, transmembrane cargo proteins of insulin SGs move toward budding reaction. Insulin granules undergo multiple sequential steps to become bioactive forms then, store under steady-state conditions [263]. (B) In the absence of VPS41, AP-3 coated insulin secretory granules could be shunted to autophagosome-lysosome mediated proteolysis leading to lower numbers of insulin granules and impaired insulin release in INS1 cells upon external stimuli.

In conclusion, the present study, in which I characterized the role of VPS41 in a β cell line model, using VPS41 KO, KD and islets isolated from VPS41β mouse model, a novel role of VPS41 as an essential factor in the insulin secretory machinery was shown through its regulation of insulin granule storage in β cells. Thus, further study of VPS41 variants that are associated with T2D risk could be used as a fundamental indicator to evaluate the risk of T2D in human populations.

References

1. Röder, P. V, Wu, B., Liu, Y. & Han, W. Pancreatic regulation of glucose homeostasis. *Exp. & Mol. Med.* 219 (2016) doi:10.1038/emm.2016.6.
2. Cerf, M. E. Beta cell dysfunction and insulin resistance. *Front. Endocrinol. (Lausanne).* **4**, 1–12 (2013).
3. Leahy, J. L. Pathogenesis of type 2 diabetes mellitus. *Archives of Medical Research* (2005) doi:10.1016/j.arcmed.2005.01.003.
4. Steiner, D. F. The biosynthesis of insulin. in *Pancreatic Beta Cell in Health and Disease* (2008). doi:10.1007/978-4-431-75452-7_3.
5. Andrali, S. S., Sampley, M. L., Vanderford, N. L. & Ozcan, S. Glucose regulation of insulin gene expression in pancreatic β-cells. *Biochem. J* **415**, 1–10 (2008).
6. GA, R., TJ, P., DJ, H. & A, M.-S. Pancreatic β-cell identity, glucose sensing and the control of insulin secretion. *Biochem. J.* **466**, 203–218 (2015).
7. Melloul, D., Marshak, S. & Cerasi, E. Regulation of insulin gene transcription. *Diabetologia* (2002) doi:10.1007/s00125-001-0728-y.
8. Du, W. *et al.* HID-1 is required for homotypic fusion of immature secretory granules during maturation. *Elife* (2016) doi:10.7554/eLife.18134.
9. Loh, Y. P., Cheng, Y., Mahata, S. K., Corti, A. & Tota, B. Chromogranin A and derived peptides in health and disease. in *Journal of Molecular Neuroscience* (2012). doi:10.1007/s12031-012-9728-2.
10. Arvan, P. & Halban, P. A. Sorting ourselves out: Seeking consensus on trafficking in the beta-cell. *Traffic* (2004) doi:10.1111/j.1600-0854.2004.00152.x.
11. Brunner, Y. *et al.* Proteomics analysis of insulin secretory granules. *Mol. Cell. Proteomics* (2007) doi:10.1074/mcp.M600443-MCP200.
12. Steiner, D. F., Rhodes, C. J., Philipson, L. H., Bell, G. I. & Chan, S. J. Biosynthesis, Processing, and Secretion of the Islet Hormones. in *Endocrinology: Adult and Pediatric* (2016). doi:10.1016/b978-0-323-18907-1.00031-7.
13. Nasteska, D. & Hodson, D. J. The role of beta cell heterogeneity in islet function and insulin release. *Journal of Molecular Endocrinology* (2018) doi:10.1530/JME-18-0011.
14. Fu, Z., R. Gilbert, E. & Liu, D. Regulation of Insulin Synthesis and Secretion and Pancreatic Beta-Cell Dysfunction in Diabetes. *Curr. Diabetes Rev.* (2012) doi:10.2174/157339913804143225.
15. Liu, M. *et al.* Biosynthesis, structure, and folding of the insulin precursor protein. *Diabetes, Obesity and Metabolism* (2018) doi:10.1111/dom.13378.
16. Olson, A. L. Regulation of GLUT4 and Insulin-Dependent Glucose Flux. *ISRN Mol. Biol.* (2012) doi:10.5402/2012/856987.
17. Konrad, D. *et al.* Need for GLUT4 activation to reach maximum effect of insulin-mediated glucose uptake in brown adipocytes isolated from GLUT4myc-expressing mice. *Diabetes* (2002) doi:10.2337/diabetes.51.9.2719.
18. Miller, T. B. & Larner, J. Mechanism of control of hepatic glycogenesis by insulin. *J. Biol. Chem.* (1973).
19. Straub, S. G. & Sharp, G. W. G. Glucose-stimulated signaling pathways in biphasic insulin secretion. *Diabetes/Metabolism Research and Reviews* (2002) doi:10.1002/dmrr.329.
20. Qaid, M. M. & Abdelrahman, M. M. Role of insulin and other related hormones in energy metabolism���A review. *Cogent Food Agric.* (2016) doi:10.1080/23311932.2016.1267691.
21. Obel, L. F. *et al.* Brain glycogen - new perspectives on its metabolic function and regulation at the subcellular level. *Frontiers in Neuroenergetics* (2012) doi:10.3389/fnene.2012.00003.
22. Edgerton, D. S. *et al.* Insulin's direct effects on the liver dominate the control of hepatic glucose production. *J. Clin. Invest.* (2006) doi:10.1172/JCI27073.
23. Dimitriadis, G., Mitron, P., Lambadiari, V., Maratou, E. & Raptis, S. A. Insulin effects in muscle

and adipose tissue. *Diabetes Res. Clin. Pract.* (2011) doi:10.1016/S0168-8227(11)70014-6.
24. James, H. A., O'Neill, B. T. & Nair, K. S. Insulin Regulation of Proteostasis and Clinical Implications. *Cell Metabolism* (2017) doi:10.1016/j.cmet.2017.06.010.
25. Da Silva Xavier, G. The Cells of the Islets of Langerhans. *J. Clin. Med.* (2018) doi:10.3390/jcm7030054.
26. DiGruccio, M. R. *et al.* Comprehensive alpha, beta and delta cell transcriptomes reveal that ghrelin selectively activates delta cells and promotes somatostatin release from pancreatic islets. *Mol. Metab.* (2016) doi:10.1016/j.molmet.2016.04.007.
27. Lammert, E. & Thorn, P. The Role of the Islet Niche on Beta Cell Structure and Function. *Journal of Molecular Biology* (2020) doi:10.1016/j.jmb.2019.10.032.
28. Ranjan, A. K., Joglekar, M. V. & Hardikar, A. A. Endothelial cells in pancreatic islet development and function. *Islets* (2009) doi:10.4161/isl.1.1.9054.
29. Nikolova, G. *et al.* The vascular basement membrane: A niche for insulin gene expression and β cell proliferation. *Dev. Cell* (2006) doi:10.1016/j.devcel.2006.01.015.
30. Aronoff, S. L., Berkowitz, K., Shreiner, B. & Want, L. Glucose Metabolism and Regulation: Beyond Insulin and Glucagon. *Diabetes Spectr.* (2004) doi:10.2337/diaspect.17.3.183.
31. Arrojo e Drigo, R. *et al.* Structural basis for delta cell paracrine regulation in pancreatic islets. *Nat. Commun.* (2019) doi:10.1038/s41467-019-11517-x.
32. Rorsman, P. & Huising, M. O. The somatostatin-secreting pancreatic δ-cell in health and disease. *Nature Reviews Endocrinology* (2018) doi:10.1038/s41574-018-0020-6.
33. Bonner-Weir, S. Morphological evidence for pancreatic polarity of β-cell within islets of Langerhans. *Diabetes* (1988) doi:10.2337/diabetes.37.5.616.
34. Gan, W. J. *et al.* Cell polarity defines three distinct domains in pancreatic β-cells. *J. Cell Sci.* (2017) doi:10.1242/jcs.185116.
35. De Marchi, U., Fernandez-Martinez, S., Fuente, S., Wiederkehr, A. & Santo-Domingo, J. Mitochondrial Ion Channels in Pancreatic β-cells: Novel Pharmacological Targets for the Treatment of Type 2 Diabetes. *Br. J. Pharmacol.* (2020) doi:10.1111/bph.15018.
36. Del Prato, S., Bianchi, C. & Daniele, G. Abnormalities of Insulin Secretion and β-Cell Defects in Type 2 Diabetes. in *Textbook of Diabetes* (2016). doi:10.1002/9781118924853.ch12.
37. Kreutzberger, A. J. B. *et al.* Distinct insulin granule subpopulations implicated in the secretory pathology of diabetes types 1 and 2. *Elife* **9**, 1–41 (2020).
38. Dolai, S. *et al.* Synaptotagmin-7 functions to replenish insulin granules for exocytosis in human islet β-cells. *Diabetes* **65**, 1962–1976 (2016).
39. Rohli, K. E., Boyer, C. K., Blom, S. E. & Stephens, S. B. Nutrient Regulation of Pancreatic Islet β-Cell Secretory Capacity and Insulin Production. *Biomolecules* **12**, 335 (2022).
40. Hinke, S. A., Hellemans, K. & Schuit, F. C. Plasticity of the β cell insulin secretory competence: Preparing the pancreatic β cell for the next meal. *J. Physiol.* **558**, 369–380 (2004).
41. Boland, B. B., Rhodes, C. J. & Grimsby, J. S. The dynamic plasticity of insulin production in β-cells. *Mol. Metab.* **6**, 958–973 (2017).
42. Hutton, J. C. Insulin secretory granule biogenesis and the proinsulin-processing endopeptidases. *Diabetologia* (1994) doi:10.1007/BF00400826.
43. Alarcon, C. *et al.* Pancreatic β-cell adaptive plasticity in obesity increases insulin production but adversely affects secretory function. *Diabetes* (2016) doi:10.2337/db15-0792.
44. PE, M. & P, R. The ins and outs of secretion from pancreatic beta-cells: control of single-vesicle exo- and endocytosis. *Physiology (Bethesda).* **22**, 113–121 (2007).
45. Liu, M., Wright, J., Guo, H., Xiong, Y. & Arvan, P. Proinsulin entry and transit through the endoplasmic reticulum in pancreatic beta cells. in *Vitamins and Hormones* (2014). doi:10.1016/B978-0-12-800174-5.00002-8.
46. Wicksteed, B., Alarcon, C., Briaud, I., Lingohr, M. K. & Rhodes, C. J. Glucose-induced Translational Control of Proinsulin Biosynthesis is Proportional to Preproinsulin mRNA Levels in Islet β-Cells but Not Regulated via a Positive Feedback of Secreted Insulin. *J. Biol. Chem.*

(2003) doi:10.1074/jbc.M303509200.
47. Molinete, M., Irminger, J. C., Tooze, S. A. & Halban, P. A. Trafficking/sorting and granule biogenesis in the β-cell. *Semin. Cell Dev. Biol.* (2000) doi:10.1006/scdb.2000.0173.
48. Spitzenberger, F. *et al.* Islet cell autoantigen of 69 kDa is an arfaptin-related protein associated with the golgi complex of insulinoma INS-1 cells. *J. Biol. Chem.* **278**, 26166–26173 (2003).
49. Germanos, M., Gao, A., Taper, M., Yau, B. & Kebede, M. A. Inside the Insulin Secretory Granule. (2021).
50. Norris, N., Yau, B. & Kebede, M. A. Isolation and proteomics of the insulin secretory granule. *Metabolites* **11**, (2021).
51. Hummer, B. H. *et al.* HID-1 controls formation of large dense core vesicles by influencing cargo sorting and trans-Golgi network acidification. *Mol. Biol. Cell* (2017) doi:10.1091/mbc.E17-08-0491.
52. Dunn, M. F. Zinc-ligand interactions modulate assembly and stability of the insulin hexamer - A review. in *BioMetals* (2005). doi:10.1007/s10534-005-3685-y.
53. Hou, J. C., Min, L. & Pessin, J. E. Chapter 16 Insulin Granule Biogenesis, Trafficking and Exocytosis. *Vitamins and Hormones* (2009) doi:10.1016/S0083-6729(08)00616-X.
54. Takeuchi, T. & Hosaka, M. Sorting Mechanism of Peptide Hormones and Biogenesis Mechanism of Secretory Granules by Secretogranin III, a Cholesterol-Binding Protein, in Endocrine Cells. *Curr. Diabetes Rev.* (2008) doi:10.2174/157339908783502406.
55. Tooze, S. A., Flatmark, T., Tooze, J. & Huttner, W. B. Characterization of the immature secretory granule, an intermediate in granule biogenesis. *J. Cell Biol.* (1991) doi:10.1083/jcb.115.6.1491.
56. Bonnemaison, M. L., Eipper, B. A. & Mains, R. E. Role of adaptor proteins in secretory granule biogenesis and maturation. *Frontiers in Endocrinology* (2013) doi:10.3389/fendo.2013.00101.
57. Schvartz, D. *et al.* Improved characterization of the insulin secretory granule proteomes. *J. Proteomics* (2012) doi:10.1016/j.jprot.2012.04.023.
58. M, V., Y, T. & K, G. A review on insulin trafficking and exocytosis. *Gene* **706**, 52–61 (2019).
59. P, R. & E, R. Insulin granule dynamics in pancreatic beta cells. *Diabetologia* **46**, 1029–1045 (2003).
60. Ferri, G. *et al.* Insulin secretory granules labelled with phogrin-fluorescent proteins show alterations in size, mobility and responsiveness to glucose stimulation in living β-cells. *Sci. Rep.* **9**, (2019).
61. Georgiadou, E. & Rutter, G. A. Age matters: Grading granule secretion in beta cells. *J. Biol. Chem.* **295**, 8912–8913 (2020).
62. Yau, B. *et al.* A fluorescent timer reporter enables sorting of insulin secretory granules by age. *J. Biol. Chem.* **295**, 8901–8911 (2020).
63. Pasquier, A. *et al.* Lysosomal degradation of newly formed insulin granules contributes to β cell failure in diabetes. *Nat. Commun.* **10**, 1–14 (2019).
64. Müller, A., Mziaut, H., Neukam, M., Knoch, K. P. & Solimena, M. A 4D view on insulin secretory granule turnover in the β-cell. *Diabetes. Obes. Metab.* **19 Suppl 1**, 107–114 (2017).
65. Tooze, S. A. Biogenesis of secretory granules in the trans-Golgi network of neuroendocrine and endocrine cells. *Biochim. Biophys. Acta - Mol. Cell Res.* (1998) doi:10.1016/S0167-4889(98)00059-7.
66. Huang, X. F. & Arvan, P. Formation of the insulin-containing secretory granule core occurs within immature β-granules. *J. Biol. Chem.* (1994).
67. Lara-Lemus, R. *et al.* Lumenal protein sorting to the constitutive secretory pathway of a regulated secretory cell. *J. Cell Sci.* (2006) doi:10.1242/jcs.02905.
68. Turner, M. D. & Arvan, P. Protein traffic from the secretory pathway to the endosomal system in pancreatic β-cells. *J. Biol. Chem.* (2000) doi:10.1074/jbc.275.19.14025.
69. Molinete, M., Dupuis, S., Brodsky, F. M. & Halban, P. A. Role of clathrin in the regulated

secretory pathway of pancreatic β-cells. *J. Cell Sci.* (2001).
70. Docherty, K. & Hutton, J. C. Carboxypeptidase activity in the insulin secretory granule. *FEBS Lett.* (1983) doi:10.1016/0014-5793(83)81065-5.
71. Wang, J. & Osei, K. Proinsulin maturation disorder is a contributor to the defect of subsequent conversion to insulin in β-cells. *Biochem. Biophys. Res. Commun.* (2011) doi:10.1016/j.bbrc.2011.06.119.
72. Cool, D. R. & Loh, Y. P. Carboxypeptidase E is a sorting receptor for prohormones: Binding and kinetic studies. *Mol. Cell. Endocrinol.* (1998) doi:10.1016/S0303-7207(98)00081-1.
73. Smith, G. D., Swenson, D. C., Dodson, E. J. & Reynolds, C. D. Structural stability in the 4-zinc human insulin hexamer. *Proc. Natl. Acad. Sci. U. S. A.* (1984) doi:10.1073/pnas.81.22.7093.
74. Emdin, S. O., Dodson, G. G., Cutfield, J. M. & Cutfield, S. M. Role of zinc in insulin biosynthesis. *Diabetologia* (1980) doi:10.1007/bf00275265.
75. Kuliawat, R. & Arvan, P. Distinct molecular mechanisms for protein sorting within immature secretory granules of pancreatic β-cells. *J. Cell Biol.* (1994) doi:10.1083/jcb.126.1.77.
76. MD, T. & P, A. Protein traffic from the secretory pathway to the endosomal system in pancreatic beta-cells. *J. Biol. Chem.* **275**, 14025–14030 (2000).
77. Kang, T. *et al.* Proteomic Analysis of Restored Insulin Production and Trafficking in Obese Diabetic Mouse Pancreatic Islets following Euglycemia. *J. Proteome Res.* **18**, 3245–3258 (2019).
78. Pottekat, A. *et al.* Insulin biosynthetic interaction network component, TMEM24, facilitates insulin reserve pool release. *Cell Rep.* (2013) doi:10.1016/j.celrep.2013.07.050.
79. Huh, Y. H., Jeon, S. H. & Yoo, S. H. Chromogranin B-induced secretory granule biogenesis: Comparison with the similar role of chromogranin A. *J. Biol. Chem.* **278**, 40581–40589 (2003).
80. Kim, T., Tao-Cheng, J. H., Eiden, L. E. & Loh, Y. P. Chromogranin A, an 'on/off' switch controlling dense-core secretory granule biogenesis. *Cell* (2001) doi:10.1016/S0092-8674(01)00459-7.
81. Stephens, S. B. *et al.* The Prohormone VGF Regulates β Cell Function via Insulin Secretory Granule Biogenesis. *Cell Rep.* (2017) doi:10.1016/j.celrep.2017.08.050.
82. Day, R. & Gorr, S. U. Secretory granule biogenesis and chromogranin A: Master gene, on/off switch or assembly factor? *Trends Endocrinol. Metab.* (2003) doi:10.1016/S1043-2760(02)00011-5.
83. Bearrows, S. C. *et al.* Chromogranin B regulates early-stage insulin granule trafficking from the Golgi in pancreatic islet β-cells. *J. Cell Sci.* **132**, 1–13 (2019).
84. Fargali, S. *et al.* The granin VGF promotes genesis of secretory vesicles, and regulates circulating catecholamine levels and blood pressure. *FASEB J.* (2014) doi:10.1096/fj.13-239509.
85. J, W. *et al.* Chromogranin A regulates vesicle storage and mitochondrial dynamics to influence insulin secretion. *Cell Tissue Res.* **368**, 487–501 (2017).
86. Holst, B. *et al.* PICK1 Deficiency Impairs Secretory Vesicle Biogenesis and Leads to Growth Retardation and Decreased Glucose Tolerance. *PLoS Biol.* (2013) doi:10.1371/journal.pbio.1001542.
87. KL, M. *et al.* Membrane localization is critical for activation of the PICK1 BAR domain. *Traffic* **9**, 1327–1343 (2008).
88. Cao, M. *et al.* PICK1 and ICA69 Control Insulin Granule Trafficking and Their Deficiencies Lead to Impaired Glucose Tolerance. *PLoS Biol.* (2013) doi:10.1371/journal.pbio.1001541.
89. Gehart, H. *et al.* The BAR Domain Protein Arfaptin-1 Controls Secretory Granule Biogenesis at the trans-Golgi Network. *Dev. Cell* **23**, 756–768 (2012).
90. Habermann, B. The BAR-domain family of proteins: A case of bending and binding? *EMBO Rep.* **5**, 250–255 (2004).
91. Li, J., Mao, Z., Huang, J. & Xiaa, J. PICK1 is essential for insulin production and the maintenance of glucose homeostasis. *Mol. Biol. Cell* **29**, 587–596 (2018).

92. Ahras, M., Otto, G. P. & Tooze, S. A. Synaptotagmin IV is necessary for the maturation of secretory granules in PC12 cells. *J. Cell Biol.* **173**, 241–251 (2006).
93. AT, H. *et al.* Cytoskeletal dependence of insulin granule movement dynamics in INS-1 beta-cells in response to glucose. *PLoS One* **9**, (2014).
94. Tomas, A., Yermen, B., Min, L., Pessin, J. E. & Halban, P. A. Regulation of pancreatic β-cell insulin secretion by actin cytoskeleton remodelling: Role of gelsolin and cooperation with the MAPK signalling pathway. *J. Cell Sci.* **119**, 2156–2167 (2006).
95. Bogan, J. S. Granular detail of β cell structures for insulin secretion. *J. Cell Biol.* **220**, 1–2 (2021).
96. Müller, A. *et al.* 3D FIB-SEM reconstruction of microtubule-organelle interaction in whole primary mouse β cells. *J. Cell Biol.* **220**, (2021).
97. Tokuo, H., Komaba, S. & Coluccio, L. M. In pancreatic β-cells myosin 1b regulates glucose-stimulated insulin secretion by modulating an early step in insulin granule trafficking from the Golgi. *Mol. Biol. Cell* **32**, 1210–1220 (2021).
98. Gaisano, H. Y. Recent new insights into the role of SNARE and associated proteins in insulin granule exocytosis. *Diabetes, Obes. Metab.* **19**, 115–123 (2017).
99. Liang, T. *et al.* SNAP23 depletion enables more SNAP25/calcium channel excitosome formation to increase insulin exocytosis in type 2 diabetes. *JCI Insight* **5**, (2020).
100. Festa, A., Williams, K., Hanley, A. J. G. & Haffner, S. M. β-cell dysfunction in subjects with impaired glucose tolerance and early type 2 diabetes comparison of surrogate markers with first-phase insulin secretion from an intravenous glucose tolerance test. *Diabetes* (2008) doi:10.2337/db07-0954.
101. Rhodes, C. J. Type 2 diabetes - A matter of ??-cell life and death? *Science* (2005) doi:10.1126/science.1104345.
102. Prentki, M. & Nolan, C. J. Islet {beta} cell failure in type 2 diabetes\r10.1172/JCI29103. *J. Clin. Invest.* (2006).
103. Steil, G. M. *et al.* Adaptation of β-cell mass to substrate oversupply: Enhanced function with normal gene expression. *Am. J. Physiol. - Endocrinol. Metab.* (2001) doi:10.1152/ajpendo.2001.280.5.e788.
104. Wolpin, B. M. *et al.* Hyperglycemia, insulin resistance, impaired pancreatic β-cell function, and risk of pancreatic cancer. *J. Natl. Cancer Inst.* (2013) doi:10.1093/jnci/djt123.
105. Van Citters, G. W. *et al.* Elevated glucagon-like peptide-1-(7-36)-amide, but not glucose, associated with hyperinsulinemic compensation for fat feeding. *J. Clin. Endocrinol. Metab.* (2002) doi:10.1210/jc.2002-020002.
106. Drucker, D. J. The biology of incretin hormones. *Cell Metabolism* (2006) doi:10.1016/j.cmet.2006.01.004.
107. Vilsbøll, T. The effects of glucagon-like peptide-1 on the beta cell. *Diabetes, Obes. Metab.* (2009) doi:10.1111/j.1463-1326.2009.01073.x.
108. Fujitani, Y. How does glucagon-like peptide 1 stimulate human β-cell proliferation? A lesson from islet graft experiments. *Journal of Diabetes Investigation* (2018) doi:10.1111/jdi.12861.
109. Hara, K., Shojima, N., Hosoe, J. & Kadowaki, T. Genetic architecture of type 2 diabetes. *Biochem. Biophys. Res. Commun.* (2014) doi:10.1016/j.bbrc.2014.08.012.
110. Fuchsberger, C. *et al.* The genetic architecture of type 2 diabetes. *Nature* **536**, 41–47 (2016).
111. Sun, J. *et al.* Proinsulin misfolding and endoplasmic reticulum stress during the development and progression of diabetes. *Mol. Aspects Med.* **42**, 105–118 (2015).
112. Arunagiri, A. *et al.* Misfolded proinsulin in the endoplasmic reticulum during development of beta cell failure in diabetes. *Ann. N. Y. Acad. Sci.* (2018) doi:10.1111/nyas.13531.
113. El-Assaad, W. *et al.* Saturated fatty acids synergize with elevated glucose to cause pancreatic β-cell death. *Endocrinology* (2003) doi:10.1210/en.2003-0410.
114. Grespan, E. *et al.* Defective amplifying pathway of β-cell secretory response to glucose in type 2 diabetes: Integrated modeling of in vitro and in vivo evidence. *Diabetes* (2018)

doi:10.2337/db17-1039.
115. Lowell, B. B. & Shulman, G. I. Mitochondrial dysfunction and type 2 diabetes. *Science* (2005) doi:10.1126/science.1104343.
116. Krauss, S. *et al.* Superoxide-mediated activation of uncoupling protein 2 causes pancreatic β cell dysfunction. *J. Clin. Invest.* (2003) doi:10.1172/JCI200319774.
117. Henquin, J. C. Triggering and amplifying pathways of regulation of insulin secretion by glucose. *Diabetes* (2000) doi:10.2337/diabetes.49.11.1751.
118. Lenzen, S., Drinkgern, J. & Tiedge, M. Low antioxidant enzyme gene expression in pancreatic islets compared with various other mouse tissues. *Free Radic. Biol. Med.* **20**, 463–466 (1996).
119. Kajimoto, Y. & Kaneto, H. Role of oxidative stress in pancreatic beta-cell dysfunction. *Ann. N. Y. Acad. Sci.* **1011**, 168–176 (2004).
120. Kaniuk, N. A. *et al.* Ubiquitinated-protein aggregates form in pancreatic β-cells during diabetes-induced oxidative stress and are regulated by autophagy. *Diabetes* **56**, 930–939 (2007).
121. Langin, D. The role of uncoupling protein 2 in the development of type 2 diabetes. *Drugs of Today* (2003) doi:10.1358/dot.2003.39.4.737960.
122. Chan, C. B., Saleh, M. C., Koshkin, V. & Wheeler, M. B. Uncoupling Protein 2 and Islet Function. in *Diabetes* (2004). doi:10.2337/diabetes.53.2007.s136.
123. Nolan, C. J. *et al.* Beta cell compensation for insulin resistance in Zucker fatty rats: Increased lipolysis and fatty acid signalling. *Diabetologia* (2006) doi:10.1007/s00125-006-0305-5.
124. Mezza, T. *et al.* Increased B-cell workload modulates proinsulin-to-insulin ratio in humans. *Diabetes* (2018) doi:10.2337/db18-0279.
125. Strawbridge, R. J. *et al.* Genome-wide association identifies nine common variants associated with fasting proinsulin levels and provides new insights into the pathophysiology of type 2 diabetes. *Diabetes* (2011) doi:10.2337/db11-0415.
126. Loopstra-Masters, R. C., Haffner, S. M., Lorenzo, C., Wagenknecht, L. E. & Hanley, A. J. Proinsulin-to-C-peptide ratio versus proinsulin-to-insulin ratio in the prediction of incident diabetes: The Insulin Resistance Atherosclerosis Study (IRAS). *Diabetologia* (2011) doi:10.1007/s00125-011-2322-2.
127. Liu, S. *et al.* Misfolded proinsulin impairs processing of precursor of insulin receptor and insulin signaling in β cells. *FASEB J.* **33**, 11338 (2019).
128. Pradhan, A. D. *et al.* Insulin, proinsulin, proinsulin:insulin ratio, and the risk of developing type 2 diabetes mellitus in women. *Am. J. Med.* (2003) doi:10.1016/S0002-9343(03)00061-5.
129. Laybutt, D. R. *et al.* Endoplasmic reticulum stress contributes to beta cell apoptosis in type 2 diabetes. *Diabetologia* (2007) doi:10.1007/s00125-006-0590-z.
130. Back, S. H. & Kaufman, R. J. Endoplasmic Reticulum Stress and Type 2 Diabetes. *Annu. Rev. Biochem.* (2012) doi:10.1146/annurev-biochem-072909-095555.
131. A.G.E.-S., A. *et al.* Diabetes before hyperglycemia. *Diabetes* (2011) doi:http://dx.doi.org/10.2337/db11-379-477.
132. Vivot, K., Pasquier, A., Goginashvili, A. & Ricci, R. Breaking Bad and Breaking Good: β-Cell Autophagy Pathways in Diabetes. *J. Mol. Biol.* **432**, 1494–1513 (2020).
133. Ebato, C. *et al.* Autophagy Is Important in Islet Homeostasis and Compensatory Increase of Beta Cell Mass in Response to High-Fat Diet. *Cell Metab.* **8**, 325–332 (2008).
134. Mészáros, G., Pasquier, A., Vivot, K., Goginashvili, A. & Ricci, R. Lysosomes in nutrient signalling: A focus on pancreatic β-cells. *Diabetes, Obes. Metab.* **20**, 104–115 (2018).
135. Mizushima, N. & Levine, B. Autophagy in mammalian development and differentiation. *Nat. Cell Biol.* **12**, 823–830 (2010).
136. Kaur, J. & Debnath, J. Autophagy at the crossroads of catabolism and anabolism. *Nat. Rev. Mol. Cell Biol.* **16**, 461–472 (2015).
137. Maiuri, M. C., Zalckvar, E., Kimchi, A. & Kroemer, G. Self-eating and self-killing: Crosstalk between autophagy and apoptosis. *Nat. Rev. Mol. Cell Biol.* **8**, 741–752 (2007).

138. Mariño, G., Niso-Santano, M., Baehrecke, E. H. & Kroemer, G. Self-consumption: The interplay of autophagy and apoptosis. *Nat. Rev. Mol. Cell Biol.* **15**, 81–94 (2014).
139. Lee, Y. ho, Kim, J., Park, K. & Lee, M. S. β-cell autophagy: Mechanism and role in β-cell dysfunction. *Mol. Metab.* **27**, S92–S103 (2019).
140. Riahi, Y. *et al.* Autophagy is a major regulator of β-cell insulin homeostasis. *Diabetologia* **59**, 1480 (2016).
141. Goginashvili, A. *et al.* Insulin secretory granules control autophagy in Pancreatic β cells. *Science (80-.).* **347**, 878–882 (2015).
142. Yamamoto, S. *et al.* Autophagy Differentially Regulates Insulin Production and Insulin Sensitivity. *Cell Rep.* **23**, 3286–3299 (2018).
143. Mir, S. U. R. *et al.* Inhibition of autophagic turnover in β-cells by fatty acids and glucose leads to apoptotic cell death. *J. Biol. Chem.* **290**, 6071–6085 (2015).
144. Las, G., Serada, S. B., Wikstrom, J. D., Twig, G. & Shirihai, O. S. Fatty acids suppress autophagic turnover in β-cells. *J. Biol. Chem.* **286**, 42534–42544 (2011).
145. Bartolome, A., Guillen, C. & Benito, M. Autophagy plays a protective role in endoplasmic reticulum stress-mediated pancreatic β cell death. *Autophagy* **8**, 1757–1768 (2012).
146. Sheng, Q. *et al.* Autophagy protects pancreatic beta cell mass and function in the setting of a high-fat and high-glucose diet. *Sci. Rep.* **7**, 1–10 (2017).
147. Masini, M. *et al.* Autophagy in human type 2 diabetes pancreatic beta cells. *Diabetologia* **52**, 1083–1086 (2009).
148. Stienstra, R. *et al.* Autophagy in adipose tissue and the beta cell: Implications for obesity and diabetes. *Diabetologia* **57**, 1505–1516 (2014).
149. Cinti, F. *et al.* Evidence of β-cell dedifferentiation in human type 2 diabetes. *J. Clin. Endocrinol. Metab.* **101**, 1044–1054 (2016).
150. Talchai, C., Xuan, S., Lin, H. V., Sussel, L. & Accili, D. Pancreatic β cell dedifferentiation as a mechanism of diabetic β cell failure. *Cell* **150**, 1223–1234 (2012).
151. Mezza, T. *et al.* B-cell fate in human insulin resistance and type 2 diabetes: A perspective on islet plasticity. *Diabetes* **68**, 1121–1129 (2019).
152. Bensellam, M., Jonas, J. C. & Laybutt, D. R. Mechanisms of β;-cell dedifferentiation in diabetes: Recent findings and future research directions. *J. Endocrinol.* **236**, R109–R143 (2018).
153. Fan, J. *et al.* Cyb5r3 links FoxO1-dependent mitochondrial dysfunction with β-cell failure. *Mol. Metab.* **34**, 97–111 (2020).
154. Zhu, Y., Liu, Q., Zhou, Z. & Ikeda, Y. PDX1, Neurogenin-3, and MAFA: Critical transcription regulators for beta cell development and regeneration. *Stem Cell Res. Ther.* **8**, 1–7 (2017).
155. Bensellam, M., Laybutt, D. R. & Jonas, J. C. The molecular mechanisms of pancreatic β-cell glucotoxicity: Recent findings and future research directions. *Mol. Cell. Endocrinol.* **364**, 1–27 (2012).
156. Efrat, S. Epigenetic Memory: Lessons From iPS Cells Derived From Human β Cells. *Front. Endocrinol. (Lausanne).* **11**, 1–5 (2021).
157. Wang, Z., York, N. W., Nichols, C. G. & Remedi, M. S. Pancreatic β cell dedifferentiation in diabetes and redifferentiation following insulin therapy. *Cell Metab.* **19**, 872–882 (2014).
158. Accili, D. *et al.* When β-cells fail: lessons from dedifferentiation. *Diabetes, Obes. Metab.* **18**, 117–122 (2016).
159. Brereton, M. F. *et al.* Reversible changes in pancreatic islet structure and function produced by elevated blood glucose. *Nat. Commun.* **5**, (2014).
160. Park, J. J., Koshimizu, H. & Loh, Y. P. Biogenesis and transport of secretory granules to release site in neuroendocrine cells. *J. Mol. Neurosci.* **37**, 151–159 (2009).
161. Loh, Y. P., Kim, T., Rodriguez, Y. M. & Cawley, N. X. Secretory Granule Biogenesis and Neuropeptide Sorting to the Regulated Secretory Pathway in Neuroendocrine Cells. *J. Mol. Neurosci.* **63**, (2004).

162. Normant, E. & Loh, Y. P. Depletion of carboxypeptidase E, a regulated secretory pathway sorting receptor, causes misrouting and constitutive secretion of proinsulin and proenkephalin, but not chromogranin A. *Endocrinology* (1998) doi:10.1210/endo.139.4.5951.
163. Montero-Hadjadje, M. *et al.* Chromogranins A and B and secretogranin II: Evolutionary and functional aspects. in *Acta Physiologica* (2008). doi:10.1111/j.1748-1716.2007.01806.x.
164. Asensio, C. S. *et al.* Self-Assembly of VPS41 Promotes Sorting Required for Biogenesis of the Regulated Secretory Pathway. *Dev. Cell* **27**, 425–437 (2013).
165. Welle, R. E. N. van der *et al. VPS41 recessive mutation causes ataxia and dystonia with retinal dystrophy and mental retardation by inhibiting HOPS function and mTORC1 signaling*. *bioRxiv* (2019). doi:10.1101/2019.12.18.867333.
166. Plemel, R. L. *et al.* Subunit organization and Rab interactions of Vps-C protein complexes that control endolysosomal membrane traffic. *Mol. Biol. Cell* (2011) doi:10.1091/mbc.E10-03-0260.
167. Auffarth, K., Arlt, H., Lachmann, J., Cabrera, M. & Ungermann, C. Tracking of the dynamic localization of the Rab-specific HOPS subunits reveal their distinct interaction with Ypt7 and vacuoles. *Cell. Logist.* (2014) doi:10.4161/cl.29191.
168. Pols, M. S., Ten Brink, C., Gosavi, P., Oorschot, V. & Klumperman, J. The HOPS Proteins hVps41 and hVps39 Are Required for Homotypic and Heterotypic Late Endosome Fusion. *Traffic* (2013) doi:10.1111/tra.12027.
169. Short, B. How Vps41 HOPS between tethering functions. *J. Cell Biol.* (2010) doi:10.1083/jcb.1914iti3.
170. Lürick, A. *et al.* Multivalent Rab interactions determine tether-mediated membrane fusion. *Mol. Biol. Cell* (2017) doi:10.1091/mbc.E16-11-0764.
171. Kleine Balderhaar, H. J. & Ungermann, C. CORVET and HOPS tethering complexes-coordinators of endosome and lysosome fusion. *J. Cell Sci.* **126**, 1307–1316 (2013).
172. Spang, A. Membrane tethering complexes in the endosomal system. *Front. Cell Dev. Biol.* **4**, 1–7 (2016).
173. Solinger, J. A. & Spang, A. Tethering complexes in the endocytic pathway: CORVET and HOPS. *FEBS Journal* (2013) doi:10.1111/febs.12151.
174. Peplowska, K., Markgraf, D. F., Ostrowicz, C. W., Bange, G. & Ungermann, C. The CORVET Tethering Complex Interacts with the Yeast Rab5 Homolog Vps21 and Is Involved in Endo-Lysosomal Biogenesis. *Dev. Cell* (2007) doi:10.1016/j.devcel.2007.03.006.
175. Amaya, C., Militello, R. D., Calligaris, S. D. & Colombo, M. I. Rab24 interacts with the Rab7/Rab interacting lysosomal protein complex to regulate endosomal degradation. *Traffic* (2016) doi:10.1111/tra.12431.
176. Lachmann, J., Glaubke, E., Moore, P. S. & Ungermann, C. The Vps39-like TRAP1 is an effector of Rab5 and likely the missing Vps3 subunit of human CORVET. *Cell. Logist.* (2014) doi:10.4161/21592780.2014.970840.
177. Khatter, D. *et al.* The small GTPase Arl8b regulates assembly of the mammalian HOPS complex on lysosomes. *J. Cell Sci.* (2015) doi:10.1242/jcs.162651.
178. Lin, X. *et al.* RILP interacts with HOPS complex via VPS41 subunit to regulate endocytic trafficking. *Sci. Rep.* **4**, 1–12 (2014).
179. Xing, R. *et al.* The Rab7 effector WDR91 promotes autophagy-lysosome degradation in neurons by regulating lysosome fusion. *J. Cell Biol.* **220**, (2021).
180. Modica, G. *et al.* Rab7 palmitoylation is required for efficient endosome-to-TGN trafficking. *J. Cell Sci.* (2017) doi:10.1242/jcs.199729.
181. Hanafusa, H. *et al.* LRRK1 phosphorylation of Rab7 at S72 links trafficking of EGFR-containing endosomes to its effector RILP. *J. Cell Sci.* (2019) doi:10.1242/jcs.228809.
182. Rehling, P., Darsow, T., Katzmann, D. J. & Emr, S. D. Formation of AP-3 transport intermediates requires Vps41 function. *Nat. Cell Biol.* (1999) doi:10.1038/14037.
183. Darsow, T., Katzmann, D. J., Cowles, C. R. & Emr, S. D. Vps41p function in the alkaline

phosphatase pathway requires homo-oligomerization and interaction with AP-3 through two distinct domains. *Mol. Biol. Cell* (2001) doi:10.1091/mbc.12.1.37.
184. Angers, C. G. & Merz, A. J. HOPS interacts with Apl5 at the vacuole membrane and is required for consumption of AP-3 transport vesicles. *Mol. Biol. Cell* (2009) doi:10.1091/mbc.E09-04-0272.
185. Feng, Q. N. *et al.* Adaptor protein-3-dependent vacuolar trafficking involves a subpopulation of COPII and HOPS tethering proteins. *Plant Physiol.* (2017) doi:10.1104/pp.17.00584.
186. Guo, Y., Sirkis, D. W. & Schekman, R. Protein Sorting at the trans -Golgi Network . *Annu. Rev. Cell Dev. Biol.* (2014) doi:10.1146/annurev-cellbio-100913-013012.
187. Cabrera, M. *et al.* Phosphorylation of a membrane curvature-sensing motif switches function of the HOPS subunit Vps41 in membrane tethering. *J. Cell Biol.* **191**, 845–859 (2010).
188. Bigay, J., Casella, J. F., Drin, G., Mesmin, B. & Antonny, B. ArfGAP1 responds to membrane curvature through the folding of a lipid packing sensor motif. *EMBO J.* (2005) doi:10.1038/sj.emboj.7600714.
189. Pols, M. S. *et al.* HVps41 and VAMP7 function in direct TGN to late endosome transport of lysosomal membrane proteins. *Nat. Commun.* (2013) doi:10.1038/ncomms2360.
190. van der Welle, R. E. N. *et al.* Neurodegenerative VPS41 variants inhibit HOPS function and mTORC1-dependent TFEB/TFE3 regulation . *EMBO Mol. Med.* **13**, 1–24 (2021).
191. CH, B. *et al.* Pancreatic β-Cell-Specific Deletion of VPS41 Causes Diabetes Due to Defects in Insulin Secretion. *Diabetes* **70**, 436–448 (2021).
192. Asensio, C. S., Sirkis, D. W. & Edwards, R. H. RNAi screen identifies a role for adaptor protein AP-3 in sorting to the regulated secretory pathway. *J. Cell Biol.* **191**, 1173–1187 (2010).
193. Newell-Liwa, K., Seong, E., Burmeister, M. & Faundez, V. Neuronal and non-neuronal functions of the AP-3 sorting machinery. *J. Cell Sci.* **120**, 531–541 (2007).
194. Peden, A. A. *et al.* Localization of the AP-3 adaptor complex defines a novel endosomal exit site for lysosomal membrane proteins. *J. Cell Biol.* **164**, 1065–1076 (2004).
195. Sirkis, D. W., Edwards, R. H. & Asensio, C. S. Widespread Dysregulation of Peptide Hormone Release in Mice Lacking Adaptor Protein AP-3. *PLoS Genet.* (2013) doi:10.1371/journal.pgen.1003812.
196. Maller, J. B. *et al.* Bayesian refinement of association signals for 14 loci in 3 common diseases. *Nat. Genet.* **44**, 1294–1301 (2012).
197. AMP T2D Knowledge Portal. http://www.type2diabetesgenetics.org/gene/geneInfo/VPS41#.
198. Keller, M. P. *et al.* A gene expression network model of type 2 diabetes links cell cycle regulation in islets with diabetes susceptibility. *Genome Res.* (2008) doi:10.1101/gr.074914.107.
199. Liu, M. *et al.* Normal and defective pathways in biogenesis and maintenance of the insulin storage pool. *J. Clin. Invest.* **131**, (2021).
200. Suckale, J. & Solimena, M. The insulin secretory granule as a signaling hub. *Trends in Endocrinology and Metabolism* (2010) doi:10.1016/j.tem.2010.06.003.
201. Tooze, S. A. & Huttner, W. B. Cell-free protein sorting to the regulated and constitutive secretory pathways. *Cell* **60**, 837–847 (1990).
202. Okita, N. *et al.* Modified Western blotting for insulin and other diabetes-associated peptide hormones. *Sci. Rep.* **7**, 1–11 (2017).
203. Harney, D. J. *et al.* Proteomics analysis of adipose depots after intermittent fasting reveals visceral fat preservation mechanisms. *Cell Rep.* **34**, (2021).
204. Obermü Ller, S., Calegari, F., King, A. ¤, Lindqvist, A. & Lundquist, I. Defective Secretion of Islet Hormones in Chromogranin-B Deficient Mice. *PLoS One* **5**, 8936 (2010).
205. Boncompain, G. *et al.* Synchronization of secretory protein traffic in populations of cells. *Nat. Methods* **9**, 493–498 (2012).
206. Pacheco-Fernandez, N., Pakdel, M. & Von Blume, J. Retention Using Selective Hooks (RUSH) Cargo Sorting Assay for Protein Vesicle Tracking in HeLa Cells. *Bio-protocol* **11**, (2021).

207. Cheisson, G. *et al.* Perioperative management of adult diabetic patients. Review of hyperglycaemia: definitions and pathophysiology. *Anaesthesia, Crit. care pain Med.* **37 Suppl 1**, S5–S8 (2018).
208. Krentz, N. A. J. & Gloyn, A. L. Insights into pancreatic islet cell dysfunction from type 2 diabetes mellitus genetics. *Nature Reviews Endocrinology* (2020) doi:10.1038/s41574-020-0325-0.
209. Moriyama, H. *et al.* Evidence for a primary islet autoantigen (preproinsulin 1) for insulitis and diabetes in the nonobese diabetic mouse. *Proc. Natl. Acad. Sci. U. S. A.* **100**, 10376–10381 (2003).
210. Schoppe, J. *et al.* AP-3 vesicle uncoating occurs after HOPS-dependent vacuole tethering. *EMBO J.* **39**, 1–17 (2020).
211. Yau, B., Hocking, S., Andrikopoulos, S. & Alamerew Kebede, M. Targeting the insulin granule for modulation of insulin exocytosis. *Biochem. Pharmacol.* 114821 (2021) doi:10.1016/j.bcp.2021.114821.
212. Zhu, X. *et al.* Severe block in processing of proinsulin to insulin accompanied by elevation of des-64,65 proinsulin intermediates in islets of mice lacking prohormone convertase 1/3. *Proc. Natl. Acad. Sci. U. S. A.* **99**, 10299–10304 (2002).
213. Iida, H. *et al.* SERCA2 regulates proinsulin processing and processing enzyme maturation in the pancreatic β cell. (2022).
214. Ashcroft, S. J. H. Glucoreceptor Mechanisms and the Control of Insulin Release and Biosynthesis*. *Diabetologia* **18**, 5–15 (1980).
215. Kolb, H., Kempf, K., Röhling, M. & Martin, S. Insulin: too much of a good thing is bad. *BMC Med.* **18**, (2020).
216. Marsh, B. J. *et al.* Regulated autophagy controls hormone content in secretory-deficient pancreatic endocrine β-cells. *Mol. Endocrinol.* **21**, 2255–2269 (2007).
217. Khilji, M. S. *et al.* The inducible β5i proteasome subunit contributes to proinsulin degradation in GRP94-deficient β-cells and is overexpressed in type 2 diabetes pancreatic islets. *Am. J. Physiol. - Endocrinol. Metab.* **318**, E892–E900 (2020).
218. Jung, H. S. *et al.* Loss of Autophagy Diminishes Pancreatic β Cell Mass and Function with Resultant Hyperglycemia. *Cell Metab.* **8**, 318–324 (2008).
219. Binger, K. J. *et al.* Atp6ap2 deletion causes extensive vacuolation that consumes the insulin content of pancreatic β cells. *Proc. Natl. Acad. Sci. U. S. A.* **116**, 19983–19988 (2019).
220. Amenta, J. S. & Brocher, S. C. Role of lysosomes in protein turnover: catch-up proteolysis after release from NH4Cl inhibition. *J. Cell. Physiol.* **102**, 259–266 (1980).
221. Wang, X. J. *et al.* A novel crosstalk between two major protein degradation systems: regulation of proteasomal activity by autophagy. *Autophagy* **9**, 1500–1508 (2013).
222. Broca, C. *et al.* Proteasome Dysfunction Mediates High Glucose-Induced Apoptosis in Rodent Beta Cells and Human Islets. *PLoS One* **9**, 92066 (2014).
223. Gies, V. *et al.* Beyond Anti-viral Effects of Chloroquine/Hydroxychloroquine. *Front. Immunol.* **11**, 1–8 (2020).
224. Bik, E. *et al.* Chloroquine-induced accumulation of autophagosomes and lipids in the endothelium. *Int. J. Mol. Sci.* **22**, 1–14 (2021).
225. Hashida, S., Kominami, E. & Katunuma, N. Inhibitions of cathepsin B and cathepsin L by E-64 in vivo. II. Incorporation of [3H]E-64 into rat liver lysosomes in vivo. *J. Biochem.* **91**, 1373–1380 (1982).
226. Bogyo, M., Verhelst, S., Bellingard-Dubouchaud, V., Toba, S. & Greenbaum, D. Selective targeting of lysosomal cysteine proteases with radiolabeled electrophilic substrate analogs. *Chem. Biol.* **7**, 27–38 (2000).
227. Zhou, Y. *et al.* RILP Restricts Insulin Secretion Through Mediating Lysosomal Degradation of Proinsulin. *Diabetes* **69**, 67–82 (2020).
228. Park, S. Y. & Guo, X. Adaptor protein complexes and intracellular transport. *Biosci. Rep.* **34**,

381–390 (2014).
229. Nakatsu, F. & Ohno, H. Adaptor protein complexes as the key regulators of protein sorting in the post-Golgi network. *Cell Struct. Funct.* **28**, 419–429 (2003).
230. Sanger, A., Hirst, J., Davies, A. K. & Robinson, M. S. Adaptor protein complexes and disease at a glance. *J. Cell Sci.* **132**, (2019).
231. Cowles, C. R., Odorizzi, G., Payne, G. S. & Emr, S. D. The AP-3 adaptor complex is essential for cargo-selective transport to the yeast vacuole. *Cell* **91**, 109–118 (1997).
232. Kos, C. H. Cre/loxP system for generating tissue-specific knockout mouse models. *Nutr. Rev.* **62**, 243–246 (2004).
233. McLellan, M. A., Rosenthal, N. A. & Pinto, A. R. Cre-loxP-Mediated Recombination: General Principles and Experimental Considerations. *Curr. Protoc. Mouse Biol.* **7**, 1–12 (2017).
234. Andrikopoulos, S., Blair, A. R., Deluca, N., Fam, B. C. & Proietto, J. Evaluating the glucose tolerance test in mice. *Am. J. Physiol. Endocrinol. Metab.* **295**, (2008).
235. Liu, K. F. *et al.* Comparison of area under the curve in various models of diabetic rats receiving chronic medication. *Arch. Med. Sci.* **18**, 1078 (2022).
236. Carstensen, M., Thomsen, C. & Hermansen, K. Incremental area under response curve more accurately describes the triglyceride response to an oral fat load in both healthy and type 2 diabetic subjects. *Metabolism* **52**, 1034–1037 (2003).
237. Small, L. *et al.* Comparative analysis of oral and intraperitoneal glucose tolerance tests in mice. *Mol. Metab.* **57**, (2022).
238. Virtue, S. & Vidal-Puig, A. GTTs and ITTs in mice: simple tests, complex answers. *Nat. Metab.* **3**, 883–886 (2021).
239. Sun, J. *et al.* β-Cell Dedifferentiation in Patients With T2D With Adequate Glucose Control and Nondiabetic Chronic Pancreatitis. *J. Clin. Endocrinol. Metab.* **104**, 83–94 (2019).
240. Weng, J. *et al.* Effect of intensive insulin therapy on beta-cell function and glycaemic control in patients with newly diagnosed type 2 diabetes: a multicentre randomised parallel-group trial. *Lancet (London, England)* **371**, 1753–1760 (2008).
241. Bonnemaison, M. L., Eipper, B. A. & Mains, R. E. Role of adaptor proteins in secretory granule biogenesis and maturation. *Front. Endocrinol. (Lausanne).* **4**, (2013).
242. Huang, X. F. & Arvan, P. Intracellular transport of proinsulin in pancreatic β-cells: Structural maturation probed by bisulfide accessibility. *J. Biol. Chem.* (1995) doi:10.1074/jbc.270.35.20417.
243. Griffin, E. F., Yan, X., Caldwell, K. A. & Caldwell, G. A. Distinct functional roles of Vps41-mediated neuroprotection in Alzheimer's and Parkinson's disease models of neurodegeneration. *Hum. Mol. Genet.* (2018) doi:10.1093/hmg/ddy308.
244. Kebede, M. A. *et al.* SORCS1 is necessary for normal insulin secretory granule biogenesis in metabolically stressed β cells. *J. Clin. Invest.* (2014) doi:10.1172/JCI74072.
245. Ohta, T. *et al.* Gender Differences in Metabolic Disorders and Related Diseases in Spontaneously Diabetic Torii-Lepr fa Rats. (2014) doi:10.1155/2014/841957.
246. Benko, F. *et al.* The impact of diabetes mellitus type 2 on the steroidogenesis of male Zucker Diabetic Fatty rats. *Physiol. Res.* **71**, 713–717 (2022).
247. Kim, B., Kim, Y. Y., Nguyen, P. T. T., Nam, H. & Suh, J. G. Sex differences in glucose metabolism of streptozotocin-induced diabetes inbred mice (C57BL/6J). *Appl. Biol. Chem.* **63**, 1–8 (2020).
248. Kautzky-Willer, A., Leutner, M. & Harreiter, J. Sex differences in type 2 diabetes. *Diabetologia* **66**, (2023).
249. Díaz, A. *et al.* Sex Differences in Age-Associated Type 2 Diabetes in Rats-Role of Estrogens and Oxidative Stress. (2019) doi:10.1155/2019/6734836.
250. Mauvais-Jarvis, F. Gender differences in glucose homeostasis and diabetes. *Physiol. Behav.* **187**, 20–23 (2018).
251. Xu, B. *et al.* Estrogens Promote Misfolded Proinsulin Degradation to Protect Insulin Production and Delay Diabetes. *Cell Rep.* **24**, 181–196 (2018).

252. Mauvais-Jarvis, F., Arnold, A. P. & Reue, K. A Guide for the Design of Pre-clinical Studies on Sex Differences in Metabolism. *Cell Metab.* **25**, 1216–1230 (2017).
253. Gannon, M., Kulkarni, R. N., Tse, H. M. & Mauvais-Jarvis, F. Sex differences underlying pancreatic islet biology and its dysfunction. doi:10.1016/j.molmet.2018.05.017.
254. Navarro, G. *et al.* Extranuclear Actions of the Androgen Receptor Enhance Glucose-Stimulated Insulin Secretion in the Male. *Cell Metab.* **23**, 837–851 (2016).
255. Pal, M. & Gupta, S. Testosterone supplementation improves glucose homeostasis despite increasing hepatic insulin resistance in male mouse model of type 2 diabetes mellitus. *Nutr. Diabetes* **6**, e236-6 (2016).
256. Salpeter, S. R. *et al.* Meta-analysis: effect of hormone-replacement therapy on components of the metabolic syndrome in postmenopausal women. *Diabetes. Obes. Metab.* **8**, 538–554 (2006).
257. Misso, M. L. *et al.* Cellular and molecular characterization of the adipose phenotype of the aromatase-deficient mouse. *Endocrinology* **144**, 1474–1480 (2003).
258. Yan, H. *et al.* Estrogen Improves Insulin Sensitivity and Suppresses Gluconeogenesis via the Transcription Factor Foxo1. *Diabetes* **68**, 291–304 (2019).
259. Damacharla, D. *et al.* Quantitative proteomics reveals novel interaction partners of Rac1 in pancreatic β-cells: Evidence for increased interaction with Rac1 under hyperglycemic conditions. *Mol. Cell. Endocrinol.* (2019) doi:10.1016/j.mce.2019.110489.
260. Zhang, X. *et al.* Quantitative proteomics reveals novel protein interaction partners of PP2A catalytic subunit in pancreatic β-cells. *Mol. Cell. Endocrinol.* (2016) doi:10.1016/j.mce.2016.01.008.
261. Figeys, D. Mapping the human protein interactome. *Cell Research* (2008) doi:10.1038/cr.2008.72.
262. Snider, J. *et al.* Fundamentals of protein interaction network mapping. *Mol. Syst. Biol.* (2015) doi:10.15252/msb.20156351.
263. Bonifacino, J. S. & Glick, B. S. The Mechanisms of Vesicle Budding and Fusion. *Cell* **116**, 153–166 (2004).

Appendix

The length of degradation inhibition is a critical factor to consider whilst studying insulin degradation under VPS41 KD conditions. Therefore, I evaluated endogenous insulin and proinsulin protein levels over different time courses by western blot to determine the timepoint/timeframe when insulin protein is being reduced. Consistent with our previous data, VPS41 KD led to reduced endogenous insulin in a time-dependent manner (**Figure 1A & C**). A reduction of endogenous insulin was observed at 24 hours post-transfection in VPS41 KD cells and insulin reduction was significant between 48-72 hours after transfection. As well, proinsulin was reduced gradually in a time-dependent manner in VPS41 KD INS1 cells however, the decrease in its expression was not as marked as for insulin (**Figure 1A, C&D**). Interestingly, proinsulin protein expression was increased in VPS41 KD INS1 cells at 24 hours post-transfection compared to control INS1 cells (**Figure 1A**). Indeed, endogenous insulin expression was still diminished at 72 hours post-transfection in KD INS1 cells while proinsulin protein expression was maintained at residual levels. There was no reduction of insulin protein expression in control cells (**Figure 1A & D**). Hence, the ratio of proinsulin over insulin at all indicated time points was much higher in VPS41 KD INS1 cells compared with control cells due to the significant decrease of insulin protein expression (**Figure 1E**). Based on the altered endogenous insulin expression and proinsulin levels at the studied time points following transfection, I showed VPS41 KD leads to rapid reduction of insulin compared to proinsulin (**Figure 1**). These results further suggest that VPS41 KD causes poor insulin storage on INS1 cells.

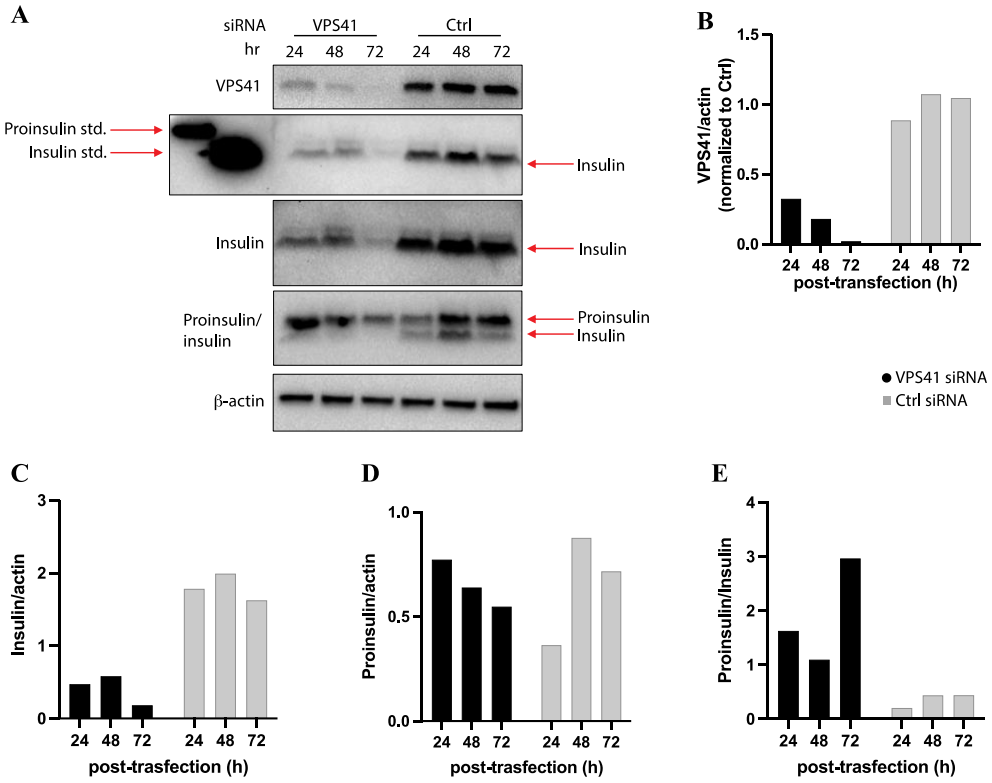

Figure 1 Protein expression of VPS41, insulin and proinsulin over a time-course in VPS41 KD and WT INS1 cells

(A) WT INS1 cells were transiently transfected with VPS41 or non-targeting control siRNA (50 pmol) and then lysed with SDS-lysis buffer at the indicated time points. Protein extracts (25µg) were resolved on an SDS-PAGE with human proinsulin (300ng) and insulin (4µg) std and immunoblotted for insulin and proinsulin. (B, C, D) The intensity values of VPS41, insulin and proinsulin protein bands were quantified by ImageJ software. (E) The ratio of proinsulin over insulin expression.

Based on the time response result for endogenous insulin levels following KD, WT INS1 cells were cultured with media containing the inhibitor, Chloroquine (CQ, 10μM) for 24 hours to prevent protein degradation after transfection with siRNA. The quantified graph of VPS41 expression and transfection efficiency of VPS41 siRNA was high with a 90% reduction of endogenous VPS41 in the VPS41 KD INS1 cells compared to control INS1 cells (**Figure 2B**). Consistently, VPS41 KD led to the significant reduction of insulin levels without CQ treatment on cells; however, inhibiting autophagosome-mediated lysosomal protein degradation with CQ did not significantly alter insulin protein expression in both VPS41 KD and control INS1 cells (**Figure 2D**). Proinsulin protein levels were increased slightly in both CQ-treated VPS41 KD and control cells compared with non-treated cells but there was no significant difference after the statistical analysis (**Figure 2C**). This unexpected result where insulin protein levels were not restored upon inhibiting autophagosome-mediated lysosomal protein degradation raised the possibility that the treatment conditions such as CQ concentration or treatment time could be the variable factor to affect insulin levels through cellular stress or damage following siRNA transfection [1]. Therefore, WT INS1 cells were cultured at different times and concentrations with the protein degradation inhibitors prior to siRNA transfection.

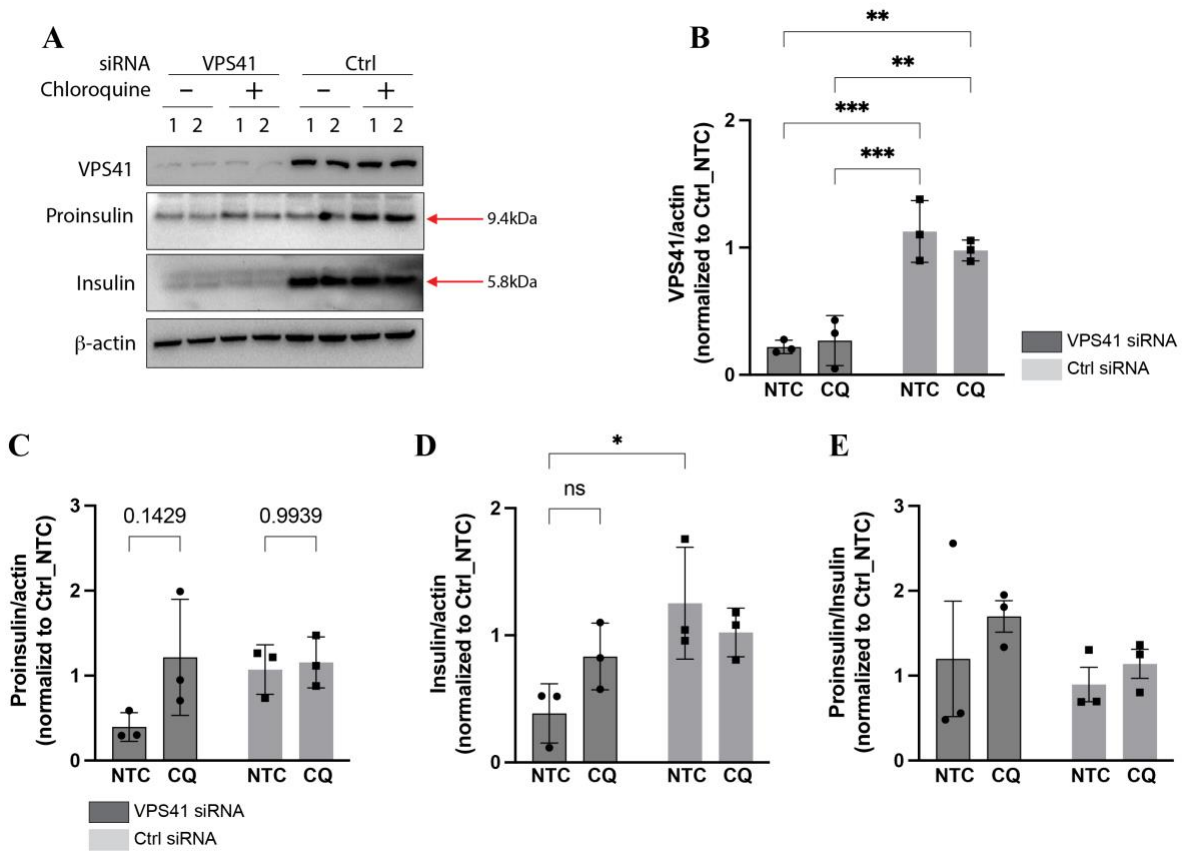

Figure 2 VPS41 and insulin protein expression in VPS41 KD or control INS1 cells treated with or without CQ

(A) At 24 hours post-transfection with VPS41 or non-targeting control siRNA (50 pmol), cells were incubated with or without CQ (10μM) for 24 hours and then lysed with SDS-lysis buffer. Protein extracts (25μg) of protein extracts were resolved in an SDS-PAGE with human (pro) insulin std and immunoblotted for VPS41, insulin and proinsulin protein expression. (B, C, D) The intensity values of VPS41, proinsulin and insulin protein bands were quantified by Image J software. (E) The ratio of proinsulin over insulin. All the data were presented as mean ± SEM, *$p < 0.05$, ** $p < 0.005$ & *** $p < 0.0005$ by Two-way ANOVA with Tukey's multiple comparisons test.

Endogenous insulin protein levels were measured in WT INS1 cells following different treatment times with protein degradation inhibitors, CQ (10μM) or MG132 (100nM). Compared to untreated conditions, both CQ and MG132 treatment in cells led to enhanced proinsulin levels in a time-dependent manner (**Figure 3A & B**). Unexpectedly, these two inhibitors, which inhibit protein degradation through different pathways had different effects on insulin levels. CQ-treatment of INS1 cells decreased insulin levels in a time-dependent manner while MG132-treated cells had increased insulin expression except at 24 hours (**Figure 3A & C**). I also observed a slight increase in proinsulin levels in INS1 cells treated with MG132 (100nM) over the time course compared to non-treated cells. Therefore, the ratio of proinsulin over insulin expression was increased in cells treated with CQ but not significantly increased in MG132-treated cells (**Figure 3D & E**). For experiments onwards, I treated the cells with CQ or MG132 for 24 hours to examine their effects on intracellular insulin protein degradation. the optimal CQ concentration was determined through a dose-response experiment (**Figure 3**).

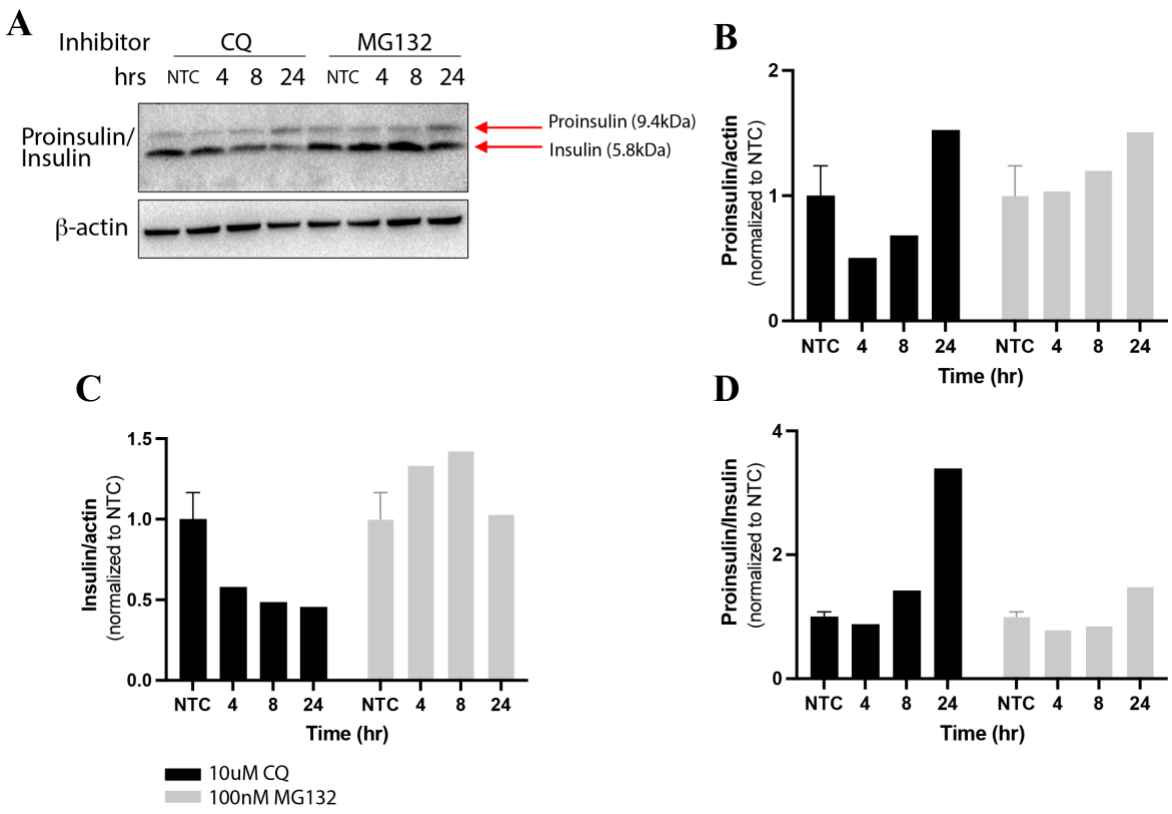

Figure 3 Proinsulin and insulin expression in INS1 cells treated with or without CQ or MG132

INS1 cells were cultured with CQ (10 μM) or MG132 (100 nM) for the indicated times before lysis (A). Protein extracts were resolved in an SDS-PAGE with human insulin and proinsulin as the standard then, immunoblotted for insulin and proinsulin. (B, C) Intensity values of proinsulin and insulin protein bands were quantified by Image J software. (D) Ratio of proinsulin over insulin.

WT INS1 cells were treated with different CQ concentrations for 24 hours. Consistent with previous results of increased proinsulin expression upon CQ (10 µM) treatment (**Figure 3**), proinsulin levels were enhanced in a dose-dependent manner up to the treatment of 2µM. (**Figure 4A & B**). Treatment of cells with lower concentrations of CQ from 0.1- 1µM caused an increase in insulin expression while no significant difference in insulin levels was observed in INS1 cells treated with higher CQ concentrations 2 - 10 µM compared to untreated cells (**Figure 4A & C**). Hence, based on the optimizations for CQ treatment time and concentration, I treated with CQ (2 µM) in WT INS1 cells for 24 hours of further experiments to prevent protein degradation especially proinsulin and insulin after VPS41 KD transfection.

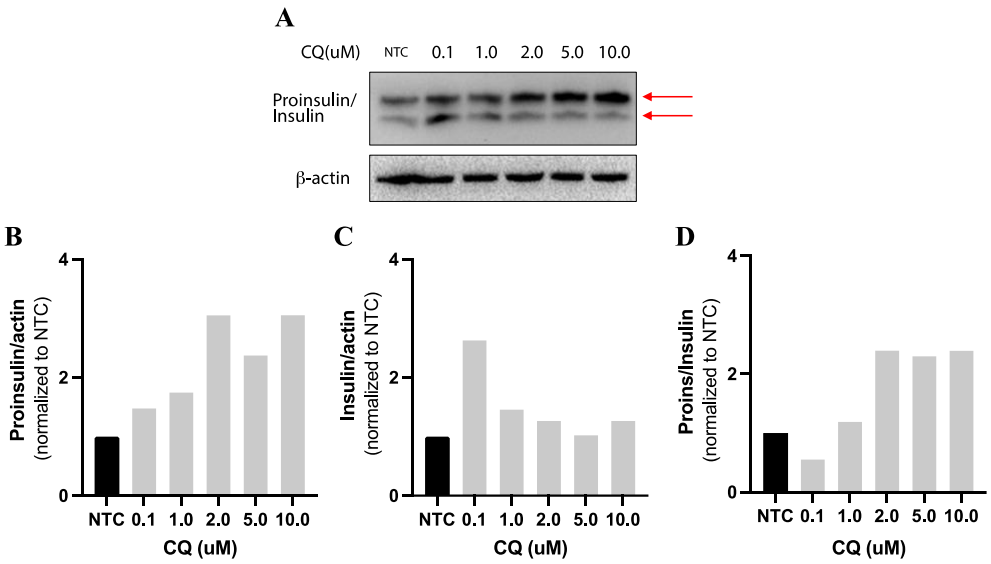

Figure 4 Proinsulin and insulin expression levels with or without CQ treatment in INS1 cells

INS1 cells were cultured for 24 hours after CQ treatment with the indicated concentrations and then lysed. (A) Protein extracts (25 µg) were resolved in SDS-PAGE with human (pro) insulin std. and immunoblotted for insulin and proinsulin. (B, C) The intensity values of proinsulin and insulin protein bands were quantified by Image J software and normalized to non-treated WT INS1 cells. (D) The ratio of proinsulin over insulin was calculated by the quantified proinsulin and insulin results.

To examine the effect of inhibiting autophagosome-mediated lysosomal protein degradation in INS1 cells lacking VPS41, the VPS41 siRNA transfected INS1 cells were cultured with or without CQ (2μM) for 24 hours before lysis. We performed different methods of siRNA transfection and CQ treatment in WT INS1 cells to determine whether pre-, co-, and/or post-CQ treatment affected endogenous insulin levels in the absence of VPS41(**Figure 5**).

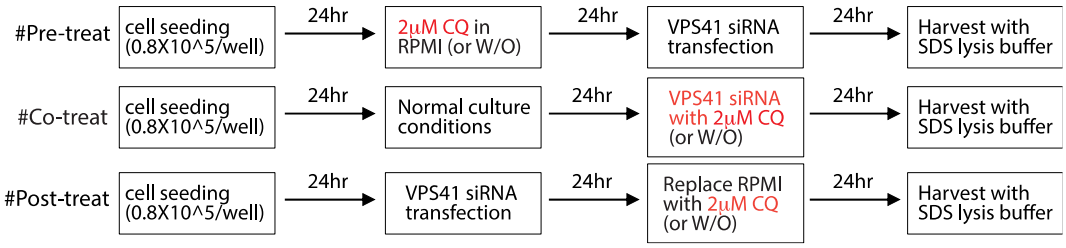

Figure 5 CQ treatment at different time points on VPS41 KD INS1 cells

After following the method variations (**Figure 5**), INS1 cells were lysed and VPS41 and insulin protein expression were examined by western blot. As shown in **Figure 6**, VPS41 was reduced by more than 50% in KD cells compared to control INS1 cells (**Figure 6A & B**). VPS41-siRNA transfection also led to the reduction of proinsulin and insulin protein in INS1 cells (**Figure 6**). Interestingly, proinsulin and insulin protein levels were different, and the difference was dependent on VPS41 levels in VPS41 KD INS1 cells. Due to the prolonged culture time following siRNA transfection in the post-treated condition (**Figure 5**), VPS41 protein expression was slightly decreased in the post-treated condition compared to - co-treated and pre-treated conditions, which might be due to the prolonged culture time following VPS41 siRNA transfection (**Figure 6A**). Thus, pre-, and co-treated VPS41 KD INS1 cells showing higher expression of VPS41 were more expressed insulin and proinsulin, compared to the post-treated VPS41 KD cells (**Figure 6)**. Additionally in the pre-treatment group, inhibiting autophagosome-mediated lysosomal protein degradation with CQ restored proinsulin and insulin protein expression in VPS41 KD INS1 cells. In the co-or post-CQ treatment groups, proinsulin and insulin protein expression was not significantly different (**Figure 6**). To further examine and confirm the restoration of insulin protein expression in the pre-treatment group, I repeated independent experiments (n=4) following the different procedures of CQ treatment in VPS41 KD and control INS1 cells (**Figure 7**).

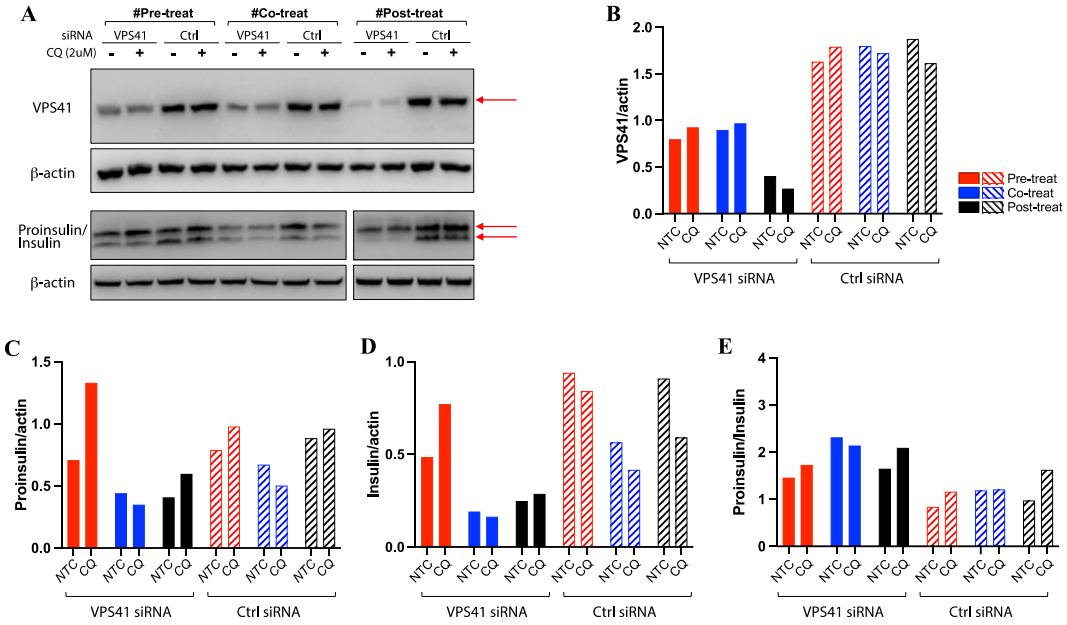

Figure 6 VPS41, proinsulin and insulin protein expression after pre-, co-, and post-CQ treatment in siRNA-transfected INS1 cells

Following pre-, co-, and post-CQ (2 μM) treatments in INS1 cells, the cells were lysed with SDS lysis buffer. (A) Protein extracts (25 μg) were resolved on SDS-PAGE with human proinsulin and insulin as the standard then immunoblotted for VPS41, insulin and proinsulin. (B, C, D) The intensity values of VPS4, proinsulin and insulin protein bands were quantified by Image J software. (E) The ratio of proinsulin over insulin results. Solid-colour bars indicate VPS41 siRNA-transfected cells while pattern-colour bars show non-targeting control siRNA-transfected cells.

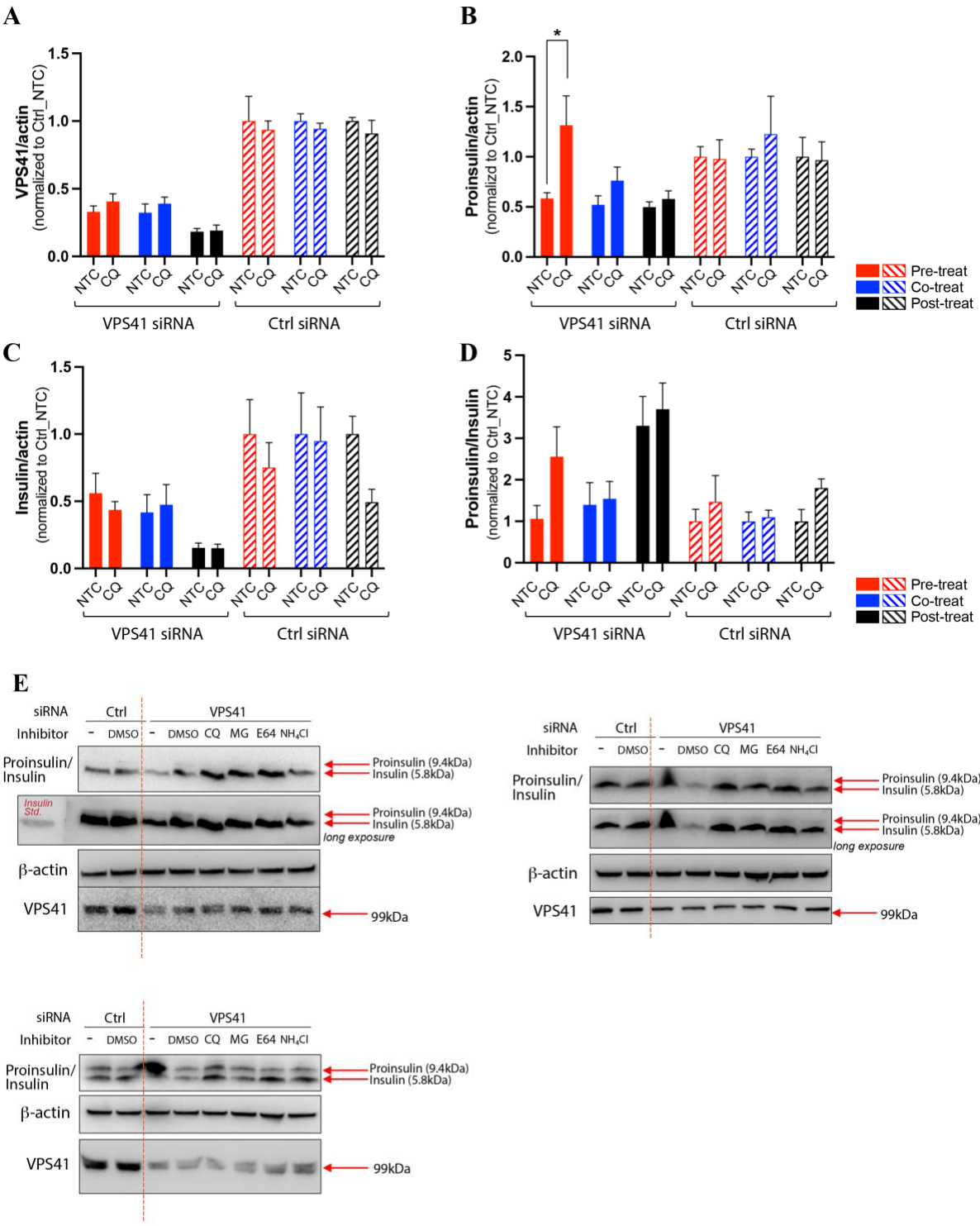

Figure 7 Quantified endogenous VPS41, proinsulin and insulin protein levels in INS1 cells after CQ treatment

Quantified intensity values of (A) VPS41, (B) proinsulin, (C) insulin, and (D) proinsulin protein expression over insulin expression was obtained from replicate experiments following CQ (2μM) treatment and siRNA transfection with VPS41 or control on WT ISN1 cells. Quantified values were obtained from presented immunoblot images (E) by Image J software. Solid-colour bars indicate VPS41 siRNA-transfected while pattern-colour bars show non-targeting control siRNA-transfected cells. The data were presented as mean ± SEM from replicated experiments (n=4) and *: $p < 0.05$ by unpaired t test.

To investigate if preventing the ubiquitin-mediated proteasomal protein degradation pathway restores insulin content in VPS41 KD INS1 cells, I examined proinsulin and insulin protein expression levels in VPS41 transfected INS1 cells treated with MG132. Based on previous reports in the literature about MG132 treatment in pancreatic β cells including mouse islets [2,3] and on the previous result (**Figure 3**), WT INS1 cells were treated with MG132 (100 nM) for 24 hours to confirm whether the concentration of 100nM would not alter critical cellular pathways through enhanced cellular stress or damage as MG132 acts an inducer of apoptosis via oxidative stress [4]. I did not observe significant alterations in proinsulin and insulin protein levels with or without MG132 (100 nM) treatment in WT INS1 cells (**Figure 8**).

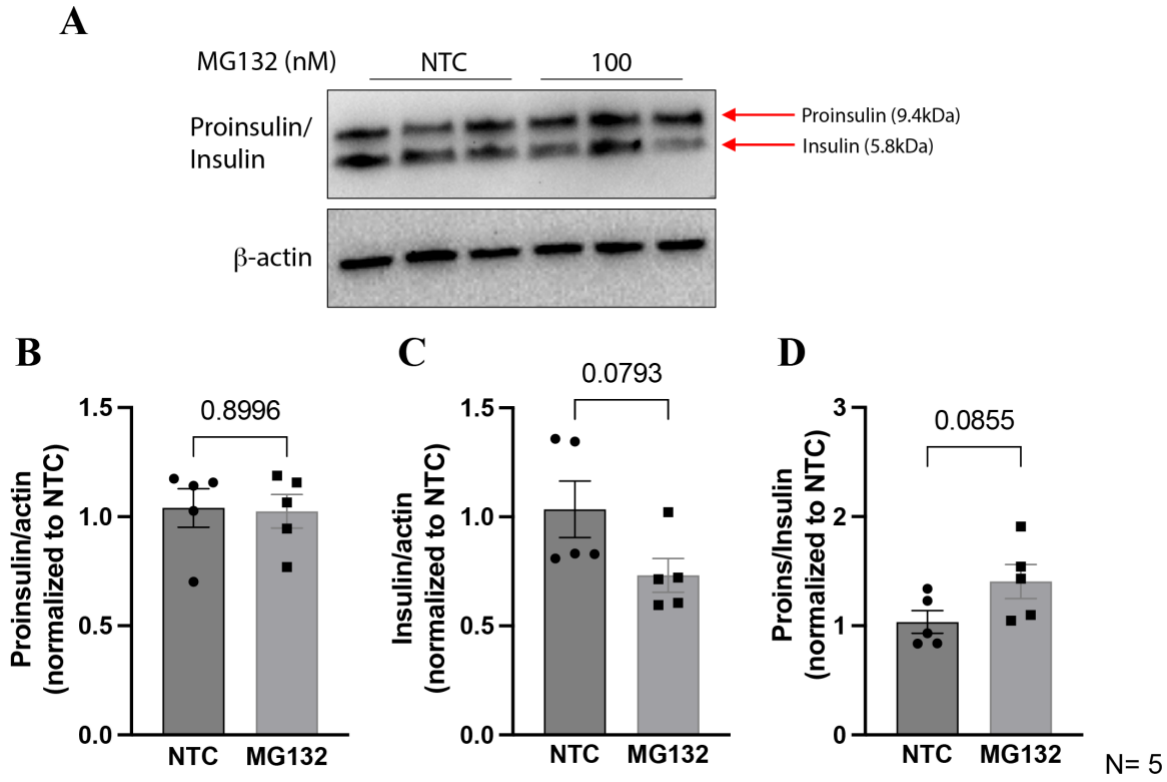

Figure 8 Proinsulin and insulin protein expression with or without MG132 treatment in INS1 cells

WT INS1 cells were treated with or without MG132 (100 nM) for 24 hours before cell lysis. (A) Protein extract (25 µg) was resolved in an SDS-PAGE with human (pro) insulin std. and immunoblotted for insulin and proinsulin. (B, C) The intensity values of proinsulin and insulin protein bands were quantified by Image J software. (D) The ratio of proinsulin over insulin was calculated by the quantified proinsulin and insulin results. All the data were collected from repeated independent experiments (n=5) and presented as mean ± SEM.

In addition to CQ and MG132 protein degradation inhibitors, different types of inhibitors, which have different mechanisms were employed to investigate their effects on protein degradation including insulin protein expression, in cells lacking VPS41. Prior to investigating the inhibitory effects of these inhibitors dose-response experiment was performed in WT INS1 cells to determine the optimal concentration.

NH_4Cl is a well-known inhibitor of autophagy-mediated lysosome degradation that prevents lysosomal protease activity via increased acidification of the lysosome [5,6]. WT INS1 cells were cultured with the indicated concentrations of NH_4Cl for 24 hours to establish the optimal NH_4Cl concentration. Enhanced proinsulin and insulin protein levels were observed in WT INS1 cells treated with a lower concentration of NH_4Cl (1mM) while the higher doses of NH_4Cl (5 and 10mM) led to a dramatic reduction of insulin expression (**Figure 9**).

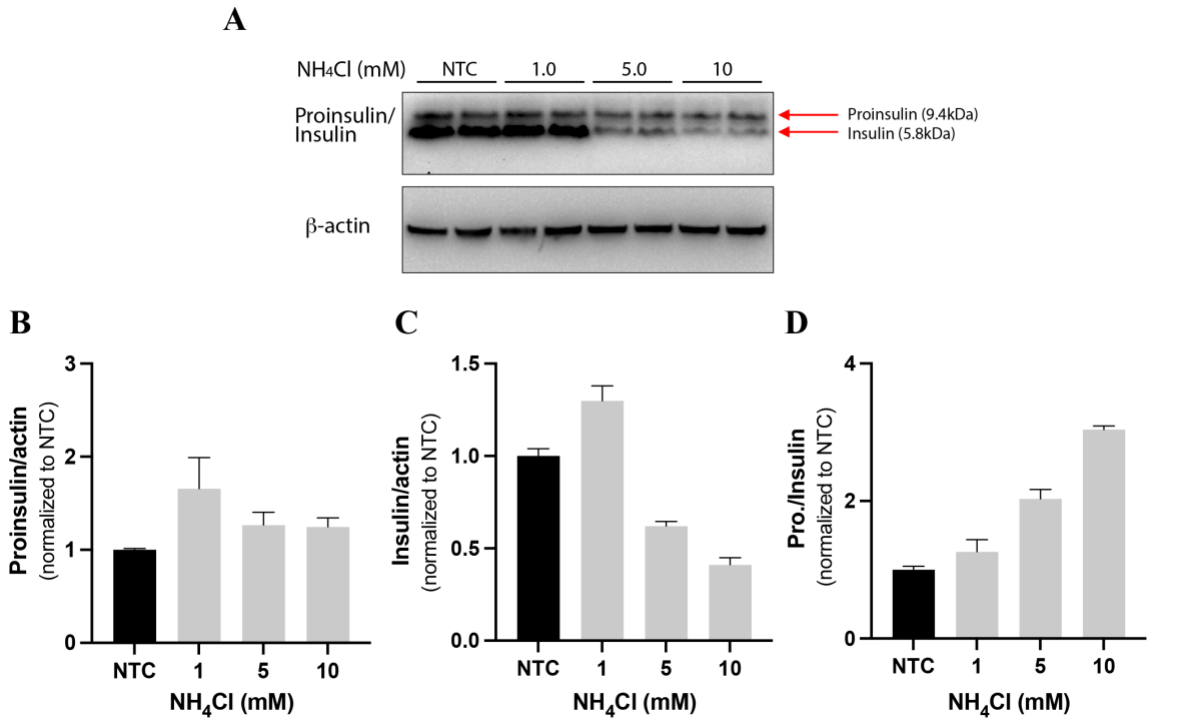

Figure 9 Proinsulin and insulin expression in WT INS1 cells after NH_4Cl treatment

WT INS1 cells were treated with NH_4Cl (1-10mM) for 24 hours. (A) After lysis, protein extracts (25µg) were resolved in an SDS-PAGE with human proinsulin and insulin as the standard, then immunoblotted for proinsulin and insulin. (B) The intensity values of proinsulin and (C) insulin protein bands were quantified by Image J software. (D) The ratio of quantified proinsulin over quantified insulin protein levels. All the data were presented as mean ± SD.

I also used another pharmacological lysosome inhibitor, named E-64, which is a selective lysosomal cysteine protease cathepsin B inhibitor [7,8]. As for NH_4Cl, a dose-response experiment was performed to determine the optimal concentration of E-64. WT INS1 cells were cultured with the indicated concentrations of E-64 for 24 hours. While endogenous proinsulin protein expression was consistent except at high concentrations (10 and 20 μM), there was a dose-dependent decrease in endogenous insulin (**Figure 10**). Therefore, the lowest concentration of E-64 (1.0 μM) was used alongside the other inhibitors in further experiments.

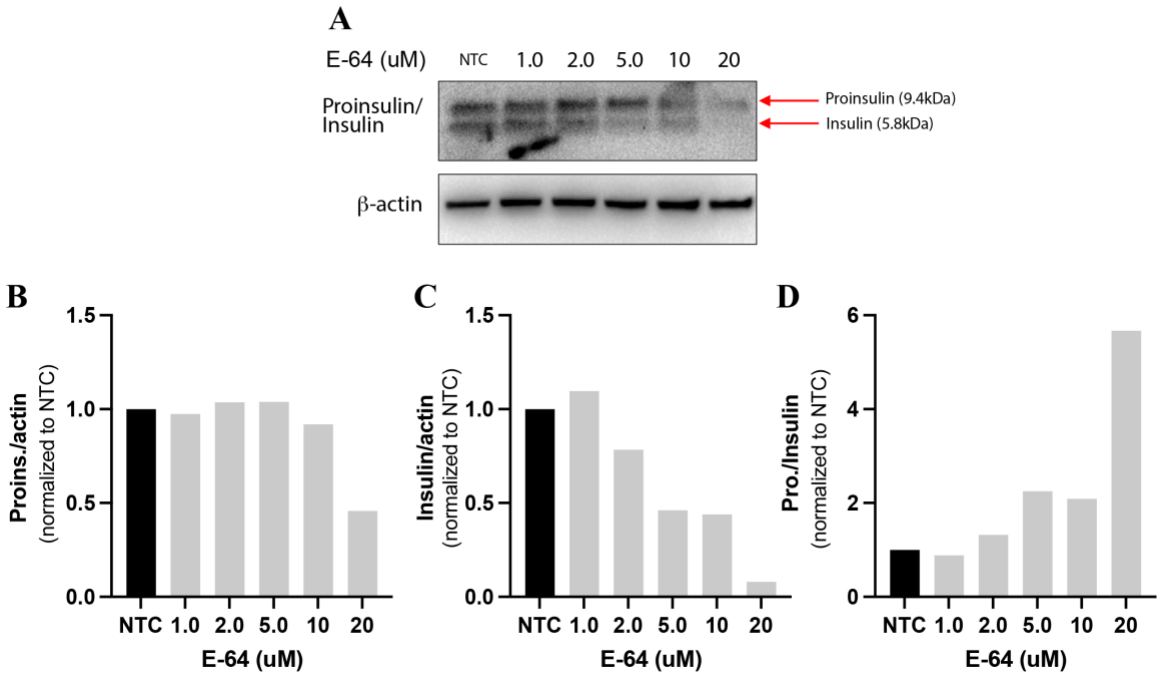

Figure 10 Proinsulin and insulin protein expression in INS1 cells after E-64 treatment

WT INS1 cells were treated with E-64 with the indicated concentrations for 24 hours before cell lysis. SDS-lysis buffer. (A) Protein extracts (25 μg) were resolved on SDS-PAGE with human insulin and proinsulin as the standard, then immunoblotted for proinsulin and insulin protein expression. (B) The intensity values of proinsulin and (C) insulin protein bands were quantified by Image J software. (D) The ratio of quantified proinsulin over quantified insulin.

1. Bartolome, A., Guillen, C. & Benito, M. Autophagy plays a protective role in endoplasmic reticulum stress-mediated pancreatic β cell death. *Autophagy* **8**, 1757–1768 (2012).
2. Liu, S. *et al.* Misfolded proinsulin impairs processing of precursor of insulin receptor and insulin signaling in β cells. *FASEB J.* **33**, 11338 (2019).
3. Broca, C. *et al.* Proteasome Dysfunction Mediates High Glucose-Induced Apoptosis in Rodent Beta Cells and Human Islets. *PLoS One* **9**, 92066 (2014).
4. Fan, W. *et al.* Proteasome inhibitor MG-132 induces C6 glioma cell apoptosis via oxidative stress. (2011) doi:10.1038/aps.2011.16.
5. Amenta, J. S. & Brocher, S. C. Role of lysosomes in protein turnover: catch-up proteolysis after release from NH4Cl inhibition. *J. Cell. Physiol.* **102**, 259–266 (1980).
6. Las, G., Serada, S. B., Wikstrom, J. D., Twig, G. & Shirihai, O. S. Fatty acids suppress autophagic turnover in β-cells. *J. Biol. Chem.* **286**, 42534–42544 (2011).
7. Hashida, S., Kominami, E. & Katunuma, N. Inhibitions of cathepsin B and cathepsin L by E-64 in vivo. II. Incorporation of [3H]E-64 into rat liver lysosomes in vivo. *J. Biochem.* **91**, 1373–1380 (1982).
8. Bogyo, M., Verhelst, S., Bellingard-Dubouchaud, V., Toba, S. & Greenbaum, D. Selective targeting of lysosomal cysteine proteases with radiolabeled electrophilic substrate analogs. *Chem. Biol.* **7**, 27–38 (2000).